REPORT DOCUMENTATION PAGE

Form Approved
OMB No. 0704-0188

1. AGENCY USE ONLY (Leave blank)	2. REPORT DATE Nov 94	3. REPORT TYPE AND DATES COVERED

4. TITLE AND SUBTITLE
Collisional Dynamics and Spectroscopic Studies of Highly Excited Rovibrational levels of $I_2X(0_g^+)$ via Stimulated Emission Pumping

5. FUNDING NUMBERS

6. AUTHOR(S)

Melvin Leonard Nowlin

7. PERFORMING ORGANIZATION NAME(S) AND ADDRESS(ES)

AFIT Students Attending:

Emory University

8. PERFORMING ORGANIZATION REPORT NUMBER
AFIT/CI/CIA

94-039-D

9. SPONSORING/MONITORING AGENCY NAME(S) AND ADDRESS(ES)

DEPRTMENT OF THE AIR FORCE
AFIT/CI
2950 P STREET
WRIGHT-PATTERSON AFB OH 45433-7765

10. SPONSORING/MONITORING AGENCY REPORT NUMBER

11. SUPPLEMENTARY NOTES

12a. DISTRIBUTION/AVAILABILITY STATEMENT

Approved for Public Release IAW 190-1
Distribution Unlimited
MICHAEL M. BRICKER, SMSgt, USAF
Chief Administration

12b. DISTRIBUTION CODE

13. ABSTRACT (Maximum 200 words)

DTIC
SELECTE
JAN 0 5 1994
F

19950103 050

DTIC QUALITY INSPECTED 3

14. SUBJECT TERMS

15. NUMBER OF PAGES
288

16. PRICE CODE

17. SECURITY CLASSIFICATION OF REPORT	18. SECURITY CLASSIFICATION OF THIS PAGE	19. SECURITY CLASSIFICATION OF ABSTRACT	20. LIMITATION OF ABSTRACT

Collisional Dynamics and Spectroscopic Studies of Highly Excited Rovibrational Levels of I_2 $X(0^+_g)$ via Stimulated Emission Pumping

by

Melvin Leonard Nowlin

Presented to the Faculty of the Graduate School of Emory University
in Partial Fulfillment of the Requirements for the Degree of Doctor of Philosophy

Nov 1994

In presenting this dissertation as a partial fulfillment of the requirements for an advanced degree from Emory University, I agree that the Library of the University shall make it available for inspection and circulation in accordance with its regulations governing materials of this type. I agree that permission to copy from, or to publish, this dissertation may be granted by the professor under whose direction it was written, or, in his absence, by the Dean of the Graduate School, when such copying or publication is soley for scholarly purposes and does not involve potential financial gain. It is understood that any copying from, or publication of, this disseration which involves potential financial gain will not be allowed without written permission.

_____

NOTICE TO BORROWERS

Unpublished dissertations deposited in the Emory University Library must be used only in accordance with the stipulations prescribed by the author in the preceding statement.

The author of this dissertation is:

Melvin Leonard Nowlin
Department of the Air Force
Headquarters, United States Air Force Academy
Department of Chemistry
USAFA, CO 80840

The director of this dissertation is:

Michael Charles Heaven
Department of Chemistry
Emory University
Atlanta, GA 30322

Users of this dissertation not regularly enrolled as students at Emory University are required to attest acceptance of the preceding stipulations by signing below. Libraries borrowing this dissertation for the use of their patrons are required to see that each user records here the information requested.

Name of User	**Address**	**Date**	**Type of Use** (Examination only or copying)
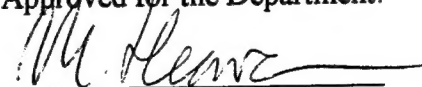
Collisional Dynamics and Spectroscopic Studies of Highly Excited Rovibrational Levels of I_2 $X(0^+_g)$ via Stimulated Emission Pumping

by

Melvin Leonard Nowlin

Advisor: Michael Charles Heaven
Department of Chemistry

Approved for the Department:

_____
Advisor

_____11/10/94_____
Date

Accepted:

_____
Dean of the Graduate School

_____
Date

Collisional Dynamics and Spectroscopic Studies of Highly Excited Rovibrational Levels of I_2 $X(0^+_g)$ via Stimulated Emission Pumping

by

Melvin Leonard Nowlin
B.S., Chemistry, Virginia Military Institute, 1982
M.E., Chemical Engineering, The University of Virginia, 1983

Advisor: Michael Charles Heaven

An Abstract of
A Dissertation Submitted to the Faculty of the Graduate School of Emory University
in Partial Fulfillment of the Requirements for the Degree of Doctor of Philosophy

Chemistry/Physical Chemistry

1994

Abstract

Highly excited vibrational levels of I_2 (X) are thought to play an important role in the mechanism of iodine dissociation in the chemical oxygen iodine laser. It has been proposed that I_2 is dissociated in the laser with processes such as
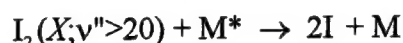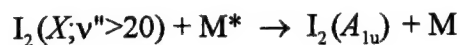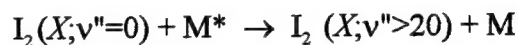
$$I_2(X;v''=0) + M^* \rightarrow I_2 (X;v''>20) + M$$
$$I_2(X;v''>20) + M^* \rightarrow I_2(A_{1u}) + M$$
$$I_2(X;v''>20) + M^* \rightarrow 2I + M$$

where M^* is $I(^2P_{1/2})$ or $O_2(^1\Delta)$, and M is $O_2(^3\Sigma)$ or $I(^2P_{3/2})$. In the chain branching mechanism, initiation would involve near-resonant E-V transfer populating vibrational levels around $v''=40$. Consequently, the relaxation dynamics of these levels are of interest as they may control the efficiency of the laser.

I have examined the nascent state distribution of the I_2 (X) product using pulsed laser photolysis and probe techniques. In these experiments, $I(^2P_{1/2})$ was generated by 496 nm photolysis of I_2. Within several microseconds after the photolysis laser, $I_2(X;23<v''<47)$ is detected by laser excitation of the D-X transition at wavelengths in the 280 - 300 nm range. Rotationally-resolved spectra under single collision conditions were recorded for the D-X transitions $4<v'<12 \leftarrow 23<v''<47$. Analysis of the data indicated that the molecular constants for the D state did not extrapolate to the $v'<30$ levels reliably. In order to improve the characterization of the D state, a least-squares analysis generated improved spectroscopic constants:

Table I: Dunham Vibrational Parameters of the $D(0^+_u)$ Ion-Pair state of I_2

Y_{00} = 41026.166

Y_{10} = 95.11746327

Y_{20} = -0.111495227

Y_{30} = -5.792874546x10^{-4}

Y_{40} = 4.205281828x10^{-6}

Y_{50} = -1.408244378x10^{-8}

Y_{60} = 2.68736882x10^{-11}

Y_{70} = -2.3114805x10^{-14}

Vibrationally excited I_2 (X) was prepared for state-to-state studies of the vibrational and rotational collision dynamics. Levels v''=42, 38 and 23 were prepared by stimulated emission pumping and then probed by laser induced fluorescence. The prepared level, and the collisionally populated levels were detected by laser excitation of the D-X system. Relaxation kinetics were determined by varying the delay between the dump and probe laser pulses. Collisions with H_2, He, Ar, H_2O, D_2O, Cl_2, N_2, O_2, and I_2 were investigated. Total loss rates were measured for all collision partners. Rotational energy transfer rate constants were determined by parametrization of experimental data by the statistical power gap. Vibrational energy transfer (Δv=-1) was observed and measured for many of the collision partners.

Acknowlegements

The author gratefully acknowledges the sponsorship and support of the United States Air Force Academy and the Air Force Institute of Technology. In particular, I wish to thank Colonel Hans J. Mueh, Professor and Head, Lt. Col. Clifford M.Utermoehlen, Deputy Head, Maj. Michael O. Killpack, Associate Professor, Maj. James P.Hogan, Program Manager, as well as all the outstanding men and women of the United States Air Force with whom I have had the privilege to serve. I will always be indebted to Lt. Col. Robert C. Ligday for his trust and guidance in support of the author's professional development. The support of Dr. Gordon D. Hager as well as the financial assistance of the USAF Phillips Laboratory and the Air Force Office of Scientific Research made the timely completion of this project possible.

I wish to express my profound gratitude to my advisor, Dr. Michael C. Heaven. His rigorous intellect and pleasant personality are indeed a rare combination. The author was truly fortunate to associate with, and have as my mentor an individual with such high standards. In addition, I wish to thank Dr. Clarence G. Trowbridge and Dr. Ernest A. Dorko, Senior Scientist and Adjunct Professor for the Air Force Institute of Technology, for their graciousness and support in serving on my committee. Dr. Dorko's ardent support during numerous management reviews prevented cancellation of this research, and his personal commitment and encouragement in a constantly changing environment are largely responsible for the success of this project.

Dedication

in memory of

Leonard Minor Nowlin

September 8, 1914 - July 1, 1979

No man is an island entire of itself; every man is part of the main ... Any man's death diminishes me because I am involved in mankind, and therefore never send to know for whom the bell tolls; it tolls for thee.   John Donne

Table of Contents

LIST OF FIGURES AND ILLUSTRATIONS

LIST OF TABLES

LIST OF EXAMPLES

CHAPTER I

INTRODUCTION

Collision induced measurements of rotational energy transfer by laser induced fluorescence are nearing almost a quarter of a century of experimentation. It was first applied to Na_2 $(B\ ^1\pi)^1$ and I_2 $(B\ ^3\pi)^2$ and has since measured OH $(A\ ^2\Sigma)$,[3] $Na_2\ (A\ ^1\Sigma)$,[4] Li_2 $(A\ ^1\Sigma)$,[5] CdH $(A\ ^2\pi)$,[6] KH $(A\ ^1\Sigma)$,[7] ZnH $(A\ ^2\pi)$,[8] CsH $(A\ ^1\Sigma)$,[9] CaF $(A\ ^2\pi)$,[10] and IF $(B\ ^3\pi)$.[11] The more recent developments of various pump-probe techniques have been useful for investigating rotational energy transfer of inelastic collisions within vibrationally excited levels of the electronic ground state for HF [v=1,[12] v=2 (Ref 13)], NO (v=2),[14] H_2(v=1),[15,16] D_2 (v=1),[15] HD (v=1),[17] HCl (v=1),[18] N_2(v=1)[19] and CN(v=2).[20] Pump-probe techniques have also been used to examine rotational energy transfer in the electronically excited states for NO $(A)^{21}$ and IF $(B^3\pi)$.[22]

Although the field of molecular dynamics is well developed, there are very few studies of energy transfer for molecules with chemically significant internal energy. The principal reason for the lack of state-to-state experimental investigations into high levels of vibrational excitation in the ground electronic state has been the difficulty in the state-selective preparation and detection of the energetic species. In order to selectively prepare these energetic molecules, spectroscopic techniques are now being employed as a means of preparing highly vibrationally excited species as well as investigating them.

Surprisingly, there are only four examples of polyatomics with internal energies in excess of 5000 cm^{-1} whose state-to-state collisional relaxations has been experimentally investigated.[23] Only experiments with C_2H_2,[24] H_2CO,[25] HCN [23] and NH_3 [26] have directly probed for energy redistribution. Even more surprising than the scarcity of polyatomic data, is the scarcity of state resolved measurements for vibrationally energetic diatomic species. Besides the vibrationally excited I_2 studies presented herein, only experiments with NO $(X^2\pi)$[27] and O_2 $(X^3\Sigma)$[28] have measured the energy transfer of highly vibrationally excited molecules in their electronic ground state.

A key motivation for studying the energy transfer of these highly vibrationally excited levels of $I_2(X)$ is because $I_2(X, v''>20)$ levels are thought to play an important role in the mechanism of iodine dissociation in the chemically-pumped oxygen iodine laser. In addition, the collisional dynamics of $I_2(B)$ have been studied extensively, and used in the development of theoretical models of energy transfer. However, there is very little information on the collisional dynamics of I_2 (X). Comparisons can yield insights concerning the influence of the electronic state on the outcome of an inelastic collision. With the advent of stimulated emission pumping for state preparation in combination with laser induced fluorescence for detection, it is feasible to populate and probe individual rovibrational levels in the ground state. Stimulated emission pumping is a folded variant of optical-optical double resonance and has the same advantage of combining rotational state selection rules for two resonant transitions, thereby eliminating rotational congestion. This dissertation examines the state-to-state

relaxation of highly vibrationally excited $I_2(X)$ selectively prepared by the technique of stimulated emission pumping. Section §1.1 of this introduction will provide an overview of the $O_2(^1\Delta) + I_2$ system and the role of vibrationally excited $I_2(X)$. Section §1.2 describes the chemical-pumped oxygen iodine laser while the energy levels of molecular and atomic iodine are presented in Section §1.3. Appendix E provides a general description of atomic and molecular term symbols.

§1.1 OVERVIEW OF THE DEVELOPMENTS OF $I_2 + O_2(^1\Delta)$

In 1966, S.J. Arnold, N. Finlayson and E. A. Ogryzlo were the first to report a "bright-yellow glow" when I_2 was introduced into a stream of $O_2(^1\Delta)$ molecules.[29] In addition to the yellow glow associated with $B^3\Pi^+_u \rightarrow X^1\Sigma^+_g$ transitions in I_2, they correctly identified atomic iodine's $I(^2P_{1/2} \rightarrow ^2P_{3/2})$ transition at 13200 Å. Iodine dissociation was hypothetically proposed as a reaction with $O_2(^1\Sigma)$ or alternatively, as multiple collisions with $O_2(^1\Delta)$ "if I_2 possesses a low-lying state (<23 kcal above ground)." The mechanisms suggested by Arnold et al. for I_2 dissociation were

$$I_2 + O_2(^1\Sigma) \text{ or } 2[O_2(^1\Delta)] \rightarrow 2I + O_2$$
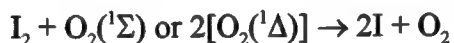
Since $O_2(^1\Sigma)$ concentration was observed as increasing 10 times its steady-state value upon addition of iodine into the $O_2(^1\Delta)$ flow, they explained iodine atoms as catalyzing the formation of $O_2(^1\Sigma)$ in the following chain processes:

$$O_2(^1\Delta) + O_2(^1\Delta) \rightarrow O_2(^3\Sigma) + O_2(^1\Sigma)$$

$$O_2(^1\Delta) + I(^2P_{3/2}) \rightarrow O_2(^3\Sigma) + I(^2P_{1/2})$$

$$O_2(^1\Delta) + I(^2P_{1/2}) \rightarrow O_2(^1\Sigma) + I(^2P_{3/2})$$
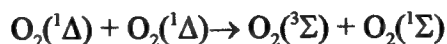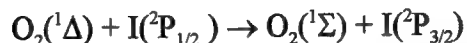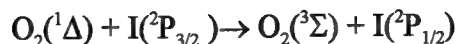
In a series of papers,[30-33] R. G. Derwent and B. A. Thrush examined the excitation of

iodine by $O_2(^1\Delta)$. They proposed the formation of atomic iodine was accounted for by

the direct excitation of I_2 by $O_2(^1\Sigma)$. They proposed

$$O_2(^1\Sigma) + I_2 \rightarrow O_2(^3\Sigma) + I_2(A^3\pi_{1u})$$
$$\rightarrow O_2(^3\Sigma) + 2I$$
$$O_2(^1\Delta) + I_2(A^3\pi_{1u}) \rightarrow O_2(^3\Sigma) + I_2(B^3\pi_{0u}).$$
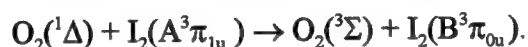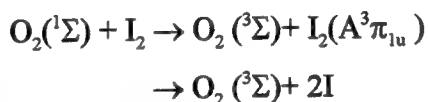
They discounted the alternative mechanism of

$$2O_2(^1\Delta) + I_2 \rightarrow 2O_2(^3\Sigma) + 2I$$
$$\rightarrow 2O_2(^3\Sigma) + I_2(A^3\pi_{1u})$$
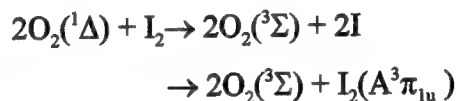
Their rationale for discounting the alternative mechanism was based upon the addition of

water vapor to the $I_2+O_2(^1\Delta)$ system which effectively quenched $O_2(^1\Sigma)$ and the emission,

as well as other quantitative considerations. Once formed, atomic iodine is subsequently

excited by $O_2(^1\Delta)$ with near-resonant (quantum defect ~279 cm^{-1}) energy transfer

where resonant energy transfer is characterized by collisions between species in which

transfer of energy occurs from the metastable to the unexcited species.

As a result of this efficient resonant energy transfer, Derwent and Thrush[34]

reported that the atomic iodine line at 1.315 µm would exhibit laser action when the

concentration of $O_2(^1\Delta)$ was significantly greater than 10%. In 1978, researchers at the

Air Force Weapons Laboratory, W. E. McDermott, N. R. Pchelkin, D. J. Benard, and R.

R. Bousek[35] were the first to demonstrate an electronic transfer laser utilizing the atomic

iodine transition $I(^2P_{1/2}) \rightarrow I(^2P_{3/2}) + h\nu$ pumped by $O_2(^1\Delta)$. The Chemical Oxygen

Iodine Laser (COIL) is the shortest wavelength chemical laser and is the only chemical

laser which operates on an electronic rather than rotational or variational transitions

(e.g. CO_2 and HF/DF lasers)[36]. Figure 1.1 shows the interrelationships between the

electronic energy levels of oxygen, and atomic and molecular iodine.

While the prediction of laser action by Derwent and Thrush[35] for the $I_2/O_2(^1\Delta)$

chemical system was realized, the mechanism for I_2 dissociation by $O_2(^1\Sigma)$ became

doubtful. Aviles et al.[37] reported that the total $O_2(^1\Sigma)$ removal rate coefficient was ten

times smaller than the value required by Derwent and Thrush to model their results.

Muller et al.[38] substantiated the finding that the rate of dissociation of I_2 by $O_2(^1\Sigma)$ was

too small. Furthermore, spectroscopic studies of the $I_2(A')$ by Tellinghuisen[39] placed the

potential minimum at 10047 cm^{-1}. As seen in Figure 1.1, the $I_2(A')$ state is energetically

too high to be accessed by a single collision with an $O_2(^1\Delta)$ molecule, thereby eliminating

this possibility of the $I_2(A')$ state as an intermediate storage state.

A chain reaction model for iodine dissociation was proposed by R.F. Heidner III,

C. E. Gardner, G. I. Segal, and T. M. El-Sayed.[40] Their analysis was derived from their

investigations with a discharge flow-tube in which they monitored $O_2(^1\Delta)$, $O_2(^1\Sigma)$,

$I(^2P_{1/2})$, $I_2(A^3\pi_{1u})$ and $I_2(B^3\pi_{0u})$ by optical emission spectroscopy. Although vibrationally

excited $I_2(X)$ was not directly observed in the flow tube experiment, the participation of

vibrationally excited I_2 was inferred from kinetic models.[41] In fact, Heidner et al.

Energy (cm^{-1}) x 10^{-3}

I$_2$ $B(^3\Pi_0^+)$

15725

15 —

4878

O$_2$ ($^1\Sigma$)

2I ($^2P_{3/2}$)

— — — — 12244

I$_2$ $A(^3\Pi_{1u})$

5239

805

I$_2$ $A'(^3\Pi_{2u})$

10 —

I ($^2P_{1/2}$)

O$_2$ ($^1\Delta$)

7603

7882

10042

1.315 μm

5 —

I ($^2P_{3/2}$)

O$_2$ ($^3\Sigma$)

I$_2$ X($^1\Sigma$)
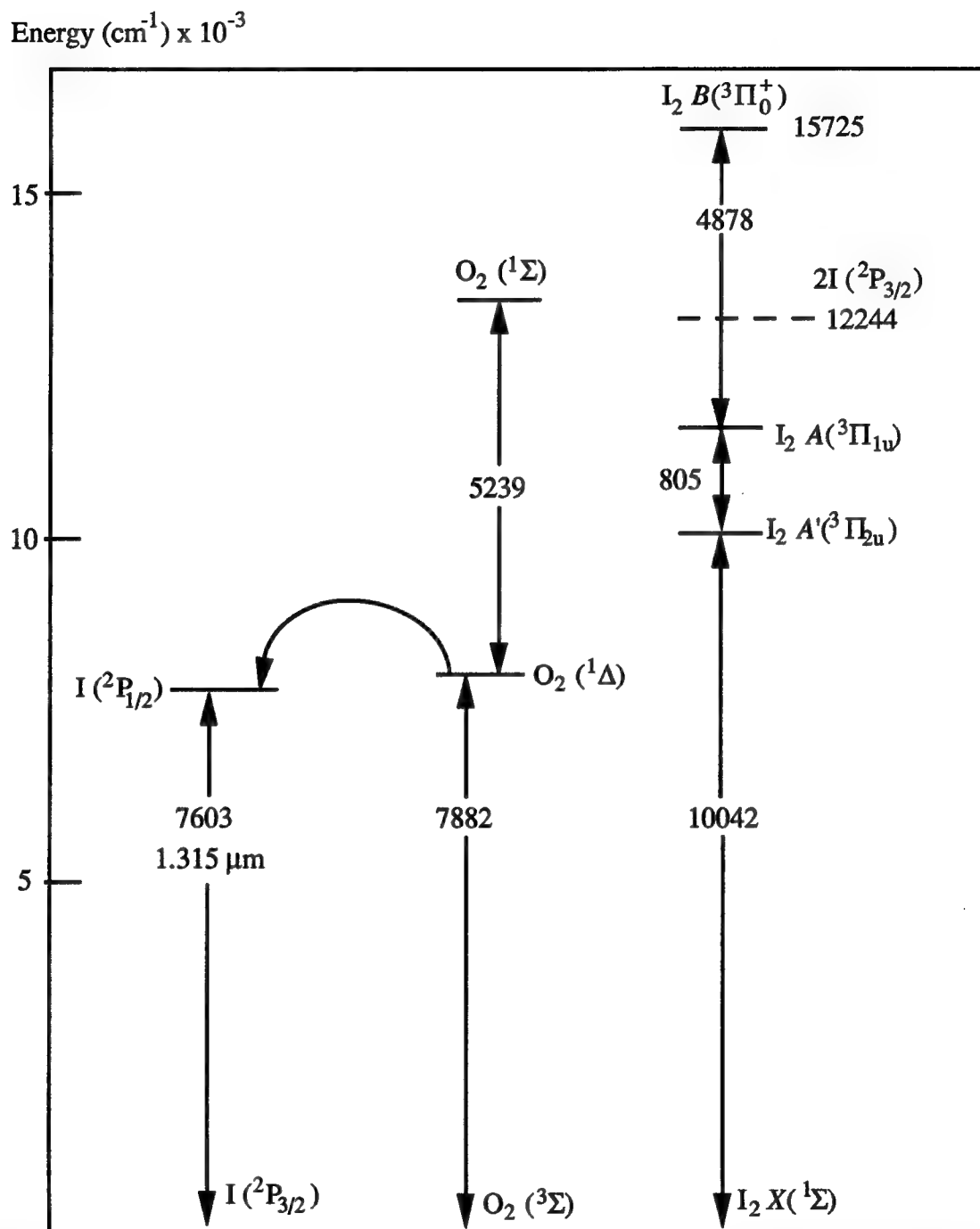
Figure 1.1: Electronic Energy Levels in the Chemical Oxygen Iodine Laser

postulated two kinetic models with the intermediate state ($I_2^\dagger$) as either $I_2(A')$ or vibrationally excited I_2 (X). The most important of these processes for iodine dissociation are

$$O_2(^1\Sigma) + I_2\ (X) \to O_2(^3\Sigma) + 2I$$

$$O_2(^1\Delta) + I_2\ (X) \to O_2(^3\Sigma) + I_2^\dagger$$

$$O_2(^1\Delta) + I_2^\dagger \to O_2(^3\Sigma) + 2I$$

$$I(^2P_{1/2}) + I_2(X) \to I_2^\dagger + I$$

$$I(^2P_{1/2}) + I_2^\dagger \to 3I$$
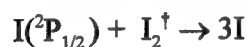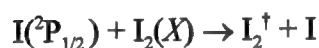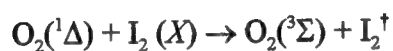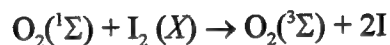
G.E. Hall, W.J. Marinelli, and P.L. Houston[42] observed the electronic to vibrational (E→V) energy transfer from $I(^2P_{1/2})$ to I_2 and proposed a chain-branching mechanism

$$I(^2P_{1/2}) + I_2(X) \to I_2\ (20<v<40) + I(^2P_{3/2})$$

$$I_2\ (20<v<40) + O_2(^1\Delta) \to 2I(^2P_{3/2}) + O_2$$

$$O_2(^1\Delta) + I(^2P_{3/2}) \to O_2(^3\Sigma) + I(^2P_{1/2})$$
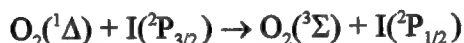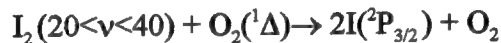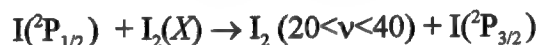
They followed the time evolution of the I_2 vibrational population distribution for $v''=29$ and 40, and measured the rate constants for deactivation of I_2 (X, $v''=40$) by He, Ar, and I_2. Using the rate constants measured by Hall et al., D. David, V. Joly and A. Fausse[43] modeled I_2 dissociation in the presence of $O_2(^1\Delta)$ using high vibrational levels of I_2 as an intermediate state, and by assuming the rate constants scaled linearly with v and $v-1$. The presence of vibrationally excited iodine was confirmed by M.H. van Benthem and S. J. Davis[44] while observing $I_2 + O_2(^1\Delta)$ by in a flow tube reactor. More recently, A.J.

Bouvier, R. Bacis, A. Bouvier, D. Cerny, S. Churassy, P. Crozet and M. Nota[45] have

proposed channels for dissociation involving the A and A' states of I_2. They suggested

either a two-step or three-step dissociation process, with both mechanisms conditional

upon the degree of relaxation of the vibrationally excited I_2 (X). Figure 1.2 illustrates

the two-step or three step dissociation process. In the two-step mechanism with little

vibrational relaxation, vibrationally excited I_2 can be dissociated by excitation directly to

the repulsive 1u state. However, if vibrational relaxation becomes dominant, then the A

or A' states are populated before dissociation occurs through 1u. Relaxation of the

vibrationally excited $I_2(X)$ forces higher consumption of $O_2(^1\Delta)$ and requires a multi-step

process. Indeed, the two-step, three-step, and multi-step dissociation mechanisms help

explain the observation of $2 \leq n \leq 6$ where n is the number of $O_2(^1\Delta)$ required to dissociate

an I_2 molecule. In fact, one of the most critical issues facing COIL modeling is the

parametric dependence of n.

Predicting the dissociation of molecular iodine has been identified as the largest

source of error in COIL performance modeling. Modeling the performance of the laser

over predicts performance and under predicts I_2 dissociation.[36] Scaling of the COIL

device to higher power has become increasingly more difficult due to inadequate

knowledge of the mechanism for iodine dissociation since the dissociation efficiency

greatly influences device geometry and operating conditions. Experimental and modeling

data have indicated that some of the performance prediction problems may be due to a

coupled mixing and dissociation process. Imperfect mixing of iodine and oxygen results

Dissociation (through 1u)

$A(1u)$

2

$v''=33\text{-}40$

$^2P_{3/2} + {}^2P_{3/2}$

1

$X(0^+_g)$

a) Two-Step Process

$B(0^+_u)$

3

$A'(2u), A(1u)$

Dissociation

$^2P_{3/2} + {}^2P_{3/2}$

$v''=33\text{-}40$

relaxation

2

$X(0^+_g)$

1
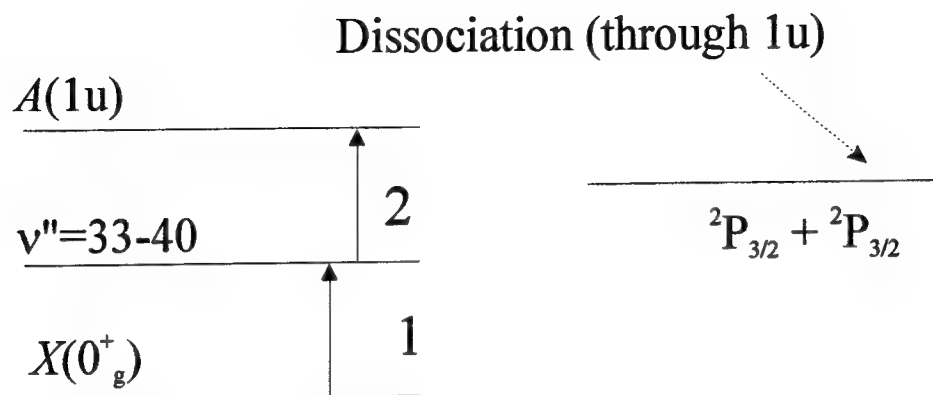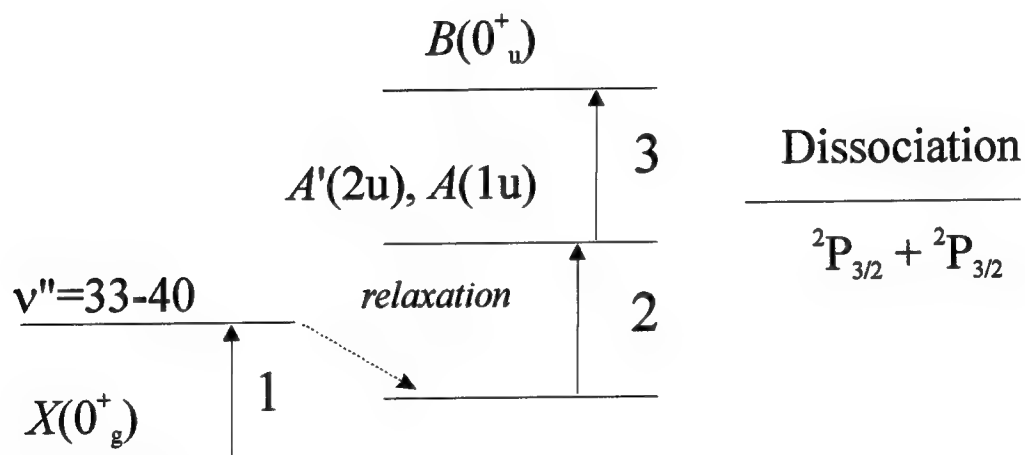
b) Three-Step Process

Figure 1.2: Illustration of the Proposed a)Two-Step and b)Three-Step Dissociation Process of Iodine by O_2 ($^1\Delta$) [Reference 45].

in initial regions of high iodine concentration leading to faster dissociation rates. In addition, estimated and inaccurate rate constants used in the kinetic model may contribute significantly to the errors in the prediction of laser performance.

§1.2 CHEMICAL OXYGEN IODINE LASER (COIL)

The COIL operates on the hyperfine components of the $5^2P_{1/2} \rightarrow 5^2P_{3/2}$ transition in atomic iodine.   A schematic diagram of the COIL device is shown in Figure 1.3. Singlet delta oxygen, $O_2(^1\Delta)$, is produced by a two phase chemical reaction of chlorine, hydrogen peroxide , and potassium hydroxide. Often referred to as basic hydrogen peroxide (BHP) due to its high pH, the typical mix is (by weight) 25% H_2O_2, 25% KOH, and 50% H_2O, and the overall stoichiometry of the generator is given by

$$Cl_2 + H_2O_2 + 2KOH \rightarrow 2KCl + 2H_2O + O_2(^1\Delta)$$
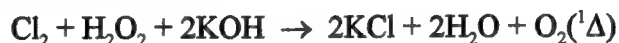
The reaction responsible for singlet oxygen generation is[36]

$$Cl_2 + 2HO_2^- \rightarrow 2Cl^- + H_2O_2 + O_2(^1\Delta)$$

This chemical reaction is exothermic (27 Kcal/mol) with yields approaching 100% $O_2(^1\Delta)$. Due to the exothermic nature of this reaction, cooling is required to remove the heat of mixing and minimize the H_2O/ H_2O_2 vapor pressure. Singlet delta oxygen's long radiative lifetime of 45 min. and relative immunity to quenching make it an almost ideal energy transfer agent. Mass transport losses of $O_2(^1\Delta)$ to the laser cavity are dominated by energy pooling where

$$O_2(^1\Delta) + O_2(^1\Delta) \rightarrow O_2(^1\Sigma) + O_2(^3\Sigma)$$
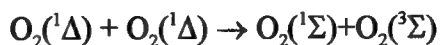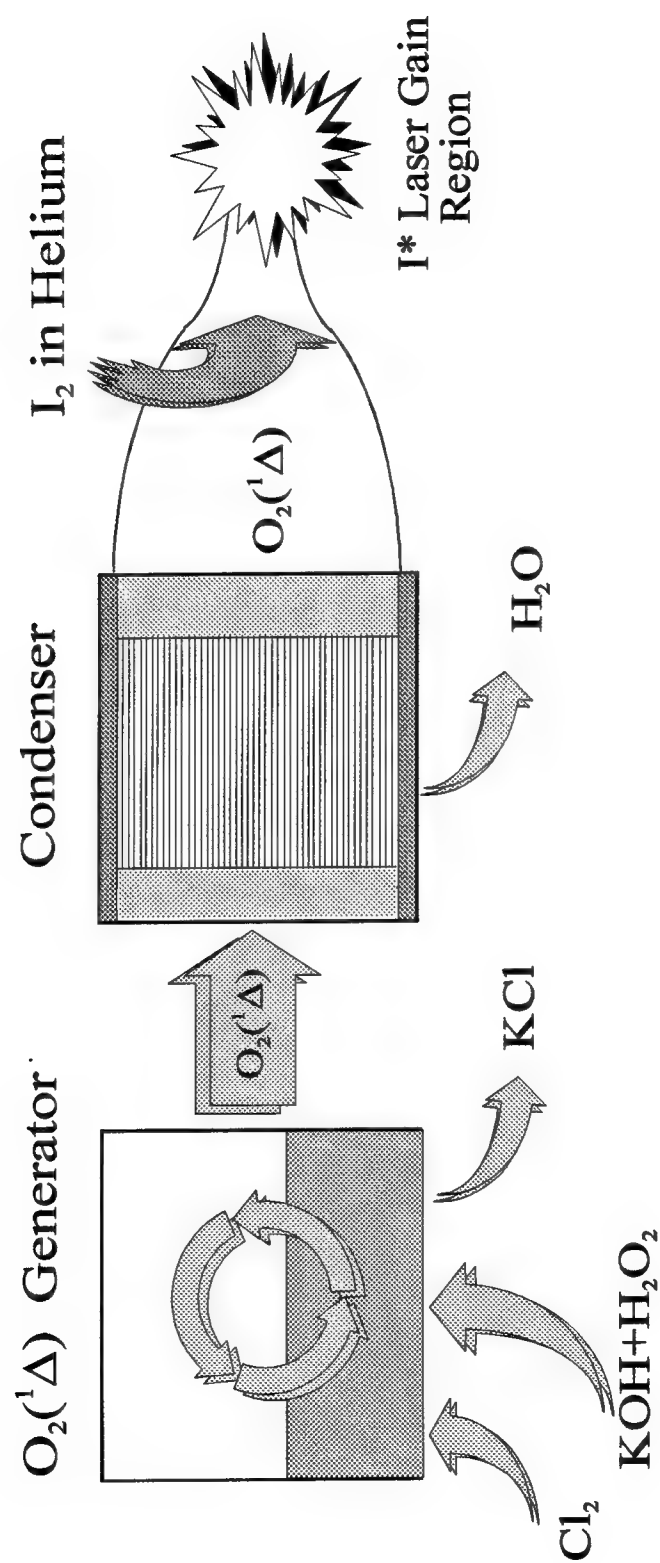
Figure 1.3: Schematic Diagram of the Chemical Oxygen Iodine Laser

In the COIL device, helium serves as a carrier gas for molecular iodine which is injected into the $O_2(^1\Delta)$ flow where it dissociates via a multi-step mechanism as discussed in Section §1.1. $I(^2P_{1/2})$ spin excited atoms are generated through the sequential dissociation and pumping of I_2 by $O_2(^1\Delta)$. The equilibrium expression for the pumping mechanism is

$$k_F[O_2(^1\Delta)][I(^2P_{3/2})]=k_R[O_2(^3\Sigma)][I(^2P_{1/2})]$$

$$K_{eq} = \frac{[O_2(^3\Sigma)][I^2P_{1/2}]}{[O_2(^1\Delta)][I^2P_{3/2}]}$$

The lasing threshold is calculated at zero gain. The gain equation is

$$\gamma_0 = A_{21}\frac{\lambda^2}{8\pi n^2}g(\upsilon)\left(N_2 - \tfrac{g_2}{g_1}N_1\right)$$

where γ_0 is the threshold gain, A_{21} is the Einstein Coefficient for spontaneous emission, $g(\upsilon)$ is the lineshape, N is the population, g is the degeneracy, and n is the index of refraction. The ratio of degeneracies of the two atomic iodine states is

$$\frac{g_2}{g_1} = \frac{g[I(^2P_{1/2})]}{g[I(^2P_{3/2})]} = \frac{2}{4}$$

Because the degeneracy ratio of $^2P_{3/2}$ to $^2P_{1/2}$ is 2, only 33% of the iodine atoms are required in the $^2P_{1/2}$ state for a population inversion to exist. At gain equal to zero, the threshold condition is

$$\frac{[I(^2P_{1/2})]}{[I(^2P_{3/2})]} = \frac{1}{2}$$

$$\gamma_0 = \sigma\left([I^2P_{1/2}] - \tfrac{1}{2}[I^2P_{3/2}]\right) = 0$$

Substituting $[O_2(^1\Delta)] + [O_2(^3\Sigma)] = [O_2]_{tot}$ into the equilibrium expression and substituting, the amount of $O_2(^1\Delta)$ required is

$$K_{eq} = \frac{[O_2(^3\Sigma)][I^2P_{1/2}]}{[O_2(^1\Delta)][I^2P_{3/2}]} = \frac{[O_2]_{tot} - [O_2(^1\Delta)]}{[O_2(^1\Delta)]} \frac{1}{2}$$

rearranging, the mole fraction is calculated[46]

$$X = \frac{1}{2K_{eq}+1}, \qquad Keq = 0.75 \exp[\tfrac{402}{T}]$$

At 298°K, a yield of 15% $O_2(^1\Delta)$ is required for threshold. With sufficient $O_2(^1\Delta)$ production, continuous-wave laser output in the COIL is sustained at 1.315 μm by stimulated emission on the $I(5^2P_{1/2})$ to $I(5^2P_{3/2})$ magnetic dipole transition

$$I(^2P_{1/2}) \rightarrow I(^2P_{3/2}) + h\nu \ (7603 \ \text{cm}^{-1})$$
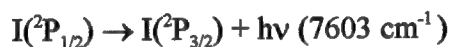
Table 1.1[46] lists some of the processes and their respective rate constants.

§1.3 Molecular and Atomic Iodine Energy Levels

Without a doubt, the spectroscopy of molecular iodine is the most extensively studied and understood of all the halogens. Initially, interest in the spectroscopy of the iodine molecule was a result of its relatively intense absorption of light in the visible and UV regions of the electromagnetic spectrum. Fluorescence of I_2 B-X was first recorded in the early 1900s by Franck and Wood[47]. Later, McLennan[48] described the diffuse

Liquid Chemistry

$HO_2^- + Cl_2 \rightarrow HOOCl + Cl^-$,	8.5×10^{10} cm^3/mole·s
$HO_2^- + HOOCl \rightarrow ClOO^- + H_2O_2$,	∞
$ClOO^- \rightarrow Cl^- + O_2(^1\Delta)$,	$10^7 \rightarrow \infty$ cm^3/mole·s
$O_2(^1\Delta) \rightarrow O_2(^3\Sigma)$,	$1/1.8$ μs
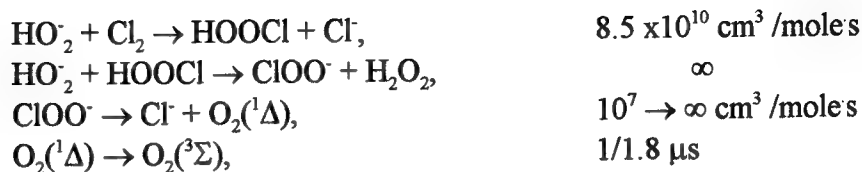
Gas Phase Kinetics [Rates in cm^3/molecule·sec]

$O_2(^1\Sigma) + I_2 \rightarrow O_2(^3\Sigma) + I_2$,	1.6×10^{-11}
$O_2(^1\Sigma) + I_2 \rightarrow O_2(^3\Sigma) + 2I$,	4.0×10^{-12}
$O_2(^1\Sigma) + He \rightarrow O_2(^1\Delta) + He$,	1.0×10^{-17}
$O_2(^1\Sigma) + H_2O \rightarrow O_2(^1\Delta) + H_2O$,	6.0×10^{-12}
$O_2(^1\Delta) + O_2(^3\Sigma) \rightarrow O_2(^3\Sigma) + O_2(^3\Sigma)$,	1.6×10^{-18}
$O_2(^1\Delta) + O_2(^1\Delta) \rightarrow O_2(^3\Sigma) + O_2(^3\Sigma)$,	1.8×10^{-17}
$O_2(^1\Delta) + O_2(^1\Delta) \rightarrow O_2(^1\Sigma) + O_2(^3\Sigma)$,	2.5×10^{-17}
$O_2(^1\Delta) + I_2 \rightarrow O_2(^3\Sigma) + I_2^*$,	7.0×10^{-15}
$O_2(^1\Delta) + I_2^* \rightarrow O_2(^3\Sigma) + 2I$,	3.0×10^{-10}
$O_2(^1\Delta) + I \rightarrow O_2(^3\Sigma) + I^*$,	7.8×10^{-11}
$O_2(^1\Delta) + I \rightarrow O_2(^3\Sigma) + I$,	1.0×10^{-15}
$O_2(^1\Delta) + H_2O \rightarrow O_2(^3\Sigma) + H_2O$,	4.0×10^{-18}
$O_2(^1\Delta) + I^* \rightarrow O_2(^1\Sigma) + I$,	1.0×10^{-13}
$O_2(^1\Delta) + wall \rightarrow O_2(^3\Sigma) + wall$,	2.0×10^{-5}
$O_2(^3\Sigma) + I^* \rightarrow O_2(^1\Delta) + I$,	$1.028 \times 10^{-10}*exp(-401.4/T)$
$O_2(^3\Sigma) + I^* \rightarrow O_2(^3\Sigma) + I$,	3.5×10^{-16}
$O_2(^3\Sigma) + I_2^* \rightarrow O_2(^3\Sigma) + I_2$,	5.0×10^{-11}
$I_2 + I^* \rightarrow I_2^* + I$,	3.5×10^{-11}
$I_2^* + He \rightarrow I_2 + He$,	4.0×10^{-12}
$I_2^* + H_2O \rightarrow I_2 + H_2O$,	3.0×10^{-10}
$I_2 + I^* \rightarrow I_2^* + I$,	3.5×10^{-11}
$Cl + I_2 \rightarrow I + ICl$,	2.0×10^{-10}

Overall

$n\, O_2(^1\Delta) + I_2 \rightarrow n\, O_2(^3\Sigma) + 2I$,	$n \sim 2$ to 5

Table 1.1: Limited Listing of Kinetic Processes with Rate Constants
in the COIL Device

structure now associated with the bound-free fluorescence of the *D-X* system.

Subsequent work revealed many intriguing phenomena, such as the changes from continuous to banded emission spectra upon the addition of inert gases, and the quenching of visible fluorescence from the *B* state by application of a magnetic field. This behavior has focused considerable interest resulting in an unusually large amount of detailed knowledge, both experimental and theoretical.

Mulliken[49] presented one of the more enlightened theoretical studies of molecular iodine and he correctly predicted the lowest excited electronic state. Using a basis of electronic configurations in which ten valence electrons were distributed among the four highest molecular orbitals $\sigma_g \pi_u \pi_g \sigma_u$, Mulliken accounted for the sub-Rydberg states of I_2. The violet color of I_2 arises as a result of the excitation of an electron from the highest occupied MO (antibonding π_g^* level) into the lowest unoccupied MO (antibonding σ_u^* level). The lower excited states may be arranged in three groups according to whether a state correlates at dissociation with two unexcited atoms ($5p^5$ ^2P_j) with $j=\frac{1}{2}$ or $\frac{3}{2}$, or one unexcited and one excited atom, I + I* (e.g. $5p^46s$) , or two oppositely charged ions, $I^+ + I^-$. Generally, members of these three groups are referred to as valence, Rydberg, or ion-pair states, respectively.[50] The *A'*, *A*, and *B* are the 2_u, 1_u, and 0^+_u spin orbit components of the $^3\Pi_u$ state. The ground state is assigned unambiguously to the $^1\Sigma_g^+ (0^+_g)$ state.

The ground state iodine atom has a $5p^5$ valence electron structure which gives rise to σ_g, π_u, π_g^*, and σ_u^* molecular orbitals (MO). Spin-orbit coupling splits the $5p^5$

configuration into $^2P_{3/2}$ and $^2P_{1/2}$ excited states. Both of these levels have the same orbital angular momentum and parity. According to the electronic-dipole selection rules, electronic-dipole transitions between the two groups are totally forbidden (but are magnetic-dipole allowed). In fact, the strength of the magnetic dipole transition is surprising since magnetic dipole transitions are normally 6-8 times weaker than the corresponding electronic-dipole transition.

Atomic nuclei are effected by the fields resulting from electronic motion and spin. There is a magnetic dipole interaction between the electron and the nucleus, and the magnetic dipole contributes to atomic iodine's nuclear spin ($I=^5/_2$). The nuclear alignment energy gives a very small (hyperfine) splitting to atomic energy levels. Figure 1.4 [note scale change on the energy axis] shows the atomic energy levels of iodine and the hyperfine splitting. Each of these levels have a Zeeman splittable degeneracy given by $g_F=2F+1$. The relatively small spacing of the $5^2P_{3/2}$ hyperfine levels allows rapid mixing whereas the $5^2P_{1/2}$ hyperfine levels are likely to be mixed only by other iodine atoms.[51] Laser action has been observed on four of the hyperfine components[52] for the transitions (in order of intensity) $3{\rightarrow}4 > 2{\rightarrow}2 > 3{\rightarrow}2 > 2{\rightarrow}3$. The gain of the $F=3{\rightarrow}F=4$ transition can be calculated assuming the population in each hyperfine level is distributed in accordance with its statistical weight.

$$[I(^2P_{1/2}, F=3)]=^7/_{12}\, \{[I(^2P_{1/2}, F=3)] + [I(^2P_{1/2}, F=2)]\}$$
$$N_2 = {}^7/_{12}\, I^2P_{1/2}$$
$$[I(^2P_{3/2}, F=4)]=^9/_{24}\, \{[I(^2P_{3/2})]\}$$
$$N_1 = {}^9/_{24}\, I^2P_{3/2}$$
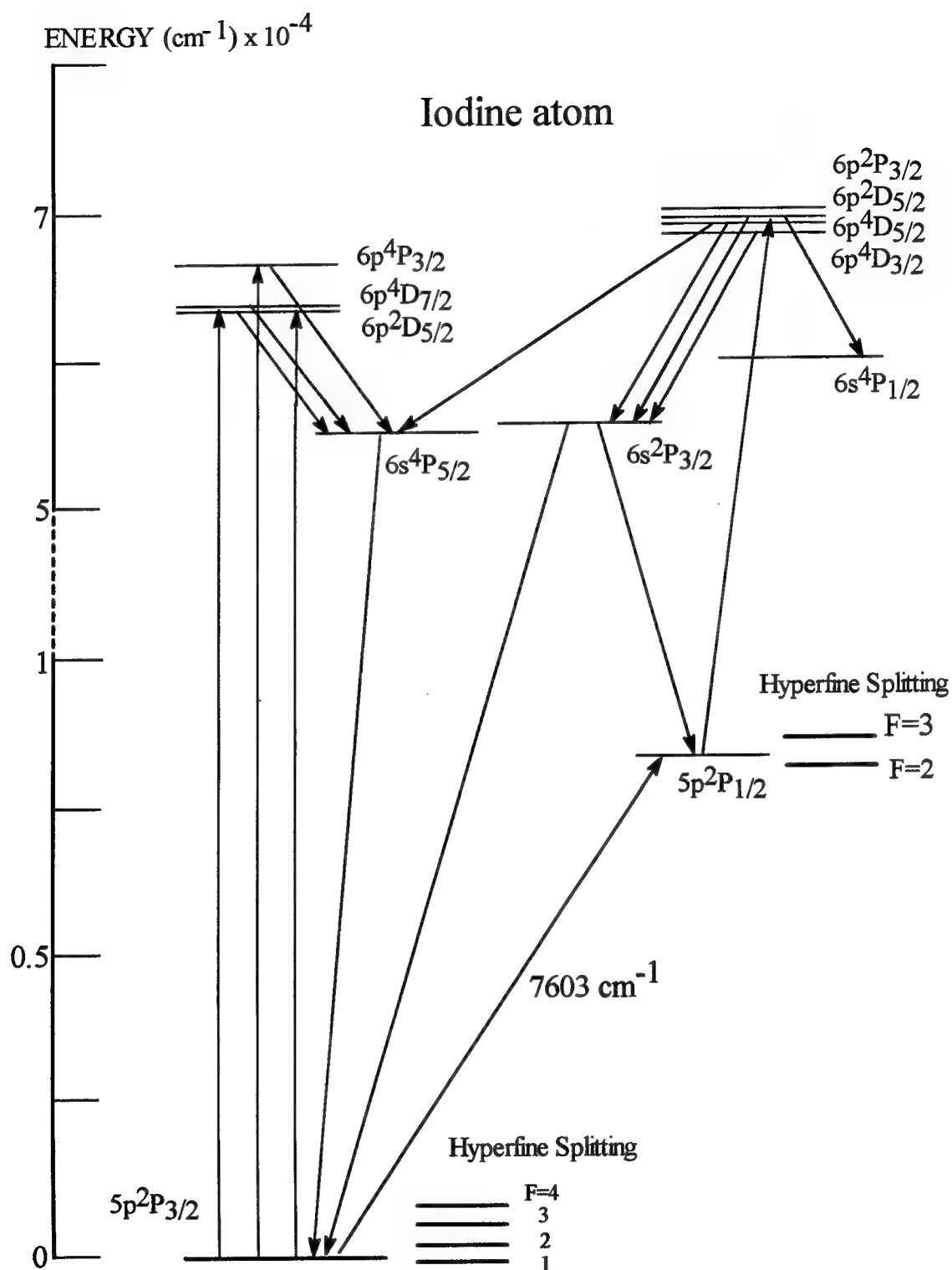
Figure 1.4: Atomic Iodine Energy Level Diagram

The small signal gain is

$$\gamma_0 = (A_{21})\frac{\lambda^2}{8\pi n^2}\left(\frac{7}{12}[I^2P_{1/2}] - \frac{7}{9}\frac{9}{24}[I^2P_{3/2}]\right)$$

evaluating[51]

$$\gamma_0 = 7.5 \times 10^{-18}([I^2P_{1/2}] - \frac{1}{2}[I^2P_{3/2}])$$

The small signal gain is not a strength of the COIL device. But gain and power output have been scaled substantially since the first demonstration at the Air Force Weapons Laboratory. Small signal gain of 1.2% cm^{-1} has been demonstrated in a supersonic device. The unsaturated gain coefficient previously described is the gain coefficient which is measured with a low intensity probe beam passing through the laser cavity without mirrors. The actual gain coefficient measuring during laser operation is less than the unsaturated gain coefficient. This is a result of the rate of stimulated emission which depletes the excited atoms until balanced by the gain saturation.

While the gain is small, the device has a high efficiency. The efficiency of a laser is determined by taking the ratio of the output power to the input pumping power. In fact, a COIL with a maximum chemical efficiency approaching 40% [comparable with the operating costs of a commercial Nd:YAG laser system] was demonstrated by K.Shimizu, T. Sawano, T. Tokuda, S. Yoshida and I. Tanaka.[53]

§1.4 REFERENCES

1. K. Bergmann and W. Demtroder, *Z. Phys.* **243**, 1 (1971); and *J. Phys. B* **5**, 1386, 2098 (1972).

2. R. B. Kurzel, J. I. Steinfeld, D. A. Hatzenbuhler, and G. E. Leroi, *J. Chem. Phys.* **55**, 4822 (1971).

3. For a concise summary see, A. Jorg, Ulrich Meier, and K. Kohse-Hoinghaus, *J. Chem. Phys.* **93**, 6453 (1990).

4. T. A. Brunner, R. D. Driver, N. Smith, and D. E. Pritchard, *Phys. Rev. Lett.* **41**, 856 (1978).

5. Ch. Ottinger and M. Schroder, *J. Phys. B* **13**, 4163 (1980).

6. J. Dufayard and O. Nedelec, *Chem. Phys.* **71**, 279 (1982).

7. M. Giroud and O. Nedelec, *J. Chem. Phys.* **77**, 3998 (1982).

8. O. Nedelec and J. Dufayard, *Chem. Phys.* **84**, 167 (1984).

9. M. Ferray, J. P. Visticot, and B. Saver, *J. Chem. Phys.* **81**, 3009 (1984).

10. C. Dufour, B. Pinchemel, M. Douary, J. Schamps, and M. H. Alexander, *Chem. Phys.* **98**, 315 (1985).

11. S. J. Davis and K. W. Holtzclaw, *J. Chem. Phys.* **92**, 1661 (1990).

12. J. J. Hinchen, *Appl. Phys. Lett.* **27**, 672 (1975).

13. R. A. Copeland, D. J. Pearson, F. F. Crim, *Chem. Phys. Lett.* **81**, 541 (1981).

14. A. S. Sudbo and M. M. T. Loy, *Chem. Phys. Lett.* **82**, 135 (1981).

15. W. Meier, G. Ahlers, and H. Zacharias, *J. Chem. Phys.* **85**, 2599 (1986).

16. R. L. Farrow and D. W. Chandler, *J. Chem. Phys.* **89**, 1994 (1988).

17. D. W. Chandler and R. L. Farrow, *J. Chem. Phys.* **85**, 810 (1986).

18. F. Menard-Bourcin, T. Delaporte, and J. Menard, *J. Chem. Phys.* **84**, 210 (1986).

19. G. O. Sitz and R. L. Farrow, *J. Chem. Phys.* **93**, 7883 (1990).

20. R. Fei, H. M. Lambert, T. Carrington, S.V. Filseth, C. M. Sadowski, and C. H. Dugan, *J. Chem. Phys.* **100**, 1190 (1994).

21. A. V. Smith and A. W. Johnson, *Chem. Phys. Lett.* **93**, 608 (1982).

22. B. K. Clark and I. M. Littlewood, *Opt. Commun.* **62**, 91 (1987).

23. J. Wu, R. Huang, M. Gong, A. Saury, and E. Carrasquillo M., *J. Chem. Phys.* **99**, 6474 (1993).

24. J. D. Tobiason, A. L. Utz, and F. F. Crim, *J. Chem. Phys.* **97**, 7437 (1992).

25. F. Temps, S. Halle, P. H. Vaccaro, R. W. Field, J. L. Kinsey, *J. Chem. Phys.* **87**, 1895 (1987).

26. T. Seelemann, P. Andresen, E. W. Roth, *Chem. Phys. Lett.* **146**, 89 (1988).

27. X. Yang and A. M. Wodtke, *J. Chem. Phys.* **96**, 5123 (1992).

28. X. Yang, J. M. Price, J. A. Mack, C. G. Morgan, C. A. Rogaski, D. McGuire, E. H. Kim, and A. M. Wodtke, *J. Phys. Chem.* **97**, 3944 (1993).

29. S. J. Arnold, N. Finlayson, and E. A. Ogryzlo, *J. Chem. Phys.* **44**, 2529 (1966).

30. R. G. Derwent and B. A. Thrust, *J. Chem. Soc. Faraday II* **68**, 720 (1972).

31. R. G. Derwent, D. R. Kearns, and B. A. Thrush, *Chem. Phys. Lett.* **6**, 115 (1970).

32. R. G. Derwent and B. A. Thrust, *Trans. Faraday Soc.* **67**, 2036 (1971).

33. R. G. Derwent and B. A. Thrust, *Discuss. Faraday Soc.* **53**, 162 (1972).

34. R. G. Derwent and B. A. Thrust, *Chem. Phys. Lett.* **9**, 591 (1971).

35. W. E. McDermott, N. R. Pchelkin, D. J. Benard, and R. R. Bousek, *Appl. Phys. Lett.* **34**, 40 (1978).

36. K. A. Truesdell and S. E. Lamberson, *SPIE Gas Flow and Chemical Lasers* **1810**, 476 (1992).

37. R. G. Aviles, D. R. Muller, and P. L. Houston, *Appl. Phys. Lett.* **37**, 358 (1980).

38. D. F. Muller, R. H. Young. P. L. Houston, and J. R. Wiesenfeld, *Appl. Phys. Lett.* **38**, 404 (1981).

39. J. Tellinghuisen, *J. Mol. Spectrosc.* **94**, 231 (1982).

40. R. F. Heidner III, C. E. Gardner, G. I. Segal, and T. M. El-Sayed, *J. Phys. Chem.* **87**, 2348 (1983).

41. M. L. Nowlin and M. C. Heaven, *J. Chem. Phys.* **99**, 5654 (1993).

42. G. E. Hall, W. J. Marinelli, and P. L. Houston, *J. Phys. Chem.* **87**, 2153 (1983).

43. D. David, V. Joly, and A. Fausse, *Proceedings of the 7th International Symposium on Gas Flow and Chemical Lasers*, Springer Proceedings in Physics (Springer, Berlin, 1987), p.156.

44. M. H. van Benthem and S. J. Davis, *J. Phys. Chem.* **90**, 902 (1986).

45. A. J. Bouvier, R. Bacis, A Bouvier, D. Cerny, S. Churassy, P. Crozet, and M. Nota, *J. Quant. Spectrosc. Radiat. Transfer* **49**, 311 (1992).

46. G. P. Perram and G. D. Hager, *The Standard Chemical Oxygen-Iodine Laser Kinetics Package*, AFWL-TR-88-50, Phillips Laboratory, NM (1989).

47. J. Franck and R. W. Wood, *Philos. Mag.* **21**, 314 (1911).

48. J. C. McLennan, *Proc. Roy. Soc. (London)* **A88**, 289 (1913); **A91**, 23 (1914).

49. R. S. Mulliken, *J. Chem. Phys.* **55**, 288 (1971).

50. J. C. D. Brand and A. R. Hoy, *Applied Spectroscopy Reviews* **23**, 285 (1987).

51. R.F. Shea, *Overview of the Singlet Oxygen-Iodine Laser System*, AFWL 84-355, Phillips Laboratory, NM (1984).

52. *Handbook of Laser Science and Technology*, CRC Press

53. K.Shimizu, T. Sawano, T. Tokuda, S. Yoshida and I. Tanaka, *J. Appl. Phys.* **69**, 79 (1991).

CHAPTER 2

THEORETICAL BACKGROUND

Studies of the inelastic collision dynamics of $I_2 B^3\Pi(0_u^+)$ have had a long and distinguished history[1-9]. Much of the attention paid to $I_2(B)$ derives from the relative ease with which individual rovibrational levels of the B state may be excited and detected. As a consequence of this experimental accessibility, collisional energy transfer data for $I_2(B)$ have been widely used in the development and evaluation of theoretical models of inelastic collisions[1-4]. For the most part, these theories have assumed the usual Born-Oppenheimer separation of the electronic and nuclear motions. Models of rotational and vibrational energy transfer have not considered the influence of electronic state mixings induced by interactions with the collision partners. However, it is well known that quenching of $I_2(B)$ is caused by collision-induced mixing of the B state with the nearby repulsive electronic states[8,9]. Such mixings have also been considered in recent discussions of the dynamics of $I_2(B)$-Ar van der Waals complexes[10-12]. Electronically nonadiabatic channels may cause significant deviations from the inelastic collision dynamics predicted using adiabatic models. In vibrational energy transfer, nonadiabatic processes may enhance the cross sections for single- and multiquantum transfer events. Burke and Klemperer[12] have suggested that the probabilities for collision-induced predissociation of $I_2 (B)$ may be dependent on the orientation of the collision partners. Should this be the case, the cross sections for angular momentum

changing collisions would be influenced by the competition between quenching and momentum exchange. These considerations imply that $I_2(B)$ may not be the best prototype for testing adiabatic models of energy transfer.

As there is a substantial energy separation between $I_2(X)$ and the first electronically excited state $[A'\ ^3\Pi(2_u)$ at 10042 cm$^{-1}]$[13], the ground state energy transfer dynamics will not be significantly influenced by electronic state mixings. Hence, energy transfer data for $I_2(X)$ are more suitable for evaluating adiabatic models than those for $I_2(B)$. Furthermore, it is conceivable that comparisons of the results for $I_2(X)$ and $I_2(B)$ can be used to identify nonadiabatic effects in the latter. Interpretations of these comparisons will be the most easily reached when the intermolecular potential energy surfaces are similar for $I_2(X)+M$ and $I_2(B)+M$. There is evidence from spectroscopic studies of the binary van der Waals complexes[14] that this condition is satisfied for M=He and Ar, and it may well hold for several other inert collision partners. From a practical standpoint, the ground state energy transfer dynamics are of relevance to the kinetics of I_2 dissociation and recombination. They also determine the performance characteristics of optically[15] and chemically[16,17] pumped iodine lasers.

This chapter will provide basic theoretical background useful for the discussions in this dissertation. Section §2.1 will briefly discuss spectroscopy while Section §2.2 considers thermal and nonradiative distributions. Section §2.3 gives an overview of scaling and fitting laws for rotationally inelastic collisions.

§2.1 SPECTROSCOPY

The angular momentum of a diatomic molecule is specified by the quantum number, J. Electronic transitions of diatomic molecules are almost always accompanied by changes in the vibrational and rotational eigenstates, giving rise to a dense rovibrational structure. A rovibrational manifold consists of a series of vibrational levels v, for which the energy difference (ΔE) decreases slightly between successive levels, and a series of rotational levels J, whose energy differences (ΔE) increase linearly with each level. The wavelength of the spectral line corresponds to the energy required for the transition. Section §2.1.1 will discuss the rotational structure and distribution. Section §2.1.2 will present vibrational distribution and Section §2.1.3 will discuss some aspects of electronic transitions. A traditional presentation of spectroscopic constants and sample calculations are included in Appendix A.

§2.1.1 ROTATIONAL TRANSITIONS

Since iodine is a homonuclear diatomic, it has no rotating dipole with which to interact with the electric field of the radiation. Therefore, no energy can be exchanged between the molecule and the radiation, and no pure rotational structure is observed. But when accompanied by an electronic transition, iodine panoplies a dense rotational structure. Molecular iodine belongs to Hund's coupling case (c). In case (c), the spin-orbit coupling is so strong that the spin and orbital momenta couple strongly at every opportunity. The rotational levels are quantized with discrete energies expressed

by E(J)=BJ(J+1), where B is the rotational constant, and J is the Jth rotational level. The

rotational fine structure is designated by the following

P Branch $\Delta J = -1$ $J_{upper} = J_{lower} - 1$

Q Branch $\Delta J = 0$ $J_{upper} = J_{lower}$

R Branch $\Delta J = 1$ $J_{upper} = J_{lower} + 1$

For the I_2 electronic states $X(0^+_g)$, $B(0^+_u)$, and $D(0^+_u)$ utilized in this dissertation, the

Q-branch transition is forbidden since it occurs only in states with nonzero orbital

angular momentum along the molecular axis as restricted by the selection rule $\Delta J \neq 0$ for

$\Omega=0 \rightarrow \Omega=0$ transitions. All spectra display a red-shaded (§2.1.3) progression of P-R

doublets.

The rotational structure of a given v', v'' transition can be represented by a single

formula using the rotational energies. The representation of the formula is known as a

Fortrat diagram[18] and is given by

$$v = v_0 + (B'_v + B''_v)m + (B'_v - B''_v)m^2$$

where $m = J+1$ [R-branch]

         $m = -J$ [P-branch]

         $v_0 =$ bandhead

A second-order polynomial fit generates both the bandhead as well as the ground and

excited state rotational constants. The vertex of the polynomial representation

corresponds to the bandhead, v_0. The rotational constants can be determined by

$B_v'' = (X+Y)/2$ and $B_v' = (X-Y)/2$ where $X = (B'_v + B''_v)$ and $Y = (B'_v - B''_v)$. An example of a

Fortrat diagram is seen in Figure 2.1.
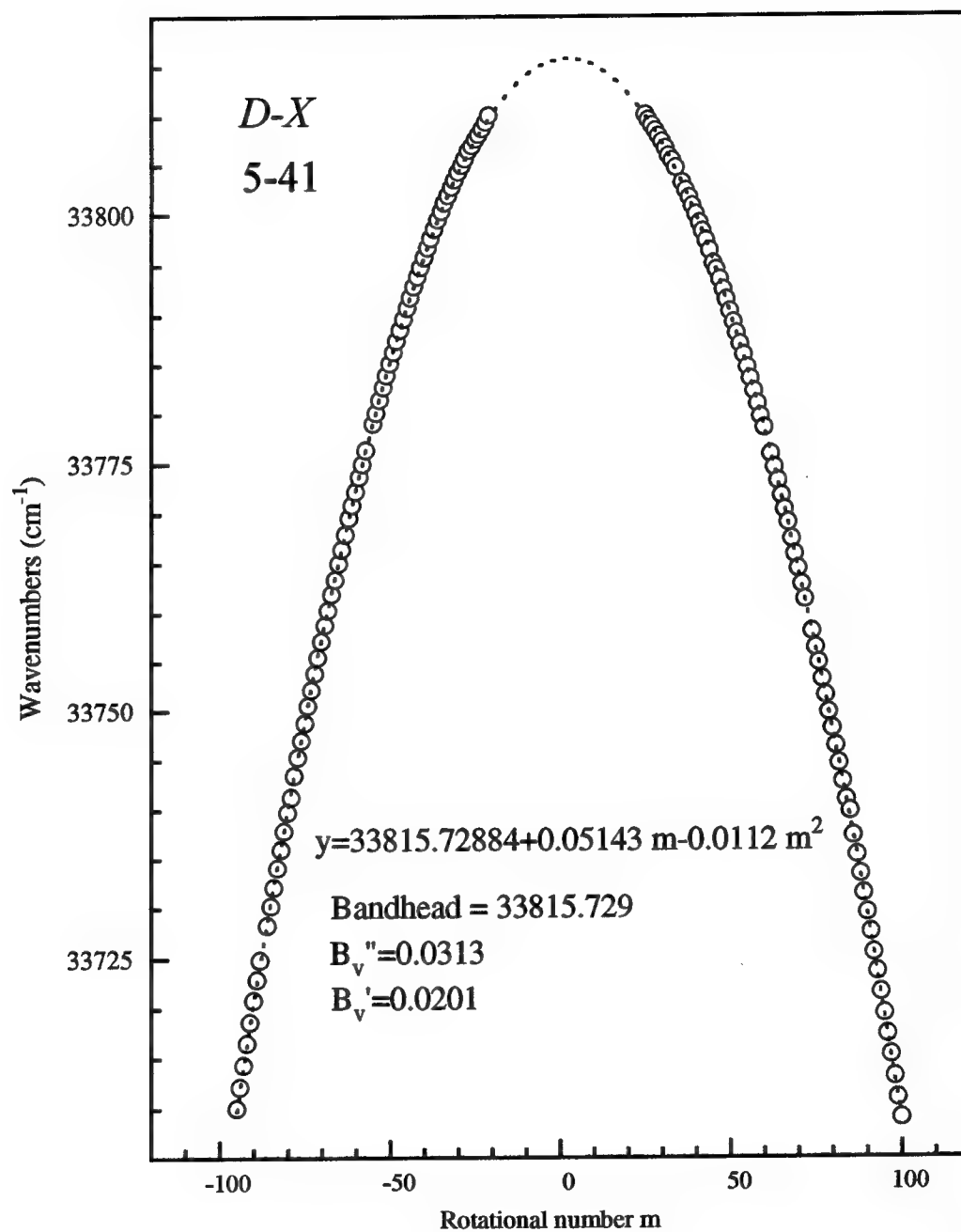
Figure 2.1: Fortrat Diagram of I_2 (D,v'=5←X,v"=41) with Second Order Polynomial Fit

The energy of a rotational level includes correction terms which account for the non-ideal behavior due to centrifugal distortion and anharmonicity. The truncated expansion of the rotational energy F_J, is given by

$$F_J = B_v J(J+1) - D_v J^2(J+1)^2 + H_v J^3(J+1)^3$$

where B_v is the rotational constant, D_v is the centrifugal distortion constant and H_v is the anharmonicity constant.

§2.1.2 VIBRATIONAL TRANSITIONS

A diatomic molecules will vibrate along its internuclear axis with a frequency commensurate with its mass and force constant. The heavier the atom, the smaller the vibrational frequency. For example, iodine has a vibrational frequency of 6.4×10^{12} Hz (214 cm^{-1}) while hydrogen vibrates at 1.3×10^{14} Hz (4395 cm^{-1}). No pure vibration-rotation transitions are observed for homonuclear diatomics between rotational states of adjacent vibrational manifolds since no amount of stretching between two identical molecules can form an electric dipole. Vibration-rotation transitions are observed when accompanied by an allowed electronic transition. The energy of a vibrational level using the anharmonic oscillator model is given by a Taylor series expansion of a Hermite polynomial

$$G(v) = \omega_e(v+\tfrac{1}{2}) - \omega_e \chi_e (v+\tfrac{1}{2})^2 + \omega_e y_e (v+\tfrac{1}{2})^3 + \ldots$$

When a vibronic transition occurs, it is usually accompanied by rotational transitions. The energies of these transitions are given by Dunham expansion coefficients discussed in Section §2.1.3 and Appendix A.

§2.1.3 ELECTRONIC TRANSITIONS

Radiation of sufficient energy to cause electronic transitions will simultaneously effect vibrational and rotational transitions. The most probable transition between vibrational levels of different electronic states is determined by the Franck-Condon principal and is discussed in Appendix B. The Franck-Condon principal states that the vibrational transition is most probable for the vibrational state whose turning point is vertically above or below the state from which the transition initiated (except for the ground vibrational state). The vertical path is the most likely because the electronic transition is so fast in comparison to the nuclear motion, that the position and momentum of the nuclei is essentially unchanged.

The shading of the bands of an electronic transition provides an indication of the relative positions of the potential energy curves of the two electronic states involved. If $B''_e > B'_e$ and $R'_e > R''_e$, the transitions progress to lower frequencies and the band is red-shaded. Likewise, if $B'_e > B''_e$, the transitions progress to higher frequencies and the band is blue-shaded. For the D-X system, $B''_v > B'_v$ and red-shaded progressions are observed. The bandhead of a red-shaded progression is formed by the R-branch. The
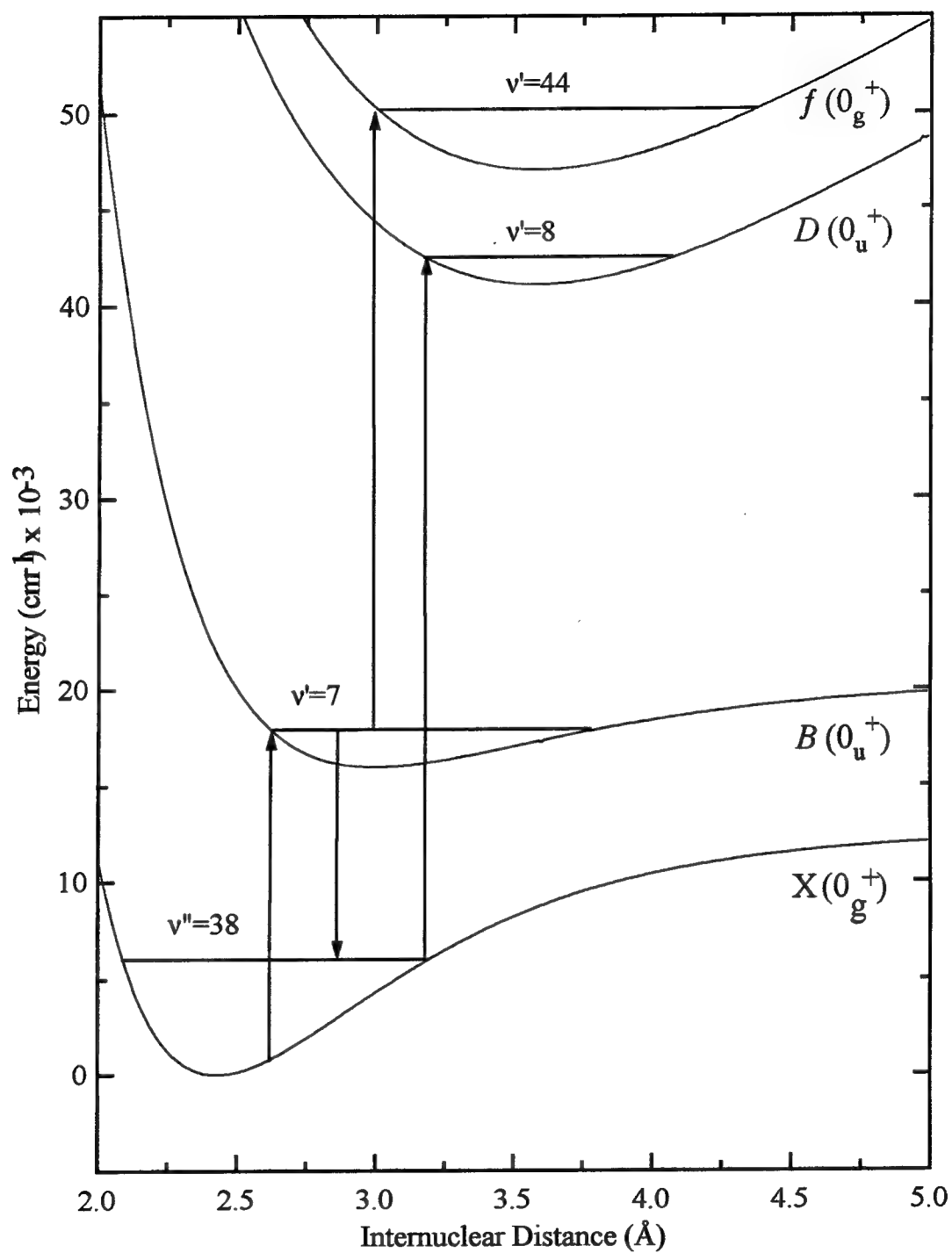
Figure 2.2: Iodine Potential Energy Diagram Showing SEP (v"=38) and OODR Transitions

electronic states used in selectively preparing $v''=38$ are illustrated in Figure 2.2 and show both SEP and OODR transitions.

The total energy E_{vJ}, of a diatomic molecule can be partitioned according to its electronic (T_e), vibrational (G_v) and rotational (F_J) energies where

$$E_{vJ} = T_e + G_v + F_J$$

Another parametrical form in which the total energy can be expressed in known as the Dunham expansion[19] and is given by

$$E_{vJ} = \sum_{k,n} Y_{nk}(v + \tfrac{1}{2})^n[J(J+1)]^k$$

where Y_{nk} are the Dunham coefficients. Definitions of the Y_{nk} terms can be found in Appendix A.

§2.2 ROTATIONAL AND VIBRATIONAL POPULATION DISTRIBUTIONS

Generally, the selection rules for radiative transitions do not hold for non-radiative transitions. Non-radiative transitions are defined as transitions in which the change of the quantum state is not accompanied by emission of radiation. For non-radiative transitions induced by collisions, only alternating J values ($J_i \rightarrow J_{i+2n}$) will be populated due to the symmetry selection rule $\Delta J = \pm 2n$. Molecular collisions cause nonradiative transitions to the other vibration-rotation levels at the expense of translational kinetic energy , thereby populating the levels in accord with the Boltzmann distribution law.
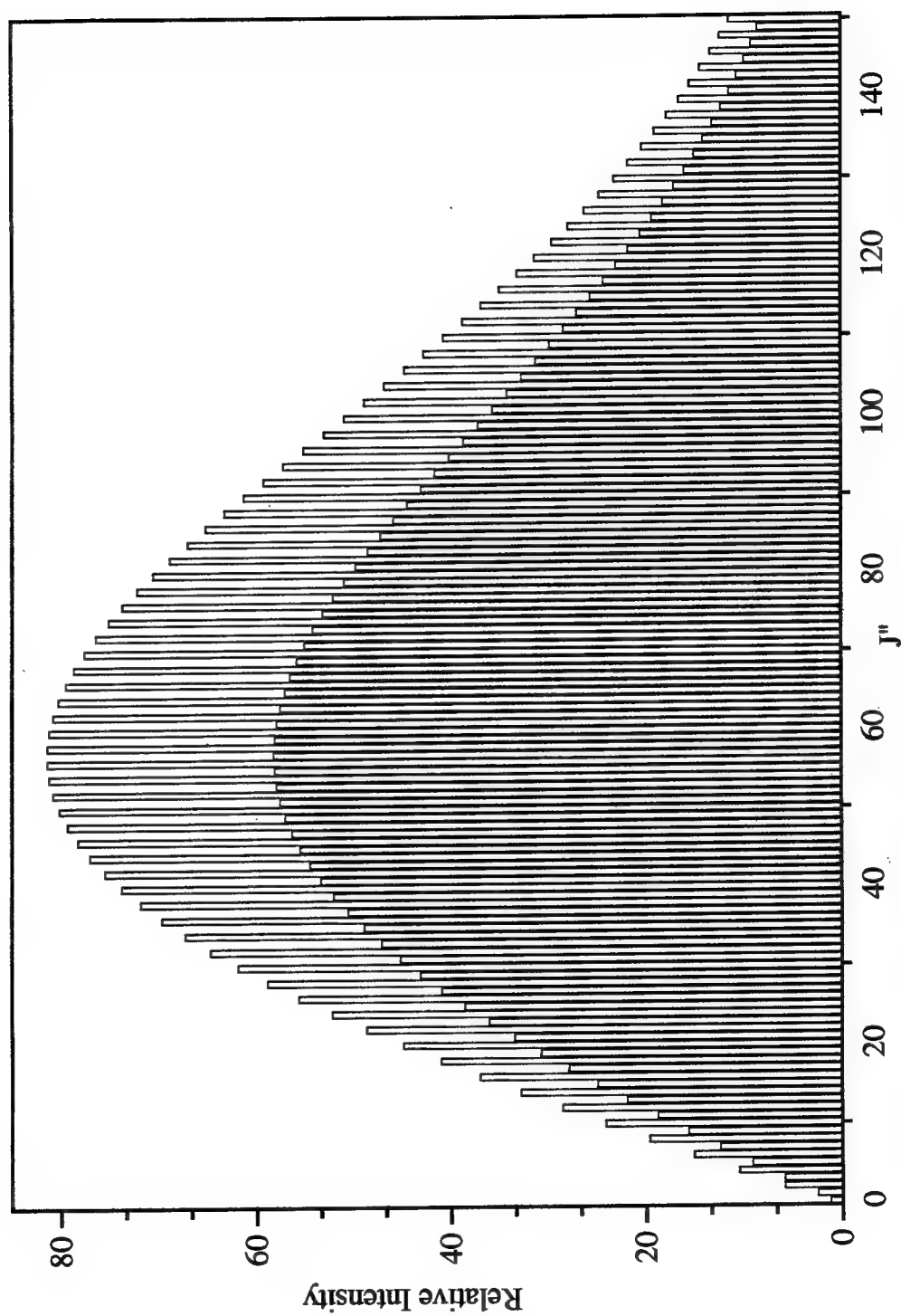
Figure 2.3: I$_2$ (X) Rotational Population Distribution at 300°K

Collisions between molecules establish a thermal population of the rotational states. The rotational population distribution is shown in Figure 2.3. The rotational manifold is extensively populated for two reasons. First, the energy spacings are much smaller than the vibrational spacings. Second, the Jth rotational level is (2J+1)-fold degenerate. The population in a rotational state J of vibrational manifold v is dictated by Boltzmann statistics according to

$$\frac{n_J}{n_0} = \frac{(2J+1)e^{\frac{-BJ(J+1)}{kT}}}{(2J_0+1)^{\frac{-BJ_0(J_0+1)}{kT}}} = \frac{(2J+1)e^{\frac{-BJ(J+1)}{kT}}}{Q_r}$$

where B is the rotational constant, Q_r is the partition function. As seen in Figure 2.3, the distribution will increase to a maximum, J_{max}, with $J_{max} = 0.5896[T(^{\circ}K)/B(cm^{-1})]^{1/2} - 1/2$. The alternation of intensities of the rotational lines is a result of the nuclear spin, and is discussed in Section §4.3.

Collisions between molecules establish a thermal population of the vibrational states as well. The vibrational population distribution at room temperature is given in Figure 2.4. The distribution for the vibrational levels v, in thermal equilibrium is given by

$$\frac{n_v}{n_0} = \frac{e^{\frac{-(v+\frac{1}{2})h\omega}{kT}}}{e^{\frac{-\frac{1}{2}h\omega}{kT}}} = \frac{e^{\frac{-vh\omega}{kT}}}{Q_v}$$

Approximately ninety-five percent of the population for $I_2(X)$ is distributed between the three lowest energy levels.
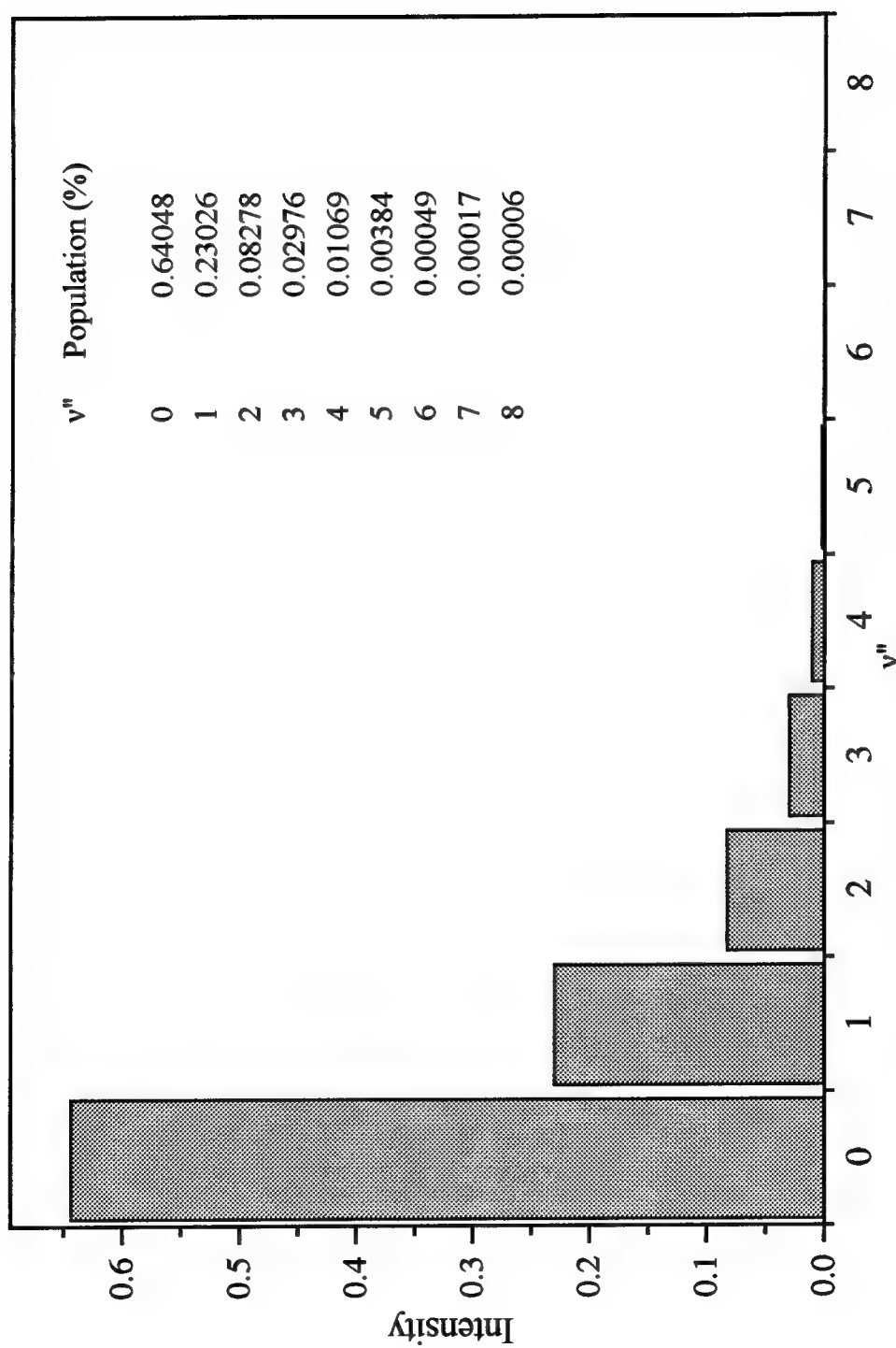
Figure 2.4: $I_2 X(^1\Sigma_g^+)$ Vibrational Population Distribution at 300°K

v"	Population (%)
0	0.64048
1	0.23026
2	0.08278
3	0.02976
4	0.01069
5	0.00384
6	0.00049
7	0.00017
8	0.00006

§2.3 ROTATIONALLY INELASTIC (RI) COLLISIONS

Nonreactive collisions are classified as either elastic collisions, where the particles interact with each other but only their directions of motion change, or as inelastic collisions, where both the motion and the internal energies of the particles change. Like elastic collisions, energy transfer collisions of the inelastic kind preserve the chemical identity of the colliding species. The inelastic collision processes involving vibration and rotation are of great importance in understanding the kinetics of gas-phase chemical reactions and energy transfer. Of all the fundamental inelastic molecular processes, rotationally inelastic collisions are the most likely. Collisional energy transfer processes[20] are often expressed by a collision cross section σ^2. The cross section is an effective area associated with colliding particles. Rotational energy transfer cross sections are typically 10^{-16} to 10^{-15} cm^2, and are one to two orders of magnitude higher than either vibrational or electronic energy transfer. The rotational energy transfer process for a diatomic is given by

$$X_2(v,j_i) + M \rightarrow X_2(v,j_f=j_i+\Delta j) + M + \Delta E$$
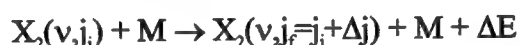
where ΔE is the amount of energy transferred from rotation to translation. Figure 2.5 illustrates the classical trajectory of an impulsive collision between an atom and a rigid rotor. In diagram of the classical trajectory, $\mathbf{r}$ is the vector from the origin to the instantaneous position of the particle, $\mathbf{p}$ is the linear momentum, $\mathbf{l}$ is the orbital angular momentum (where $\mathbf{l}=\mathbf{r}\times\mathbf{p}$), and $\mathbf{j}$ is the rotor angular momentum. As a collision partner increases in mass, more of the orbital angular momentum of the collision will be made
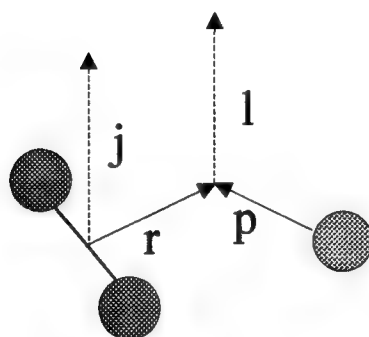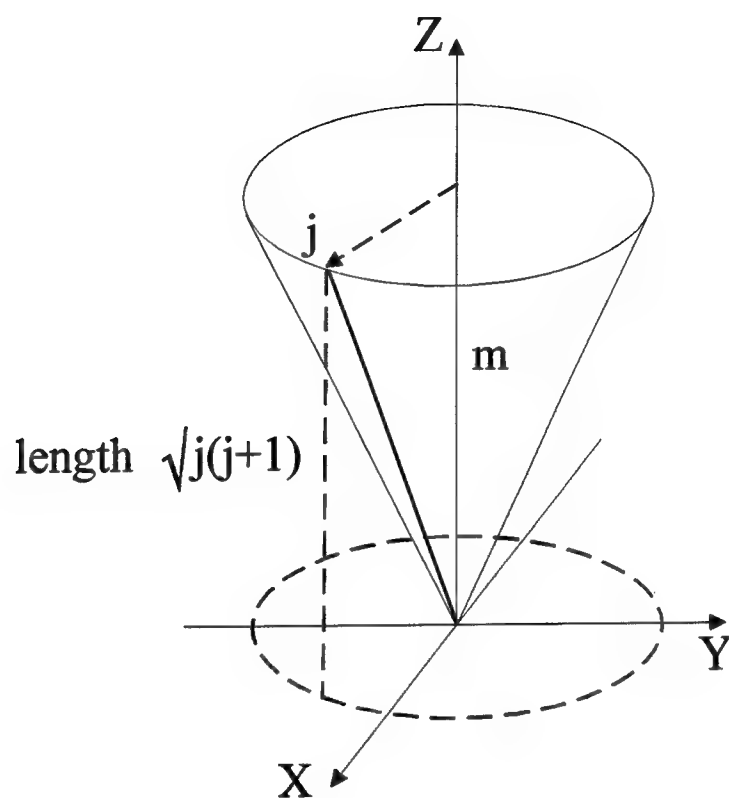
Figure 2.5: Illustration of the classical trajectory

available to the rotational angular momentum of the molecule. Light collision partners like hydrogen and helium exhibit a high degree of persistence of the initial rotational state, while the transfer efficiencies of heavy collision partners vary with the square root of the reduced mass of the collision pair.[7,21]

The efficiency of vibrational energy transfer in diatomic molecules depends to a large extent on the relative energy gap between vibrational levels and the translational energy of the bath gas. Dynamic effects which determine the outcome of a collision between a diatom and an atomic collision partner are revealed by a time dependent perturbation treatment of the harmonic oscillator problem.[22] For vibrational energy transfer, a simple physical interpretation is given by Ehrenfest's Adiabatic Principle. For a changing force acting on a quantized periodic motion, the process will be: adiabatic (no energy transfer) if the change of force is small during a period of motion; or non-adiabatic (efficient energy transfer) if a change of force is large during the period of motion. The adiabaticity parameter, which is applicable for rotational energy transfer as well, provides a criterion for which the adiabatic or non-adiabatic nature of a collision may be estimated

$$\xi = \frac{\tau_c}{t_v} = l_c v \left(\frac{\pi\mu}{8kT}\right)^{\frac{1}{2}}$$

where τ_c is the duration of the collision, t_v is the period of the oscillation, l_c is the mean interaction distance and v is the vibrational frequency. Large values of ξ correspond to adiabatic collisions. Qualitatively, energy transfer is favored for collision partners with small mass, low vibrational frequency, and a steep intermolecular potential. Both the

classical Landau and Teller, and the quantum mechanical Schwartz, Slawsky and Hertzfeld (SSH) theories[23] encompass the adiabatic principle[21].

Non-adiabatic energy transfer processes are state-to-state events in which no net chemical change occurs, but energy is exchanged among vibrational, rotational and translational degrees of freedom. In a chemical laser, energy transfer competes with radiative decay. Therefore, understanding the collisional energy transfer processes is essential for laser optimization. Table 2.1 lists some common energy transfer processes. Relative insight on the magnitude of the rate constants for energy transfer processes may be gained from the frequencies of the natural periods of motion. For example, within the framework of the adiabatic approximation, the translational motion is considered slow in comparison to the internal motion. Representative frequencies of these natural periods are

$$
\begin{array}{lll}
\text{radiative period} & \tau=10^{-16}\ \text{s} \\
\text{vibrational period} & \tau=10^{-14}\ \text{s} \\
\text{rotational period} & \tau=10^{-12}\ \text{s}
\end{array}
$$

With a typical average molecular velocity of $10^5\ ^{cm}/_s$, a molecule can travel about 10 Å in a picosecond or one rotational period. Ten Å is the outer limit for long-range interactions. Short-range interactions occur within 1 Å and the collision is considered irrotational. Consider that during each rotation, the average molecule will vibrate 100 times. But in comparison, rotational energy spacings are much smaller, so R-R and R-T energy transfer are very efficient. Typical relaxation times for rotation-translation (RT)

Table 2.1: Electronic, Vibrational and Rotational Energy Transfer Processes

	Collisional process
$X^* \rightarrow X + h\nu$	radiative decay[a]
$X^* \rightarrow X^{\dagger}$	non-radiative decay
$X^* + M^b \rightarrow X + M$	collisional quenching
$N_2\,(v{=}1) + CO_2\,(000) \rightarrow N_2\,(v{-}1) + CO_2\,(001)$	V-V (10^{-8})[c]
$X_2\,(v{=}1) + X_2\,(J{=}1) \rightarrow X_2\,(v{=}0) + X_2\,(J{=}7)$	V-R (10^{-6})[c]
$X_2\,(v{=}1) + M \rightarrow X_2\,(v{=}0) + M$	V-T (10^{-4})[c]
$X_2\,(J{=}1) + X_2\,(J{=}1) \rightarrow X_2\,(J{=}2) + X_2\,(J{=}0)$	R-R (10^{-10})[c]
$X_2\,(J{=}1) + M \rightarrow X_2\,(J{=}0) + M$	R-T (10^{-8})[c]

[a] Radiative lifetime is the decay process that occurs in the absence of all collisions where $\dfrac{1}{\tau_r} = \sum\limits_{n<j} A_{jn}$

[b] M is non-reacting collision species e.g. Ar, He, N_2

[c] Typical relaxation time $p\tau$ (atm sec)

transfer is on the order of 10^{-8} while vibration-translation (VT) energy transfer is on the order of 10^{-4} atm sec. A rate coefficient can also be expressed as an effective cross section by

$$k=v\sigma$$

where v is the mean thermal velocity and σ has units of cm^2 molecule^{-1}.

Experimental spectra of the state-to-state energy transfer events exhibit a pattern of modulating intensity which is characteristic of the molecule, the states involved, and the collision partner. From an analysis of the spectra, an array of state-to-state rotational energy transfer rates for $J_i \rightarrow J_f$ can be determined and parametrically fitted with constants. This process can be repeated for all values of $J_i \rightarrow J_f$, and the resulting rates can be represented as a matrix of rate constants for the initial and final states.

The two distinct classes of simplified representations of a matrix which enable the prediction of rotationally inelastic rate constants from some basis are known as either fitting or scaling laws. In a scaling theoretic approach, an *a priori* (deductive) equation relates one row from the rate matrix of cross sections to the entire matrix. These dynamically based angular momentum scaling laws express rate constants in terms of a subset of the matrix, typically one column or row (the basis rate constant). On the other hand, fitting laws are empirical expressions which parametrize the entire state-to-state array. Section §2.3.1 will discuss the angular momentum based scaling laws while Section §2.3.2 summarizes the energy-gap based fitting laws.

§2.3.1 SCALING LAWS

The S-matrix formalism was applied by A. DePristo, S. Augustin, R. Ramaswamy and H. Rabitz[24] to RT energy transfer by deriving a scaling relationship in which the coefficients were calculated by incorporating the internal energy level spacing and wavefunctions, and the kinetic energy. The application of classical S-matrix theory to an inelastic scattering problem involves three steps:[25] first, finding the critical paths which connect the initial and final state; second, evaluating the probability amplitude; and third superimposing the probability amplitudes to obtain S-matrix elements and then squaring to obtain transition probabilities.

The two angular momentum based scaling laws are the limited infinite order sudden[26] (IOS) and the energy corrected sudden[24] (ECS) models. The IOS model is based on the sudden approximation in scattering theory. The fundamental precept of the IOS approximation is that the rotationally inelastic collision is instantaneous and in the sudden limit, $\tau \rightarrow 0$, and the molecule does not rotate during collision (where τ is the reduced duration of a collision). This approximation requires the collision time τ_c, be much less than the rotational period τ_{rot}. The IOS rate constant is related to the basis rate constant by

$$k_{IOS} = (2j_f + 1)\exp\left\{\frac{E_{ji}-E_{j>}}{kT}\right\}\sum_l \begin{pmatrix} j_i & l & j_f \\ 0 & 0 & 0 \end{pmatrix}^2 (2l+1)k(l \rightarrow 0)$$

where $j_>$ is the larger of (j_i, j_f), $k(l \rightarrow 0) = a[l(l+1)]^{-\gamma}$, a is a parameter, T is the ambient translational temperature, and $(\cdots)$ is a 3-j symbol. The exponential factor ensures detailed balancing. The basis rates $k(l \rightarrow 0)$ are multiplied by the 3-j symbol to obtain rotational averaging. Rotational transfer is restricted to coplanar geometry (via the 3-j symbol) and indicates that an amount of angular momentum equal to the change in rotational angular momentum is simply added to that already present as though the molecule is non-rotating. In a sudden collision, all angular momenta are in a plane perpendicular to z which explains why all the m's in the 3-j symbols are zero[27]. The infinite order sudden approximation is valid for light, short range systems at high energy. At lower energies and/or heavy systems, energetic corrections become necessary.

The less restrictive and more realistic assumption of a collision with a finite rotation duration is given by the energy-corrected sudden[28,29] approximation. The rotation in radians of the diatom during the collision is known as the reduced duration

$$\tau_j = \omega_j x T_d$$

where ω_j=angular velocity of the molecule when it has angular momentum quantum number j and T_d is the duration of collision where $T_d = l_c/v$ which is the characteristic interaction length velocity of target atom relative to the molecule. The ECS model scaling law for a transition from an initial rotational state j_i to a final rotational state j_f may be expressed by:

$$k_{ECS} = (2j_f + 1) \exp\left\{\tfrac{E_{ji} - E_{j>}}{kT}\right\} \sum_l \begin{pmatrix} j_i & l & j_f \\ 0 & 0 & 0 \end{pmatrix}^2 (2l+1)[A_l^{j>}]^2 k(l \rightarrow 0)$$

where
$$A^{j>} = \frac{1+\frac{\tau^2}{6}}{1+\frac{\tau_>^2}{6}}$$

and $\tau_1 = 4\pi l_c cB(j+^1/_2)/v$. The parameter l_c is interpreted as the collision length, v is the mean velocity, and τ_1 is an effective collision time. The ECS approximation is by far the best scaling law for RI data (for Na_2^*-rare gas systems ECS introduced less than 5% error).

§2.3.2 FITTING LAWS

In contrast to the angular momentum based scaling laws, fitting laws[4,30-34] are statistical in nature (N_Δ) and based on the amount of energy transferred $[BJ(J+1)]$. Fitting laws are empirical expressions with freely adjustable parameters used in analyzing experimental data for rotationally inelastic collisions. There are three general forms of the energy based fitting laws: (1) exponential gap law (EGL), (2) statistical power gap (SPGL), and (3) hybrid statistical power-exponential gap (SPEG) laws. The exponential gap law is given by an exponential decay of the rate with respect to the amount of energy transferred in the collision. In fact, the EGL can be derived from the entropy maximization principal of information theory.

This method is known as the information theoretic approach and it has been applied for treating the final energy state distribution for rotational energy transfer. The information theoretic approach uses a comparison of the actual final state distribution $P(E_j)$ to a calculated *a priori* distribution $P^o(E_j)$, which is derived by assuming that all

quantum states at a total given energy are equally probable. The entropy deficiency, which is equal to the information content of the actual distribution is given by

$$\Delta S = R \ln (P^{\circ}(Ej)/P(E_j))$$

The comparison can also be expressed as a surprisal, which is a measure of the deviation between the probability of the final distribution from that of the *a priori* distribution:

$$I(E_j) = -\ln(P(E_j)/P^{\circ}(Ej))$$

where
$$P(E_j) = P^{\circ}(E_j)\exp[-I(E_j)].$$

The product $I(E_j)$ has been called the *surprisal* of the product state distribution. The usage of the label *surprisal* acquired a certain opprobrium, but was direct in the sense if you don't get what was expected, then by definition you are surprised[35].

First proposed by J. E. Polanyi and K. B. Woodall[36], the EGL appeared to be an accurate representation of the experimental data for HF. The EGL is given by

$$k^{EGL} = a \exp\text{-}(-\Theta|\Delta E|)R(\Delta E)(2J_f+1)$$

where a and Θ are fitting parameters and $R(\Delta E)$ is the ratio of the final to initial density of translational states. However, significant deviations were noted with this representation as more precise data became available.

An alternate formalism was proposed by D. E. Pritchard, N. Smith, R. D. Driver and T. A. Brunner[30] which scales the RT rates to a power gap law. The statistical power gap law is given by

$$k^{SPGL} = a \, |\Delta E/B_v|^{-\alpha} \cdot N_{\lambda}(J_i,J_f)(R(\Delta E,T))$$

where a, and α are fitting parameters, B_v is the rotational constant, N_λ is the factor that allows for a restriction on Δm during the collision, and $R(\Delta E, T)$ is the average ratio of final to initial density of translational states at temperature T. Interestingly, if maximum entropy is applied to ln (ΔE), the SPGL is obtained. However, there is no *a priori* justification for doing so.

The two major innovations of the SPGL are the assumption of a power law dependence on the energy defect and the flexible angular momentum factor as given[4] by

$N_\lambda(j_i, j_f) = [(2n_2+1)(2n_3+1) - \alpha(\alpha+1)]/2j_i+1$ where of the three numbers $\{j_i, j_f, \lambda\}$, $n_1 > n_2 > n_3$ and α is the greater of zero or $n_2 + n_3 - n_1$. This angular factor allows fitting from m-conserving N_0 ($\lambda=0$) to m-randomized N_Δ ($\lambda=\infty$) and in between with intermediate values of λ. In studies covering a wide range of diatomics, RT is invariably observed to occur with minimal reorientation of the **j** vector. Rotational transfer is accompanied by retention of the original orientation of the rotor[27].

In order to increase the flexibility and extend the applicability of the SPGL, a three-parameter hybrid scaling law has been proposed. The hybrid statistical power exponential gap (SPEG) scaling law has the form given by

$$k^{SPEG} = a\{(E_f - E_i)/B_0\}^{-\delta} \exp\{-\beta((E_f - E_i)/kT\}$$

where a, δ, and β are fitting parameters.

Comparison between various scaling laws is usually reported in terms of the goodness-of-fit statistic[37] chi-squared χ^2/ν, and given by

$$\frac{\chi^2}{\upsilon} = \frac{1}{\upsilon} \sum_{J_F=J_i} \frac{k_{exp}-k_{calc}}{\sigma_k^2}$$

where k_{exp} and k_{calc} are the experimental and calculated rate constants, respectively, σ_k is the error associated with the experimental datum, and ν is the number of independent degrees of freedom in the fit. When $\chi^2/\nu \approx 1$, the data is being fit on average to within the reported experimental deviation σ. A large χ^2/ν value indicates the expression used to describe the fit is an inadequate representation.

The principle of detailed balancing can be applied to reverse processes involving radiation, electron collisions, chemical reaction, nuclear reaction, or any combination. Generally, this principle is invoked to obtain unmeasured rates from measured rates. This principle states that the rate of transition from state m to state n is related to the rate of the reverse transition (n→m). For example, if the ratio for levels m=3 and n=4 has not been measured, but the ratio for $k(3,4)/k(3,2)$ is known. Then, the rate coefficients are related by[38]

$$\frac{k_{i \to f}}{k_{f \to i}} = \frac{g_f}{g_i} e^{-\frac{\Delta E}{kT}}$$

Even for a system not in thermal equilibrium, the rates of the isolated collision events obey the above relationship.

§2.4 REFERENCES

1. For a concise summary see D.J. Krajnovich, K.W. Butz, H. Du, and
    C.S. Parmenter, *J. Chem. Phys.* **91**, 7725 (1989).

2. J. I. Steinfeld, *J. Phys. Chem. Ref. Data* **13**, 445 (1984); **16**, 903 (1987).

3. S. L. Dexheimer, M. Durand, T. A. Brunner, and D. E. Pritchard, *J. Chem. Phys.* **76**, 4996 (1982).

4. T. A. Brunner and D. E. Pritchard, *Adv. Chem Phys.* **50**, 589 (1982).

5. J. Derouad and N. Sadeghi, *Chem. Phys. Lett.* **102**, 324 (1983).

6. J. Derouad and N. Sadeghi, *Chem. Phys.* **88**, 171 (1984).

7. J. I. Steinfeld and W. Klemperer, *J. Chem. Phys.* **42**, 3475 (1965).

8. R. L. Brown and W. Klemperer, *J. Chem. Phys.* **41** 3072 (1964).

9. K. Nakagawa, M. Kitamura, K. Suzuki, T. Kondow, T. Munakata, and T. Kasuya, *Chem. Phys.* **106**, 259 (1986).

10. J.A. Beswick, R. Monot, J. -M. Philippoz, and H. van den Berg, *J. Chem. Phys.* **86**, 3965 (1987).

11. M. L. Burke and W. Klemperer, *J. Chem. Phys.* **98**, 1797 (1993).

12. M. L. Burke and W. Klemperer, *J. Chem. Phys.* **98**, 6642 (1993).

13. J. Tellinghuisen, *J. Chem. Phys.* **78**, 2374 (1983).

14. D. H. Levy, *Adv. Phys. Chem.* **47**, 323 (1980), and references therein.

15. J. B. Koffend, F. J. Wodarczyk, R. Bacis, and R. W. Field, *J. Chem. Phys.* **72**, 478 (1980).

16. W. E. McDermott, N. R. Pchelkin, D. J. Benard, and R. R. Bousek, *Appl. Phys. Lett.* **32**, 469 (1978).

17. See, S, Churassy, R. Bacis, A. J. Bouvier, C. Pierre dit Mery, B. Erba, J. Bachar, and S. Rosenwaks, *J. Appl. Phys.* **62**, 31 (1987), and references therein.

18. W. A. Bingel, *Theory of Molecular Spectra*, Verlag Chemie, Berlin (1969).

19. C. H. Townes and A. L. Schwalow, *Microwave Spectroscopy*, McGraw-Hill, New York (1955).

20. J. D. Lambert, *Vibrational and Rotational Relaxation in Gases*, Clarendon Press, Oxford (1977).

21. P.J. Wolf and S. J. Davis, *J. Chem. Phys.* **87**, 3504 (1987).

22. R. D. Levine and R. B. Bernstein, *Molecular Reaction Dynamics*, Clarendon Press, Oxford (1974).

23. R. N. Schartz, Z. I. Slawsky, and K. F. Herzeld, *J. Chem. Phys.* **20**, 1591 (1952).

24. A. E. DePristo, S. T. Augustin, R. Ramaswamy, and H. Rabitz, *J. Chem. Phys.* **71**, 850 (1979).

25. D. J. Krajnovich, C. S. Parmenter, and D. L. Catlett Jr., *Chem. Rev.* **87**, 237 (1987).

26. R. Goldflam, S. Green, and D. J. Kouri, *J. Chem. Phys.* **67**, 4149 (1977).

27. A. J. McCaffery, Z. T. Alwahabi, M. A. Osborne, and C. J. Williams, *J. Chem. Phys.* **98**, 4586 (1993).

28. N. Smith and D. E. Pritchard, *J. Chem. Phys.* **74**, 3939 (1981).

29. T. A. Brunner, N. Smith, and D. E. Pritchard, *Chem. Phys. Lett.* **71**, 358 (1980).

30. D.E. Pritchard, N. Smith, R. D. Driver, and T. A. Brunner, *J. Chem. Phys.* **70**, 2115 (1979).

31. T. A. Brunner, R. D. Driver, N. Smith, and D.E. Pritchard, *J. Chem. Phys.* **70**, 4155 (1979).

32. T. A. Brunner, N. Smith, A. W. Karp and D.E. Pritchard, *J. Chem. Phys.* **74**, 3324 (1981).

33. S. L. Dexheimer, M. Durand, T. A. Brunner, and D. E. Pritchard, *J. Chem. Phys.* **76**, 4996 (1982).

34. J. I. Steinfeld, P. Ruttenberg, G. Millot, G. Fanjoux, and B. Lavorel, *J. Phys. Chem.* **95**, 9638 (1991).

35. J. I. Steinfeld, J. S. Francisco, and W. L. Hase, *Chemical Kinetics and Dynamics*, Prentice Hall, Englewood Cliffs, New Jersey (1984).

36. J. E. Polanyi and K. B. Woodall, *J. Chem. Phys.* **56**, 1563 (1972).

37. J. Mandel, *The Statistical Analysis of Experimental Data*, Dover, NY (1984).

38. R. K. Lengel and D. R. Crosley, *J. Chem. Phys.* **67**, 2085 (1977).

CHAPTER 3

EXPERIMENTAL

Chapter 3 discusses the experiment techniques and apparatuses used in this dissertation. Section §3.1 reviews laser induced fluorescence (LIF) spectroscopy which is inclusive of the free-jet and SEP techniques as well as the $I(^2P_{1/2}) + I_2$ energy transfer studies. Free-jet expansion is detailed in Section §3.2 and the apparatuses employed in the stimulated emission pumping studies are discussed in Section §3.3. Additional information on lasers, dyes, and optical materials is provided in Appendix B. A description of lineshapes important for characterizing the frequency response in molecular spectroscopy is included in Appendix F.

§3.1 LASER INDUCED FLUORESCENCE (LIF) AND $I_2 + I(^2P_{1/2})$ ENERGY TRANSFER

In LIF measurements, molecules are typically excited from the ground electronic state to an excited electronic level by absorption of radiation. The excited molecules can then decay back to the ground electronic state through spontaneous emission of a photon. The intensity of the fluorescence is proportional to the excited state number density. The energy of the absorbed photon corresponds to the energy required to transition from one eigenstate to another.

The study of collisional transfer processes in this dissertation was accomplished through utilization of two LIF techniques: excitation and fluorescence (emission) spectroscopy. In excitation spectroscopy, the excitation spectrum is obtained as the

fluorescence intensity as a function of the excitation wavelength. This type of LIF may be further classified as wavelength-resolved or undispersed if a monochromator was or was not used, respectively. With the monochromator, the detection wavelength is fixed at a position of strong fluorescence and is generally similar in appearance to the absorption spectrum. In fluorescence (emission) spectroscopy, the wavelength of the exciting laser is fixed while the fluorescent wavelength is dispersed with a scanning monochromator. The fluorescence spectrum is obtained as a function of the emission intensity vs. the emission wavelength.

Wavelength resolved fluorescence excitation spectroscopy was used in the studies of electronic to vibrational (E→V) energy transfer between $I(^2P_{1/2})$ + I_2. A schematic diagram of the experimental apparatus used in obtaining the spectra is shown in Figure 3.1. Iodine vapor (P≈0.3 Torr) in equilibrium with the crystalline solid at room temperature was introduced into the vacuum chamber. The third harmonic (355 nm) of the fundamental 1064 nm beam produced by a Quanta-Ray Nd:YAG DCR-2 pumped a pulsed dye laser (Coumarin 500 dye) which photodissociated I_2 at 496 nm. $I(^2P_{1/2})$ was produced from the photolysis of I_2 by the photodissociation of the $B^3\Pi(0^+_u)$ state. After a 5 µs delay, a Lambda-Physik tunable pulsed dye laser was fired. The output from the probe dye laser was frequency doubled with an autotracking KDP crystal. LIF spectra from 268 - 303 nm were collected using C540, R560, R6G, and R590 laser dyes. In order to increase dye laser output near 295 nm (590 nm undoubled), R6G dye was red-shifted by the addition of a 5% mixture of ethanol and R590 dye. Energy transfer
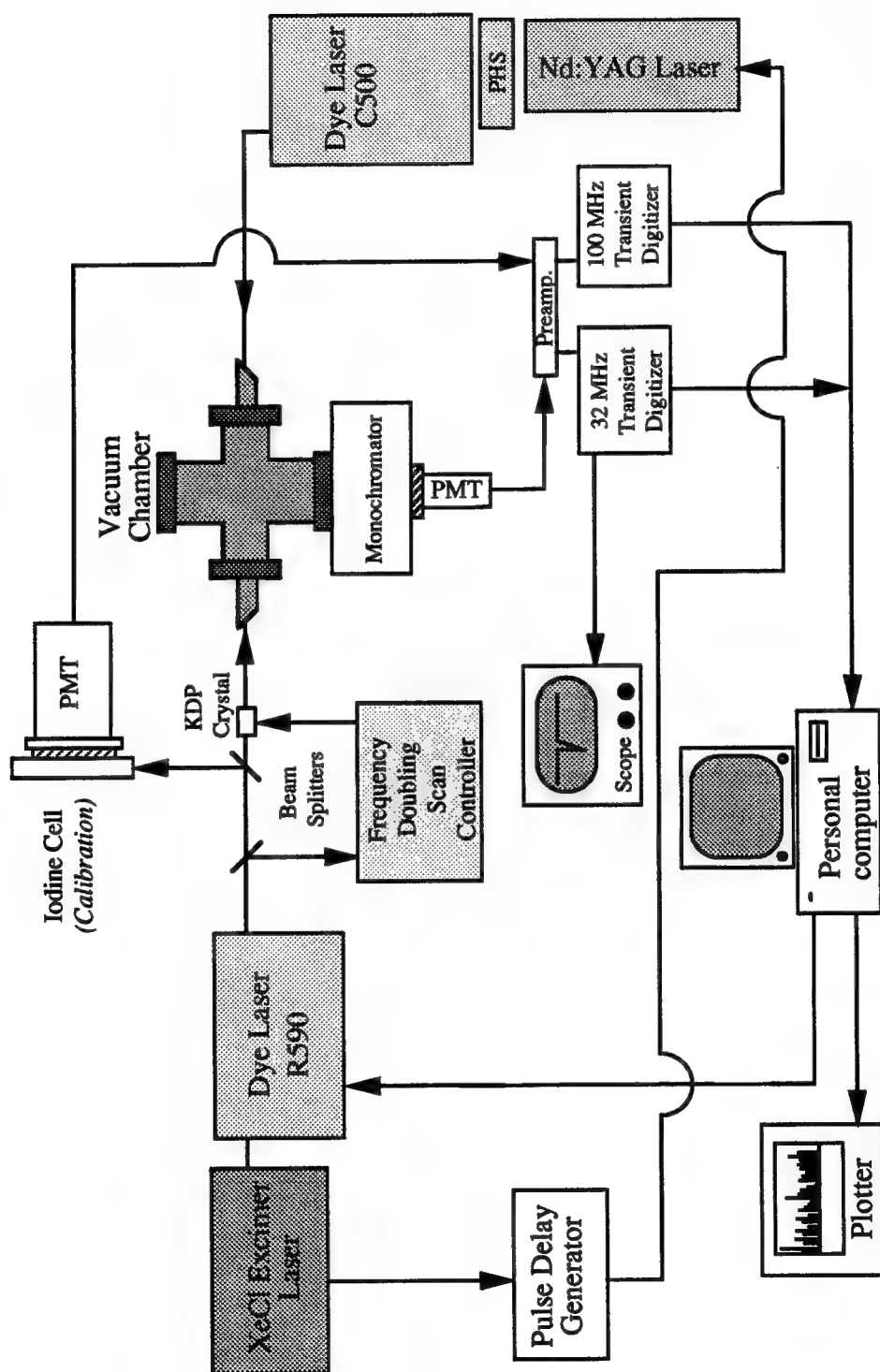
Figure 3.1: Experimental Apparatus for $I_2(X; 25 < v'' < 48)$ Energy Transfer

was recorded by interrogation of the iodine system by scanning the probe laser and monitoring the $D\text{-}X$ fluorescence at 321 nm. The LIF was resolved using a 0.25 m Jarrell-Ash monochromator and detected by an EMI 9558 photomultiplier. The wavelength resolved excitation fluorescent signals from the photomultiplier were preamplified and then captured by a LeCroy 32MHz transient digitizer. Simultaneously, an iodine calibration cell was collected on a 100 MHz transient digitizer and later utilized for absolute calibration of the probe laser. Rotationally-resolved spectra for the $D\text{-}X$ transitions $4<v'<13\leftarrow23<v''<47$ were recorded after adjusting the delay to the shortest time necessary in order to minimize multiple collisions.

Figure 3.2 shows an example of the high-resolution rotationally resolved LIF spectra of energy transfer between $I(^2P_{1/2}) + I_2$. The LIF spectra is characterized by its red-shifted and extremely dense progression of P and R branches (both even and odd J) and no distinguishing features (i.e. no vibrational bandheads are prominent). The lack of notable features are due to the 18 different bands which have Franck-Condon factors of 1×10^{-4} or better in a typical 15 cm^{-1} scan. The dense structure of the rotationally resolved spectra made assignments non-trival, therefore free-jet expansion was used to reduce spectroscopic congestion and simplify assignments.

§3.2 FREE-JET EXPANSION

During the free-jet expansion of a high pressure gas expanding through a nozzle into a low pressure environment, the translational temperature of the gas is significantly

Calibration Spectra
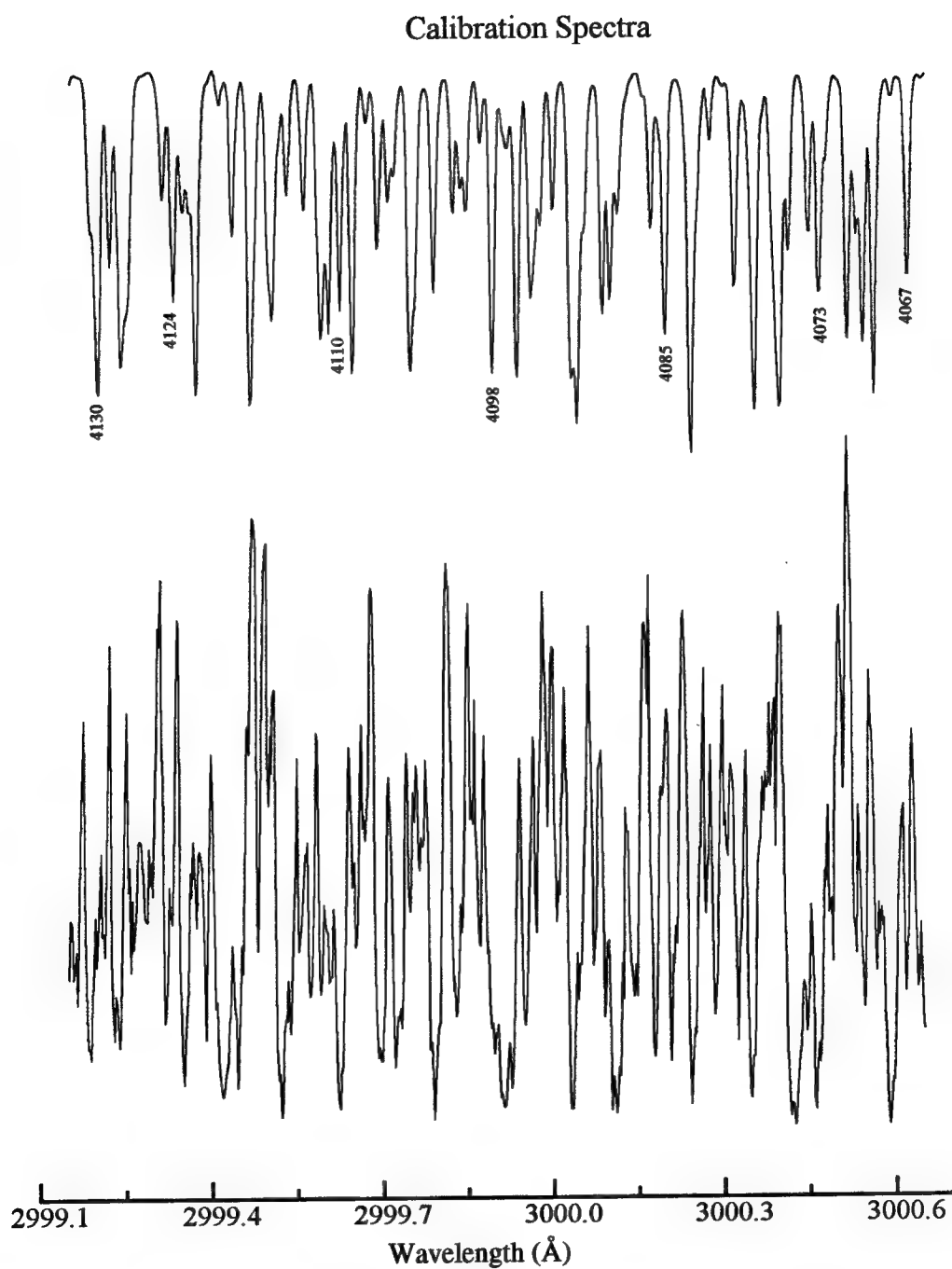
Figure 3.2: Typical High Resolution LIF Spectrum of I_2+I*
Energy Transfer with Simultaneous I_2 $B{\leftarrow}X$
Aborption Shown Inverted (top).

cooled. The high velocity flow of an ideal gas through a nozzle is described by an isentropic (reversible adiabatic) flow in steady state. In expansion with a stagnation temperature of $T_0=T_{rot}$, the gas is rapidly cooled at a rate approaching 10^9 °K/sec. Initially, the rotational relaxation is rapid where the density is high. The number of collisions decrease significantly and the rotational degrees of freedom can no longer be equilibrated, and the rotational temperature becomes fixed. If the stagnation pressure is increased, the number of collisions will increase and the rotational temperature will decrease. However, the translational temperature will decrease until all collisions have stopped. The rotational temperature can be determined from the final average speed u of the expansion and the velocity distribution[1]

$$\int_{T_{rot}}^{T_0} C_{rot}(T)dT = \tfrac{1}{2}mu^2 - C_t(T_0 - T_t)$$

where C is the heat capacity. A free-jet expansion differs from a supersonic expansion by the fact that the free-jet beam is not collimated downstream.

This technique is useful in reducing spectroscopic congestion by producing molecules which are rotationally and vibrationally cold. Cold samples are produced by seeding the molecule in an inert carrier gas. Then flowing the sample through a nozzle, random thermal motion on the high pressure side is converted to a highly directional flow near the continuum region of the nozzle. As a result, the translational degrees of freedom are cooled as the distribution of molecular velocities narrow.

In addition to cooling of the translation degrees of freedom in the expanding jet, clustering of the molecules is induced. Figure 3.3 shows a schematic representation of the

532 nm
excitation-dissociation
$I_2(B) \rightarrow I + I$

Recombination,
relaxation, and cluster
recombination producing
rotationally cold, vibrationally
excited $I_2(X)$
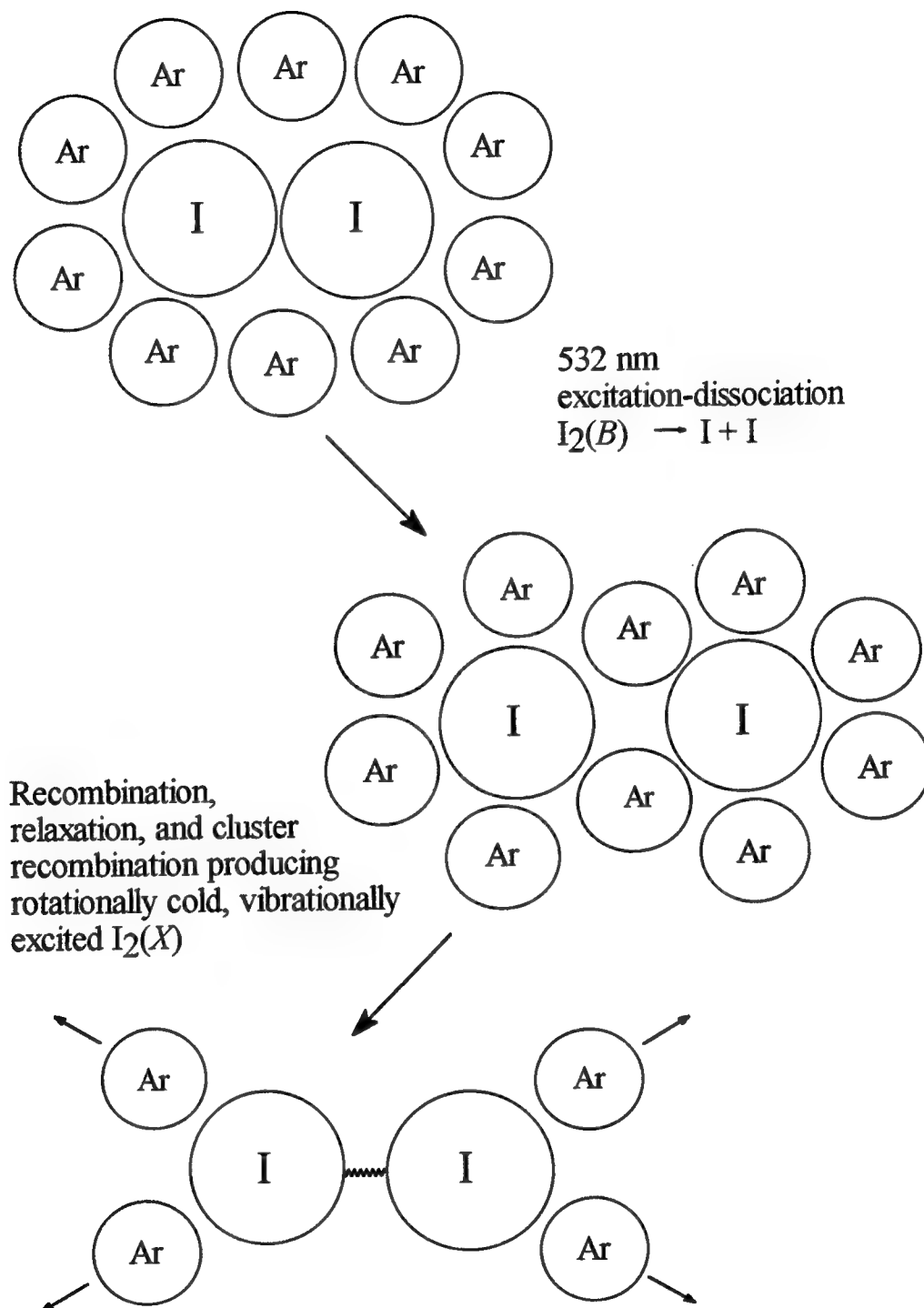
Figure 3.3: Iodine/Argon in a Free-Jet Expansion

clustering of iodine and argon in a free-jet expansion. Photofragmentation of I_2Ar_n clusters populated highly excited vibrational levels of the ground state when $I_2\dagger$ was ejected from the fragmenting clusters. Condensation processes are the most efficient at the nozzle where the collision frequency is the greatest. Under these conditions, very low rotational temperatures (13°K) were attained, yielding relatively uncongested spectra.

The cooling effect is enhanced by monatomic gases since they do not have any rotational and vibrational degrees of freedom. Cooling of the sample is generated by the high pressure differential with supersonic flow through a nozzle, and for the continuous free-jet expansion, a large pumping capacity is required. Our vacuum system consisted of a Roots blower and a Stokes vacuum pump with a 500 cfm capacity. The Roots blower was attached to the sample chamber via a flexible stainless steel bellows for vibration absorption. The sample chamber was a six-way stainless steel cavity with baffled arms. Injection of the gas sample through the nozzle was accomplished by an x,z translation mount with Cajon Ultra-Torr fittings. The translation mount allowed continuous adjustment of nozzle position under vacuum conditions. Detailed discussions and drawings of the apparatus can be found in dissertations by M. McQuaid,[2] Y. Lin,[3] or X. Zheng.[4]

A free-jet expansion was utilized to produce rotationally cold, vibrationally excited $I_2(X; v''=40)$. Previously, Fei et al.[5] had observed vibrationally excited $I_2 X$ in a free-jet expansion, but they did not attempt any high resolution LIF. For this study, I_2 vapor (P≈0.3 Torr) was seeded in argon with a backing pressure of 1.4 atm. The sample

was injected as a continuous-flow expansion through a 1 mm nozzle into a chamber evacuated with a Roots blower. The chamber pressure was maintained at 140 mTorr. The experimental apparatus shown in Figure 3.1 for the $I_2(X) + I(^2P_{1/2})$ studies is almost identical to the free-jet apparatus except the continuous-flow expansion replaced the static cell and the pulsed dye laser (PDL) was not used. Instead of the PDL output, clusters of I_2Ar_n were directly excited at 532 nm by the frequency doubled Nd:YAG laser (Quanta-Ray DCR-2). This excitation produced metastable-excited complexes and vibrationally excited I_2 molecules in the ground electronic state. The UV radiation for probing the $D{\leftarrow}X$ transition was generated by frequency doubling the output from an excimer pumped dye laser (Lambda Physik EMG 101, FL3002E, R6G) with a KDP crystal. Absolute wavelength calibration was obtained by simultaneous recording of the iodine $B{\leftarrow}X$ absorption spectra prior to the frequency doubling of the probe dye laser fundamental. After a 5 μs delay, the frequency doubled output of the Lambda Physik laser was focused approximately 5 mm below the 532 nm beam. With the monochromator set at 390 nm, the relative laser and nozzle position, delay, and flow were optimized for detection of fluorescence from the I_2Ar_n clusters. After fluorescence signal optimization, the monochromator was set to 321 nm to monitor $D{\rightarrow}X$ fluorescence. Vibrationally hot $I_2(X)$ was then characterized through UV excitation to the ion-pair state. The signal was dispersed by a 0.25 m monochromator and detected by a photomultiplier (EMI 9558 QB). An average of 200 shots per step and a PMT voltage of 2200 V was required for a reasonable signal to noise ratio. The signal from the

photomultiplier was preamplified, digitized (LeCroy TR8837F, 32MHz sampling rate) and recorded on a personal computer.

§3.3 STIMULATED EMISSION PUMPING (SEP)

Electrical discharges, exothermic chemical reactions, and UV photodissociation are the three most common and naturally occurring examples by which highly vibrationally excited molecules are produced. The major reason for the lack of state-resolved energy transfer measurements for highly vibrationally excited molecules is the difficulty in cleanly populating individual rovibrational levels. This problem can be overcome by use of the spectroscopic technique of stimulated emission pumping. Stimulated emission pumping[6] (SEP) is a folded variant of optical-optical double resonance (OODR). A crucial distinction between SEP and any single resonance technique is that the rovibrational spectra are freed of rotational congestion[7] since the rigorous electric dipole $\Delta J=\pm1$ limits the possible *dump* transitions from a SEP intermediate.

§3.3.1 SAMPLE CHAMBER

An illustration of iodine sample chamber is shown in Figure 3.4. The cylindrical chamber was constructed of stainless steel with dimensions 65 cm high and 20 cm in diameter. Standard Conflat (Del-Seal) type flanges with copper gaskets sealed the top, bottom, and pump connections. The chamber arms were 30 cm long and contained
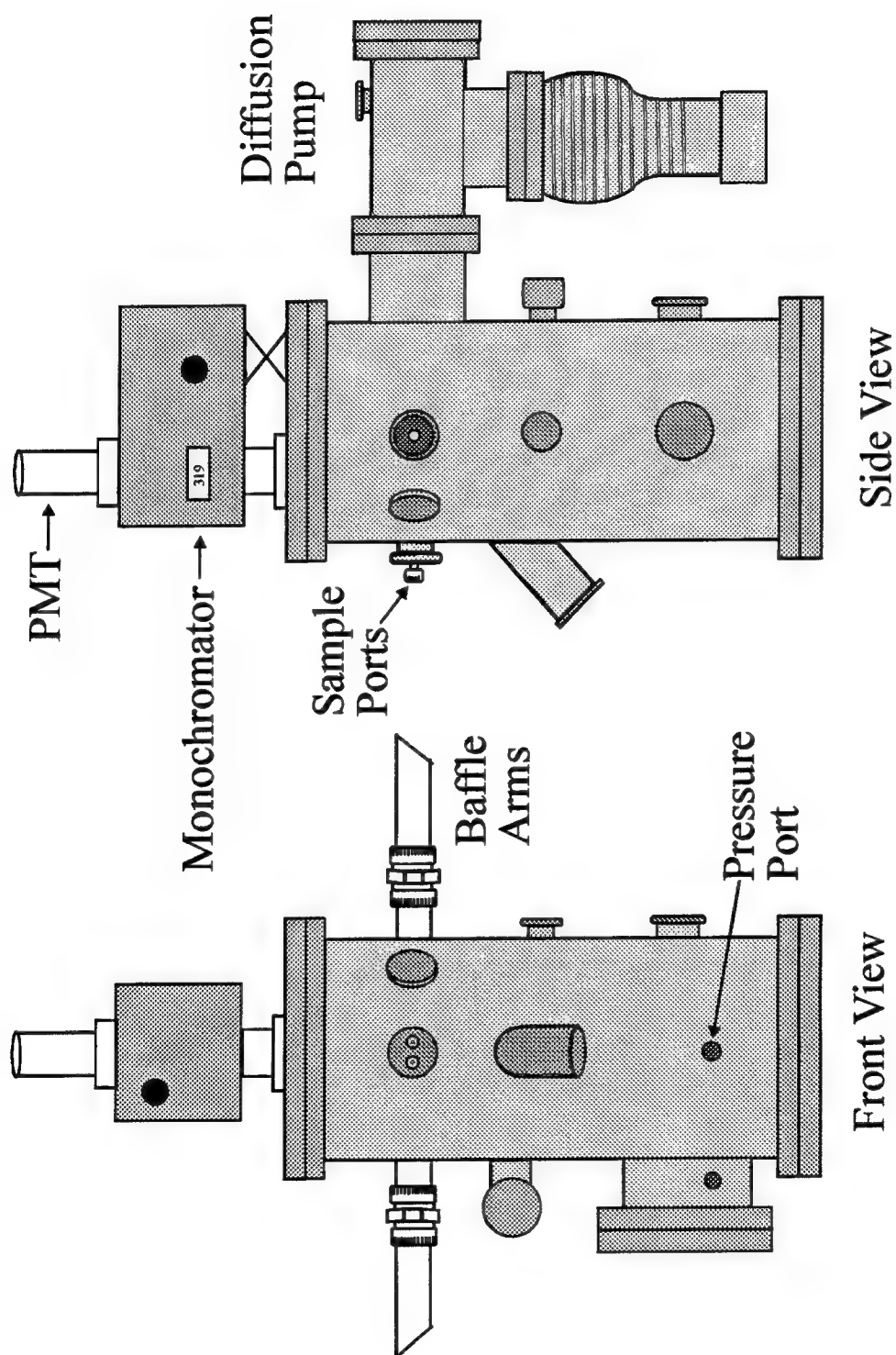
Figure 3.4: Illustration of Sample Chamber Configuration for SEP-LIF Studies

blackened baffles with 6 mm centers to reduce laser scatter. Quartz windows were oriented at Brewster angle (56°39') to transmit radiation without reflection for one polarization of the electric field. The arms are connected to the chamber with one inch Cajon Ultra-Torr fittings for removal and cleaning of the windows. Numerous smaller fittings on the chamber consist of Kwik-Flange or quick disconnect, both with Viton O-rings. Two ports with $1/4$ " Cajon Ultra-Torr fittings were used for connecting the iodine and diluent gas.

The chamber was evacuated by an Alcatel direct connect or Welch DuoSeal mechanical pump to a baseline pressure of 1-5 mTorr. A Varian differential pump with an ultimate vacuum of 10^{-6} Torr was employed for chamber bake-out and leak detection. When leaks were detected, they were sealed with Torr-Seal or epoxy. Removal of the epoxy was accomplished with glacial acetic acid. Pressure in the chamber was measured with a McLeod mercury gauge or a MKS Baratron Type 222 capacitance manometer (100 Torr) with digital display.

A biconvex quartz lens (f = 45 mm) was installed in an adjustable mount inside the sample chamber. Biconvex , or symmetric-convex lenses, have positive focal lengths and form real and virtual images. These lenses are best for imaging close to 1:1. The biconvex lens focuses the fluorescence of the sample through a quartz window located on the top of the chamber into the entrance slit of the monochromator. Because of its symmetry, the biconvex lens provides the lowest minimum aberration[12] possible with a

single element. Minimizing chromatic, spherical aberrations are important because the behavior of the lens depends on the wavelength of the light since shorter wavelength light is focused at a closer point to the lens than longer wavelengths.

After focusing the light onto the entrance slit of the monochromator, the fluorescence was then dispersed with a grating monochromator. The Czerney-Turner grating monochromator used in these experiments contains an entrance slit, collimating and focusing mirrors, a dispersing element (grating), and an exit slit. The basic grating equation[13] is defined as $m\lambda=d(\sin D + \sin I)$, where m is the order of diffraction (spectral order), λ is the diffracted wavelength, I and D are the incident and diffracted angle, respectively, and d is the grating spacing. Usually, only first order is desired since it is the most intense. The monochromator used in these experiments was a 0.25 m Jarrell-Ash. Since gratings are not efficient for all wavelengths, the monochromator contained two externally interchangeable gratings: low blaze 1180 g/mm, 180-5000 Å; and high blaze 2360 g/mm, 5000 Å- 1 μm. The efficiency of the grating may be improved by changing the groove facet angle. The optimization of the grating for a wavelength range is known as blazing. In addition to optimizing the blaze of the grating, aligning the long dimension of the source with the long dimension of the slit ensures maximum signal. The intensity of the dispersed fluorescence is measured with a photomultiplier tube (PMT). The PMT connected to the monochromator in these experiments was an EMI 9558 QB. The signal intensity as a function of the PMT voltage is shown in Figure 3.5. Berkeley Nucleonics Corp (BNC) connectors attached the PMT to the data acquisition system.

$y = A0 + A1 x + A2 x^2 + A3 x^3 + ...$

Parameter	Value	sd
A0	9.3584072	1.10771
A1	-0.019389167	0.00161
A2	1.0490221E-5	5.7243E-7

R = 0.99941
R^2 = 0.99881
SD = 0.10319

$y = 9.35841 - 0.01939 x + 0.00001 x^2$
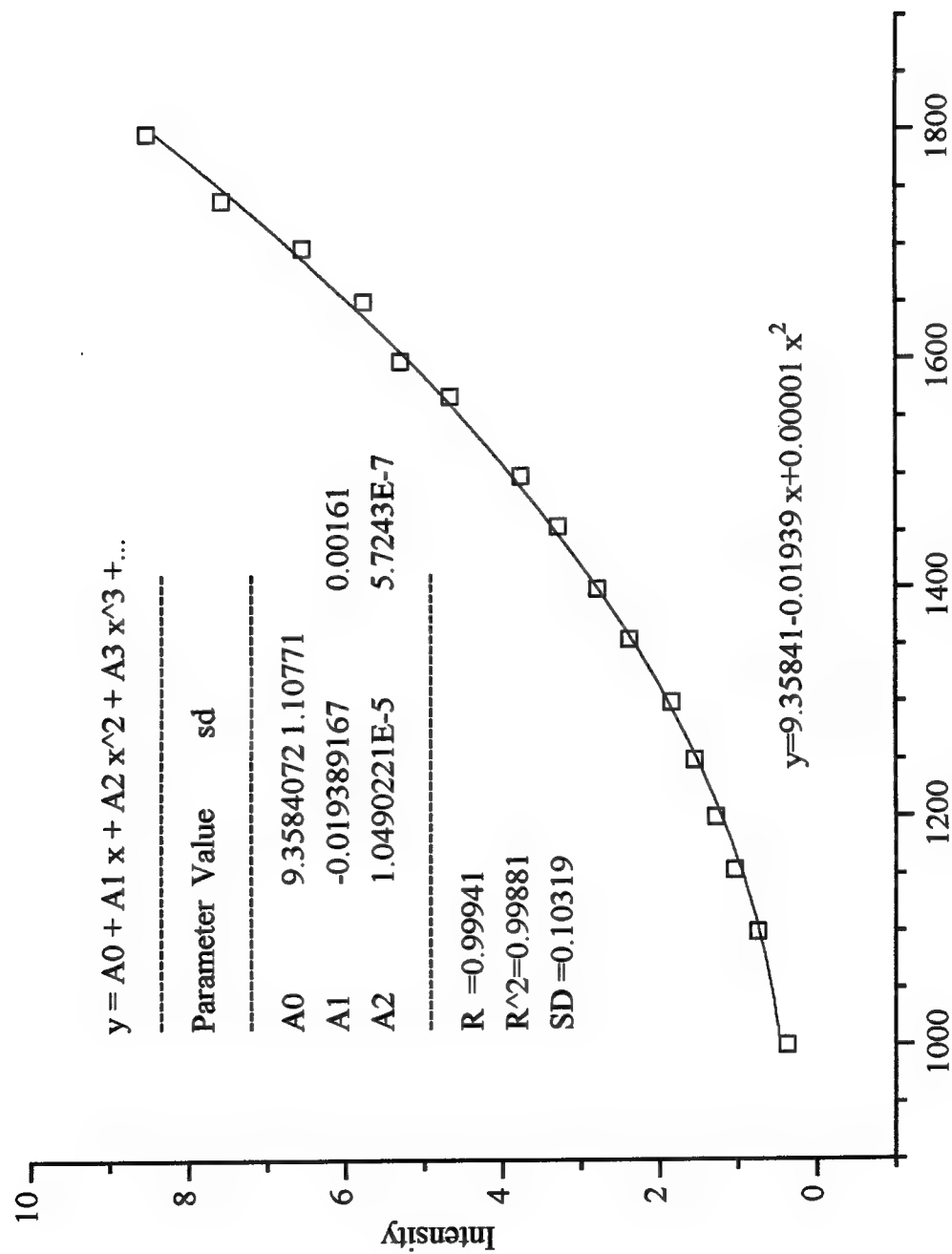
Intensity

Figure 3.5: Signal Intensity vs PMT Voltage

§3.3.2   DATA ACQUISITION

After capturing the fluorescence with the PMT, the output was processed by either a transient digitizer or boxcar integrator. Figure 3.6 shows a schematic of the digital data acquisition system with the transient digitizer. The heart of the data acquisition system is the Computer Automated Measurement and Control (CAMAC) interface. CAMAC is an internationally agreed upon electrical, organizational and mechanical standard for data collection equipment containing a standard highway bus based on IEEE-583. External clock and trigger interconnects to each module create a single clock and trigger input for the entire acquisition system. Once triggered, the CAMAC system records all channels simultaneously.

Signals from the PMT were preamplified and digitized by a transient digitizer. The preamp boosts the signals for the transient digitizers, arming the analog to digital converter (ADC). Once armed, the ADC digitizes the signal continuously and feeds the sample into memory using circular addressing. In this manner, the transient digitizer can record both transient and repetitive signals capturing both pre- and post-trigger information. While the 32 MHz transient digitizer was used in signal processing, the 100 MHz transient digitizer simultaneously collected and processed the iodine calibration signal. Usually, less than 4% of the output from the *probe* pulse dye laser was focused into an iodine reference cell where undispersed LIF was detected with a Amperex CVP (S1) photomultiplier tube. When possible, the first-order Fresnel reflection from the Schott UV transmitting black glass was reflected into the calibration cell.
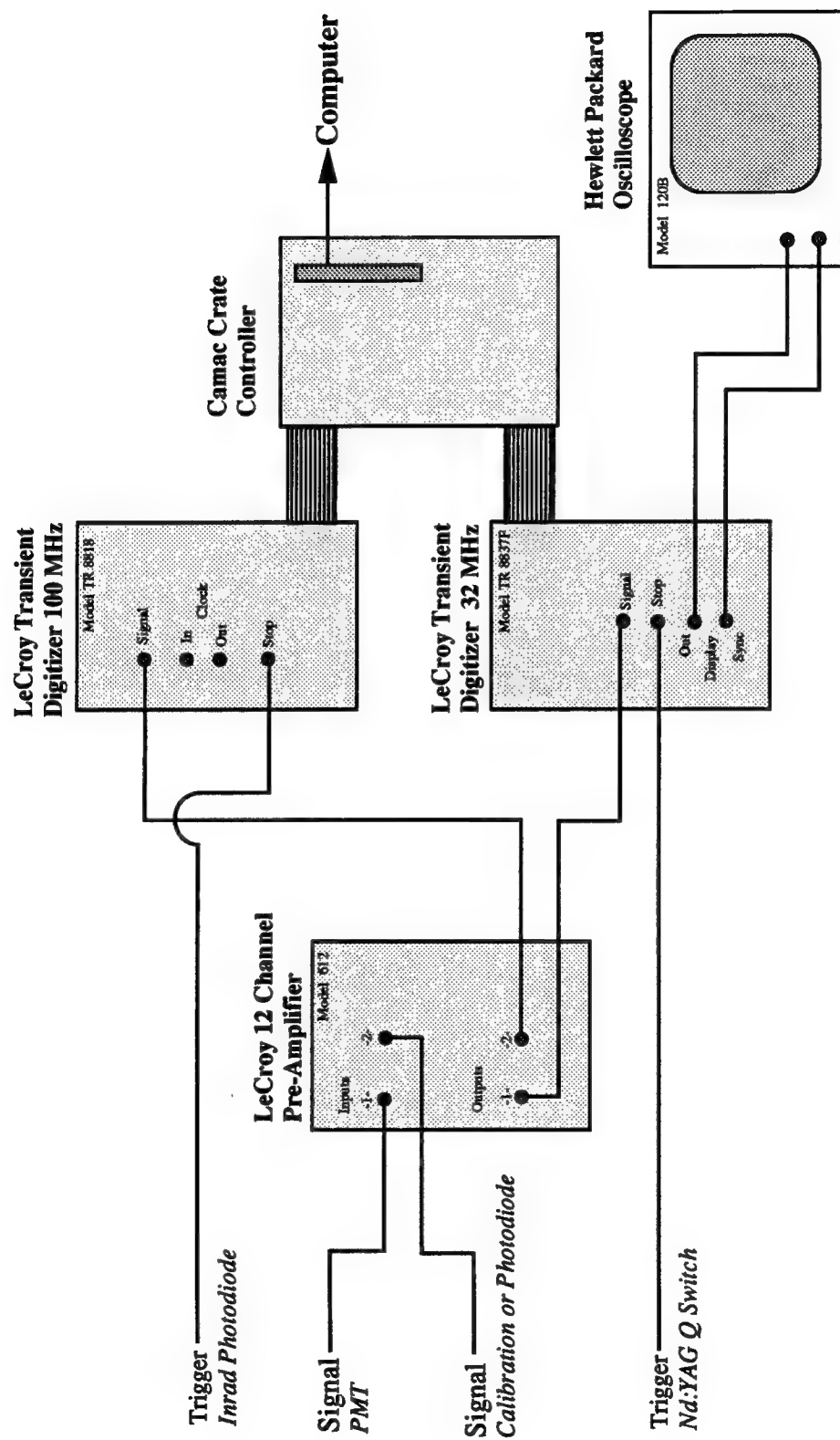
Figure 3.6: Digitial Data Acquisition System

In collecting time resolved excitation spectra, a boxcar integrator was used in place of the transient digitizer and CAMAC crate. The PMT signal was connected to the gated boxcar integrator (SR 250) and an oscilloscope. A reference signal from the gated 50Ω output of the boxcar was also displayed on the oscilloscope. The signal representing the integration gate was adjusted with the boxcar delay and width controls for maximum signal. The average output from the boxcar was recorded from the digital meter. In this manner, the probe laser was fixed on a transition (usually the parent peak) while the delay between the *dump* and *probe* was adjusted. The signal strength from the digital meter was recorded as a function of the delay between the *dump* and *probe* lasers.

A personal computer (Zenith ZW158) was used for interfacing with the CAMAC crate system. A DAS-8 analog to digital converter board in the Zenith drives the FL3002E pulsed dye laser or pressure scans as directed by the user through four computer programs for use in data acquisition and control. *LASER* was utilized for all scans which required pressure tuning of the pulsed dye laser's oscillator cavity. *LAMBOX2* was used for both low and high resolution scanning of the probe laser. *SIGNAV* and *SIGN32* were used in recording the output of the 100 MHz and 32 MHz transient digitizers, respectively. Since the memory of the 100 MHz transient digitizer could not be displayed on the Hewlett-Packard oscilloscope, *SIGNAV* was the only means available to observe signal output from the 100 MHz.

§3.3.3 RADIATION SOURCES

The three (pump) laser systems used in these experiments were: Spectra-Physics neodymium doped yttrium aluminum garnet (Nd:YAG; Nd^{3+}: $Y_3Al_5O_{12}$) laser model DCR-2[14], with harmonic generator (HG) for frequency conversion of the 1064.5 nm output, prism harmonic separator (PHS) for separating the outputs, pumping a dye laser (PDL-1); Lambda-Physik (EMG-101 MSC) XeCl excimer laser at 308 nm pumping a Lambda Physik dye laser (FL-3002E), and INRAD autotracker for frequency doubling; and a Lambda-Physik (Lextra 200) air-cooled XeCl laser pumping a single stage dye laser (FL-3001). Of the three pump lasers, the Nd:YAG laser was the only laser in which its fundamental and frequency-doubled output were utilized without dye lasers.

The Nd:YAG is a solid state laser medium which is optically pumped with krypton flashlamps whose output matches the principle absorption bands in the red and near IR of the Nd^{3+} ion. The output of the fundamental at 1064 nm has a linewidth of less than 1 cm^{-1} and a beam divergence less than 0.5 mrad. A KD*P crystal was used for generating 532 and 355 nm output. Separating the fundamental from the frequency doubled or tripled output was accomplished with a prism harmonic separator as shown in Figure 3.7. Since the laser output traversed 20 foot to the sample chamber, a Gaussian beam expander was utilized to collimate the beam to minimize divergence and power loss. The beam expander consisted of a negative lens followed by a positive collimating lens.

The three laser systems in this dissertation were used to pump dye lasers. All three dye lasers contained a Littrow type oscillator with a grating angle of 42.5° to 72.5° and

right-angle prism adjusted
for total internal reflection

half-wave plate

$\lambda/2$

$\lambda/2$

355nm

532nm

1064nm

Pellin Broca
Prism

Laser output
from
Harmonic
Generator (HG)
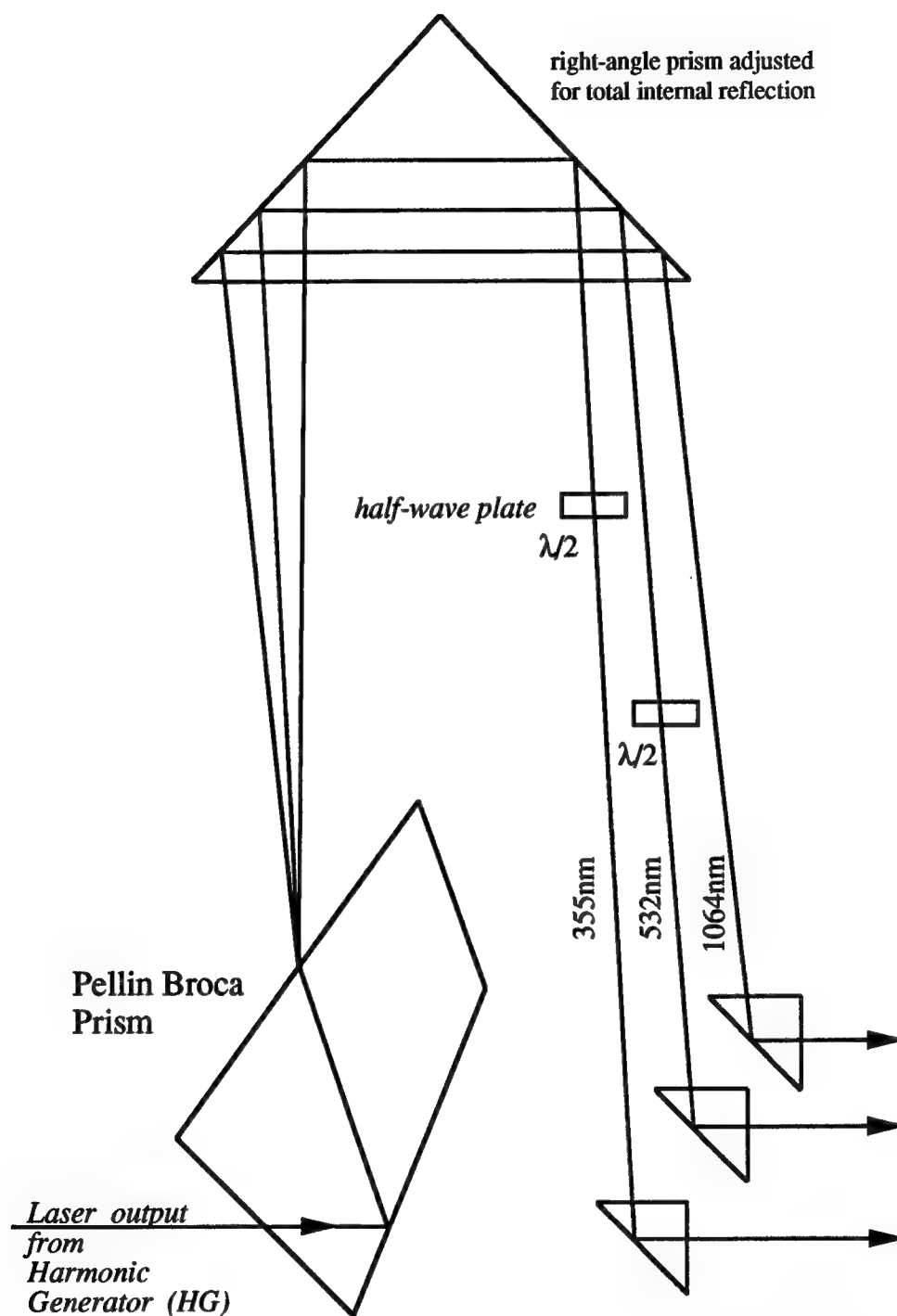
Figure 3.7: Prism Harmonic Separator (PHS) for Separating and
Isolating Nd:YAG Laser Output

intracavity etalons as shown in Figure 3.8. The dye lasers could be operated in the low

resolution mode (Δv=2.0 cm^{-1}) or high resolution mode (Δv=0.04 cm^{-1}) with the etalon.

Only the Lambda FL3002E had an electromechanical drive for simultaneous angle tuning

of the grating and etalon. In order to achieve high resolution mode with the other two

dye lasers (PDL-1 and FL3001), pressure tuning of the oscillator cavity was employed.

Pressure tuning works by changing the refractive index of the pressure box containing the

grating and etalon. Since these tuning devices utilize multiple interference, the

wavelengths change by the amount $d\lambda = \lambda_o(n-1) \times dP$ where n is the refractive index of

the gas, and dP is the change in pressure of the tuning chamber. Dry nitrogen with a n-1

value of 3×10^{-4} was slowly leaked into the pressure box. Pressure tuning from vacuum to

atmosphere provided a 3.5 cm^{-1} scan range with the wavelength changing to the *red*.

§3.3.4   EXPERIMENTAL APPARATUSES

For the purposes of this dissertation, *pump* refers to the photon which is absorbed

by a molecule in a single thermally populated level in the ground electronic state and

populates an electronically excited level in a well-resolved quantum state. *Dump* refers to

the photon which stimulates emission back into the ground electronic state. *Probe* refers

to the absorption of a photon from the state-prepared or collisionally populated level in

the ground electronic state to a resonant quantum level in an electronically excited state.

A typical SEP experiment uses a dual-beam arrangement to compensate for

pulse-to-pulse variations in laser intensity. The *pump* beam is split into equal-intensity
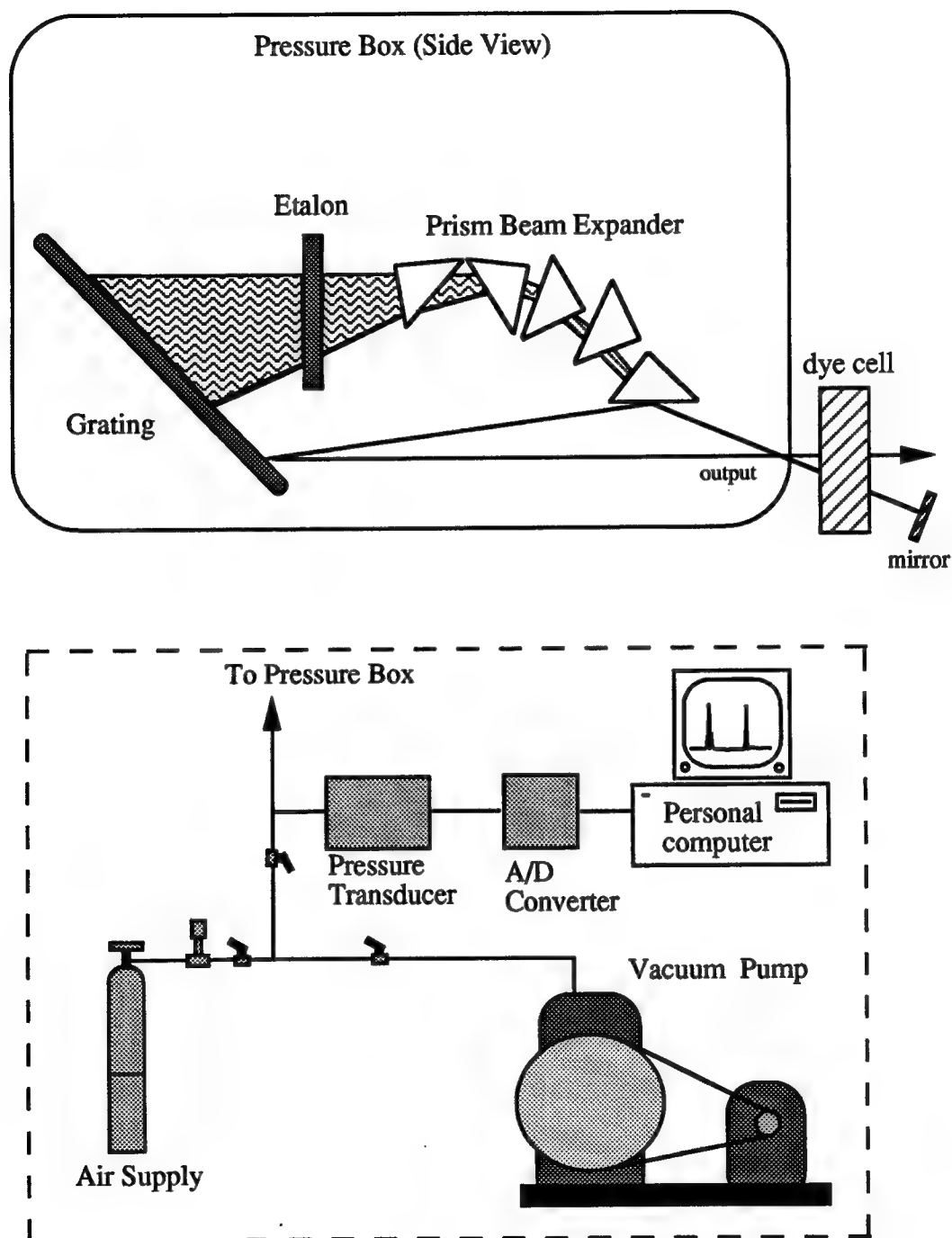
Figure 3.8: Schematic of (top) Littrow Configuration Dye
Oscillator and (bottom) Pressure Tuning Apparatus

signal and reference beams through a common sample cell. The signal is a depletion of the side fluorescence in the sample cell as the *dump* laser is scanned across a downward transition. The decrease in side fluorescence is due to an increase of stimulated emission propagating along the axis of the *dump* beam. Matched photomultipliers detect side fluorescence in both signal and reference cells. The outputs are fed to a fast differential amplifier, the reference fluorescence is subtracted from the sample signal which generates a null in the absence of downward resonant transitions.

In cases where the *pump* transition was saturated, the fluorescence signal in the absence of the *dump* laser is proportional to 0.5 times the total number of molecules in the selected quantum state, 0.5N. When the dump transition is saturated, then $1/3$ of the molecules will be in each of the three levels, so that the fluorescence signal is proportional to $N/3$. The fluorescence dip at the saturation limit is[8]

$$\frac{0.5N - \frac{N}{3}}{0.5N} = \frac{1}{3}$$

The experiments conducted in this dissertation utilized the folded triple resonance of stimulated emission pumping-laser induced fluorescence (SEP-LIF). A typical experimental setup for SEP-LIF is shown in Figure 3.9. Ideally, the *pump* laser populates a single rovibronic level of an excited electronic state where the pump laser locks onto a single rotational line of the $B \leftarrow X$ system. A second laser, the *dump*, was tuned through resonance onto a transition terminating on a rovibrational level in the ground electronic state. The dump laser is locked onto a single rotational line of a $B \rightarrow X$ transition which
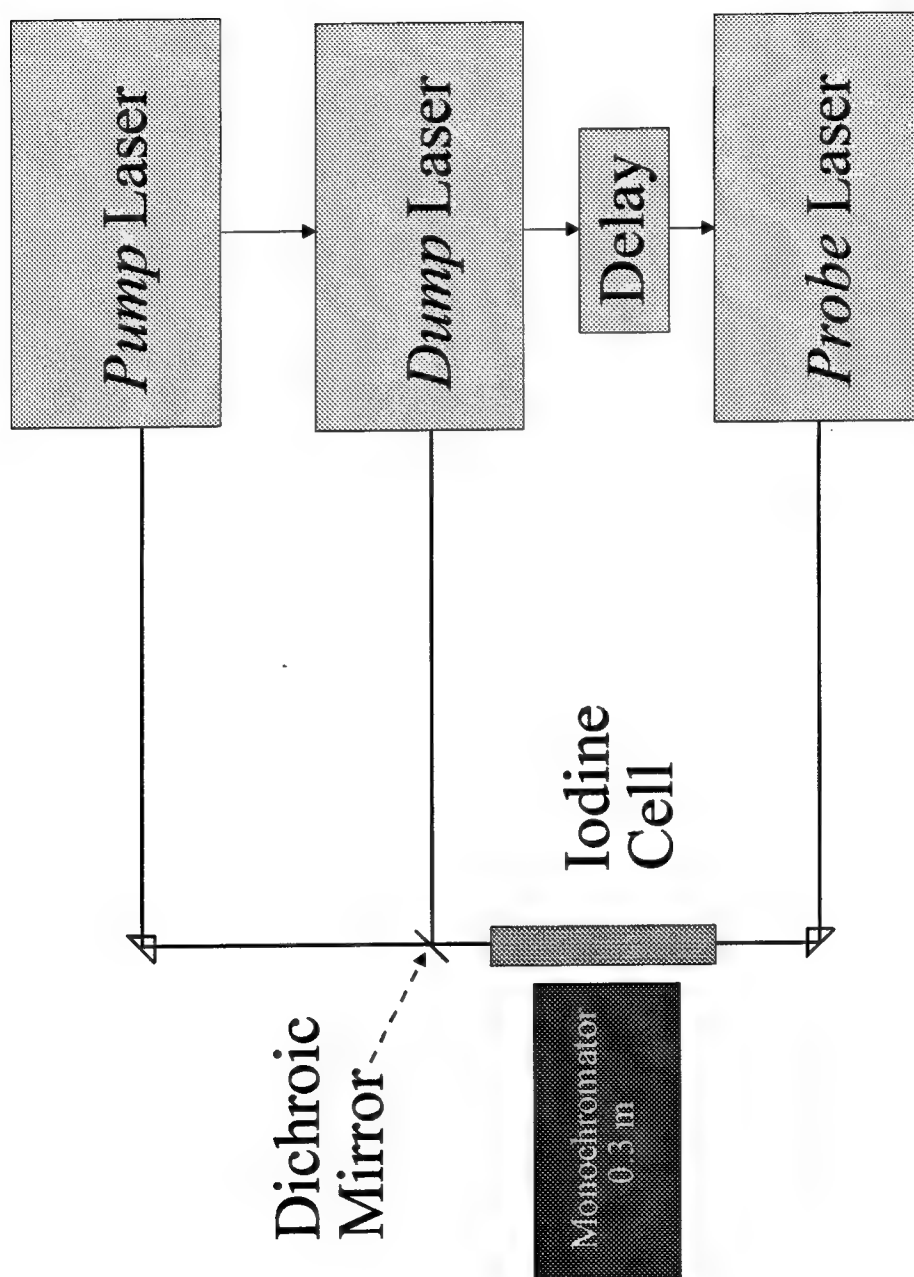
Figure 3.9: Typical Experimental Setup for SEP-LIF (Stimulated Emission Pumping-Laser Induced Fluorescence)

stimulated emission to the selected state. The $B^3\Pi^+_0$ of iodine is subject to both spontaneous and collision-induced predissociation. As a result of the curve crossing between the repulsive and bound states, the effective spontaneous lifetime of the excited levels and their dependence on diluent gas pressure are complicated and vary widely for different vibrational levels.[9]

A third laser, the *probe*, was tuned to a third resonance from the SEP prepared state to an emitting electronic state. Calculating the ground state populations can sometimes be complicated by the fact that species can be transferred into or out of the laser excited upper level through collisions with other atoms or molecules (aka Franck-Condon pumping). In these experiments, the probe was tuned between resonant transitions in the X state to the $I_2 D(0^+_u)$ ion-pair state due to the numerous advantages of this system. The D-X transition is more intense than the B-X, the short D state lifetime circumvents problems associated with quenching of the monitored fluorescence, and the D-X emission occurs at wavelengths well removed from the scattering and fluorescence associated with the SEP pump and dump pulses. In detection of the $D \rightarrow X$ fluorescence, a useful property of the bound-free region of this system was exploited.[10] All bound vibrational levels of the D state have strong transitions to the X state continuum region. Due to the occurrence of a maximum in the Mulliken difference potential, the most intense bound-free emission appears at 321 nm, regardless of the D state vibrational level.[11]

Wavelength resolved fluorescence excitation spectra were collected by fixing the monochromator at 321 nm. The *pump* and *dump* lasers would be tuned to resonant transitions for preparation of the vibrationally excited state. The parent (initially prepared level) and satellite (collisionally populated levels) were then scanned with the *probe* laser. The state prepared level was selectively monitored on a nanosecond time scale. In all three experiments, fast silicon photodetectors (Electro-Optics ET2000) were measured the delay between the *dump* and *probe* lasers. The nominal delay between the *pump* and *dump* laser was 20 ns.

The transition frequencies for the three SEP-LIF experiments conducted for this dissertation are listed in Table 3.1. The three vibrational levels selected for study by SEP-LIF in this dissertation, v"=42, 38, and 23, are consistent with the range of vibrational levels proposed as an iodine intermediate before its dissociation in the COIL device. Section §3.3.4.1 details the experimental preparation of I_2 (X, v"=42, J_i=17). This level was chosen as it is in the upper range of vibrational levels populated by $I_2+I(^2P_{1/2})$ and $I_2+O_2(^1\Delta)$. Section §3.3.4.2 describes the second SEP-LIF experiment which prepared I_2 (X, v"=38, J_i=49) for study by excitation to $I_2(D;v'=5-12)$. This transition was chosen because the 1064 nm fundamental from the Nd:YAG was resonant with a rovibrational level in I_2 (X; v"=38). Section §3.3.4.3 discusses the third SEP-LIF experiment which prepared I_2 (X, v"=23, J_i=57) for study by excitation to I_2 ($D;v'=30-37$). This vibrationally prepared state corresponds with the lower range of vibrational levels for which it is energetically possible to dissociate I_2 by one $O_2(^1\Delta)$ or

Table 3.1: Transition Frequencies for SEP-LIF Energy Transfer Studies

	ν (nm)	$\nu(cm^{-1})$	electronic transition	vibrational transition	rotational transition
ν''=42					
Pump	514.71	19,428.42	B-X	43-0	R(15)+P(13)
Dump	857.9	11,656.37	B-X	43-42	P(17)
Probe	$\approx$300	$\approx$33,333	D-X	6-42	
ν''=38					
Pump	620.45	16,117.15	B-X	7-2	R(47)+P(41)
Dump	1,064.55	9,393.64	B-X	7-38	P(49)
Probe	$\approx$290	$\approx$34480	D-X	8-38	
ν''=23					
Pump	569.64	17,767.97	B-X	19-1	R(55)
Dump	756.16	13,189.76	B-X	19-23	P(57)
Probe	$\approx$253	$\approx$39,525	D-X	23-34	

one $I(^2P_{1/2})$ atom. Inelastic collisions were investigated and kinetic rates were determined by measuring the fluorescence intensities from the initially prepared and collisionally populated levels as a function of the delay between the *dump* and *probe* lasers.

§3.3.4.1 SEP v"=42

The experimental apparatus consisted of three pulsed dye lasers operating at 10 Hz repetition frequency. The *pump* dye laser (Lambda Physik, Coumarin 500 dye, 25 mJ) was excited by a XeCl excimer laser at 308 nm. In order to extend the half-life of the Coumarin dye, DABCO (triethlylene diamine or 1,4 Diazobicyclo[2.2.2]octane) was added to the dye (0.07 m/l).[15] The addition of DABCO extends the life of blue dyes (nominally 8 hrs) by a factor of three. The *dump* dye laser (Quanta-Ray PDL-1, LDS 867 dye, 5 mJ) was pumped by the second harmonic of a Quanta-Ray DCR-3 Nd:YAG laser at 532 nm. The *probe* laser (Quanta-Ray PDL-2, R610 dye, 7 mJ) also was pumped by the second harmonic of a Quanta-Ray DCR-2 Nd:YAG laser. The output of the *probe* pulse dye laser was doubled by a KD*P crystal in a Quanta-Ray WEX-1 wavelength extender. The laser outputs were calibrated by a Burleigh WA4500 pulsed wavemeter with an accuracy to 0.02 cm^{-1}. The output of the three lasers were then directed through the iodine cell.

The iodine cell was constructed of Pyrex glass, approximately 35 cm long with brewster angled quartz windows (≈56°), and externally blackened Wood's horn located at each end. Iodine crystals were placed in a cold finger located in the bottom of the Pyrex

cell. Gas pressure was monitored with a MKS 10 Torr capacitance manometer. For measurements of I_2 self-transfer, vapor in equilibrium with crystalline solid at room temperature was used (~287 mTorr). For studies of transfer caused by other collision partners, the I_2 pressure was reduced by cooling the I_2 crystals located in a cold-finger to 0°C with an ice bath. Iodine vapor pressure as a function of temperature can be obtained from the following relationship[16]

$$Log\ P = 12.1891 - 0.001301T - 0.3523\ Log\ T - (3410.71/T)$$

where P = pressure (Torr)
T = temperature (°K)

Diluent gas pressures in the 0.5-1 Torr range were used to ensure that collisions with the bath gas dominated and that the time scale for energy transfer was short compared to the rate at which molecules diffused out of the probe laser beam (~1 mm).

The delay between the *dump* and *probe* laser pulses was controlled by a precision pulse generator (SRS DG535). The Stanford Research Systems pulse generator was initiated by an external trigger from the dump laser and could be programmed for any delay interval between 0 and 1000 s with 5 ps of resolution and jitter of less than 50 ps.

The pump laser was tuned to the $B \leftarrow X$, 43-0, R(15) line at 514.7 nm. An intracavity air spaced etalon was used to obtain a *pump* laser linewidth of Δv_p ~0.07 cm^{-1}. The *dump* laser was tuned through resonance and stimulated the $B \rightarrow X$, 43-42, P(17) line at 858.9 nm. The energy spacings between allowed *dump* transitions were sufficient to permit clean single state preparation when the *dump* laser was operated without an etalon

($\Delta v_D \approx 0.2$). A dichroic mirror (transmit 514 nm, reflect 850 nm) combined the *pump* and *dump* beams for copropagation through the sample cell. The *probe* beam was counterpropagated through the sample cell coincident with the *pump* and *dump* laser beams. Wavelengths from 295-300 nm probed the highly vibrationally excited state by interrogation of the prepared and collisionally populated levels via the $D \leftarrow X$ transition. Sampling with the probe laser in both high (0.08 cm^{-1}) and low (0.4 cm^{-1}) resolution scans was obtained by pressure-tuning of the air-spaced etalon and mechanical tuning by grating rotation, respectively. With the narrower linewidth, power broadening of the $D \leftarrow X$ lines was frequently observed. A variable attenuator was used to reduce the power to levels that did not cause measurable broadening.

Wavelength resolved fluorescence excitation spectroscopy was used exclusively in this experiment. A 0.3 m monochromator, set to transmit a 2 nm wide band centered at 321 nm, was used to monitor the probe laser fluorescence. This scheme eliminated interference from scattered laser light and fluorescence resulting from the *pump* or *dump* pulses. However, an unexpected complication was encountered. The *probe* laser also excited the $f(0^+_g) \leftarrow B(0^+_u)$ transition via pump/probe optical-optical double resonances (OODR). The bound-free emission of the $f \rightarrow B$ system is also maximized around 320 nm, so this interference could not be removed by wavelength selected fluorescence detection. In a few instances the OODR spectra were used to compare the B and X state energy transfer dynamics.

Fluorescence signals were detected by a photomultiplier (Burle C31034) and recorded by a boxcar integrator (SRS 250). For low resolution scans, the output from the boxcar was collected and stored in a personal computer using the program *SCANNER*. High resolution scans were recorded on X-Y stripchart recorder, with the Y axis representing the signal output from the boxcar and the X axis being the output of the pressure transducer from the *probe* laser's oscillator cavity.

§3.3.4.2 SEP v"=38

Figure 3.10 shows a schematic diagram of the apparatus used in preparing v"=38. This SEP-LIF experiment prepared $I_2(X; v"=38)$ for subsequent analysis by $I_2(D; v'=5$ to 12). A single Nd:YAG (Quanta Ray DCR-2) operating at 20 Hz was used to generate both the *pump* and *dump* laser pulses. The *pump* laser was the frequency doubled Nd:YAG output at 532 nm which pumped a dye laser (PDL-1) that was tuned to the $B \leftarrow X$, 7-2, R(47) line at 620.46 nm. The dye laser grating operated fourth order at 24819 with a sulforhodamine 640 dye. An intracavity air-spaced etalon produced a *pump* laser linewidth of $\Delta v_p \approx 0.04$ cm^{-1}. The Nd:YAG fundamental was isolated in the prism harmonic separator (PHS) stimulating emission of the $B \rightarrow X$, 7-38, P(49) line at 1064.55 nm. After expanding the fundamental beam, an optical path temporally delayed the dump beam 10 ns after the pump laser. Due to the long distance that the *dump* beam was required to traverse (25 ft), a Gaussian beam expander was employed to maintain beam integrity. With the relatively high power (60 mJ/pulse) being utilized, the fundamental
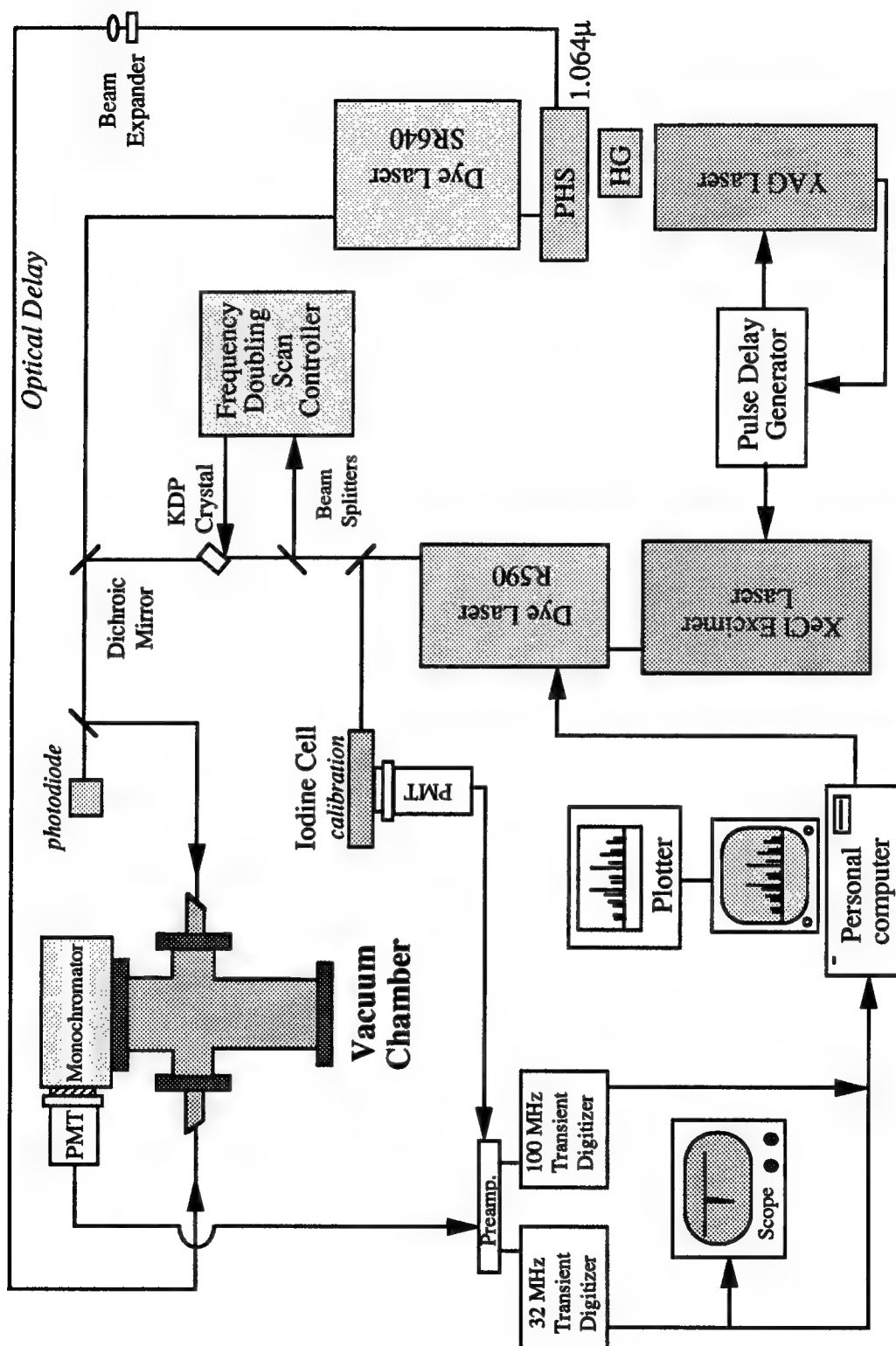
Figure 3.10: Experimental Apparatus for Stimulated Emission Pumping of $I_2(X;v''=38)$

beam was enclosed in 3-inch diameter PVC tubing. With the dump beam being invisible, an infrared display card was used for alignment, monitoring beam shape and size, and detecting Fresnel back reflections from the optics. A plano-convex lens with a 1000 mm focal length focused the fundamental beam into the sample chamber.

The probe laser was a Lambda-Physik (FL3002E, R6G) dye laser operating with an intra-cavity etalon. The output of the dye laser was frequency doubled by continuously matching the KDP phase angle with an autotracker as the probe laser was scanned. Absolute wavenumber calibration of the probe laser was achieved by directing a portion of the fundamental beam through an I_2 cell and simultaneously recording the B-X absorption spectra. Wavenumbers for the B-X lines were taken from the iodine atlas of Gerstenkorn and Luc.[17] A dichroic mirror combined the *pump* and *probe* beams counterpropagating to the *dump* beam in the sample chamber. Once again, conditions were determined under which diffusion effects out of the *probe* beam did not influence the results. Ideally, making the *probe* beam substantially larger than the *dump*, and in turn, both larger than the *pump* would have eliminated any concern. However, this was not feasible with our experimental apparatus.

The delay between laser pulses was measured by a fast silicon photodetector with a rise time of less than 200 ps. Since the wavelength range of the photodetector was from 350 to 1100 nm, recording the probe pulse required removing the Schott UV transmitting black glass filter and measuring the delay with the undoubled laser output. The delay for each scan was captured by the 100 Mhz transient digitizer. The output was recorded on

an HP7404 plotter using the *SIGNAV* program. The delay was then calculated by measuring the distance (channels) between peaks and multiplying the channels by 10 (each channel represented a 10 ns segment). Delay between the *dump* and *probe* pulses was controlled as shown in Figure 3.11.

In finding a *pump* level which was resonant with the *dump* Nd:YAG fundamental, an extensive survey of R-lines surrounding 1064.1 nm (literature value for line center) was undertaken. Even with the broad fundamental linewidth of $\Delta v_D \approx 1.0$ cm^{-1} , the search for resonant transitions was non-trivial. In order to speed the quest, vibrationally excited $I_2(X)$ was prepared by $I_2 + I^*$ energy transfer (see Chapter 4). The Nd:YAG fundamental pumped the vibrationally excited iodine and dispersed fluorescence spectra were recorded. The results of this search are shown in Figure 3.12. The information provided in this spectrum was twofold. First, it provided positive conformation that a resonant transition with the Nd:YAG fundamental existed between the vibrationally excited levels of the ground state and $I_2 B$. Second, a rough approximation on which vibrational transitions to probe was obtained.

The line center for our Nd:YAG DCR-2 was approximately 1064.55 nm. There are six resonant transitions possible with this line-center (cf Table A.1) As a point of interest, W. Ubachs et al.[18] used a frequency-doubled Nd:YAG for studying the $E(0_g^+)$ ion-pair state of iodine. They reported a line center of 18788.39 cm^{-1} (1064.49 nm fundamental) using a Quanta-Ray GCR-3 injection seeded Nd:YAG laser.
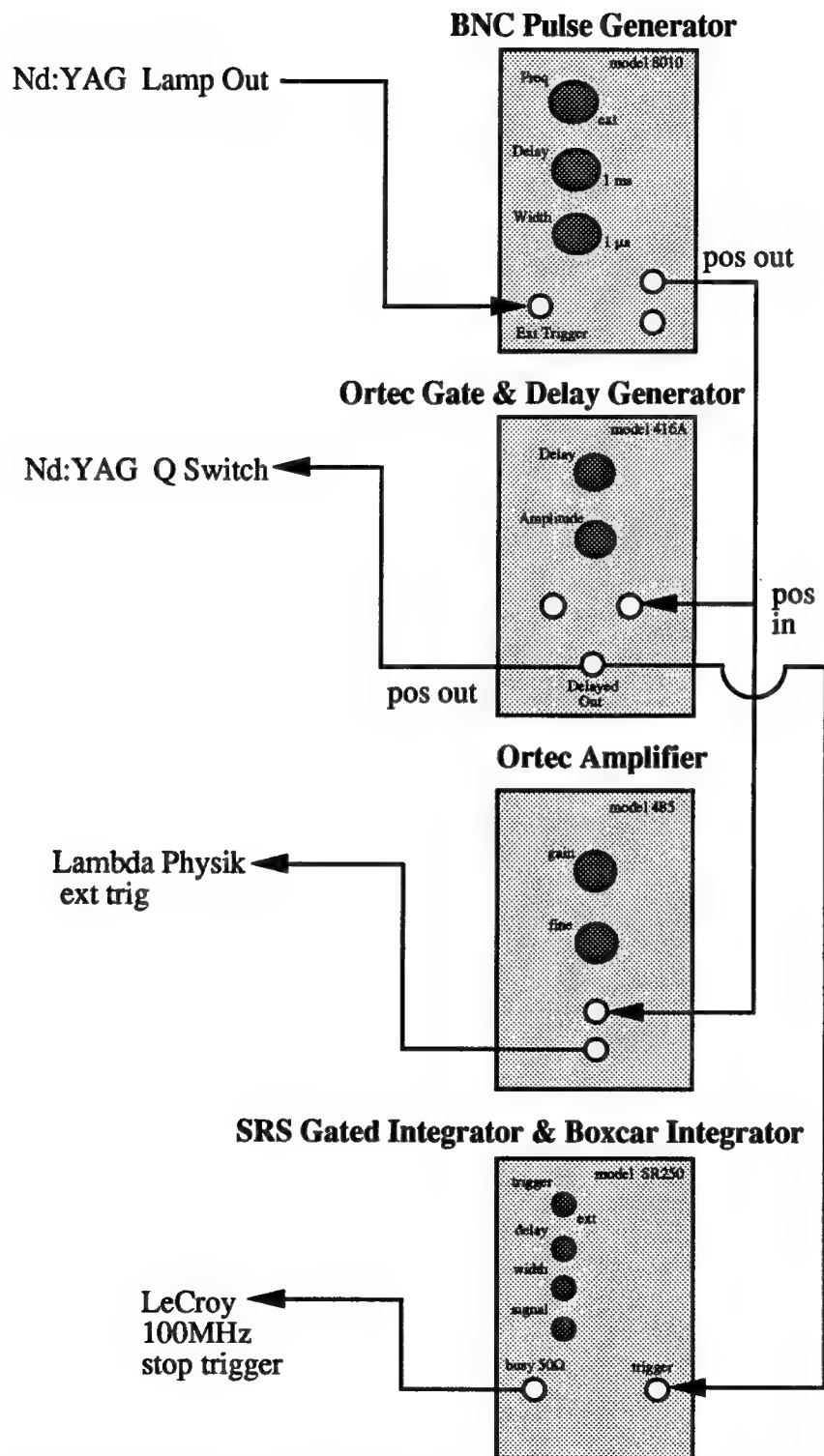
Figure 3.11: Delay Pulse Generator for Two Laser Triggering
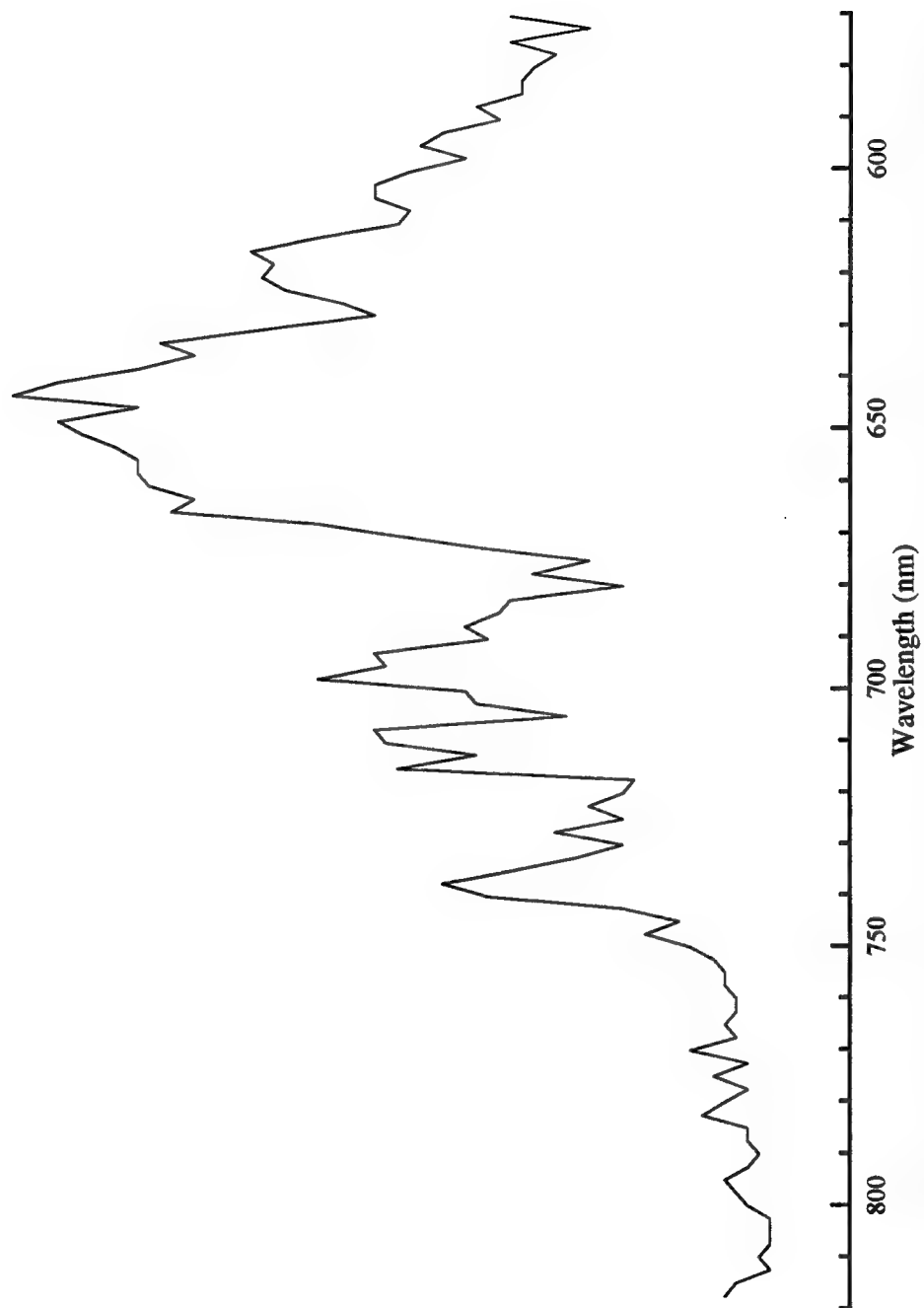
Figure 3.12: Dispersed Fluorescence of $I_2\dagger + I^*$ System with 1.064μ Nd:YAG

In first detecting the SEP-LIF signal, the *pump* laser of the SEP-LIF apparatus was pressure scanned onto successive R-lines of the I_2 *B-X* absorption spectrum while the *probe* laser was scanned until a SEP signal was observed. Pressure tuning of the *pump* laser onto the resonant line was accomplished in conjuction with the *LASER* program, which monitored the cavity pressure and the I_2 *B-X* absorption signal. The *pump* laser was pressure tuned onto resonance by slowly increasing cavity pressure until the desired wavelength was reached as indicated by the I_2 *B-X* absorption spectrum while the monochromator fixed at 634 nm. The *B-X* absorption spectra with the pump transition labeled is shown in Figure 3.13.

However, while the cavity was locked on the appropriate frequency, the pressure cavity box of PDL-1 slowly leaked and the frequency of the *pump* laser drifted. Efforts were made to adjust the grating and tilt angle of the etalon to ambient conditions as much as possible. In addition, a ballast task was added to the pressure system to reduce fluctuation inside the cavity. But the *pump* laser still required retuning after approximately four scans. In order to determine if the pump laser could be operated without an etalon, scans were made with and without the etalon as shown in Figure 3.14. The proximity of other near-coincident resonant transitions required the narrower line-width provided by the etalon and pressure tuning, so the *pump* laser was retuned as required. After tuning the two lasers to resonance, the monochromator was set at 328 nm and the SEP-LIF spectra recorded.
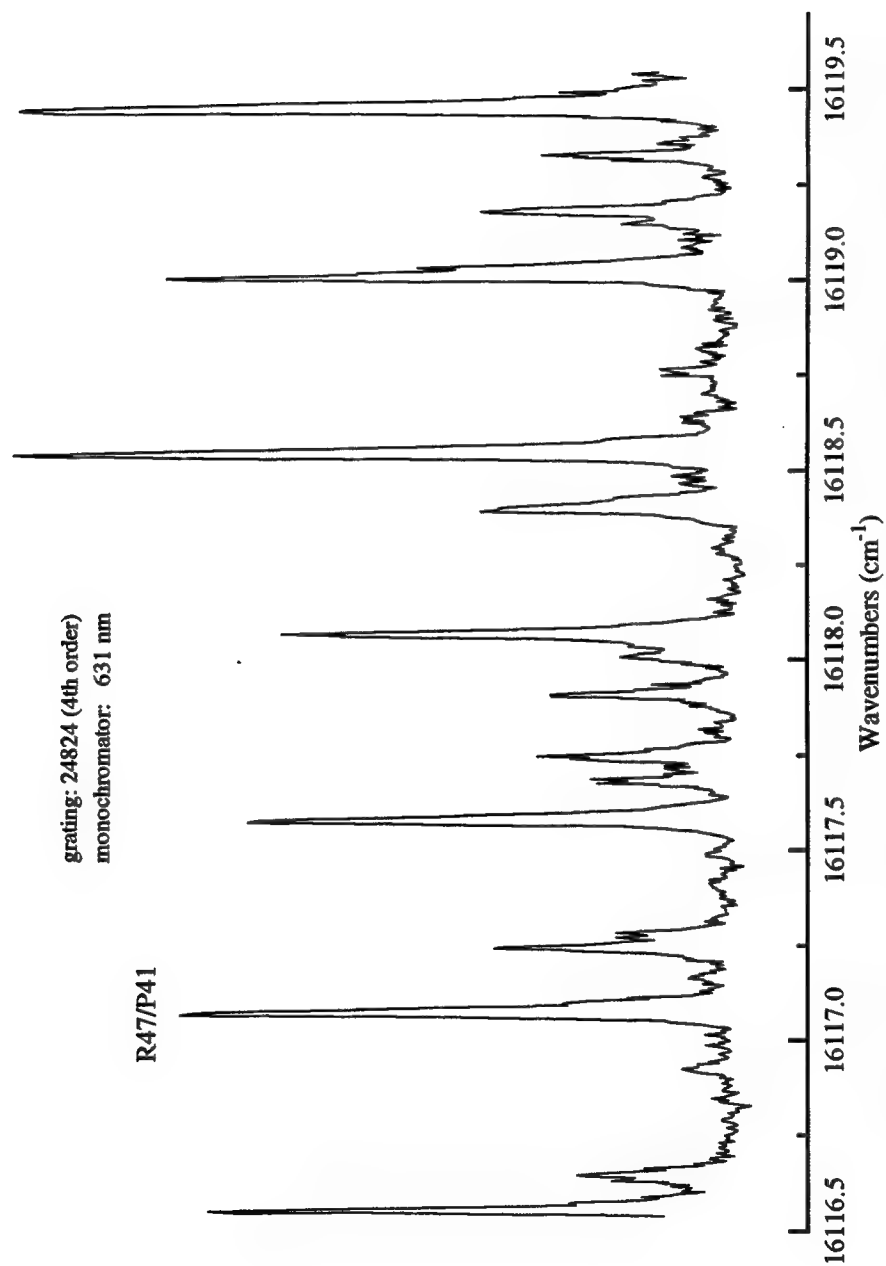
Figure 3.13: LIF Spectrum of I_2 $B \leftarrow X$, $v''=2$ Obtained Through Pressure Tuning the Pump Pulsed Dye Laser.
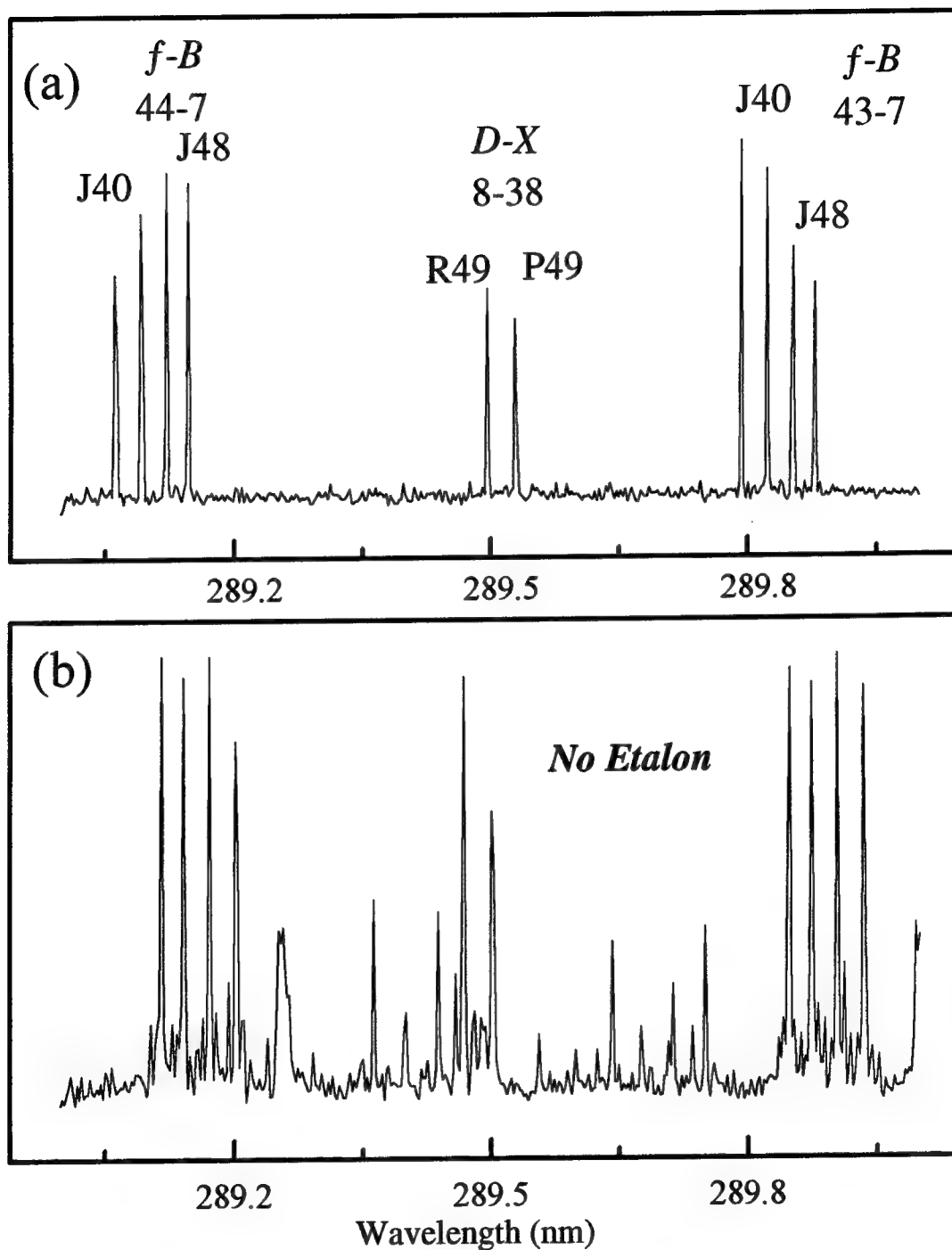
Figure 3.14: Comparison of Low Resolution SEP Spectra with
D-X and f-B transitions Showing Effects of the
Pump Laser (a) With and (b) Without Etalon.

§3.3.4.3 SEP v"=23

The experimental apparatus for stimulated emission pumping of v"=23 is shown in Figure 3.15. The *pump* dye laser (Lambda Physik Lextra 200, FL3001, R560) was tuned to the $B \leftarrow X$, 19-1, R(55) line at 569.63 nm. The dye laser was utilized with an intracavity etalon and pressure-tuning to achieve a pump laser linewidth of $\Delta v_p \approx 0.04$ cm^{-1}. The *dump* dye laser (Quanta Ray DCR-2, PDL-1, LDS 751) stimulated emission of the $B \rightarrow X$, 19-23, P(57) line at 758.16 nm. The *probe* dye laser (Lambda Physik EMG-101, FL3002E, C500 with 0.07 m/l DABCO) observed D-X lines originating from the initially prepared and collisionally populated levels. The output of the *probe* laser was doubled by a BBO crystal whose phase matching angle was continuously tuned with an autotracker. A Schott UV transmitting black glass filter separated the fundamental dye laser from the frequency doubled output. A dichroic mirror combined the *pump* and *dump* beams counterpropagating to the *probe* beam. The three laser beams were aligned (overlap) in the iodine chamber for maximum signal intensity. Delay between the *pump*, *dump*, and *probe* pulses was controlled by a convoluted triggering apparatus. Since both Lambda-Physik excimer lasers required a triggering pulse 1-1.2 µs before firing, the flash lamp sync output of the Nd:YAG laser provided the initial trigger. A BNC pulse generator was used to delay the flash lamp sync output. After triggering the excimer lasers, the Q switch would be triggered. The laser light pulse followed 50 ns after the Q-switch trigger. Figure 3.16 gives the schematic of the delay pulse generator for three laser operation.
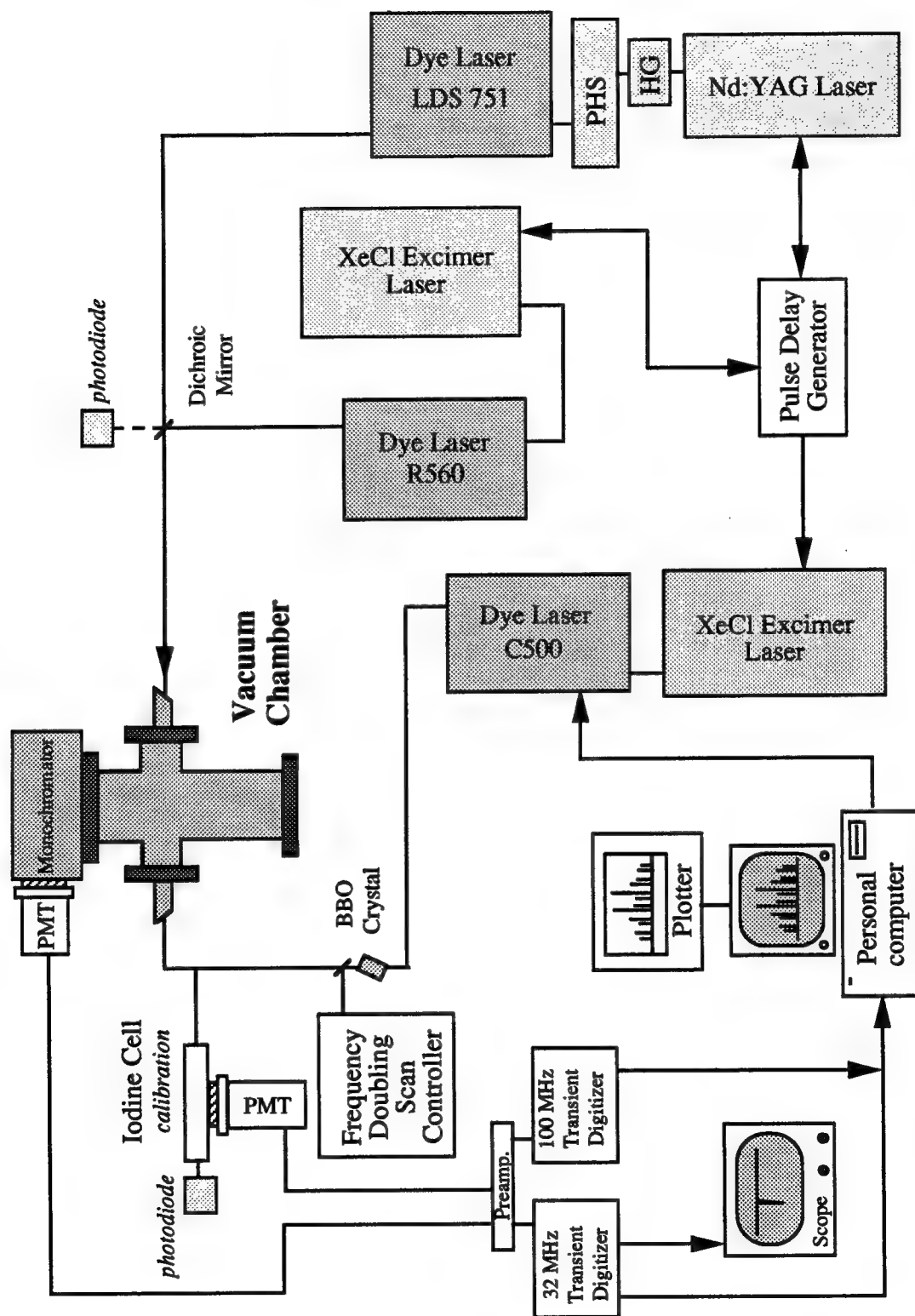
Figure 3.15: Experimental Apparatus for Stimulated Emission Pumping of $I_2(X, v''=23)$

BNC Pulse Generator

Nd:YAG Lamp Out

Lambda Physik
ext trig
probe laser

Ortec Gate & Delay Generator

pos out

SRS Gated Integrator & Boxcar Integrator

ext trig

Lambda Physik
Lextra 200
pump laser

sync out

Ortec Amplifier

Nd:YAG Q Switch
dump laser
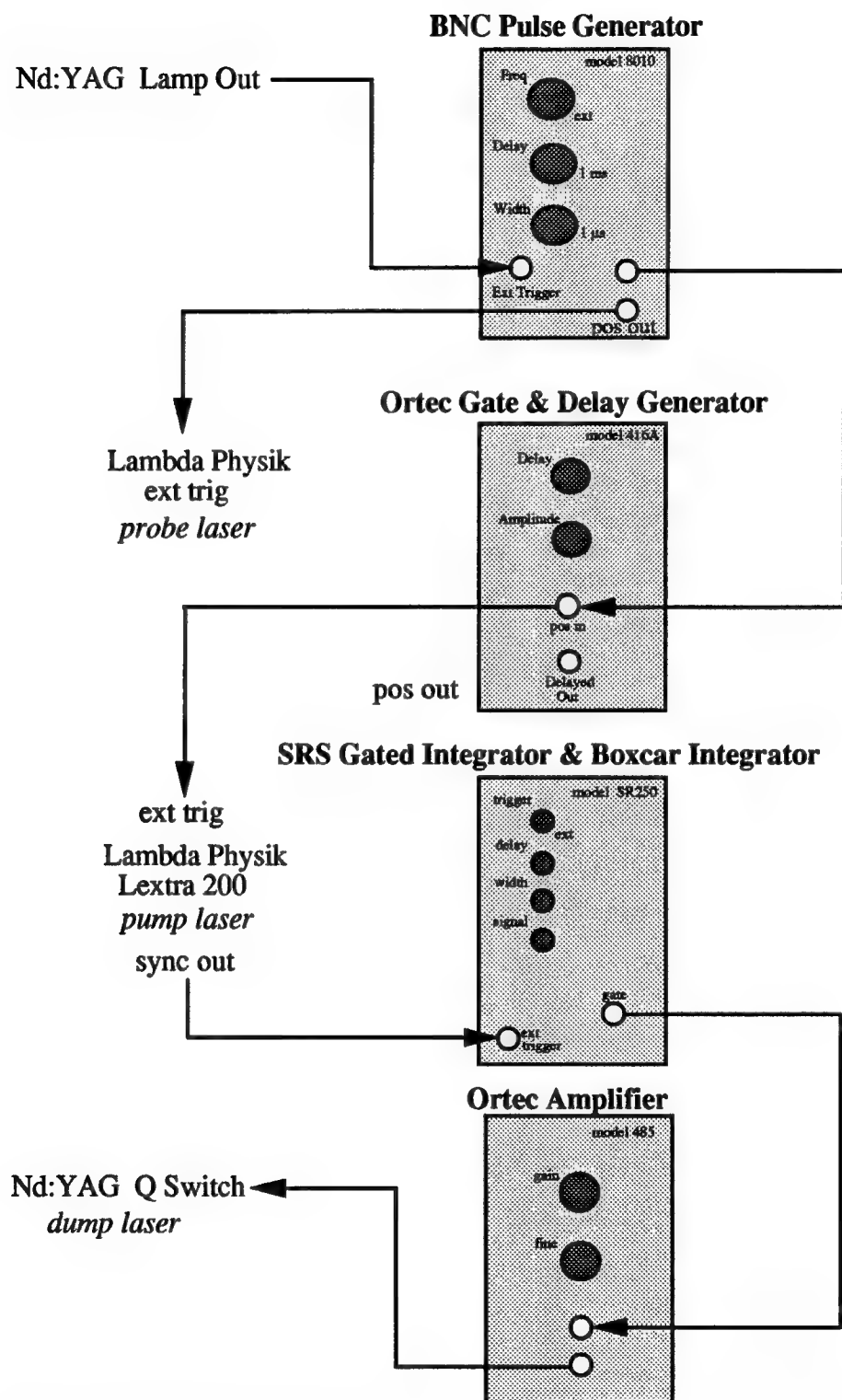
Figure 3.16: Delay Pulse Generator for Three Laser Triggering

The *pump* laser grating was set to 562.98 nm. With the monochromator fixed at 601 nm, the wavelength resolved fluorescence spectrum was obtained by pressure scanning the *pump* laser and is shown in Figure 3.17. The etalon was aligned and the grating was pressure-tuned onto resonance by slowly increasing cavity pressure until the desired wavelength as indicated by the I_2 *B-X* absorption spectrum. Using the *LASER* program to monitor the pressure scan, the cavity of the *pump* dye laser was locked at the appropriate pressure.

The *dump* dye laser was pumped by the Nd:YAG second harmonic at 532 nm and the grating operated third order at 22746 with LDS 751 dye. Due to the long distance that the *dump* beam was required to traverse (18 ft), a Gaussian beam expander was employed to maintain beam integrity. With the *dump* and *pump* beams combined, the monochromator was fixed at 319 nm while the *probe* dye laser was tuned to resonance.

§3.4 REFERENCES

1. J. Peter Toennies, *Ann. Rev. Phys. Chem.* **27**, 225 (1976).

2. Michael J. McQuaid, *Spectroscopic Characterization of Metal-Based Complexes and Metal-Based Complex Oxidation Processes*, Dissertation, Georgia Institute of Technology, Atlanta (1989).

3. Yaomin Lin, *Spectroscopic and Dynamic Studies of Br₂ and Open-Shell van der Waals Complexes*, Dissertation, Emory University, Atlanta (1991).

4. Xiaonan Zheng, *Laser Spectroscopy of Metastable and Transient Species*, Dissertation, Emory University, Atlanta (1993).

5. Suli Fei, Xiaonan Zheng, Michael C. Heaven, and Joel Tellinghuisen, *J. Chem. Phys.* **97**, 6057 (1992).
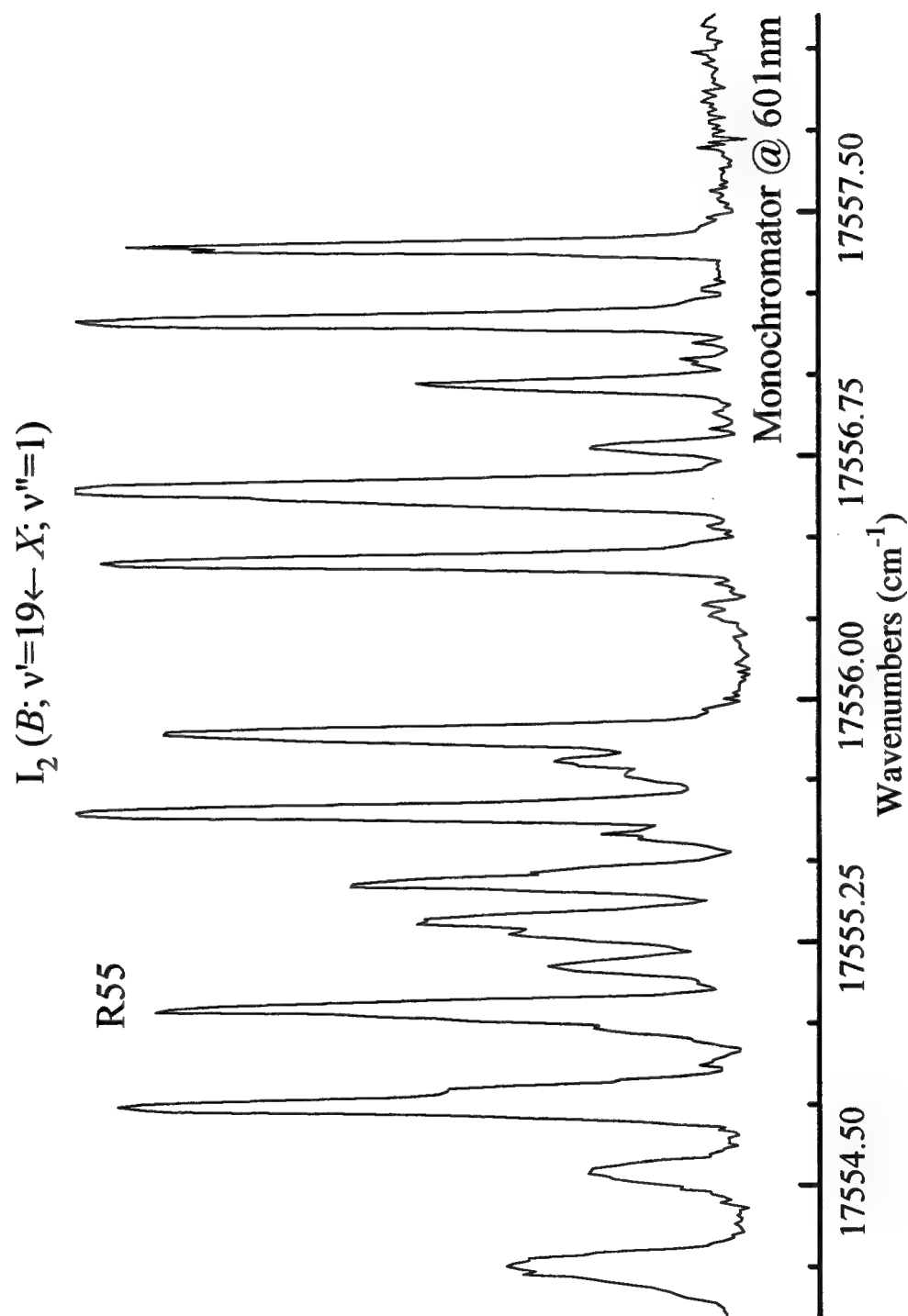
Figure 3.17: Pressure Scan of Iodine with the Pump Dye Laser

6. C. Kittrell, E. Abramson, J. L. Kinsey, S. A. McDonald, D. E.Reisner, R. W. Field and D. H. Katayama, *J. Chem. Phys.* **75,** 2056 (1981).

7. C. E. Hamilton, J. L. Kinsey, and R. W. Field, *Ann. Rev. Phys. Chem.* **37,** 493 (1986).

8. X. Yang and A. M. Woddtke, *J. Chem. Phys.* **92,** 116 (1990).

9. H. Chun, H. Ruiping, and Z. Cunhao, *Appl. Phys. B* **41,** 251 (1986).

10. M. L. Nowlin and M. C. Heaven, *J. Chem. Phys.* **99,** 5654 (1993).

11. J. Tellinghuisen, *Chem. Phys. Lett.* **99,** 373 (1983).

12. *Optics and Filters,* Oriel Corp.,Vol. III Catalog , Stratford, CT (1990).

13. *Light Sources, Monochromators and Detection Systems,* Oriel Corp.,Vol. II Catalog , Stratford, CT (1990).

14. DCR - Diffraction Coupled Resonator

15. R. Treba and T. Koch, *Chem. Phys. Lett.* **93,** 315 (1982).

16. C. Hampel, *The Encyclopedia of the Elements,* Reinhold, New York (1968).

17. S. Gerstenkorn and P. Luc, *Atlas du Specter d'Absorption de la Molecule d'Iode,* Laboratoire Aime Cotton, CNRS II, Orsay, France (1977).

18. W. Ubachs, I. Aben, J.B. Milan, G. J. Somsen, A. G. Stuiver, and W. Hogervorst, *Chem. Phys.* **174,** 285 (1993).

Chapter 4

REANALYSIS OF THE *D-X* SYSTEM AND I*+ I$_2$ ENERGY TRANSFER

Chapter 4 examines vibrationally excited I$_2$(X) in which the vibrationally excited

molecule was prepared either in a free-jet expansion of I$_2$Ar$_n$ clusters or by E→V energy

transfer between I$_2$(X) + I(^{2}P$_{1/2}$). Highly excited vibrational levels of I$_2$ (X; 23<v"<48)

were prepared by energy transfer between

$$I_2(X) + I(^2P_{1/2}) \rightarrow I_2(X; 23<v"<48) + I(^2P_{3/2})$$
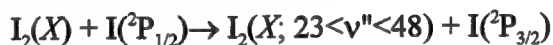
and then characterized by UV excitation to the I$_2$ $D(0^+_u)$. Analysis of this data revealed

an error in the energy predicted from the spectroscopic constants for the low vibrational

levels of the $D(0^+_u)$ ion-pair state of approximately 2 cm^{-1}. Improvement of the $D(0^+_u)$

state spectroscopic constants was necessary before any reliable population distribution

could be inverted from the spectra. For example, an error of 2 cm^{-1} would mean the

difference of approximately four peaks in the highly congested I$_2$(X) + I(^{2}P$_{1/2}$) system.

Therefore, the free-jet expansion experiment was undertaken as a means of obtaining

uncongested I$_2$ *D-X* data for spectroscopic analysis. Section §4.1 includes improved

spectroscopic constants for I$_2$D(0^+_u) as well as the analysis of the data. In determining

the $D(0^+_u)$ constants, all applicable spectroscopic data from the *D-X* experiments

performed in this dissertation were included. Section §4.2 discusses the

photofragmentation of I$_2$Ar$_n$ clusters in preparing the vibrationally excited level I$_2$(X,

v"=40) and presents the analysis and results. Section §4.3 vividly illustrates the necessity

of accurate spectroscopic constants. The nascent vibrational distribution of $I_2(X) +$ $I(^2P_{1/2})$ was examined using pulsed laser photolysis . Rotationally resolved spectra for the D-X system were recorded producing dense spectroscopic spectra. The density of states in this experiment require the predictions of the spectroscopic constants to within ± 0.04 cm^{-1} for the inversion of line intensity data.

§4.1 SPECTROSCOPIC CONSTANTS FOR I_2 $D(0^+_u)$

The molecular constants of Ishiwata and Tanaka[1] were reported with a standard deviation of 0.052 cm^{-1} for $76 \leq v' \leq 124$ and 0.31 cm^{-1} for $v' < 76$. During the analysis of the $I_2(X) + I(^2P_{1/2})$ energy transfer data (Section §4.3), attention was drawn to the spectroscopic constants for the $D(0^+_u)$ ion-pair state when the existing electronic term energy and vibrational constants did not accurately predict the band origins of transitions terminating on low vibrational levels of the $D(0^+_u)$ state.

The large mass of iodine and the shallow potential energy curves of the ion-pair states result in large densities of discrete levels. The profuse profile of the laser excitation spectra for iodine means that even relatively small errors may lead to erroneous assignments. Combination differences analysis of the energy transfer spectra indicated a 2 cm^{-1} discrepancy for the low-lying vibrational levels of the D state. The analysis by combination differences ($\Delta_2 F$) was accomplished using the following equations:

$$\Delta_2 F'' = R(J-1)-P(J+1) = 4B_{v'}(J+1/2)$$

$$\Delta_2 F' = R(J)-P(J) = 4B_v(J+1/2)$$

Plotting Δ_2F versus J gave a line with slope $4B_v$ passing through point (0,-1/2). While this systematic approach for the rotational analysis confirmed the assignment and accuracy of the rotational constants, line positions were not in agreement with predictions. In order to improve the quality of the fit, vibrational energies using Ishiwata and Tanaka[1] values for $76 \leq v \leq 124$ were combined with our data at low v. Vibrational term energies for the D state were calculated by adding the ground state vibrational energies to the fitted band origins. Initially, a fifth order polynomial[2] was fit to this data set and used for predicting line positions in the energy transfer data. Numerous Fortrat parabolas from v'=5 to 9 were generated from the $I_2(X) + I(^2P_{1/2})$ data. However, the dense rovibrational structure and low J intensity near the bandhead made this process non-trivial. An example of a successful fit of the energy transfer data to the Fortrat parabola is shown in Figure 2.5.

In an effort to improve the spectroscopic ground work, first, a free-jet expansion was conducted as detailed in Section §4.1. Then the free-jet and energy transfer line position data were combined with SEP-LIF spectra. Because SEP-LIF spectroscopy is a triple resonance method, assignment of the spectrum is greatly simplified. The addition of diluent gases produced satellite bands induced by collisions with the SEP prepared level. Assignments of the collisionally populated lines were straightforward due to the rigorous even $\Delta J = \pm 2n$ selection rule for transfer between the levels of a homonuclear diatomic. Spectra were recorded for the D-X bands for $(X;v''=38 \rightarrow D;4 \leq v' \leq 11)$ and $(X;v''=23 \rightarrow D;30 \leq v' \leq 37)$. Line positions were extracted from the energy transfer

spectra and the band origins were obtained from Fortrat parabolas. Table 4.1 lists the

vibrational energies and range of J values associated with these measurements. When

sufficient line positions were not available, I simply extracted the band origins using

existing rotational constants. This procedure was necessary for $v'=11, 30, 31, 36$ and 37.

Band origins and rotational constants were also obtained by fitting the line positions to

the expression

$$v=v_0+B'_v J'(J'+1)-B''_v J''(J''+1) \qquad 4.1$$

(trial fits to an expression that included the centrifugal distortion constants did not yield

statistically significant values for these parameters for J<60). Once again, the lower

state rotational constants were found to be in good agreement with those obtained by

Bacis et al.[3] and Tellinghuisen et al.[4] As these studies were of greater precision than our

measurements, the final fits to Equation 4.1 were made with the lower rotational

constants fixed at the values given by Bacis et al.[3]

The methodology in developing an improved global fit for the $D(0^+_u)$ ion-pair

state was to combine our analysis from the energy transfer, free-jet, and SEP-LIF

experiments for $v'=4$ to 11 and $v'=30$ to 37 with the vibrational energies from: Ishiwata

and Tanaka[1] for $76 \leq v \leq 124$; Bartels et al.[5] for $125 \leq v \leq 201$; and Hoy and Lipson[6] for

$202 \leq v \leq 290$. A least-squares analysis was performed on the combined data set using

the matrix formulation

$$\beta=(X^TWX)^{-1}X^TWy$$

Table 4.1: Wavenumbers (cm^{-1}) of Vibrational Energies for
I$_2$ $D(0^+_u)$ Calculated from Fortrat Parabolas with
Uncertainties, and Range of Measured J Values

v'	υ (cm^{-1})[a]	$\pm\delta$ (cm^{-1})	J
4	41451.971	0.15	23-55
5	41545.835	0.13	21-99
6	41639.559	0.13	19-87
7	41733.007	0.14	36-96
8	41826.277	0.08	7-90
9	41919.192	0.13	19-99
10	42011.985	0.13	23-61
11	42104.469	0.14	49
30	43810.369	0.14	57
31	43897.365	0.14	57
32	43984.051	0.11	33-63
33	44070.471	0.09	17-67
34	44156.549	0.09	17-95
35	44242.345	0.11	21-89
36	44327.845	0.14	57
37	44413.091	0.14	57

[a] Determined by adding the ground state vibrational energies of Bacis et al.[3] to the fitted band origins.

where β is the vector of m parameters to be estimated (m is the degree of the polynomial fit), W is the weight matrix, X is the n x m matrix of independent variables $\{(v+1/2)^m\}$ (n is the number of variables to fit), X^T is the transpose of X, and y is a 1D array containing the vibrational term energies. The size of the polynomial expansion was determined by increasing the order until the lowest standard deviation was obtained. The most accurate fit was achieved with a seventh order polynomial (m=7). W was weighted as the inverse of the standard deviation squared. The results are presented in Table 4.2 and for completeness, I have included Tanaka's Dunham rotational parameters. The solution for the entire matrix formulation presented herein is provided in Appendix A. The molecular constants in Table 4.2 were used to construct an RKR potential curve for v'=0 to 280 of the $D(0^+_u)$ ion-pair state as listed in Table 4.3.

The estimated variance is obtained by

$$\sigma^2 = \sum_{k=1}^{n} \frac{\delta_k^2}{n-m} = \frac{(y-X\beta)^T W (y-X\beta)}{n-m}$$

The estimated variances of the parameters as given by the variance-covariance matrix is

$$V = \sigma^2 (X^T W X)^{-1}$$

and the standard deviation of parameter β can be obtained as $\sqrt{V}$. The standard deviation of the global fit is 0.362 cm^{-1}, while the standard deviation for the fit from v'=0 to 124 is 0.032 cm^{-1}. Statistical errors from the least-squares fit for the vibrational energy and the residuals for the new $D(0^+_u)$ constants are shown in Figure 4.1. When the new term energies are compared with the energies predicted using the constants of

Table 4.2: Dunham Parameters[a,c] of the $D(0^+_u)$ of the Ion-Pair State of I_2

$$Y_{00} = 41026.166\ (291)$$

$$Y_{10} = 95.11746327\ (037)$$

$$Y_{20} = -0.111495227\ (001)$$

$$Y_{30} = -5.792874546 \times 10^{-4}$$

$$Y_{40} = 4.205281828 \times 10^{-6}$$

$$Y_{50} = -1.408244378 \times 10^{-8}$$

$$Y_{60} = 2.68736882 \times 10^{-11}$$

$$Y_{70} = -2.3114805 \times 10^{-14}$$

$$Y_{01}{}^{b} = 0.0207149(64)$$

$$Y_{11}{}^{b} = -4.374(38) \times 10^{-5}$$

$$Y_{21}{}^{b} = -8.99(79) \times 10^{-8}$$

$$Y_{31}{}^{b} = 6.58(48) \times 10^{-10}$$

$$Y_{02}{}^{b} = -4.93(27) \times 10^{-9}$$

[a] Coeffients are based on gobal refit of Ishiwata and Tanaka, *Laser Chem.* **7** ,79(1987) using levels of v'= 74 through 124; Bartels et al., *J. Chem. Phys.* **91**, 12 (1989) using data for levels v'= 125 through 201; and Hoy and Lipson, *Chem. Phys.* **140**, 187 (1990) for levels v'= 202 through 285; with data from SEP-LIF experiments for levels v'= 4 through 11 and v'= 30 through 37.

[b] Dunham parameter from T. Ishiwata and I. Tanaka, *Laser Chem.* **7** , 79(1987).

[c] The rovibrational energy levels are determined from the Dunham polynomial expansion:

$$T_{vj} = \sum_{n,k} Y_{nk}(v + \tfrac{1}{2})^n J^k (J+1)^k$$

Table 4.3:   RKR Potential Curve for I$_2$ $D(0^+_u)$

v	$T_v(cm^{-1})$	$B_v(cm^{-1})$	R_{min}	R_{max}	v	$T_v(cm^{-1})$	$B_v(cm^{-1})$	R_{min}	R_{max}
0	47.54	0.020693	3.508	3.658	57	5028.54	0.018028	2.981	4.709
1	142.43	0.020649	3.458	3.717	58	5107.47	0.017980	2.978	4.723
2	237.10	0.020605	3.424	3.759	59	5186.09	0.017932	2.974	4.737
3	331.53	0.020561	3.397	3.794	60	5264.41	0.017885	2.970	4.751
4	425.73	0.020516	3.374	3.825	61	5342.43	0.017838	2.967	4.765
5	519.69	0.020472	3.355	3.853	62	5420.14	0.017790	2.963	4.779
6	613.41	0.020427	3.337	3.880	63	5497.56	0.017743	2.959	4.792
7	706.86	0.020382	3.320	3.904	64	5574.68	0.017696	2.956	4.806
8	800.12	0.020337	3.306	3.927	65	5651.50	0.017649	2.952	4.820
9	893.09	0.020292	3.292	3.950	66	5728.02	0.017602	2.949	4.864
10	985.83	0.020246	3.278	3.971	67	5804.24	0.017555	2.946	4.848
11	1078.30	0.020201	3.266	3.992	68	5880.16	0.017508	2.943	4.862
12	1170.52	0.020155	3.254	4.012	69	5955.78	0.017461	2.940	4.875
13	1262.48	0.020110	3.244	4.032	70	6031.10	0.017415	2.936	4.889
14	1354.18	0.020064	3.233	4.051	71	6106.13	0.017368	2.933	4.903
15	1445.61	0.020018	3.223	4.070	72	6180.86	0.017322	2.930	4.917
16	1536.78	0.019972	3.214	4.088	73	6255.29	0.017275	2.927	4.930
17	1627.68	0.019925	3.204	4.106	74	6329.43	0.017229	2.924	4.944
18	1718.32	0.019879	3.196	4.123	75	6403.27	0.017183	2.921	4.958
19	1808.67	0.019833	3.187	4.141	76	6476.81	0.017137	2.918	4.972
20	1898.76	0.019786	3.179	4.158	77	6550.06	0.017091	2.915	4.986
21	1988.57	0.019739	3.171	4.175	78	6623.02	0.017045	2.912	4.999
22	2078.11	0.019693	3.163	4.192	79	6695.68	0.017000	2.909	5.013
23	2167.36	0.019646	3.156	4.208	80	6768.05	0.016954	2.906	5.027
24	2256.34	0.019599	3.148	4.225	81	6840.13	0.016909	2.903	5.040
25	2345.03	0.019552	3.142	4.241	82	6911.90	0.016864	2.900	5.054
26	2433.44	0.019505	3.135	4.257	83	6983.41	0.016819	2.897	5.068
27	2521.57	0.019458	3.128	4.272	84	7054.60	0.016774	2.895	5.082
28	2609.41	0.019410	3.121	4.288	85	7125.53	0.016729	2.892	5.096
29	2696.96	0.019363	3.115	4.304	86	7196.16	0.016684	2.889	5.109
30	2784.22	0.019316	3.109	4.319	87	7266.50	0.016640	2.886	5.123
31	2871.20	0.019268	3.103	4.334	88	7336.55	0.016596	2.884	5.137
32	2957.88	0.019221	3.097	4.350	89	7406.32	0.016551	2.881	5.151
33	3044.28	0.019173	3.091	4.365	90	7475.80	0.016508	2.878	5.164
34	3130.38	0.019126	3.086	4.380	91	7545.00	0.016464	2.876	5.178
35	3216.18	0.019078	3.080	4.395	92	7613.91	0.016420	2.873	5.192
36	3301.70	0.019031	3.075	4.409	93	7682.53	0.016377	2.870	5.206
37	3386.92	0.018983	3.069	4.424	94	7750.88	0.016334	2.868	5.220
38	3471.84	0.018935	3.064	4.439	95	7818.95	0.016291	2.865	5.234
39	3556.47	0.018887	3.059	4.454	96	7886.73	0.016248	2.863	5.247
40	3640.79	0.018840	3.054	4.468	97	7954.24	0.016205	2.860	5.261
41	3724.83	0.018792	3.049	4.483	98	8021.46	0.016163	2.858	5.275
42	3808.56	0.018744	3.044	4.497	100	8155.08	0.016079	2.853	5.303
43	3892.00	0.018696	3.040	4.511	102	8287.59	0.015995	2.843	5.330
44	3975.13	0.018648	3.035	4.526	104	8419.01	0.015913	2.838	5.358
45	4057.97	0.018601	3.030	4.540	106	8549.33	0.015831	2.833	5.386
46	4140.50	0.018553	3.026	4.554	108	8678.58	0.015751	2.828	5.414
47	4222.74	0.018505	3.022	4.569	110	8806.75	0.015671	2.824	5.441
48	4304.68	0.018457	3.017	4.583	112	8933.85	0.015593	2.819	5.469
49	4386.31	0.018409	3.013	4.597	114	9059.89	0.015515	2.814	5.497
50	4467.64	0.018361	3.009	4.611	116	9184.88	0.015439	2.810	5.525
51	4548.68	0.018314	3.005	4.625	118	9308.83	0.015364	2.833	5.553
52	4629.41	0.018266	3.001	4.639	120	9431.75	0.015290	2.805	5.581
53	4709.84	0.018218	2.997	4.653	122	9553.63	0.015217	2.800	5.609
54	4789.98	0.018170	2.993	4.667	124	9674.51	0.015145	2.796	5.637
55	4869.79	0.018123	2.989	4.681	126	9794.37	0.015075	2.791	5.665
56	4949.32	0.018075	2.985	4.695	128	9913.23	0.015006	2.787	5.693

Table 4.3: RKR Potential Curve for I$_2$ $D(0^+_u)$ (continued)

ν	T_v(cm^{-1})	B_v(cm^{-1})	R_{min}	R_{max}	ν	T_v(cm^{-1})	B_v(cm^{-1})	R_{min}	R_{max}
128	9913.23	0.015006	2.787	5.693	242	15306.58	0.014205	2.438	7.274
130	10031.10	0.014938	2.782	5.782	244	15381.37	0.014264	2.429	7.300
132	10147.98	0.014872	2.777	5.749	246	15455.61	0.014326	2.419	7.326
134	10263.89	0.014806	2.773	5.777	248	15529.30	0.014391	2.410	7.352
136	10378.83	0.014743	2.768	5.805	250	15602.42	0.014460	2.400	7.378
138	10492.81	0.014681	2.763	5.834	252	15675.00	0.014532	2.390	7.404
140	10605.84	0.014620	2.759	5.862	254	15747.04	0.014607	2.380	7.430
142	10717.94	0.014560	2.754	5.890	256	15818.52	0.014685	2.370	7.456
144	10829.09	0.014503	2.750	5.918	258	15889.47	0.014767	2.360	7.482
146	10939.33	0.014446	2.745	5.947	260	15959.88	0.014852	2.350	7.508
148	11048.65	0.014392	2.741	5.974	262	16029.75	0.014940	2.339	7.533
150	11157.06	0.014339	2.736	6.003	264	16099.08	0.015032	2.328	7.559
152	11264.57	0.014288	2.731	6.031	266	16167.87	0.015128	2.317	7.585
154	11371.20	0.014238	2.726	6.060	268	16236.12	0.015226	2.306	7.610
156	11476.94	0.014190	2.721	6.088	270	16303.83	0.015329	2.295	7.636
158	11581.82	0.014144	2.717	6.116	272	16371.01	0.015435	2.283	7.662
160	11685.82	0.014099	2.712	6.144	274	16437.64	0.015544	2.272	7.687
162	11788.98	0.014057	2.707	6.173	276	16503.73	0.015657	2.259	7.713
164	11891.28	0.014016	2.702	6.201	278	16569.27	0.015774	2.249	7.740
166	11992.75	0.013977	2.696	6.229	280	16634.27	0.015894	2.236	7.764
168	12093.39	0.013940	2.692	6.257					
170	12193.21	0.013905	2.686	6.286					
172	12292.21	0.013872	2.681	6.314					
174	12390.41	0.013841	2.676	6.342					
176	12487.82	0.013812	2.671	6.370					
178	12584.43	0.013785	2.665	6.398					
180	12680.27	0.013760	2.659	6.426					
182	12775.34	0.013738	2.654	6.455					
184	12869.64	0.013717	2.648	6.483					
186	12963.19	0.013699	2.642	6.511					
188	13055.99	0.013682	2.637	6.539					
190	13148.05	0.013669	2.631	6.567					
192	13239.39	0.013657	2.625	6.595					
194	13330.00	0.013648	2.619	6.623					
196	13419.89	0.013641	2.613	6.651					
198	13509.08	0.013637	2.606	6.678					
200	13597.56	0.013635	2.600	6.706					
202	13685.36	0.013635	2.594	6.734					
204	13772.47	0.013638	2.587	6.761					
206	13858.90	0.013643	2.580	6.789					
208	13944.66	0.013651	2.573	6.817					
210	14029.76	0.013662	2.566	6.844					
212	14114.21	0.013675	2.560	6.872					
214	14198.00	0.013690	2.552	6.899					
216	14281.16	0.013709	2.545	6.926					
218	14363.67	0.013730	2.537	6.953					
220	14445.56	0.013754	2.530	6.980					
222	14526.83	0.013780	2.522	7.008					
224	14607.48	0.013810	2.514	7.034					
226	14687.52	0.013842	2.506	7.061					
228	14766.96	0.013877	2.498	7.088					
230	14845.80	0.013915	2.490	7.115					
232	14924.05	0.013956	2.482	7.142					
234	15001.71	0.014000	2.473	7.168					
236	15078.78	0.014046	2.465	7.195					
238	15155.29	0.014096	2.456	7.221					
240	15231.22	0.014149	2.447	7.248					
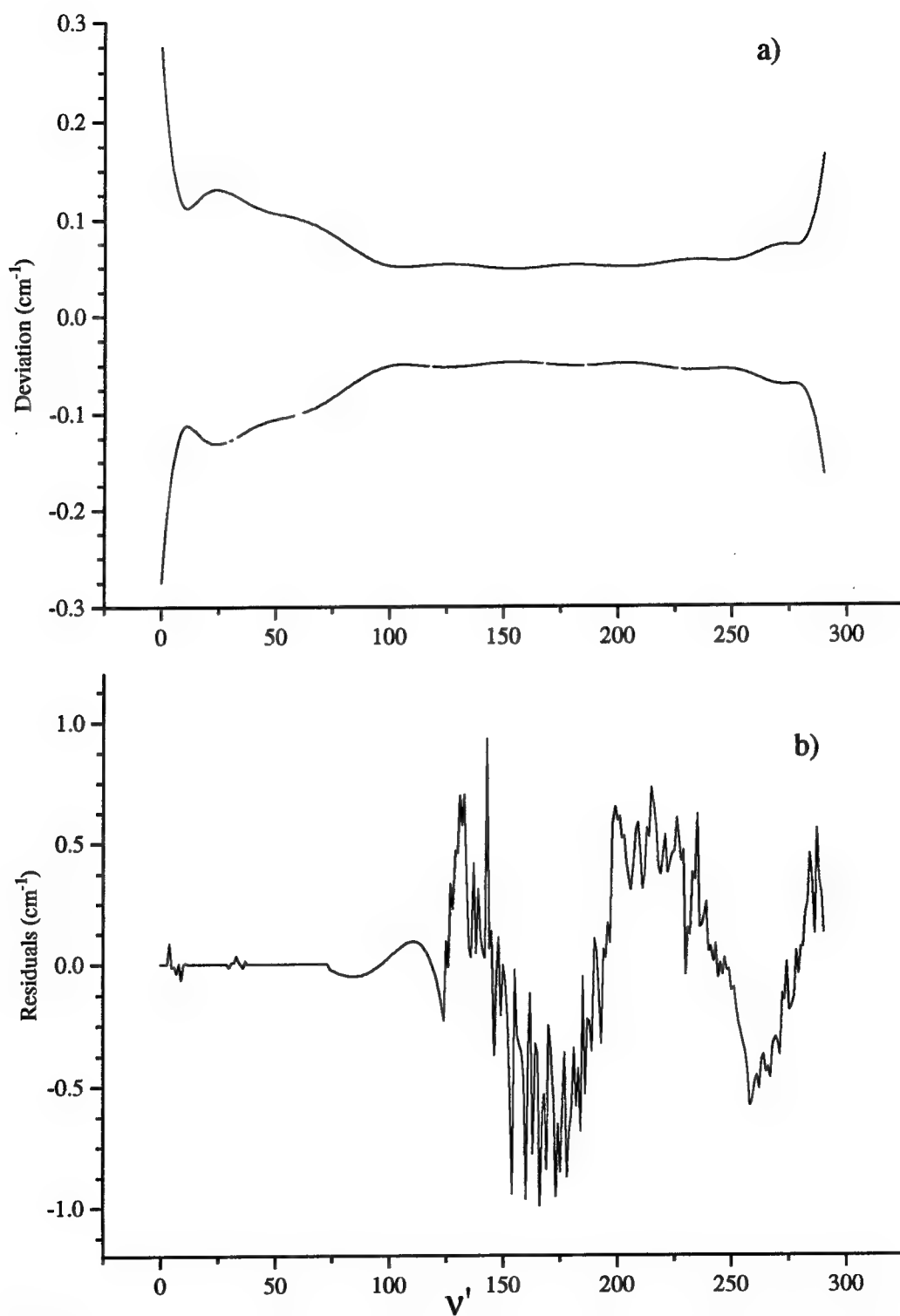
Figure 4.1: a) Statistical Error Band and b) Residuals for Vibrational Energy in I_2 D

Ishiwata and Tanaka, a difference of 0.29 cm^{-1} is noted for $v'=34$. This difference

increases with decreasing v', reaching a value of 1.82 cm^{-1} at $v'=4$.

§4.2 JET COOLING OF THE D-X SYSTEM

The spectra of rotationally cold, vibrationally excited $I_2(D,v'=8 \leftarrow X,v''=40)$ in a

free-jet expansion are shown in Figures 4.2 and 4.3. Free-jet expansion was necessary

because of the congestion of the vibrational and rotational manifolds made assignments

difficult to resolve near the band origin. After supersonic expansion of the gases through

the nozzle, photolysis of the I_2Ar_n cluster ejected vibrationally excited $I_2(X)$ in which the

rotational structure was frozen to a near Boltzmann distribution. The rotational

contours of the high resolution data were consistent with rotational temperatures of

approximately 13°K as shown in Figure 4.4. The rotational temperature can be

calculated using the approximation that the fluorescence intensity (I_J) is proportional to

the number density and given by

$$\ln \frac{I_J}{2J+1} \approx -(\frac{B_v hc}{k_B T_R}) * J(J+1)$$

c = speed of light (2.9979×10^{10} cm/sec)
h = Planck's constant (6.626×10^{-34} J sec)
B_v = Rotational constant ($v'(8)=0.02033$ cm^{-1})
k_B=Boltzmann constant (1.38062×10^{-23} J sec)

A plot of $\ln[I_J / (2J+1)]$ vs. $J(J+1)$ produces a line with slope $-(B_v hc/k_B T_R)$ from which

the rotational temperature T_R can be determined. Low rotational temperatures
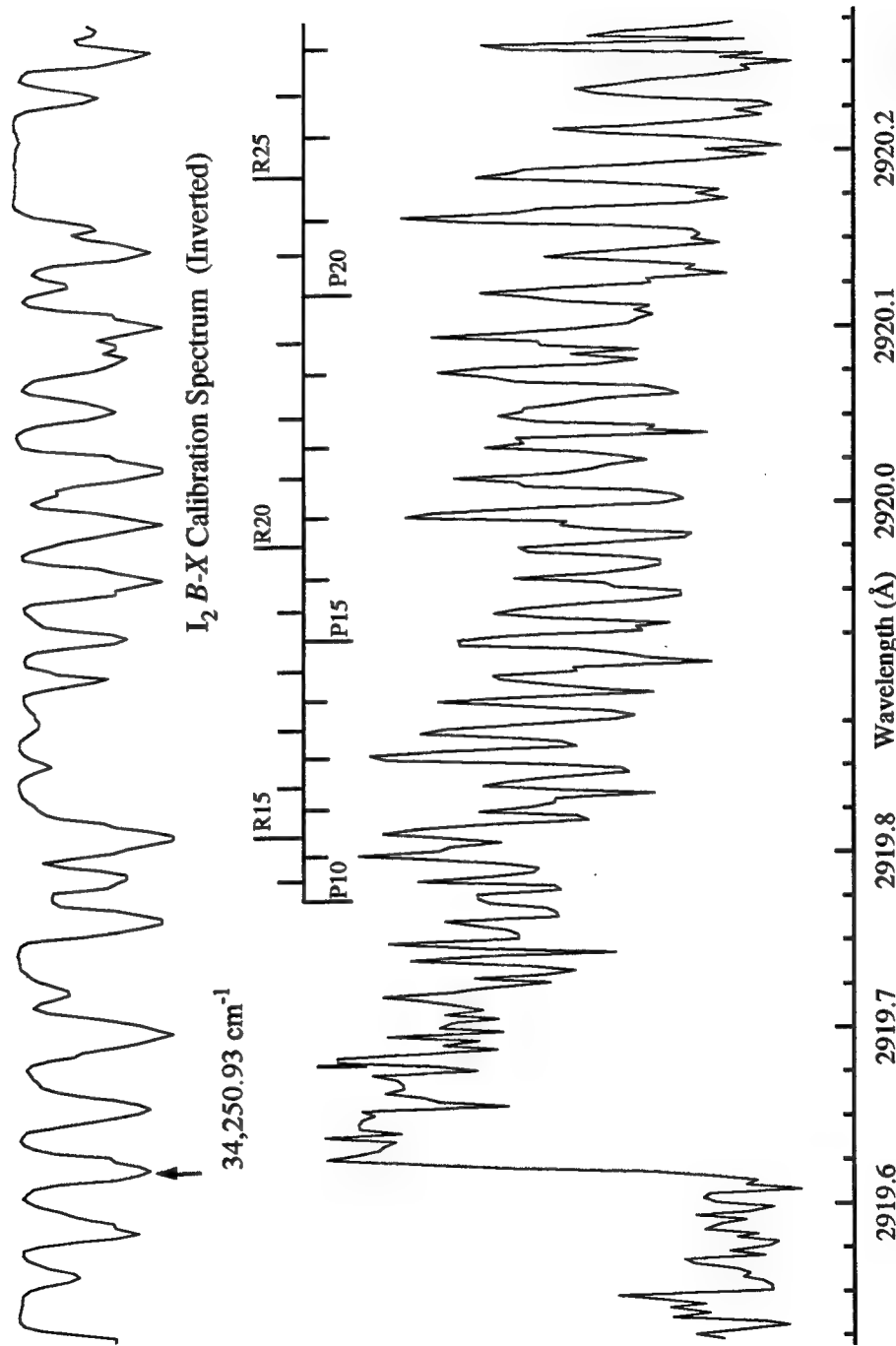
Figure 4.2: Rotationally Cold, Vibrationally Excited Spectrum of $I_2(D, v'=8 \leftarrow X, v''=40)$ in a Free-Jet Expansion
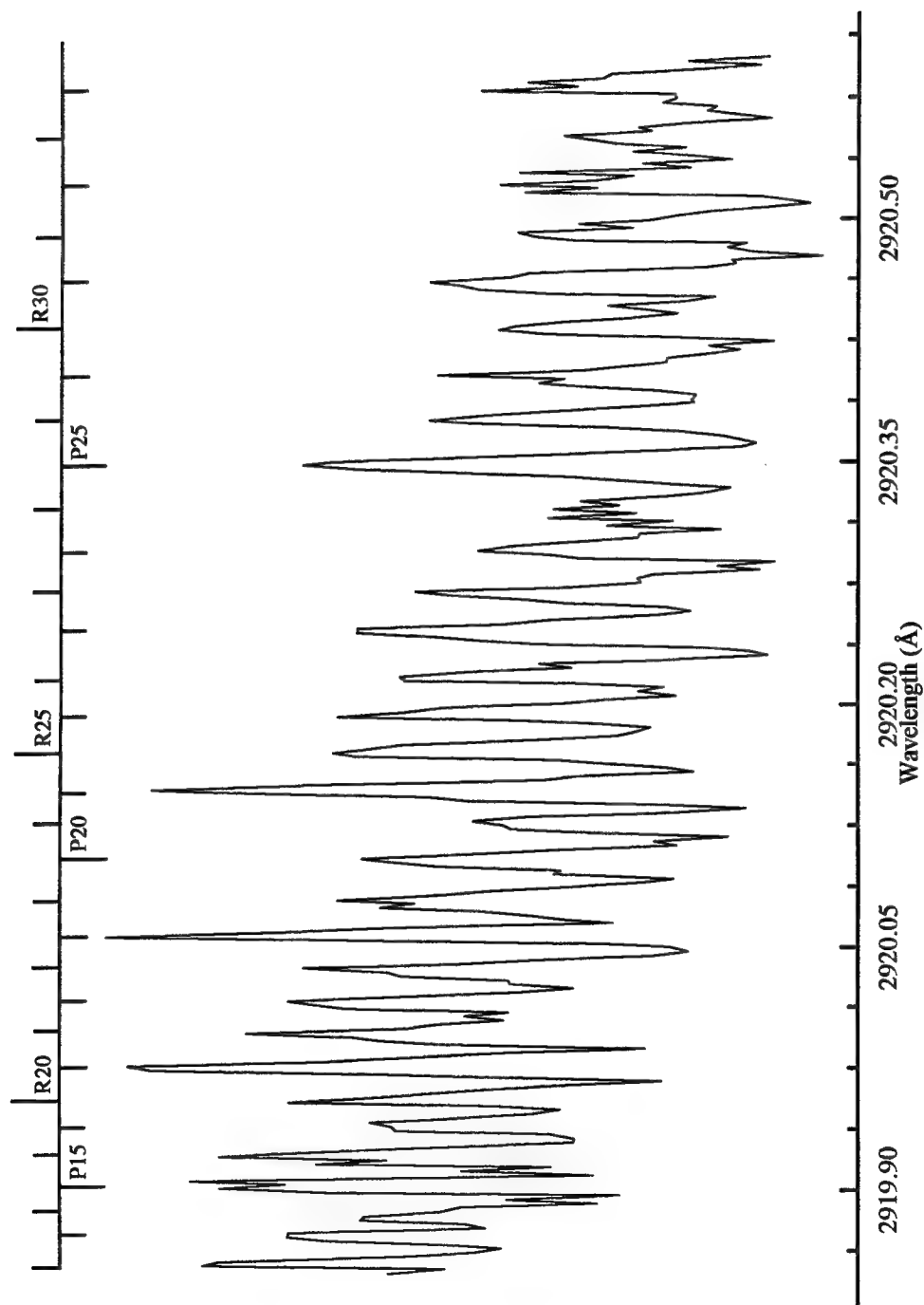
Fig 4.3: Spectrum of Vibrationally Excited $I_2(D, v'=8 \leftarrow X, v''=40)$ in a Free-Jet Expansion
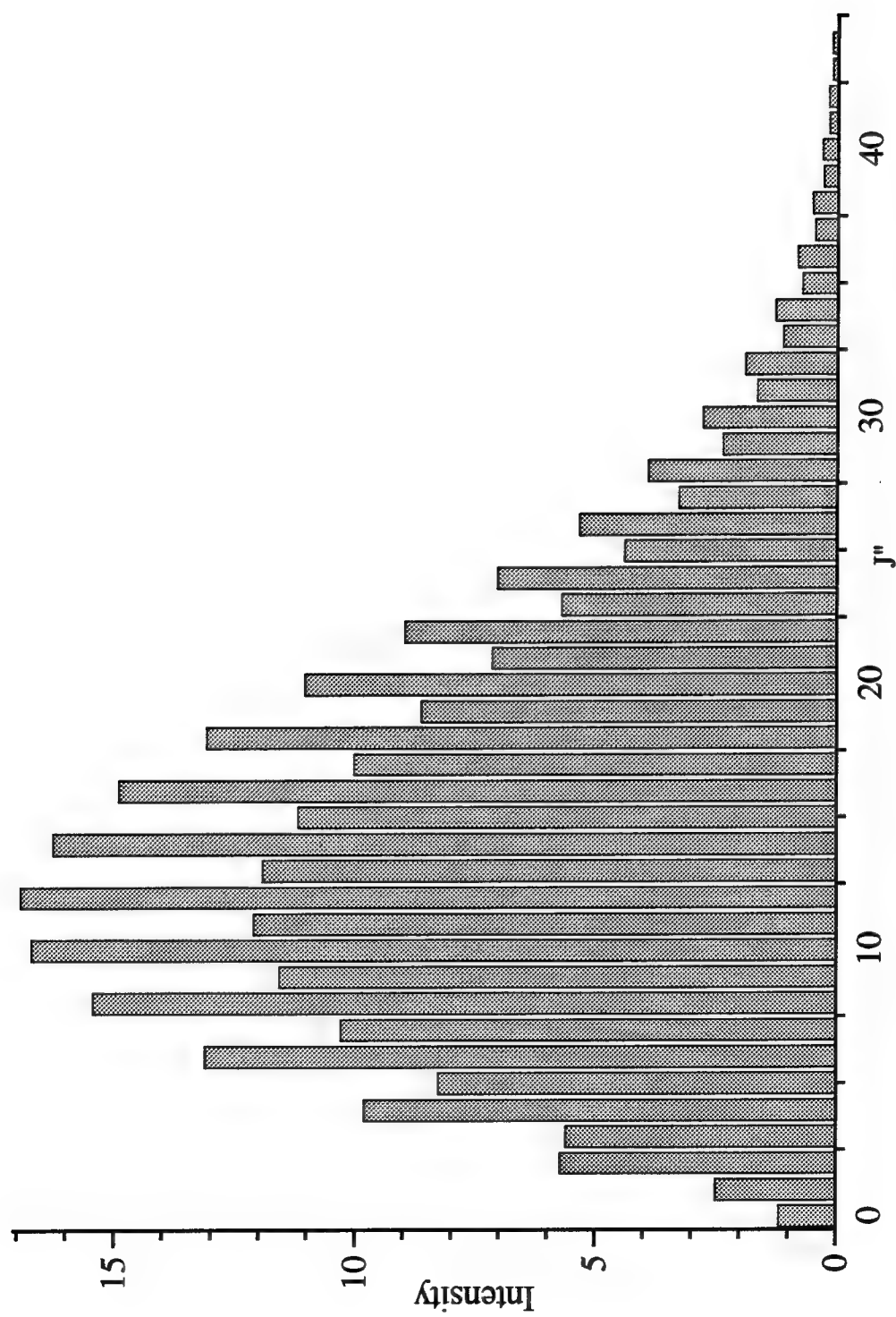
Figure 4.4: $I_2(X)$ Rotational Population Distribution at $13^{\circ}K$

corresponding to a relaxed rotational manifold markedly reduces the interference from other vibrational bands. Our spectrum shows a well-defined band-head with a progression of P and R branches. The most notable feature of this spectrum is the readily identifiable, unambiguous position of the bandhead. The absolute positions are determined from the calibration spectrum and the iodine atlas of Gerstenkorn and Luc.[7] The band head is coincident with the iodine calibration line (line 961) at 17125.4648 cm^{-1}. Since our probe laser was doubled, the band head position was calculated at 34250.93 cm^{-1}. Band origins and rotational constants were obtained by fitting the line positions to the expression

$$\nu = \nu_{v,v'} + (B'_v + B''_v)m + (B'_v - B''_v)m^2$$

The plot of the Fortrat diagram of $I_2(D,v'=8 \leftarrow X,v''=40)$ from the line positions in the free-jet expansion are shown in Figure 4.5. The Fortrat parabola incorporates line positions from both the free-jet for $J<30$ and from the $I_2(X) + I(^2P_{1/2})$ energy transfer experiment for $J>30$. While the rotational constants, $B_{v'}$ and $B_{v'}$, from this fit were in excellent agreement with the literature (X state,[3,4] D state[1]), our analysis of the band head location with the literature's vibrational constant revealed a difference of 1.51 cm^{-1}. Molecular constants published by Ishiwata and Tanaka[1] predicted a band origin at 34,252.35 cm^{-1} [A typographical error in Reference 5 incorrectly gives Y_{50} as a positive value; the correct value is $Y_{50} = -7.61 \times 10^{-9}$]. Meanwhile, the analysis of our experimental results indicated a band origin at 34,250.82 cm^{-1} or a difference of 1.53 cm^{-1}.

$$y = 34250.838 + 0.05219m - 0.01154m^2$$

where $m = -J$ for the P branch
$m = J+1$ for the R branch

Rotational Number m

Wavenumbers (cm^{-1})
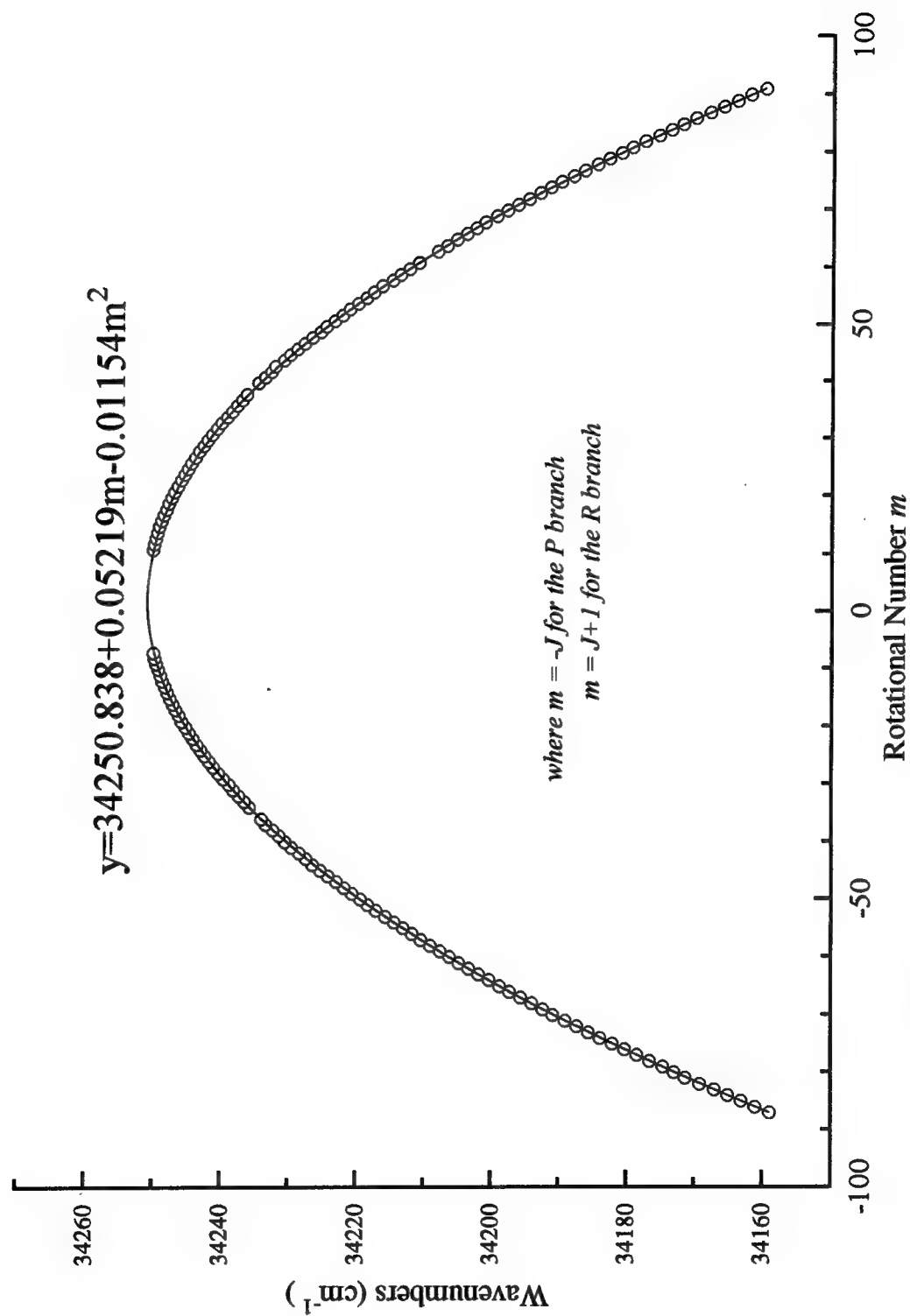
Figure 4.5: Fortrat Parabola for L$_2$ ($D,v'=8 \leftarrow X,v''=40$)

Despite the obvious success of the free-jet expansion experiment, there were two major drawbacks which hindered data collection. With an average of 200 shots per step, each scan (≈ 4.4 cm^{-1}) required well over two hours to collect and challenged the performance envelope of both the equipment and operator alike. Changes in alignment, laser timing drift, and plugging of the 1 mm nozzle provided constant challenges in maintaining signal integrity. In addition, the relatively weak signal and the optimal performance required for all equipment and operating conditions made this technique arduous. While the technique of SEP-LIF was primarily intended for analysis of inelastic collisions, it also proved useful in completing the spectroscopy for the low vibrational levels of $I_2 D(v'<38)$.

§4.3 $I_2 + I(^2P_{1/2})$ ENERGY TRANSFER

The need for highly accurate spectroscopic constants is illustrated with the spectra for $I(^2P_{1/2}) + I_2(X)$ energy transfer. The transfer of energy between $I(^2P_{1/2})$ and $I_2(X)$ produces vibrationally excited iodine through electronic-to-vibrational (E→V) energy transfer. The transfer between $I(^2P_{1/2})$ and $I_2(X)$ is efficient because the interaction is strong enough to break down the diatomic quantization. But the distinction between E→V transfer and reactive quenching is difficult because identical atoms are involved. However, based on the large rate for I_2 quenching by $I(^2P_{1/2})$ and the poor match of electronic and vibrational energies (7603 cm^{-1} vs. 215 cm^{-1}), the reactive path

through an I_3 intermediate seems more likely.[8] Vibrational excitation of $I_2(X)$ by $I(^2P_{1/2})$

through near resonant transfer is

$$I(^2P_{1/2}) + I_2(X) \rightarrow I(^2P_{3/2}) + I_2(X; 23 < v'' < 48)$$
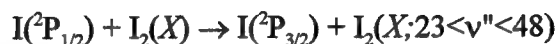
This E→V energy transfer process was initially studied by G. E. Hall, W. J. Marinelli,

and P. L. Houston,[9] who probed the vibrationally excited levels by Raman-shifting the

output of a Nd:YAG pumped dye laser with a linewidth of 0.6 cm^{-1}. Their experimental

results were consistent with a nascent I_2 product distribution which is inverted.

However, they did not deduce a population distribution of $I_2(X)$.

Energetically, $I(^2P_{1/2})$ is 7603 cm^{-1} above its ground state. Resonant energy

transfer between $I(^2P_{1/2})$ and $I_2(X)$ generates population up to $I_2(X, v''=47)$. A schematic

representation of this energy transfer in shown in Figure 4.6. In order to populate the

$v''=44$ level, energy transfer must occur between I* and $I_2(X, v''=1)$. With approximately

64%, 23%, and 8% of the vibrational populations are distributed in $v''=0$, $v''=1$, and

$v''=2$, respectively, population above $v''=40$ is easily detected.

The alternating intensity of the rotational distribution is a result of the symmetry

restrictions on the nuclear-spin states. In a homonuclear diatomic, the total wavefunction

must be antisymmetric with respect to the nuclear interchange if the nuclei are fermions.

The ground electronic state of iodine $X^1\Sigma_u^+$ is symmetric. Of the $(2I+1)^2$ possible nuclear

spin states, $(2I+1)(I+1)$ are symmetric and $(2I+1)I$ are antisymmetric. Iodine is a fermion

and has a nuclear spin (I) of $^5/_2$. Then of the 36 possible nuclear spin states, 21 are

symmetric and 15 are antisymmetric. In order to maintain an overall antisymmetric
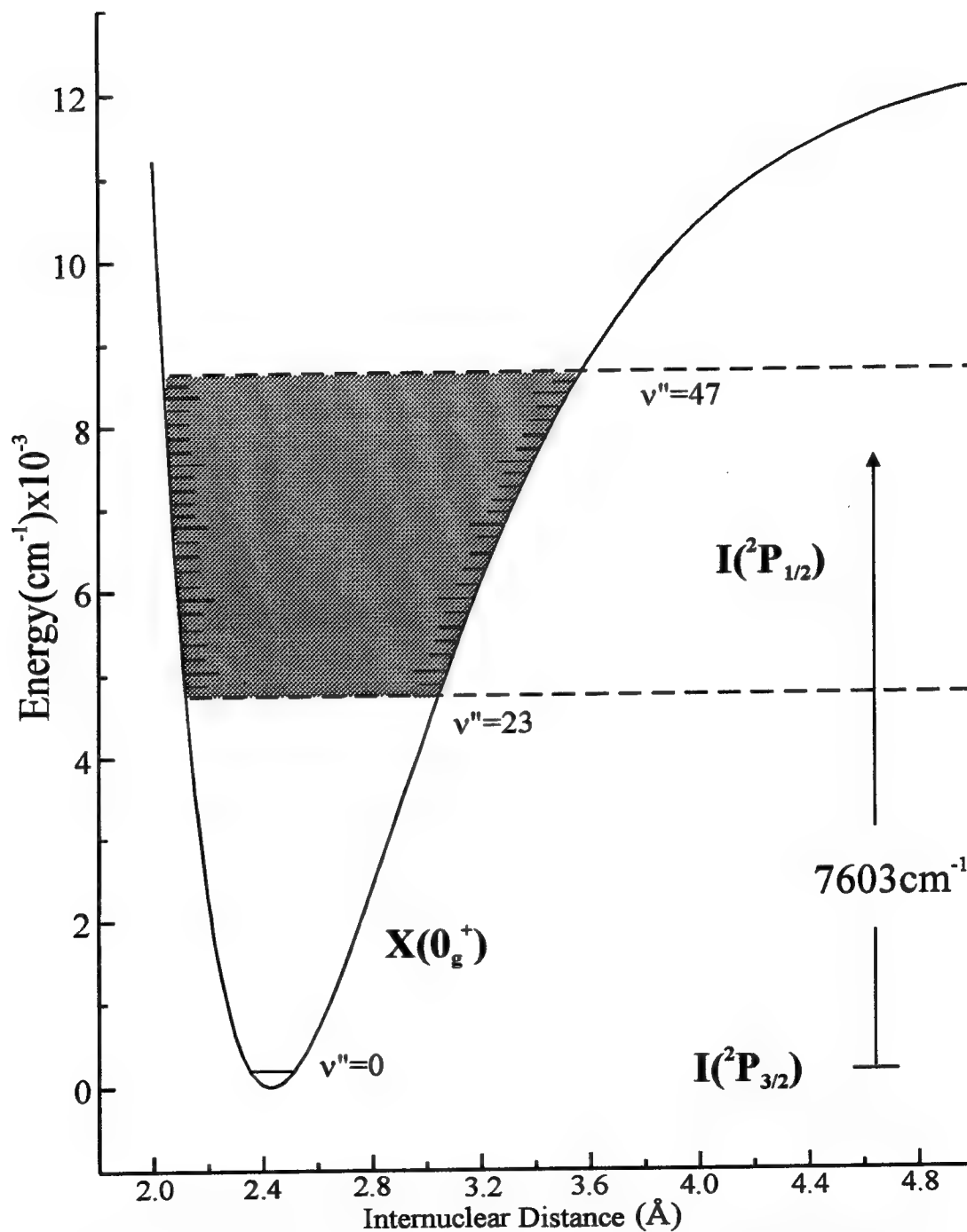
Figure 4.6: Potential Energy Diagram Illustrating
$I_2\,X(^1\Sigma_g^+) + I(^2P_{1/2}) \rightarrow I_2{}^\dagger + I(^2P_{3/2})$

wavefunction, the even J states (symmetric) must combine with odd nuclear spin states (antisymmetric), while the odd J states (antisymmetric) must combine with even nuclear-spin states (symmetric). Therefore, the odd J states combining with the symmetric nuclear spin states have a weight of $^7/_{12}$. Likewise, the even J states combining with the antisymmetric nuclear-spin states have a weight of $^5/_{12}$. Indeed, a 7:5 intensity alternation is predicted and observed for $I_2(X)$.

The inverted calibration curve of the excitation spectrum of iodine's $B \leftarrow X$ system is shown at the top of the spectrum. Utilizing the *Atlas Du Spectre D'Aborption De La Molecule D'Iode*[7], I was able to make absolute measurements for each $D \leftarrow X$ line. Assignment of two bands with v"=37 and 38 are shown in Figure 4.7. Approximately one calibration point per wavenumber was utilized to ensure accuracy of the spectral linepositions. The convolution of the numerous vibrational bands did not permit inversion of the line intensities directly from the spectra. Instead, I developed a computer model for simulating spectra based on the number density, line position and fluorescence signal strength. From the relative weightings of the vibrational bands, the nascent vibrational population of the $I(^2P_{1/2}) + I_2$ energy transfer process could be inferred. A complete listing of the FORTRAN code (MS FORTRAN V5.0) is included in Appendix D.

In the absence of predissociation, the LIF signal is essentially an absorption spectrum. The fluorescence signal strength ($S_{v,v'}$) for a v'v" transition is
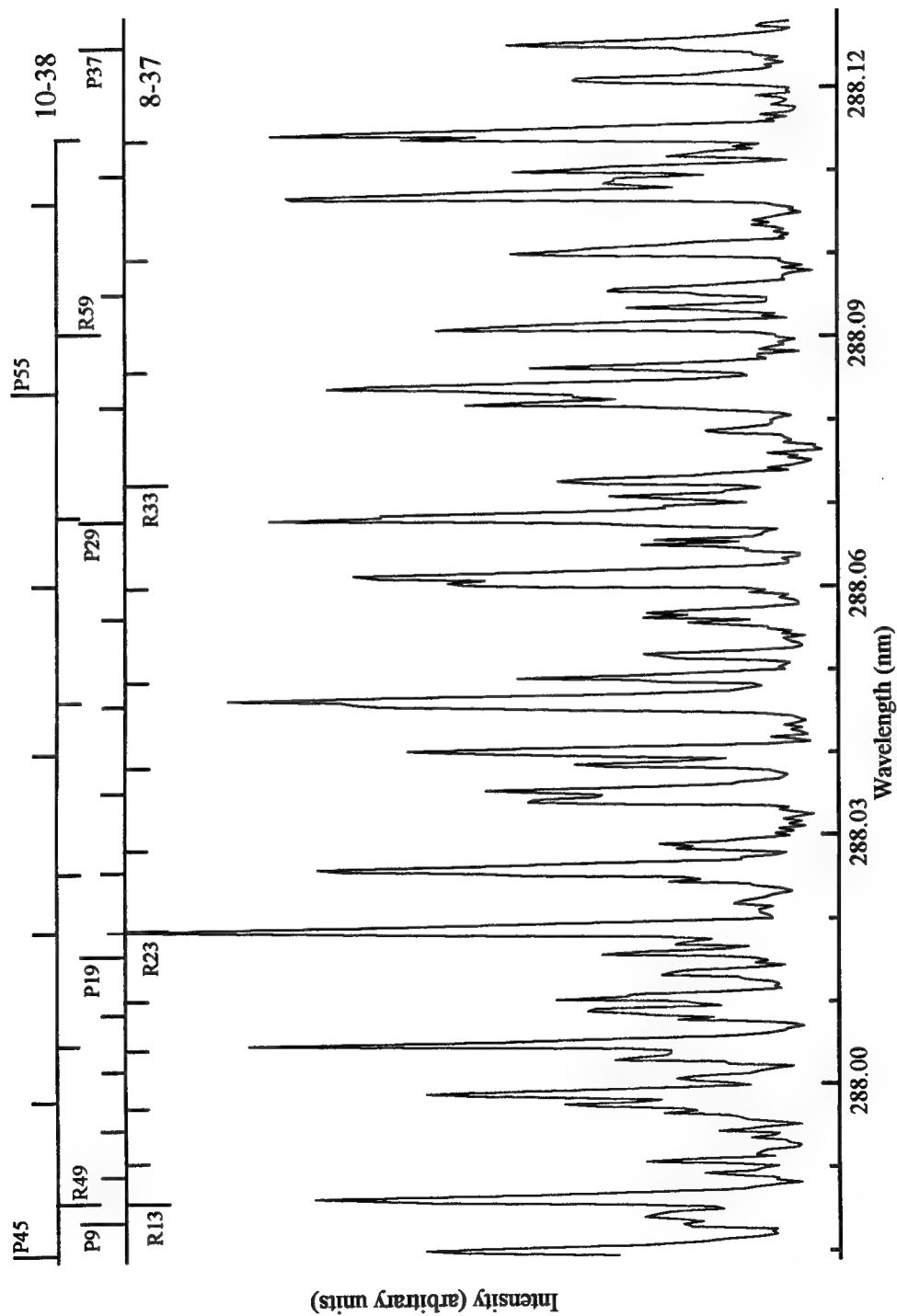
Figure 4.7: Rotationally Resolved Excitation Spectrum for I_2 *D-X*
Showing Rotational and Vibrational Energy Transfer

$$(S_{v,v'}) \propto \frac{1}{(2J''+1)} \, P_{v',v''} N_{v''} S_{J'J''} \nu_{v',v} q_{v',v''} f_{ns} <R_e>^2$$

where $P_{v',v''}$ - laser power pumping the v' v" transition
$N_{v''}$ - I_2 number density in level v"
$S_{J'J''}$ - rotational line strength (Honl-London factor)
$\nu_{v',v''}$ - frequency of the v' v" transition (cm^{-1})
$q_{v',v''}$ - Franck-Condon factor
$<R_e>$ - average of the transition moment
f_{ns} - nuclear spin factor

The line center of the function was determined using the molecular constants of the

$D(0^+_u)$ state presented in Section §4.1 and the $X(0^+_g)$ constants of Tellinghuisen et al.[4]

Many of the bands contained rotationally 'hot' lines with J>120. This complicated the

modeling of the energy transfer due to the lack of rotational D_v constants for the D

state. While the error without the D_v constants was normally on the order of 0.06 to

0.09 cm^{-1}, the spectra was dense enough that this small of error could shift the

population to the surrounding peaks. The width of the Gaussian lineshape was adjustable

but was nominally 0.08 cm^{-1}. A Lorentzian lineshape was also used for comparison. The

laser power and frequency of transition were assumed constant within each 15 cm^{-1} scan.

Within a vibrational level, the rotational populations were partitioned according to a

thermal Boltzmann distribution

$$n_J = (2J+1)\exp(-hcB_v J(J+1)/kT)$$

Table 4.4 lists the rotational temperatures used in modeling the energy transfer spectra.

The rotational temperatures for the strongest vibrational bands (typically 5-10 bands)

Table 4.4: Rotational Temperature and Relative Intensity
for $I_2 + I(^2P_{1/2})$ Energy Transfer Modeling

v''	Rotational Temperature (°K)	Relative Intensity
26	280	0.2
27	280	0.3
28	260	0.3
29	270	0.6
30	280	1.3
31	280	1.5
32	280	1.2
33	360	1.7
34	370	1.4
35	380	2.6
36	380	3.2
37	310	4.5
38	330	4.5
39	310	5.7
40	310	5.9
41	310	5.3
42	340	4.9
43	330	4.2
44	320	3.5
45	298	2.2
46	270	2.5
47	278	1.0

were fixed by determining J_{max} for that level. J_{max} was determined for a vibrational band by visual inspection of the adjoining spectra and locating the maximum intensity of the band.

For the rotational line strengths, the Honl-London factors appropriate for the $^1\Sigma$-$^1\Sigma$ transition, S^P=J and S^R=J+1, were used. Franck-Condon factors as detailed in Appendix C were calculated for inclusion into the simulation package. Relative intensities of the vibrational distribution were determined using computer simulation of the experimental spectra. The computer simulation source code is contained in the subroutines *DXSIM, DXSIMTWO,* and *DXONETIME* included in Appendix D. The simulation would draw the experimental spectrum and overlay the simulation, whose parameters were adjusted an adequate representation by inspection was obtained. Each spectra was then divided into 5 cm^{-1} segments and the relative populations adjusted for best fit. The vibrational population distribution was determined by fitting 15 cm^{-1} segments at 5 nm increments from 270-300 nm. The 5 nm spacing allowed overlap of three to five vibrational bands and provided for continuity between the fitted spectra. Generally, the PMT voltage and chamber pressure were consistent throughout the experiment. Relating the intensities of spectra taken on different days and at different wavelengths was accomplished by ensuring common overlap of over half of the vibrational bands. Approximately 25 to 30 bands were fit for each 15 cm^{-1} segment and the relative weight and rotational temperature adjusted by visual inspection for best fit.

Figure 4.8 shows the relative nascent vibrational distribution for $I(^2P_{1/2}) + I_2$ energy transfer.

The distribution of Figure 4.8 may be described as Lorentzian with a maximum at $v''=40$ and insignificant vibrational population above $v''=47$. Rotational temperatures ranged from 280°K ($v''=46$) to 380°K ($v''=35$). The vibrational distribution results are consistent with those of Hall et al.[9,10] who observed a nascent vibrational distribution as asymmetrically shaped with a peak at $v''=40$ and half-maximum points at $v''=41$ and $v''=35$. M. H. van Benthem et al.[11] obtained a bimodal distribution in their flow-tube experiments of $O_2(^1\Delta) + I_2$ with $v''_{max}=35$. These results of van Benthem and Davis are compatible considering their distribution was not nascent and suggests vibrational relaxation was occurring before the measurement was recorded at a fixed position 0.5 cm downstream of the I_2 injector.

§4.4 REFERENCES

1. T. Ishiwata and I. Tanaka, *Laser Chem.* **7**, 79 (1987).

2. M. L. Nowlin and M. C. Heaven, *Journal De Physique IV* **4**, C4-729 (1994).

3. R. Bacis, D. Cerny, and F. Martin, *J. Mol. Spectrosc.* **118**, 434 (1986).

4. J. Tellinghisen, M. McKeever, and A. Sur, *J. Mol. Spectrosc.* **82**, 225 (1980).

5. M. Bartels, R. J. Donovan, A. J. Holmes, P. R. R. Langridge-Smith, M. A. MacDonald, and T. Ridley, *J. Chem. Phys.* **91**, 7355 (1989).

6. A. J. Hoy and R. H. Lipson, *Chem. Phys.* **140**, 187 (1990).
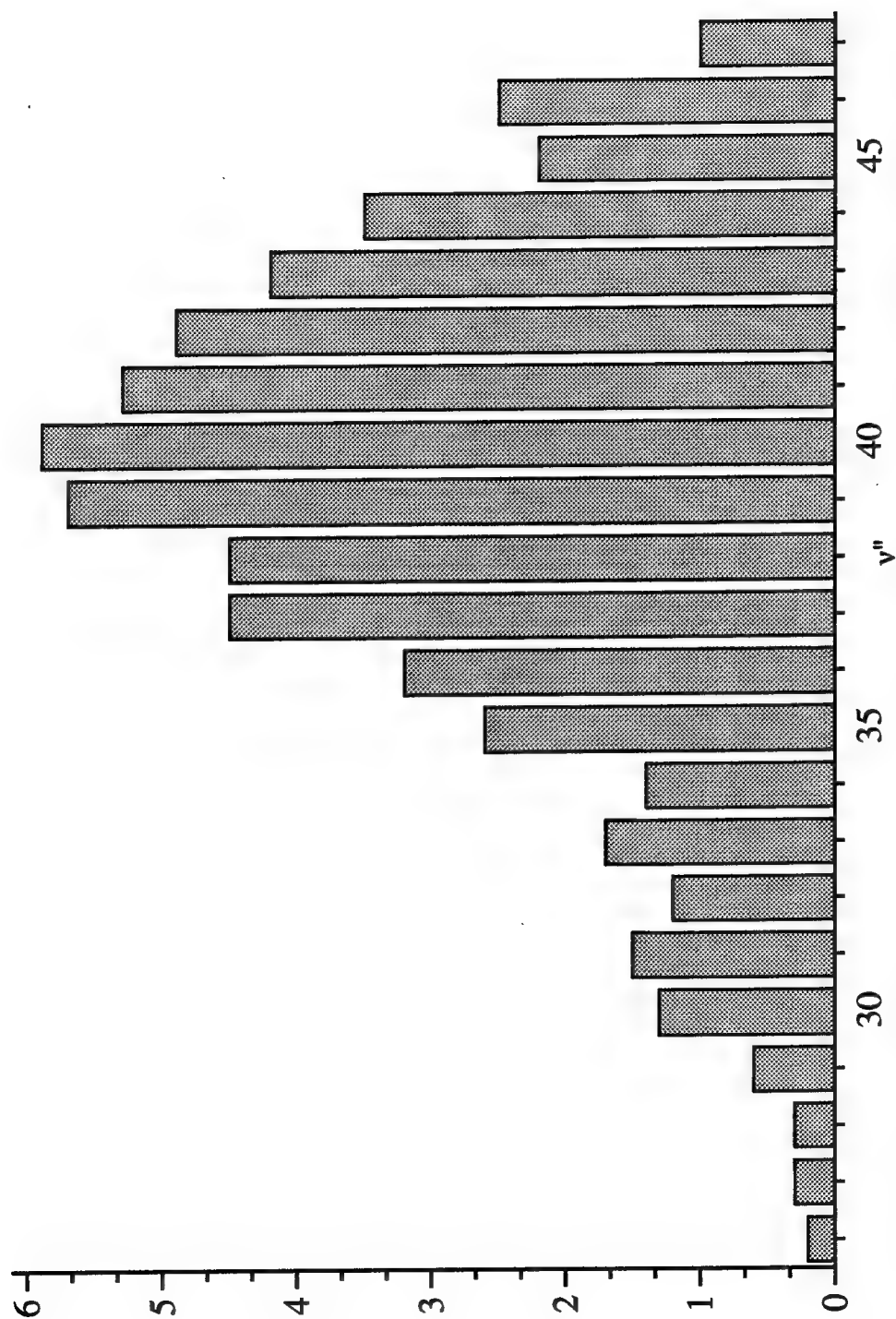
Figure 4.8: Relative Vibrational Population Distribution for $I_2 X(^1\Sigma_g^+) + I\,(^2P_{1/2})$

7. S. Gerstenkorn and P. Luc, *Atlas du Spectre d'Absorption de la Molecule d'Iode*, Laboratoire Aime Cotton, CNRS II, Orsay, France (1977).

8. G. E. Hall, S. Arepalli, P. L. Houston, and J. R. Wiesenfeld, *J. Chem. Phys.* **82**, 2590 (1985).

9. G. E. Hall, W. J. Marienelli, and P. L. Houston, *J. Phys. Chem.* **87**, 2153 (1983).

10. P. L. Houston, *Energy Diposal in Electronically Excited Halogen Atoms and Oxygen, AFOSR Final Scientific Report for Nov 1, 1981 through Oct 31, 1982*. Defense Technical Information Center, Alexandria, Virginia.

11. M. H. van Benthem and S. J. Davis, *J. Phys. Chem.* **90**, 902 (1986).

CHAPTER 5

STIMULATED EMISSION PUMPING v"= 42

§5.1   RESULTS

Figure 5.1 shows an example of a low resolution *pump-dump-probe* spectrum,

taken for pure I_2 vapor with a 20 ns delay between the *dump* and *probe* pulses. Features

belonging to the $D\leftarrow X$ and $f\leftarrow B$ transitions are evident in this scan. In many

experiments, spectra were recorded in pairs; one with the dump laser present, and one

with the dump laser blocked. A typical pair of scans can be seen in Figures 5.1 (I_2 self-

transfer) and 5.2 (I_2 + He).   Interfering OODR features were then removed from the

pump-dump-probe spectra by subtracting the two laser signal (*dump* blocked) from the

three laser signal (Figure 5.3a). As the *dump* laser depleted the B state population, a

modest scaling of the OODR spectrum prior to subtraction was required. Scale factors

in the range of 0.90-0.98 were typically obtained from the ratio of the intensities of the

strongest OODR peaks with and without the dump laser present.

At high resolution each $D\leftarrow X$ peak resolved into a single pair of P and R lines as

seen in Figure 5.4, demonstrating clean preparation of the state v"=42, J_i"=17.

Rotational energy transfer, induced by self or bath gas collisions, was easily observed in

the high resolution scans. Figure 5.5 illustrates rotational transfer caused by collisions

with Ar. The high resolution scans ranged over approximately 15 cm^{-1}. Two features

of this spectrum are worth noting. First, only levels with odd J values are observed, in
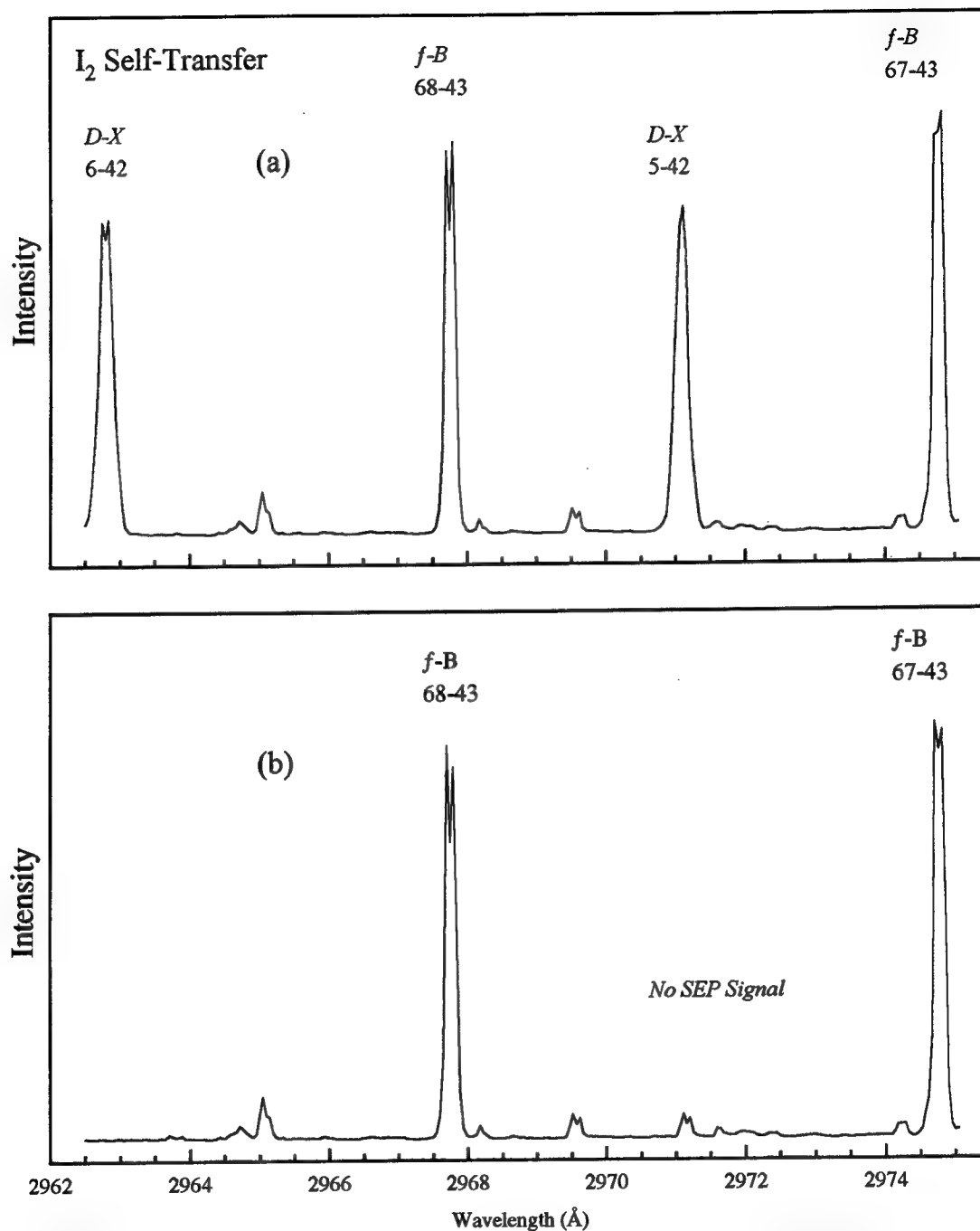
Figure 5.1: Low-Resolution Spectra Showing Observed
Transitions (a) SEP: Pump-Dump-Probe Sequence
(b) OODR: Pump-Probe Sequence
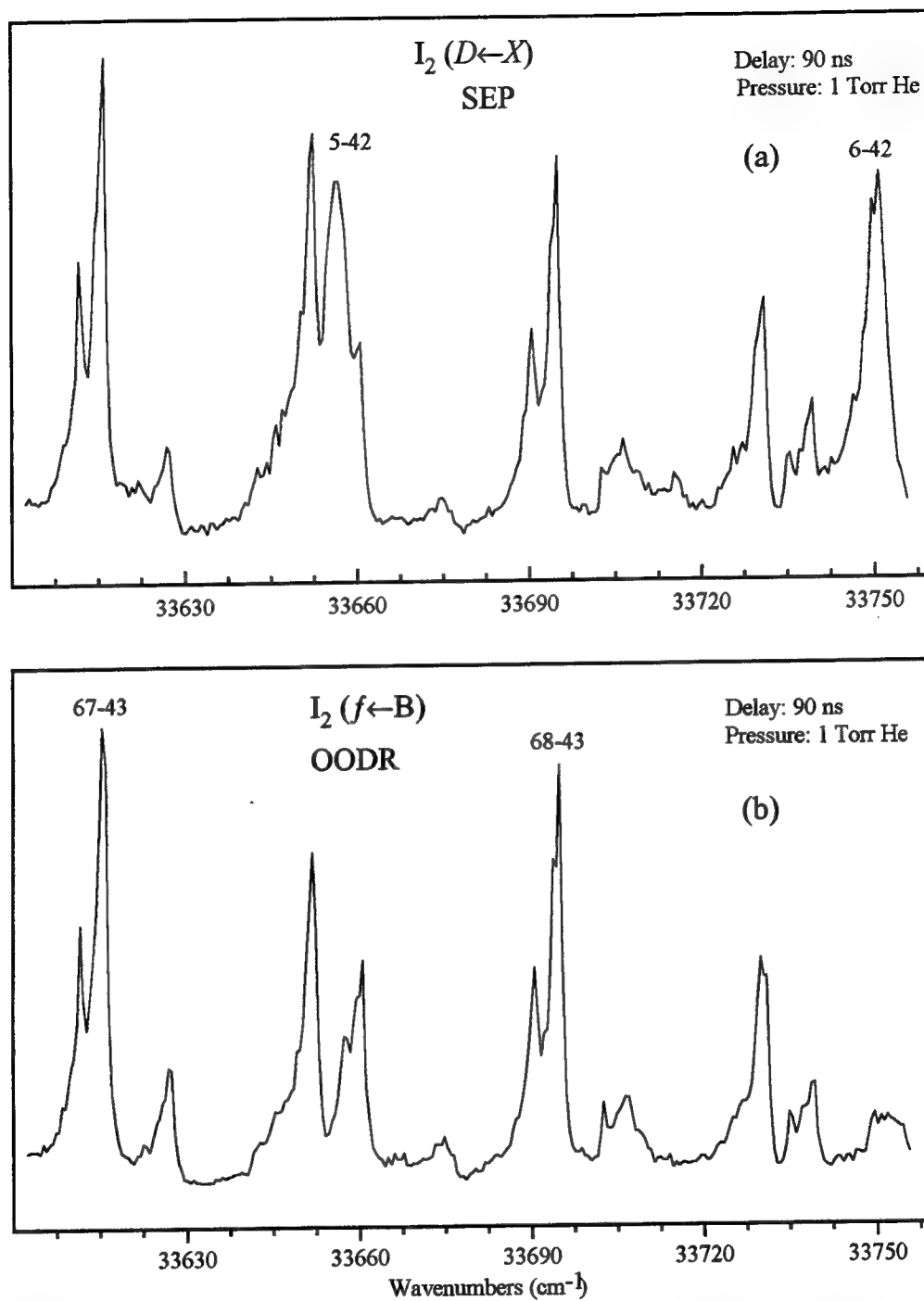
Figure 5.2: Low-Resolution Spectra Showing Energy Transfer Induced by Collisions with He. (a) SEP Pump-Dump-Probe Sequence. (b) OODR *Pump-Probe* Sequence
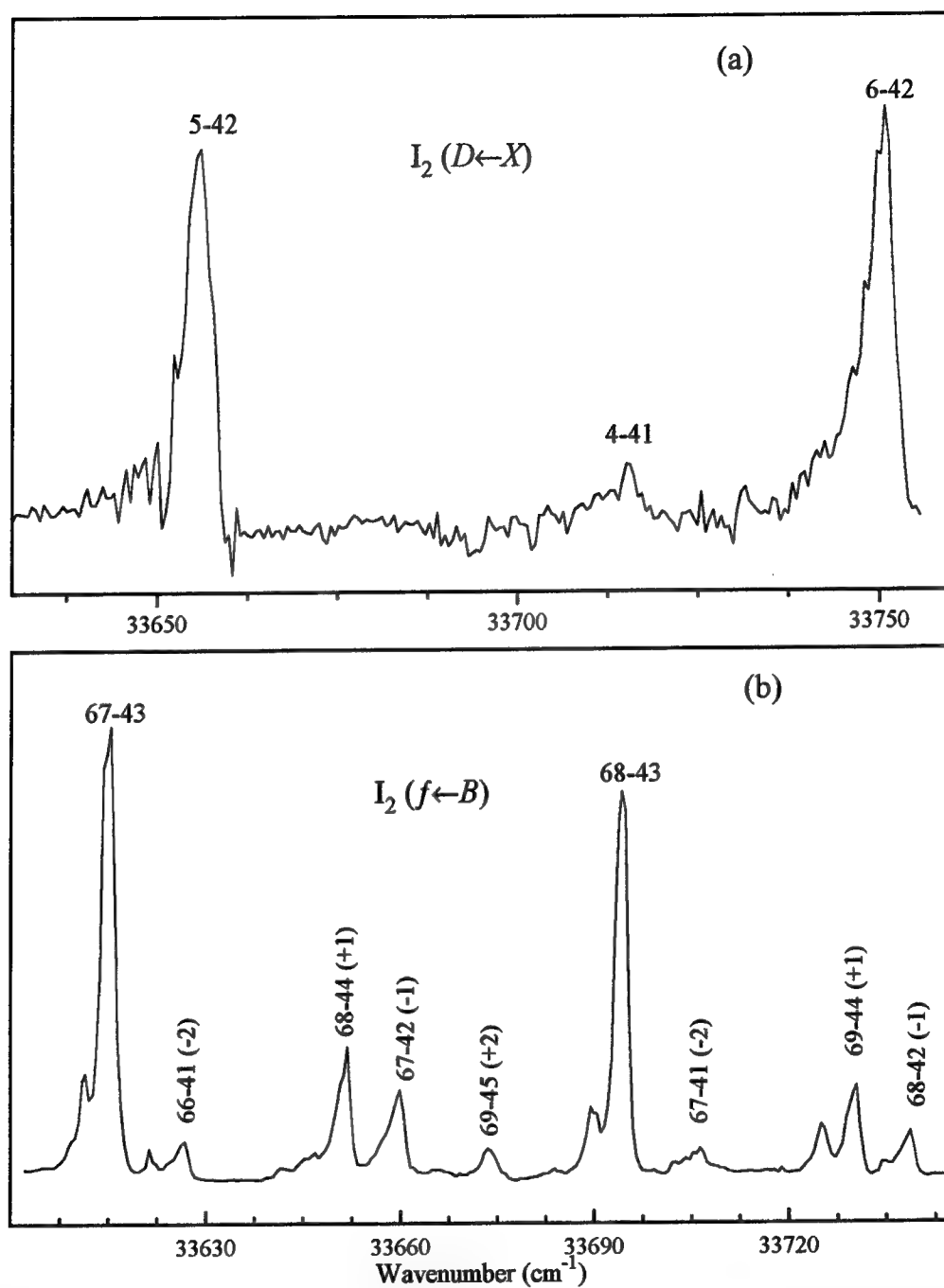
Figure 5.3: Low-resolution spectra showing vibrational energy transfer induced by collisions with He. (a) Ground state transfer observed by SEP sequence (b) B state observed by OODR

$I_2 (D, v'=7 \leftarrow X, v''=42, J_i=17)$

Pressure: 38 mTorr

Delay: 71 ns

(P17)

R(17)
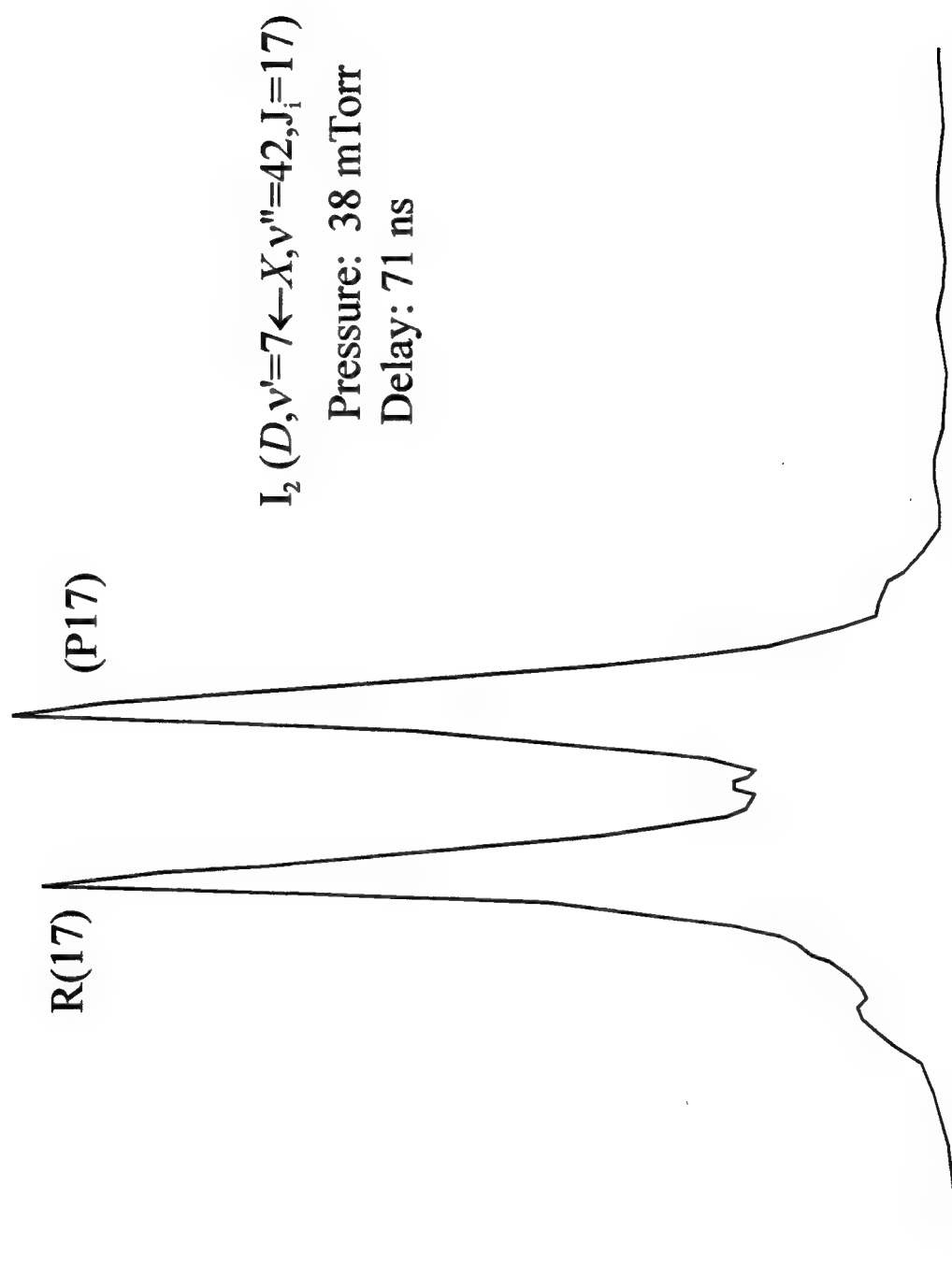
Figure 5.4: High Resolution SEP-LIF of I_2 (X) $v''=42$, $J_i=17$ Self Transfer
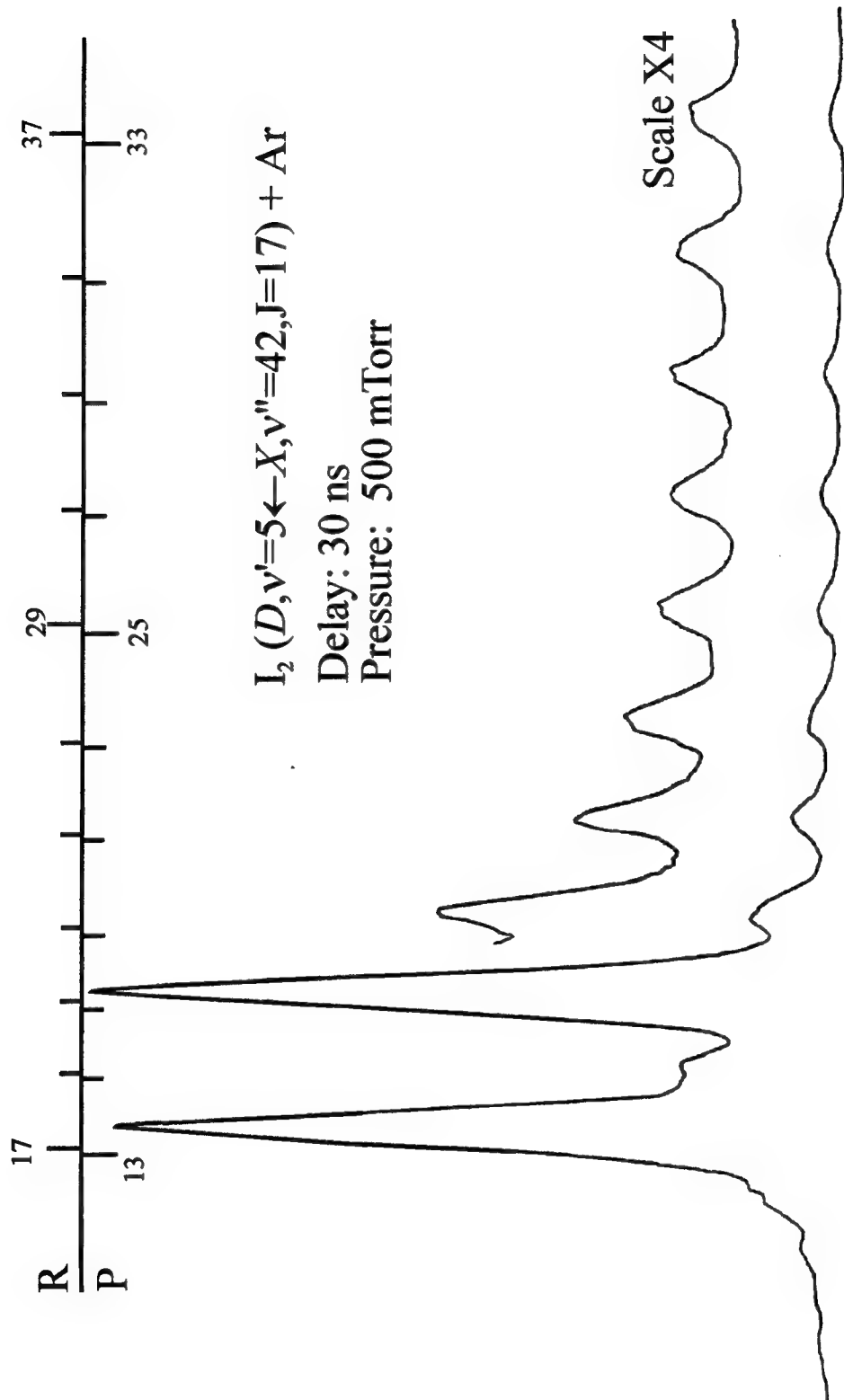
Figure 5.5: High Resolution SEP- LIF Showing Rotational Energy Transfer Between I₂ (X) v"=42, J=17 with Ar

accordance with the rigorous even ΔJ selection rule for transfer between the levels of a homonuclear diatomic. Second, the P(J) and R(J+4) lines were superimposed at a resolution of 0.1 cm^{-1}. This spectral overlap problem was present in all the bands examined, and it complicated the process of extracting energy transfer rate constants from the line intensity data.

Measurements of the total rates at which molecules were transferred out of the $v''=42$, $J''=17$ level were accomplished as shown in Figure 5.6. This was done by fixing the probe laser on the R(17) line, and monitoring the fluorescence intensity as a function of *dump-probe* pulse delay time. Good single exponential decays were observed. These decays are defined by the expression $I(t)=Ae^{-kt}$, where A is a constant and $k=k'_{I2}[I_2]+k'_M[M]$. k'_{I2} and k'_M are the total transfer rate constants for collision with I_2 and M, respectively. Rate constants determined by fitting the initial state decay curves are listed in Table 5.1. The values for He, Ar, and O_2 were obtained using an I_2 partial pressure of 30 mTorr, and have been corrected for self-transfer. Model calculations indicated that these measurements were relatively insensitive to the spectral overlap problem. Although R(17) was overlapped by P(13), the fraction of the total population transferred to $J''=13$ was predicted to be quite small. Rate constants for state-to-state rotational energy transfer ($J_i{\rightarrow}J_f$) can be determined from rotationally resolved spectra taken under single collision conditions. An indirect method was used to verify that multiple collision events were not modifying the intensity distributions seen in these experiments. Spectra were taken at a variety of pressures and delay times for each
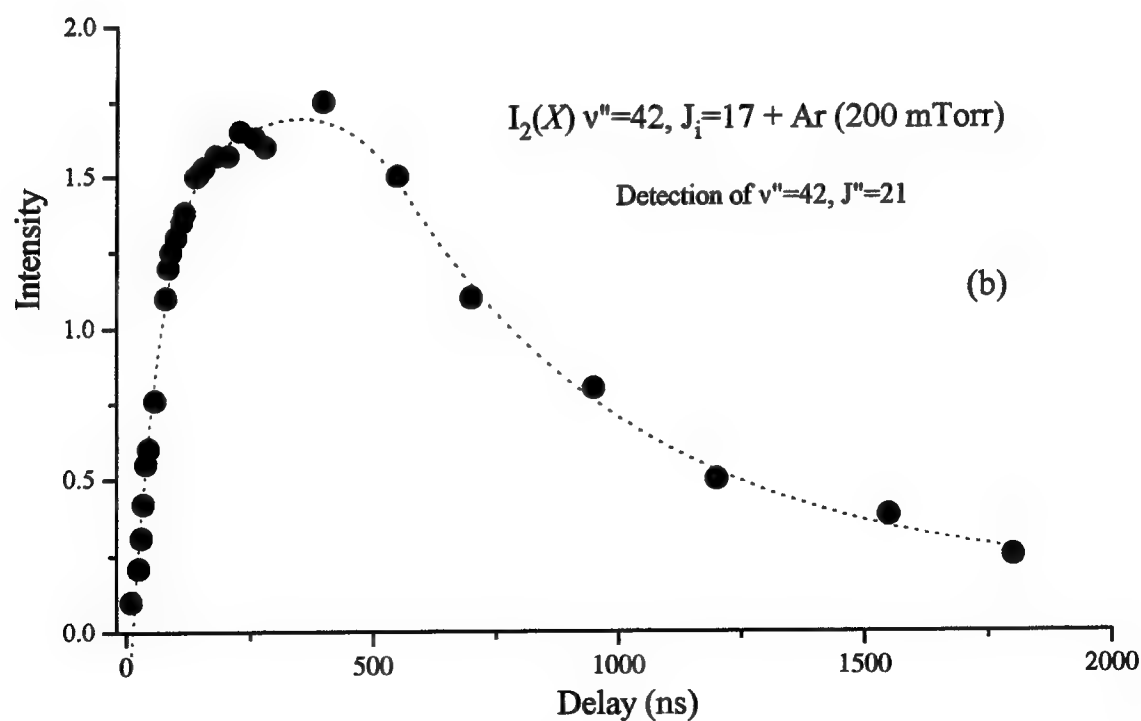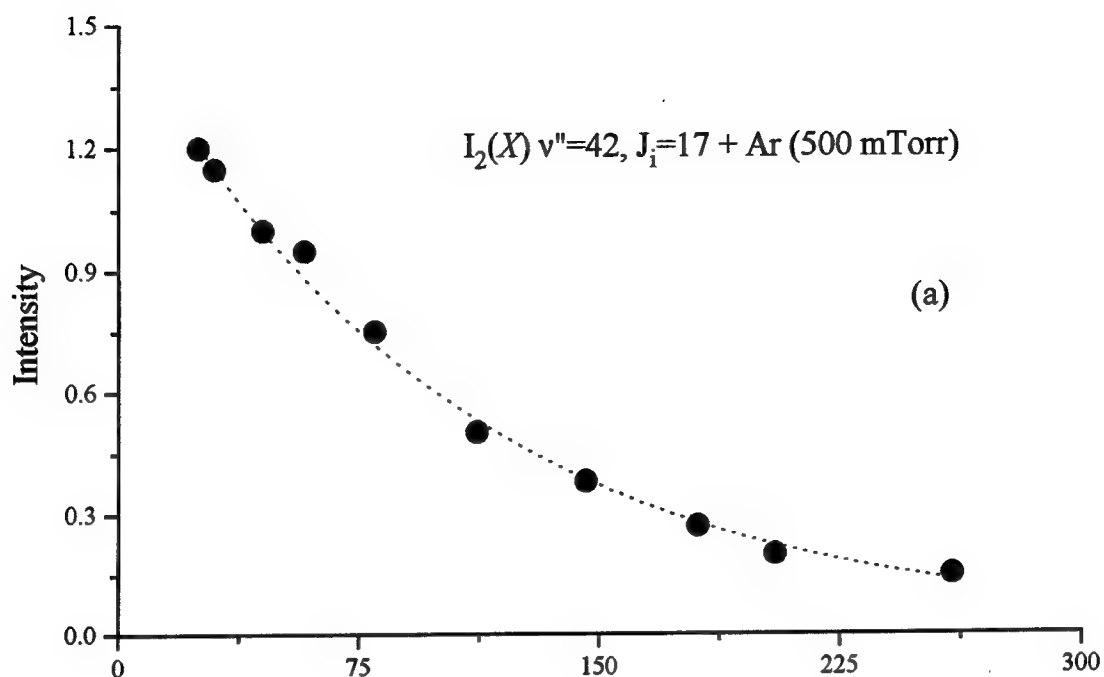
Figure 5.6: (a) Decay of Initially Pumped Level and (b) Detection of Satellite, J"=21

Table 5.1: Rate Constants for Total Population Loss from Individual Rovibronic Levels for I_2 (X) v"=42, J"=17 and Comparison with I_2 (B) v'=15, J'=33

Collision partner	$k[I_2(X)]^a$ $(10^{-10}$ cm^3 s$^{-1})$
I_2	8.6
Ar	5.0
He	6.6
O_2	7.8

a. Error limits $\pm 0.5 \times 10^{-10}$ cm^3 s^{-1}

Collision partner	$k[I_2(B)]^b$ $(10^{-10}$ cm^3 s$^{-1})$
I_2	6.5±0.6
Ar	6.8±0.7
He	7.2±0.5
O_2	.....

b. J. Derouad and N. Sadeghi, *Chem. Phys. Lett.* 102, 324 (1983).

collision partner, and conditions where the intensities of the collisionally populated

spectral features began to show nonlinear time or pressure dependence were identified.

Collision induced rotational energy transfer of I_2 with He, N_2, and O_2 are shown in

Figures 5.7, 5.8, and 5.9, respectively. Spectra used to characterize rotational energy

transfer were then recorded at pressure/delay combinations that were well below those

that revealed the effects of multiple collisions. For example, under the conditions used

to record Figure 5.2, the rate of population loss from J"=17 was 8.4×10^{-6} s^{-1} . Thus an

average of 0.25 energy transfer collisions occurred during the 30 ns between the *dump*

and *probe* pulses.

Low and high resolution scan were made to search for $D \leftarrow X$ bands resulting

from vibrational energy transfer. Surprisingly, it proved to be difficult to find conditions

that clearly produced these band. By comparison with the behavior of the B state v'=43

level, we found vibrational transfer out of the X, v"=42 level to be an inefficient process

for all the collision partners investigated. This point is graphically illustrated in Figure

5.3. The upper panel shows a *pump-dump-probe* spectrum for and I_2/He mixture taken

with a *dump-probe* delay of 90 ns (OODR features were removed from this spectrum by

subtraction). Note that the rotational contours of the bands arising from X, v"=42 have

been broadened by rotational energy transfer. The weak band at 33717 cm^{-1} was

produced by v"=42$\rightarrow$v"=41 transfer. For comparison, the Figure 5.4b shows transfer

occurring in the B state. This is an OODR spectrum (no *dump* pulse) taken with a delay

of 60 ns between the *pump* and *probe* pulses. Bands resulting from both upward and
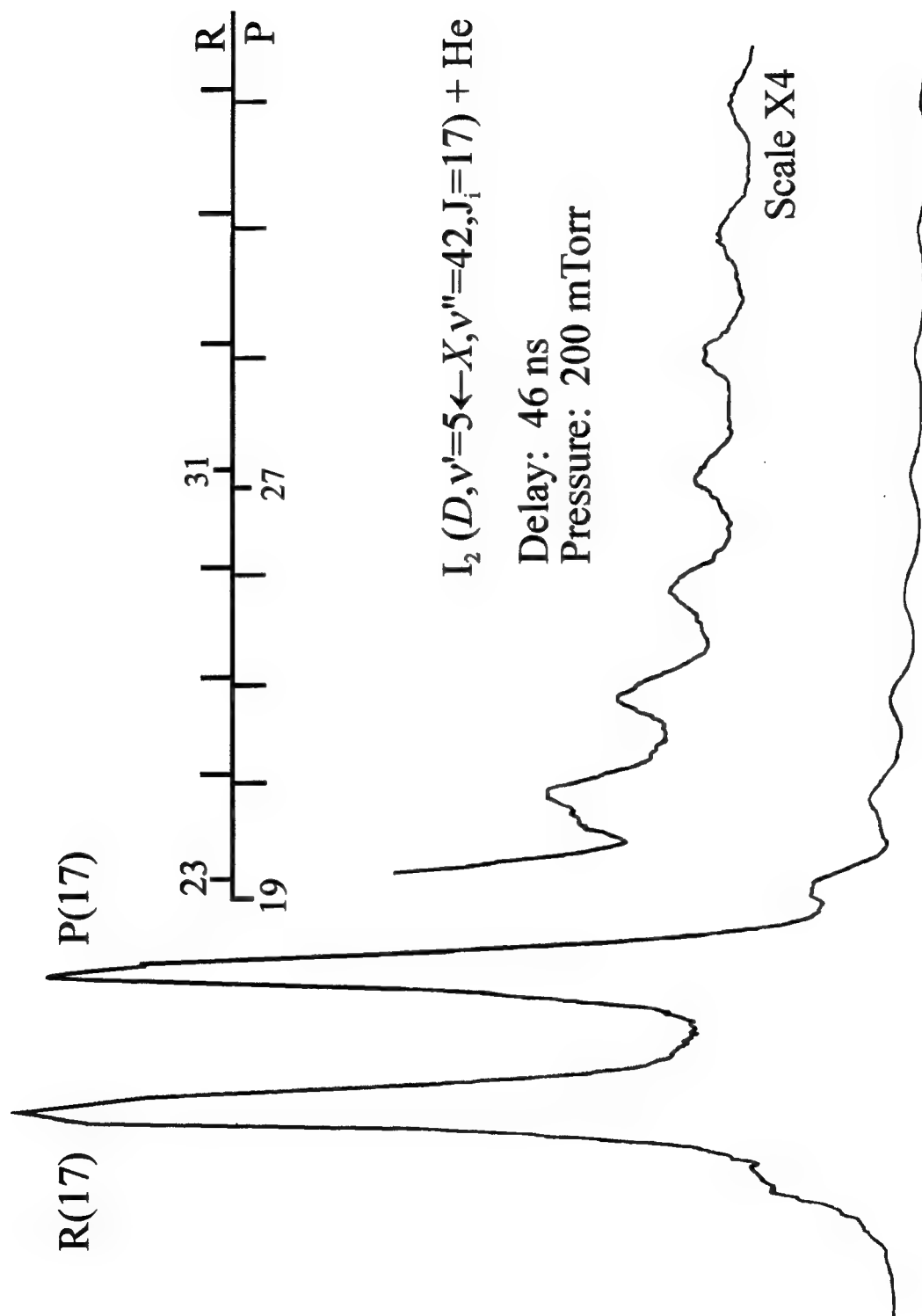
Figure 5.7:   SEP-LIF of I_2 (X) v''=42, J_i=17 with He

$I_2 (D; v'=5 \leftarrow X; v''=42, J_i=17) + N_2$

Delay: 43 ns
Pressure: 500 mTorr

P(17)

R(17)
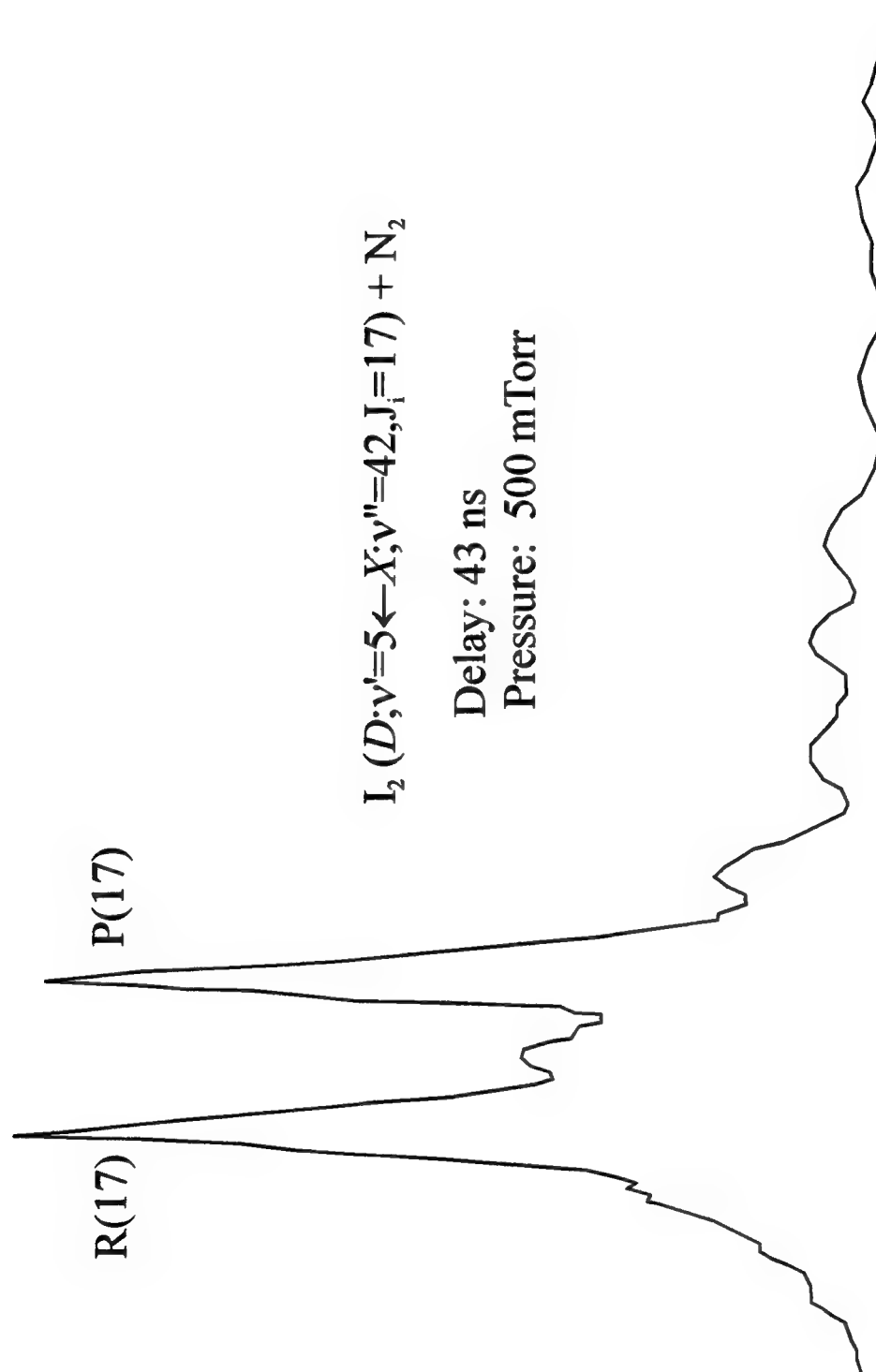
Figure 5.8: SEP-LIF of I_2 (X) v''=42, J_i=17 with N_2

$I_2 (D, v'=5 \leftarrow X, v''=42, J_i=17) + O_2$

Delay: 38 ns
Pressure: 500 mTorr

R
P

R(17)

P(17)

Scale X4

23
19

33
29
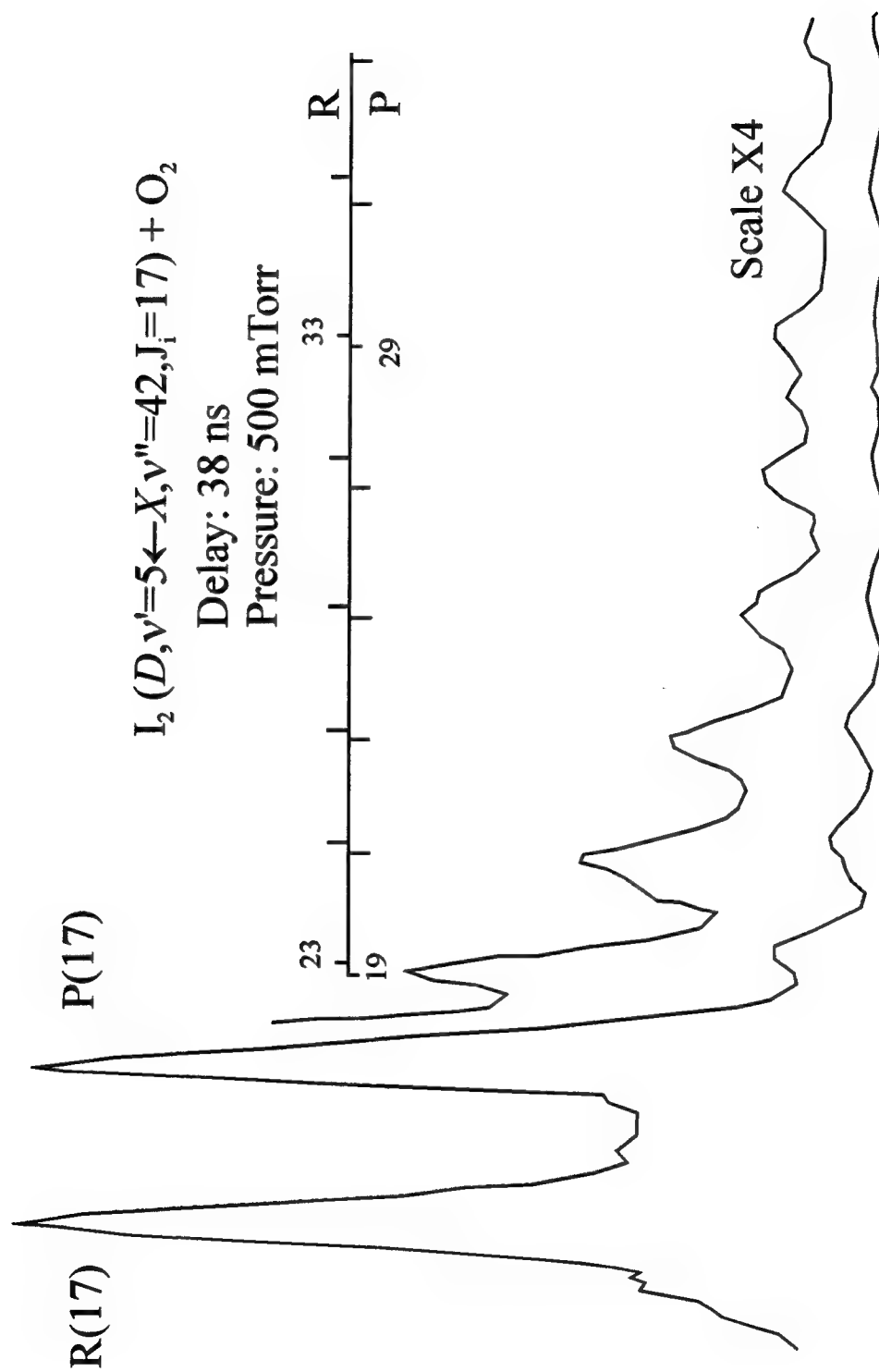
Figure 5.9: SEP-LIF of I_2 (X) $v''=42$, $J_i=17$ with O_2

downward vibrational energy transfer are evident in this trace. The rotational contours indicate that vibrational transfer within the B state was not accompanied by large changes in the angular momentum. Ground state vibrational energy transfer was observed for collisions with He and O_2. The populations transferred to $v''=41$ were sufficient to permit the recording of rotationally resolved spectra. In contrast vibrational transfer caused by collisions with I_2 or Ar could not be detected. The sensitivity of these measurements was limited by the fact that lines resulting from pure rotational transfer masked the weak levels originating from $v''=41$ levels.

§5.2 ANALYSIS

Computer simulations of the pump-dump-probe spectra were used to estimate the state-to-state energy transfer rate constants. This approach was necessitated by the fact that the spectra were not fully resolved. The computer model was based on a kinetic analysis that assumed single collision conditions and that collisions with a single species, M, dominated. As previously noted, efforts were made to ensure that these conditions prevailed. Starting with all the molecules in the prepared level $v_i=42$, $J_i=17$, the equations that describe the time evolution of the ground state population distribution[1] are

$$\frac{-d[\upsilon_i J_i]}{dt} = k_i[\upsilon_i J_i], \quad \text{and} \quad \frac{d[\upsilon_f J_f]}{dt} = k_f[\upsilon_i J_i]$$

where $[v_iJ_i]$ and $[v_fJ_f]$ are the populations in the initial and final states, respectively. Constants k_i and k_f are defined by the equations

$$k_i = \sum_{\upsilon_f} \sum_{J_f} k_M(\upsilon_iJ_i \rightarrow \upsilon_fJ_f)[M],$$

$$k_f = k_M(\upsilon_iJ_i \rightarrow \upsilon_fJ_f)[M],$$

where $k_M(v_iJ_i \rightarrow v_fJ_f)$ is a state-to-state transfer rate constant. Integration of the rate equations yields the results

$$[v_iJ_i] = [v_iJ_i]_0 e^{-kt} \text{ and } [v_fJ_f] = [v_iJ_i]_0 \, k_f/k_i \, (1-e^{-kt}).$$

Rovibrational population distributions, calculated from above equations and trial values for the rate constants, were used to generate synthetic spectra that could be compared with the experimental results. In principle, all of the rate constants could be varied until an optimum fit was achieved. However, the quality of our data was not sufficient to warrant this approach. Consequently, we used scaling laws to parametrize the rate constants, and then adjusted the parameter values to obtain agreement with experiment. For analysis of the pure rotational transfer data, a simplified version of the statistical power gap law[2] (SPG) was used, vis.,

$$k_M(J_i \rightarrow J_f) = CN_\Delta|\Delta E/B|^{-\gamma}$$

C and γ are fitted parameters. B is the rotational constant, ΔE is the difference in energy between the initial and final states and N_Δ is a statistical factor that depends on the extent to which the angular momentum projection quantum number, m, is modified by collisions. On the basis of this relationship, graphical simulations were used to obtain

best estimates for the parameters C and γ. Computer simulations of I_2 self transfer, and

I_2 with He and Ar are shown in Figures 5.10-5.12, respectively. The C coefficients were

constrained to give total rotational transfer rate constants $[k_{rot}=\Sigma_{J_f}k_M(J_i\rightarrow J_f)]$ that were

compatible with the decay rate constants given in Table 5.1. One set of fittings was

performed with the assumption that m is randomized by collision. A second set was

made with the constraint that Δm=0. The fits obtained with either assumption were

comparable, so I cannot comment on the efficiency of collisions that cause reorientation.

Parameters determined for the m-randomizing limit ($N_\Delta=2J_f+1$) and the associated k_{rot}

values are listed in Table 5.2. The individual rotational transfer rate constants for I_2 +He

is graphically illustrated in Figure 5.13.

Vibrational energy transfer (v_i=42$\rightarrow v_f$=41) was observed for collisions with He

and O_2. Features corresponding to upward transfer or multiquantum downward transfer

could not be detected. The rotational contours of the bands originating from v=41 were

consistent with a tendency to conserve angular momentum. From trial simulations it was

found that rate constants defined by the expression

$$k_M(v_i=42\ J_i=17 \rightarrow v_f=41\ J_f) = C_{42\text{-}41}\ N_\Delta\ |\Delta E_{rot}/B|^{-\gamma}$$

yielded distributions that were in good agreement with experiment. Here ΔE_{rot} is the

difference in rotational energy between the initial and final states. Note that the equation

has a singularity at ΔE_{rot}=0. This problem was avoided by setting

$$k_M(v_i=42\ J_i=17 \rightarrow v_f=41\ J_f=17) = k_M(v_i=42\ J_i=17 \rightarrow v_f=41\ J_f=19).$$

$$k_{i \to f} = 0.34 N_< \ |\Delta E/B|^{-0.7}$$
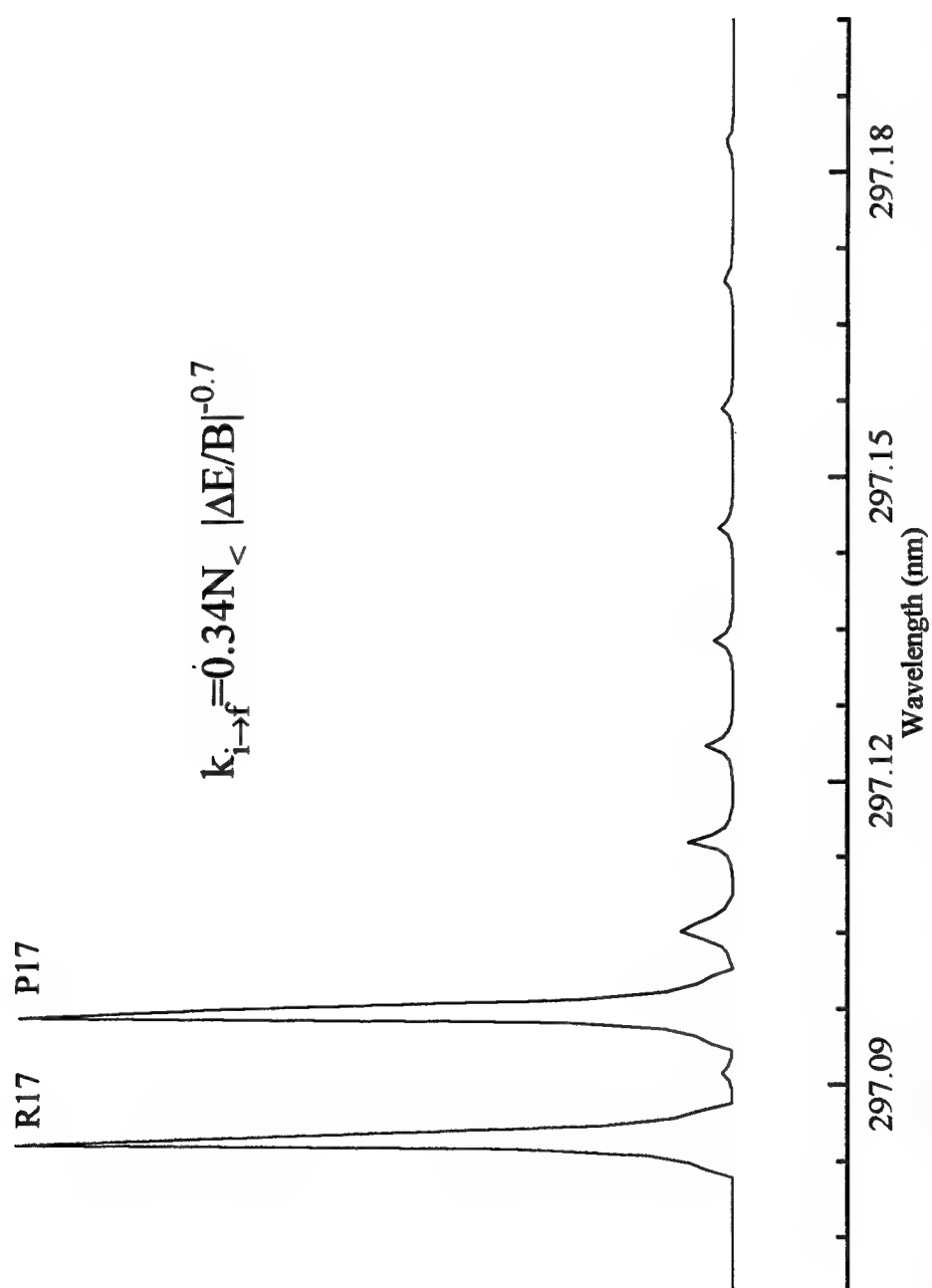
Figure 5.10: Simulation of Rotational Energy Transfer of I_2 Self Transfer for D, $v=5 \leftarrow X, v=42, J_i=17$

$$k_{i \to f} = 4.5 N_j \ |\Delta E/B|^{-1.2}$$

Scale X4

R17

P17

Wavelength (nm)

297.09   297.12   297.15   297.18   297.21   297.24
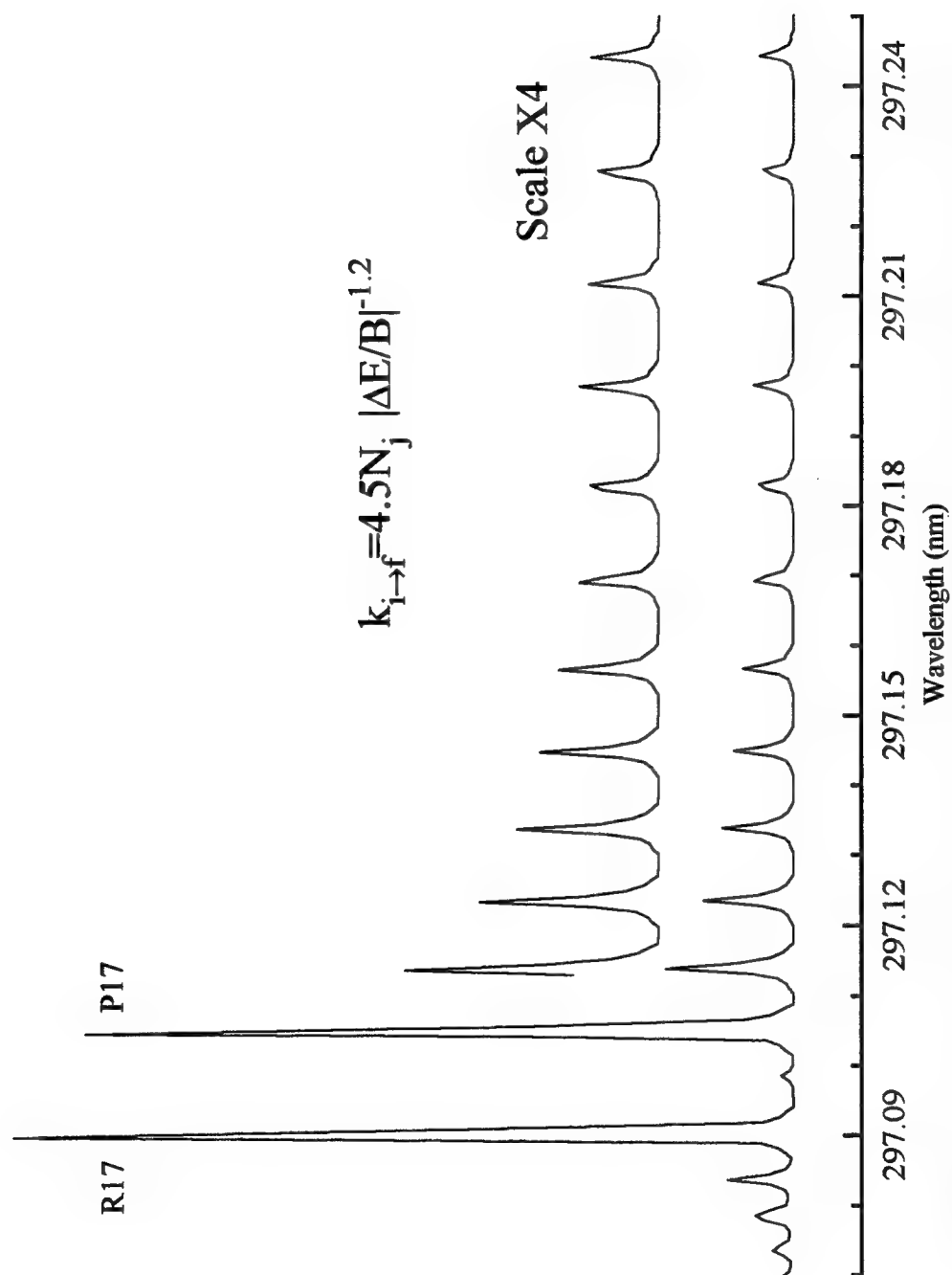
Figure 5.11: Simulation of Rotational Energy Transfer of I_2 + He for $D, v=5 \leftarrow X, v=42, J_i=17$
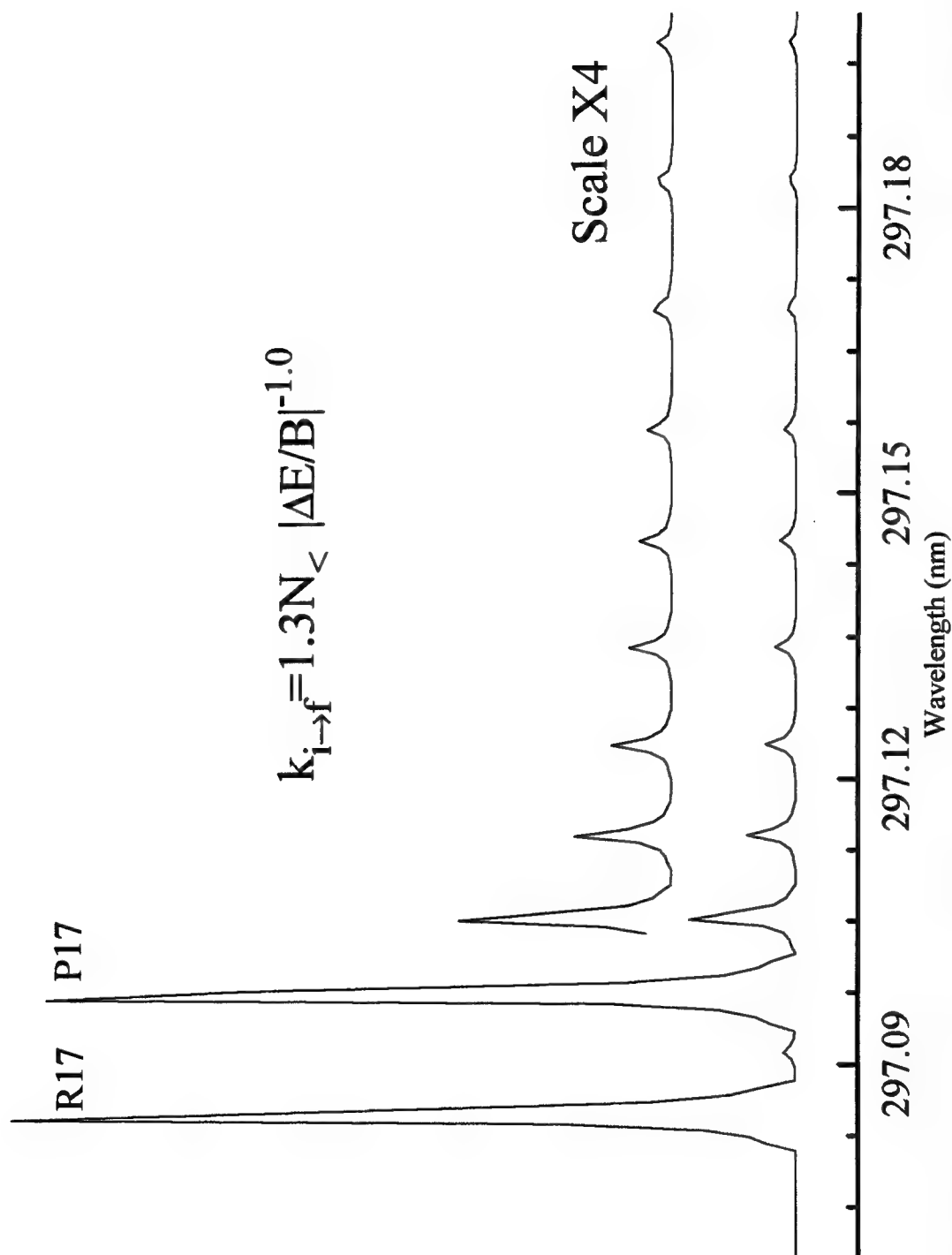
Figure 5.12: Simulation of Rotational Energy Transfer of I_2 + Ar for $D, v=5 \leftarrow X, v=42$, $J_i=17$

Table 5.2: Rotational Energy Transfer Rate Constants
and Statistical Power Gap Law Coefficients

Collision partner	I_2 (X) v"=42		
	γ	C^{ab}	$k_{rot}{}^{b,c}$
He	1.2	4.5	6.0
Ar	1.0	1.3	5.0
O_2	1.0	1.9	7.2
I_2	0.7	0.3	8.6

a. Coefficients calculated by considering $1 \leq J_f \leq 101$.
b. Units of 10^{-10} cm^3 s^{-1}
c. Error limits $\pm 0.5 \times 10^{-10}$ cm^3 s^{-1}.

Collision partner	I_2 (B)		
	γ	C	k_{rot}
He	1.40[d]	1.18[d]	5.5[e]
Ar	1.41[f]	....	4.6[g]
O_2	....	....	3.8[h]
I_2	1.49[f]	....	1.7[g]

d. S. Dexheimer, M. Durand, T. Brunner, and D. Pritchard, *J. Chem. Phys.* **76**, 1996 (1982). v'=13, J' =41 to 113
e. I_2(B) v_i=15, J_i=59. Reference 4
f. I_2(B) v_i=11, J_i=79. Reference 9
g. I_2(B) v_i=15, J_i=33. Reference 4
h. I_2(B) v_i=25, J_i=34. Reference 8

$$k \approx CN_\lambda \Delta E^{-1.2}$$
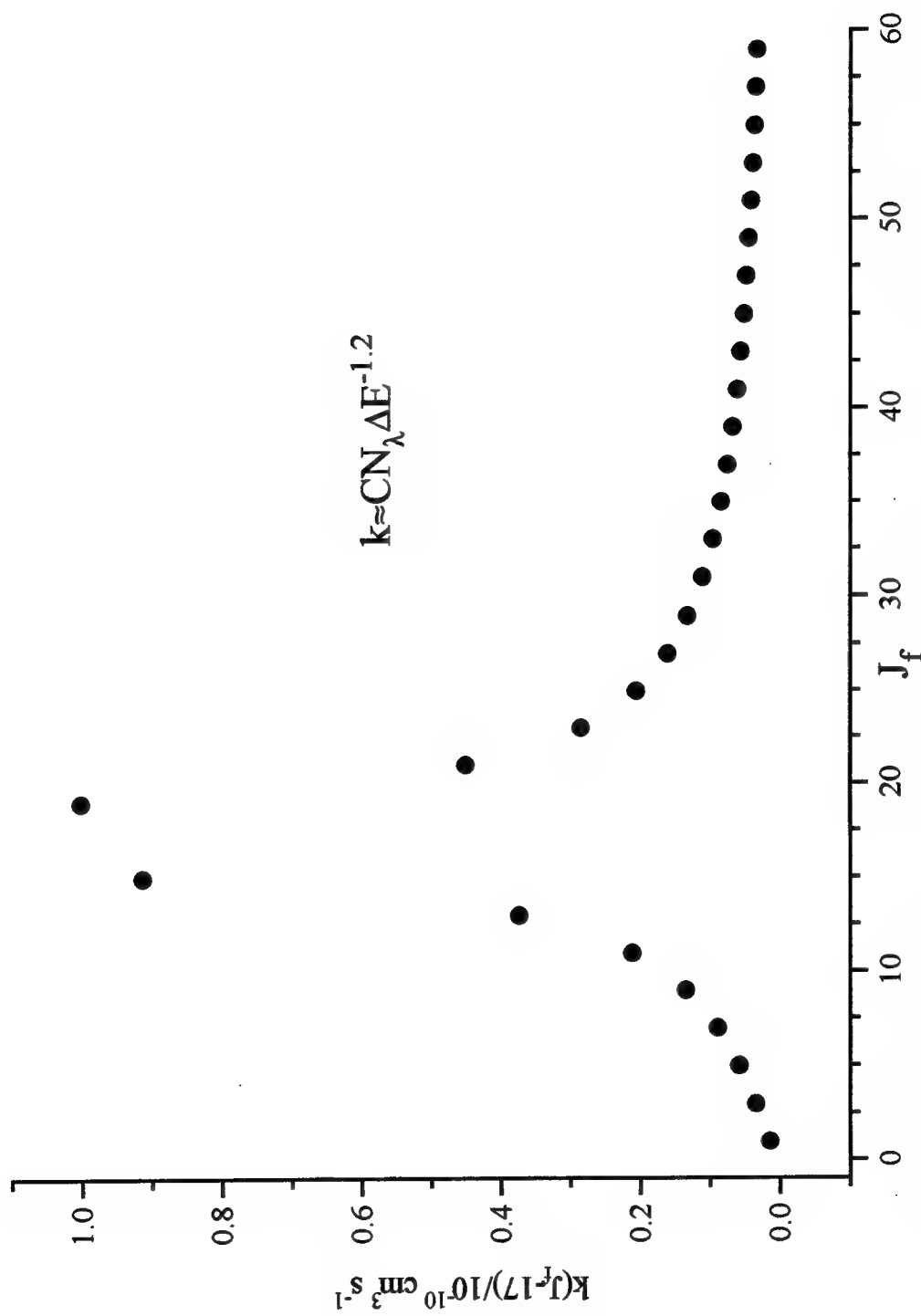
Figure 5.13: Rotational Transfer Rate Constants for $I_2(X, v''=42, J_i=17)+He$

The values of γ used in these simulations were taken from Table 5.2, leaving only the $C_{42\text{-}41}$ coefficients to be determined from the fits. Overall rate constants for transfer from v_i=42 to v_f=41 were evaluated by summing the state-to-state rate constants. These are given in Table 5.3. The vibrational model was also used to investigate the upper limits for the rate constants for relaxation induced by Ar or I_2. The upper limits given in Table 5.3 were estimated by finding values for the constants that were on the threshold of producing discernible featues in the simulated spectra.

§5.3 DISCUSSION

The rate constants for removal of population from the v''=42, J''=17 level of $I_2(X)$ indicate, for all collision partners investigated, that transfer occurs on every collision. There is only one other measurement that can be compared directly with these results. Koffend et al.[3] examined the self-relaxation of a group of rotational levels (J''=11, 13, 15 and 17) in the v''=42 manifold. They reported a lower limit for the removal rate constant of 2.1×10^{-10} cm^3 s^{-1}, with which the result of the present study is compatible. For collisions with He, Ar, and I_2 the total removal rate constants for $I_2(X)$ are very similar to those reported by Derouard and Sadeghi[4] for various rotational levels of I_2 $B(v'$=15).

The present rate constants for vibrational energy transfer are compared with results for I_2 $X(v''$=40) from the work of Hall et al.[5] in Table 5.3. For collisions with Ar and I_2, the SEP results are significantly lower than the rate constants reported by Hall et

Table 5.3: Vibrational Energy Transfer Rate Constants for I_2 (X)

Collision partner	$k_v/10^{-11}$ cm^3 molecule^{-1} s^{-1}		
	$v_i=42^a$	$v_i=40^b$	$v_i>20^c$
He	5.5±1.0	3.1±0.6	-
Ar	<1	2.3±0.1	<0.5
O_2	4.5±1.0	-	0.5
I_2	<1	5.6±1.2	-

a. Present study (SEP-LIF)
b. Hall et al.(v_i=40)
c. Hiedner et al. Note: Overall deactivation to levels below v''=20 for I_2 (X).

al. The discrepancy is reversed and less pronounced for He. I am not aware of any obvious reasons for these differences. One possibility is that vibrational energy transfer induced by Ar or I_2 involves large changes in the angular momentum and /or significant $|\Delta v|>1$ processes. Partitioning of the transferred population into a large number of final states would then require very high sensitivities and signal-to-noise ratios for detection. Under these circumstances transfer could have occurred with the rate constants proposed by Hall et al., without producing detectable $\Delta v=-1$ features in the present SEP measurements. The vibrational rate constants are consistent with van Benthem and Davis[6] observation that He relaxed $I_2 X(v''>33)$ more rapidly than Ar, and the low estimate of Heidner et al.[7] for the rate at which I_2 is activated by Ar. Relaxation by $O_2(X)$ was also considered in the Heidner et al. model of the flow tube kinetics. Two sets of rate constants were found to be in reasonable agreement with experiment. The oxygen deactivation terms in these models were 5×10^{-11} and 5×10^{-12} cm^3 s^{-1}, respectively. Given the multi-step nature of the deactivation process, the latter is more compatible with the present results.

§5.4 ACKNOWLEDGMENT

The experiment discussed in Chapter 5 of this dissertation was performed at the Air Force Phillips Laboratory, NM while assigned to the Chemistry Section, Advanced Concepts Branch, Laser Systems Division. I wish to acknowledge the assistance of 2Lt Shawn Gaffney whose long hours of support were exceeded only by his enduring

friendship and excellence. Data collection was greatly simplified by D. Christopher Burst whose outstanding programming talent was so skillfully demonstrated in his *Scanner* program. My deepest thanks go to Dr. Ernest Dorko, who supported the author and this experiment under difficult and sometimes adverse circumstances.

§5.5 REFERENCES

1. M. L. Nowlin and M. C. Heaven, *J. Phys. Chem.* **99**, 5654 (1993).

2. T. A. Brunner and D. E. Pritchard, *Adv. Chem. Phys.* **50**, 589 (1982).

3. J. B. Koffend, F. J. Wodarczyk, R. Bacis, and R. W. Field, *J. Chem. Phys.* **72**, 478 (1980).

4. J. Derouad and N. Sadeghi, *Chem. Phys. Lett.* **102**, 324 (1983).

5. G. E. Hall, W. J. Marienelli, and P. L. Houston, *J. Phys. Chem.* **87**, 2153 (1983).

6. M. H. van Benthem and S. J. Davis, *J. Phys. Chem.* **90**, 902 (1986).

7. R. F. Heidner, C. E. Gardner, G. I. Segal, and T. M. El-Sayed, *J. Phys. Chem.* **87**, 2348 (1983).

8. J. I. Steinfeld and W. Klemperer, *J. Chem. Phys.* **42**, 3475 (1970).

9. H. Chun, H. Ruiping, and Z. Cunhao, *Appl. Phys. B* **41**, 251 (1986).

CHAPTER 6

STIMULATED EMISSION PUMPING $v''= 38$

§6.1 RESULTS

Figure 6.1 shows a typical SEP-LIF spectrum taken under low resolution. The two notable features of this spectrum are the SEP prepared J"=49 lines and the inadvertent optical-optical double resonance (OODR) J'=40 and J'=48 lines. A sample calculation for line positions in $v''=38$ is provided in Appendix A. The resonant three-photon SEP-LIF technique has the advantage of eliminating the rotational congestion through rotational state selection rules. However, the conditions for the preparation and analysis of $I_2(X; v''=38)$ were also favorable for OODR of the $f(0^+_g){\leftarrow}B(0^+_u)$ via the *pump-probe* sequence. Fortunately, sufficient separation ($\approx$40 cm^{-1}) between the SEP and OODR transitions provided for clean and uncongested spectra near the initially prepared levels. In order to remove any ambiguities in assignment and analysis at high and low J, scans were run with and without the *dump* laser as shown in Figures 6.2 and 6.4. Interestingly, a comparison of collisionally induced rotational energy transfer between the X state and the B state indicates an intriguing result. When comparing RT transfer between the two states for I_2+Ar as shown in Figure 6.2, angular momentum occurs over more rotational states as indicated by the relative intensity of the spread surrounding each parent peak.
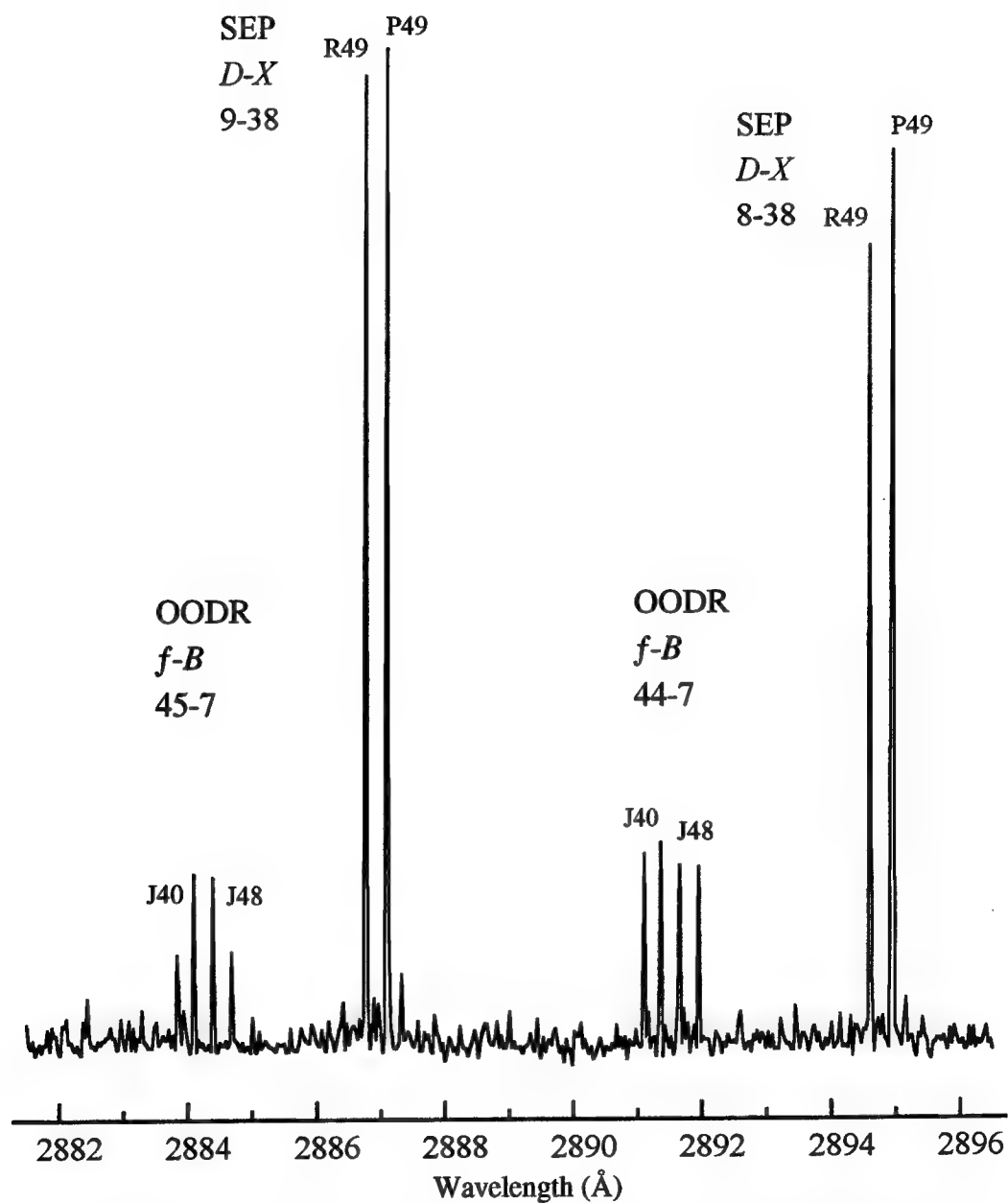
Figure 6.1: Low Resolution LIF Spectrum Showing OODR
and SEP for *f-B* and *D-X*, respectively.
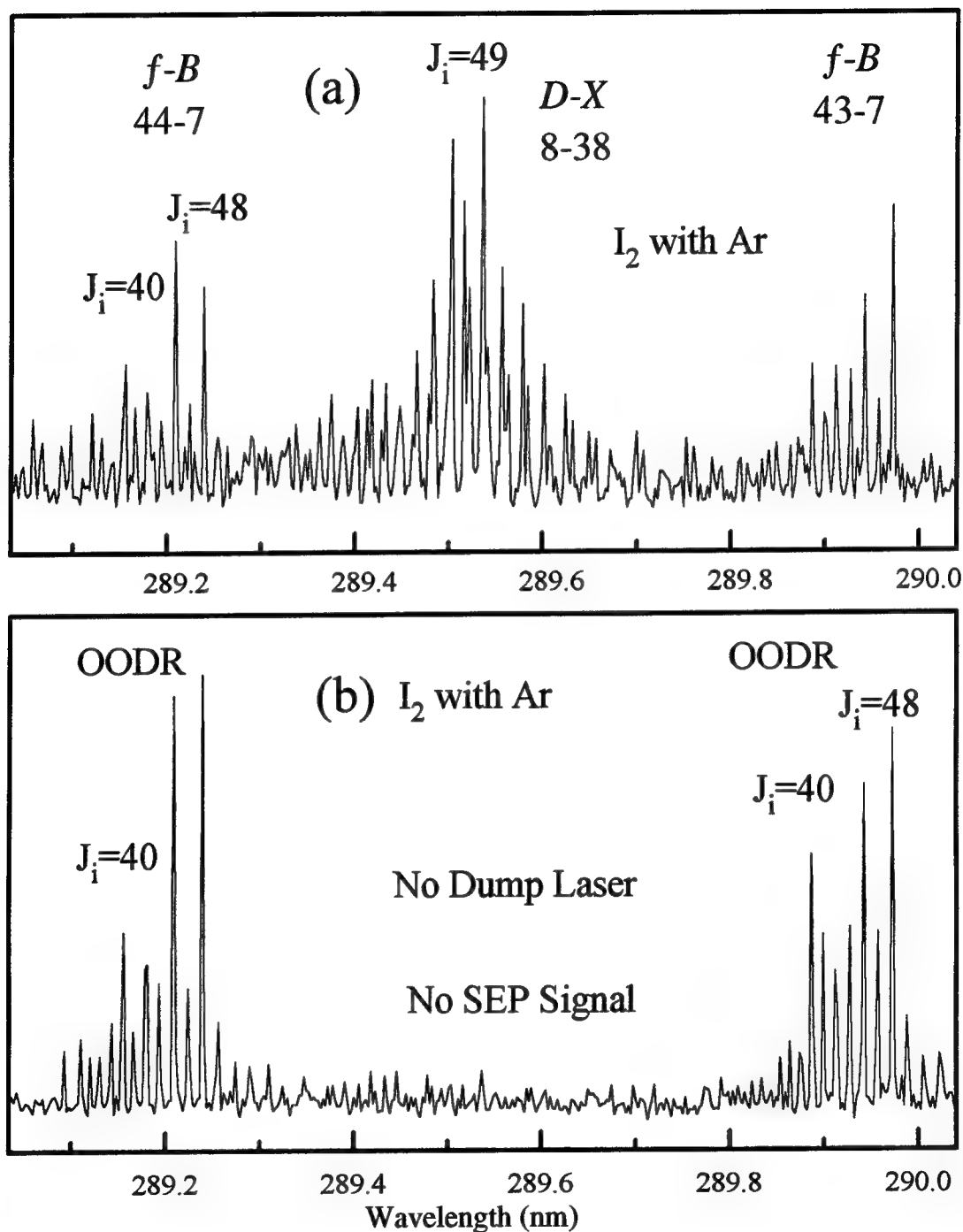
Figure 6.2: Comparison of Low Resolution Spectra of I_2+Ar With
D-X and f-B Transitions Showing Rotational Energy
Transfer (a) With and (b) Without Dump Laser

Experimentally determining the energy transfer rate coefficients required recording the rotationally resolved fluorescence spectra and following the laser excitation of individual rovibrational levels. Under high resolution, the initially prepared parent peaks are observed in Figure 6.3. Rotational transfer by collisions result in the appearance of satellite peaks in the fluorescence spectrum. Under mild experimental conditions, the progression of the P and R doublets resulting from rotational energy transfer with helium is cleanly resolved under the high resolution scans. Since the initial J value for this SEP-LIF experiment was odd (J_i =49), only odd J values were populated due to the rigorous symmetry selection rule $\Delta J=\pm 2n$ for a homonuclear diatomic because nuclear spin states are not easily changed by collisions. Once again, many scans were collected in pairs as shown in Figure 6.4; one with the *pump-dump-probe* (SEP) sequence, and one with the *dump* laser blocked (OODR). Unlike $v"$=42 SEP spectra, the OODR was sufficiently isolated and interference with RT energy transfer was minimal. In addition, the B_v constants for the levels investigated were such that both the P and R branches were cleanly resolved under our experimental conditions. This eliminated the spectral overlap problem which was present in the $v"$=42 SEP experiment.

Collecting experimental data for determining the kinetics was accomplished through two different methods. The first method involved fixing the delay between the *dump* and *probe* lasers, while the second method involved fixing the pressure and adjusing the delay. The second method was the manner in which the majority of the
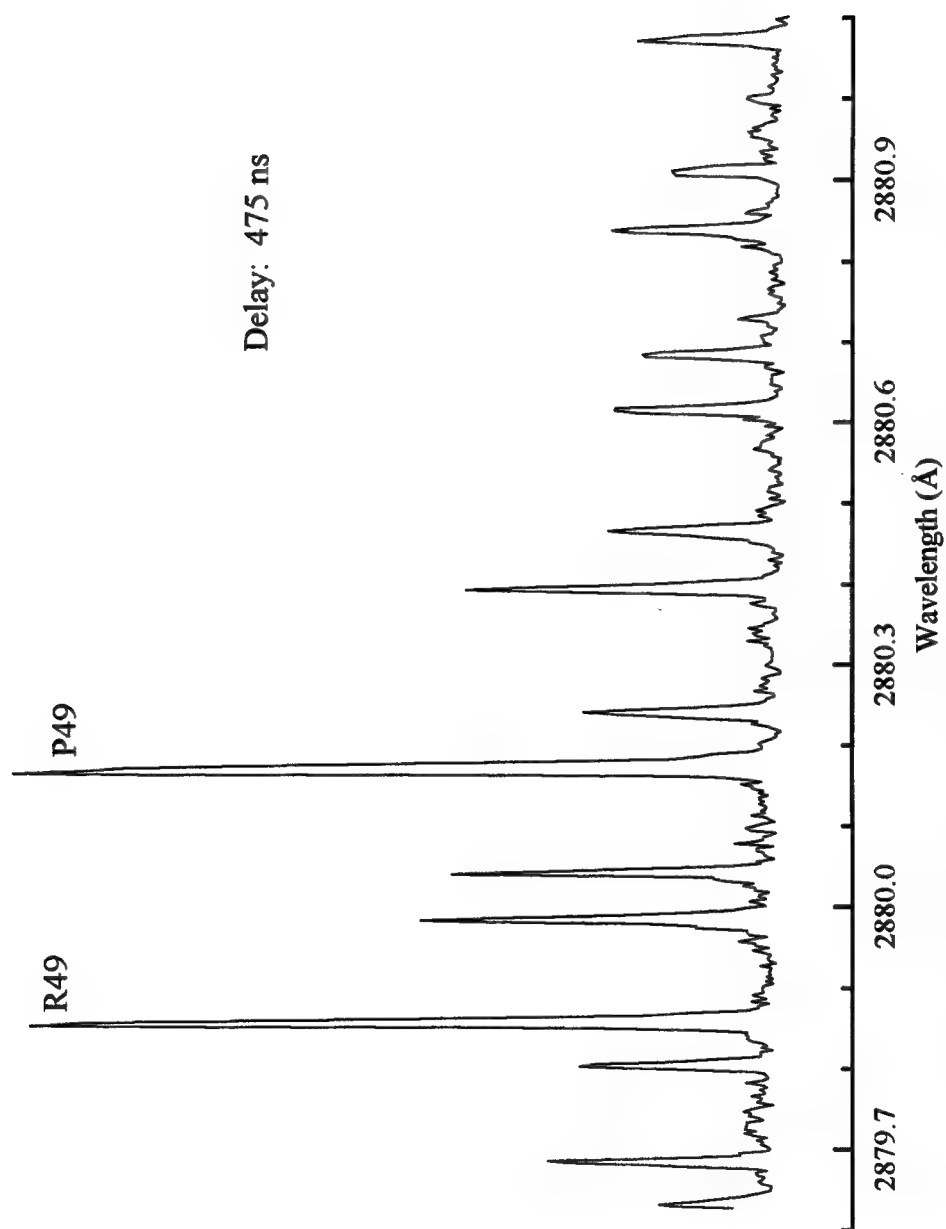
Figure 6.3: SEP-LIF of I_2 ($D, v'=10 \leftarrow X, v''=38$) with He
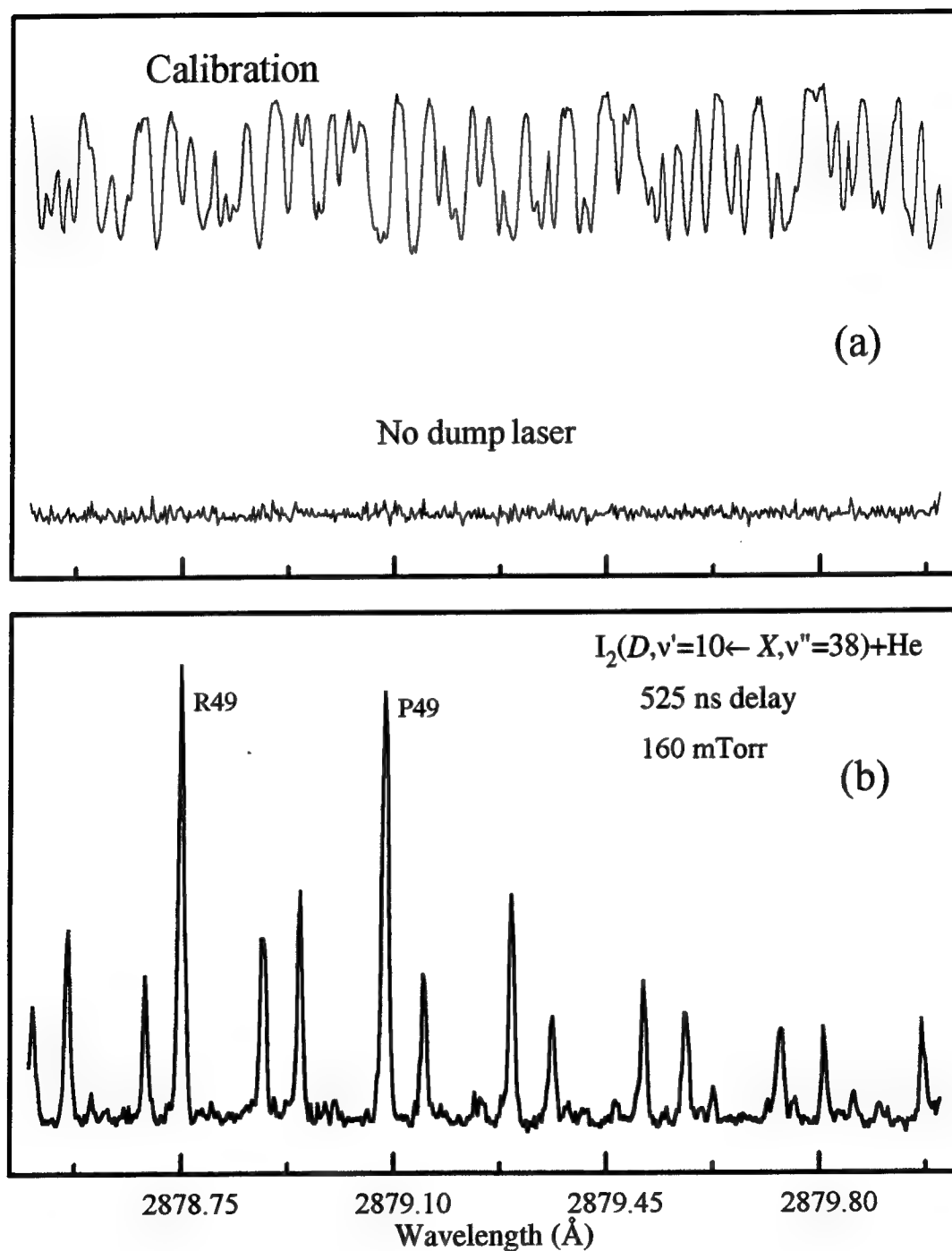
Figure 6.4: High-Resolution Spectra of I_2 $D{\leftarrow}X$ With He Showing (a) No (OODR) Signal from *pump-probe* Sequence (*dump* Laser Blocked) and (b) Transitions from *pump-dump-probe*

energy transfer data was collected. With the delay fixed, numerous scans with different pressures would be collected. Figure 6.5 shows effects of quenching with increasing pressure. Initially, the lack of an accurate and calibrated baratron hindered data collection in this manner. A McLeod mercury manometer (10^{-4} - 0.2 Torr) was connected to the sample chamber. While providing absolute pressure determinations, the McLeod gauge suffered several inherent problems. First, measurements could not be made on a continuous basis and were time-consuming since the mercury reservoir had to be raised and lowered each time a measurement was recorded. Second, the iodine reacted with the mercury forming a red-orange solid, HgI_2 in the capillary tubes which required cleaning with an ethanol/acid rinse. And third, mercury has a measurable vapor pressure at room temperature. No cold trap was installed between the mercury manometer and the sample chamber in order to prevent mercury streaming error.[1] So in order to minimize contamination, a shut-off valve was installed and kept in the closed position until measuring of the chamber pressure was required. In addition, spectra were collected with increasing diluent pressure to prevent any reflux from the manometer into the sample chamber.

Since iodine self-transfer must be accounted for in all spectra, a thorough characterization of iodine was performed. Figure 6.6 shows a high resolution scan of iodine self-transfer. In comparison with other spectra, the obvious feature of all iodine self-transfer spectra is the relative lack of rotational energy transfer. In addition, efforts
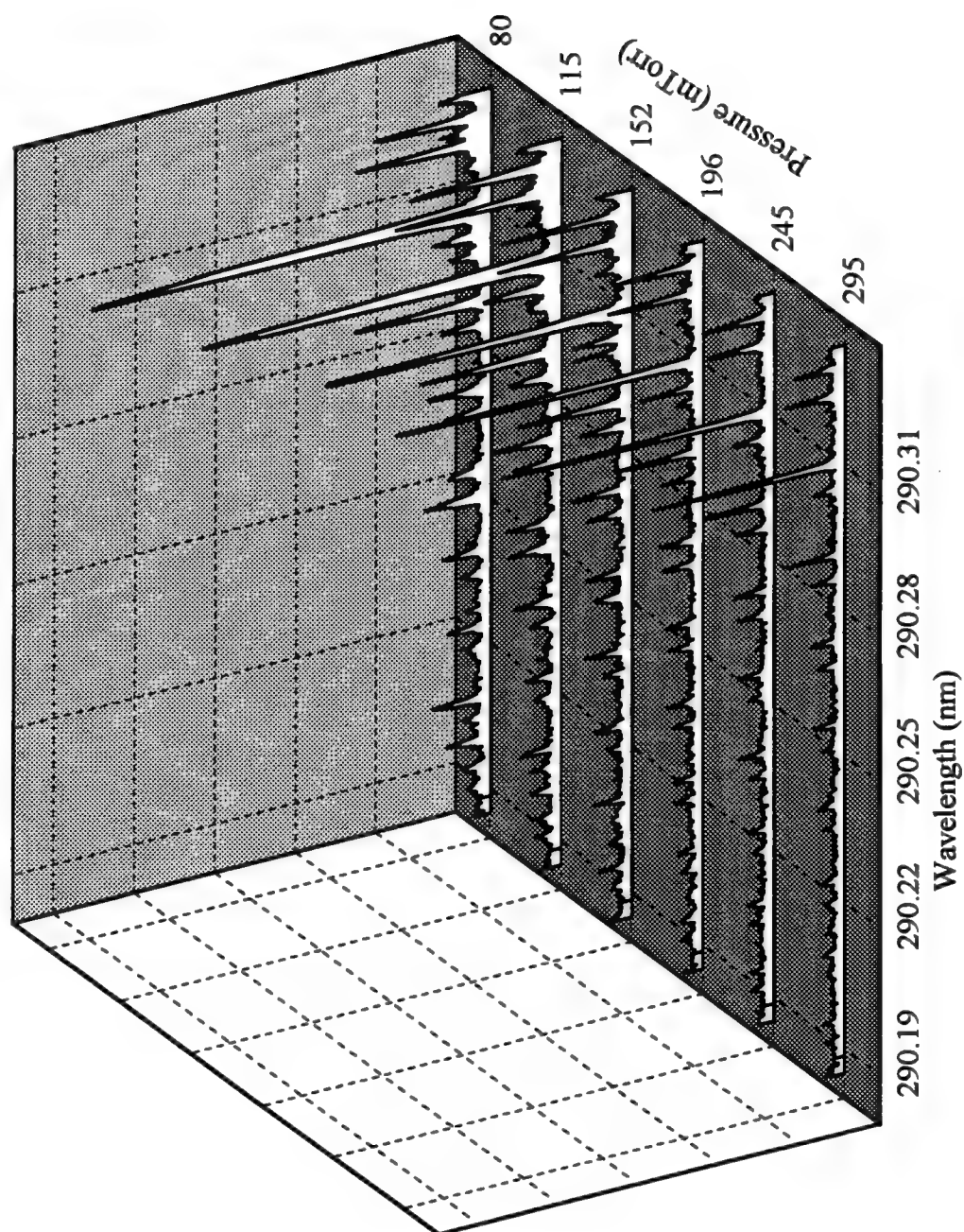
Figure 6.5: Spectra of I$_2$ (D;v'=7←X;v''=38) and Ar with increasing diluent pressure at 280 ns delay
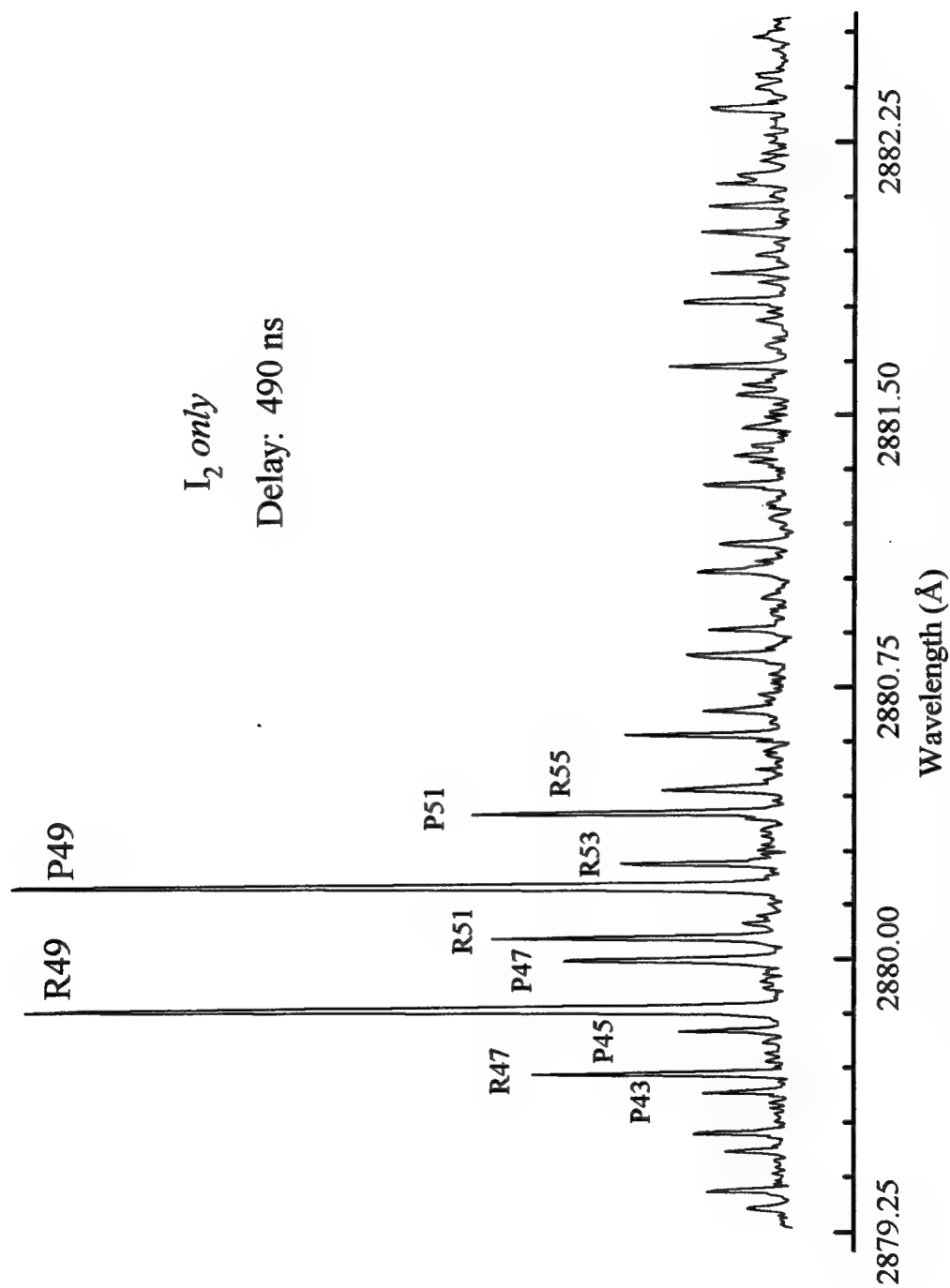
Figure 6.6: SEP-LIF Spectrum of I_2 ($D, v'=10 \leftarrow X, v''=38$)

were made to characterize energy transfer in terms of the colliding mass. RET spectra of N_2 and O_2 are shown in Figures 6.7 and 6.8, respectively.

Collision partners which are relevant to the COIL device such as Cl_2, H_2O, and He were examined as well. Experimentally, the introduction of Cl_2 into the chamber produced a unique pressure decrease. Upon adding Cl_2 to the iodine sample chamber, the pressure would experience a rather steep drop as if a chemical reaction between I_2 and Cl_2 was occurring. While the reaction $I_2 + Cl_2 \rightarrow 2ICl$ proceeds at room temperature, and inspection of the sample chamber revealed no unusual deposits. ICl consists of two crystalline forms[2]: the α form which crystallizes as large transparent ruby red needles; or the metastable β form which is obtained as brownish red crystals. Obtaining a RET spectrum with chlorine as shown in Figure 6.9 would require constant monitoring and a periodic addition of Cl_2 to maintain constant pressure ($\pm$ 5 mTorr).

Besides Cl_2, H_2O and D_2O were difficult diluents for recording RET spectra due to the large pressure fluctuations upon adding of the gas into the sample chamber. Both liquids (H_2O and D_2O) were subjected to numerous *freeze-pump-thaw* cycles to remove any dissolved gases from the sample. While the sample was still frozen, the chamber was opened to the diluent until the desired pressure was obtained. The observed pressure fluctuation can be described by the non-ideal behavior of H_2O and D_2O in iodine. Spectra were collected after the pressure stabilized (usually 20-30 mins). Examples of RET for H_2O and D_2O are shown in Figures 6.10 and 6.11, respectively.

Vibration-translation energy transfer was observed for all the collision partners for which spectra were collected. For the collisional partners examined, vibrational
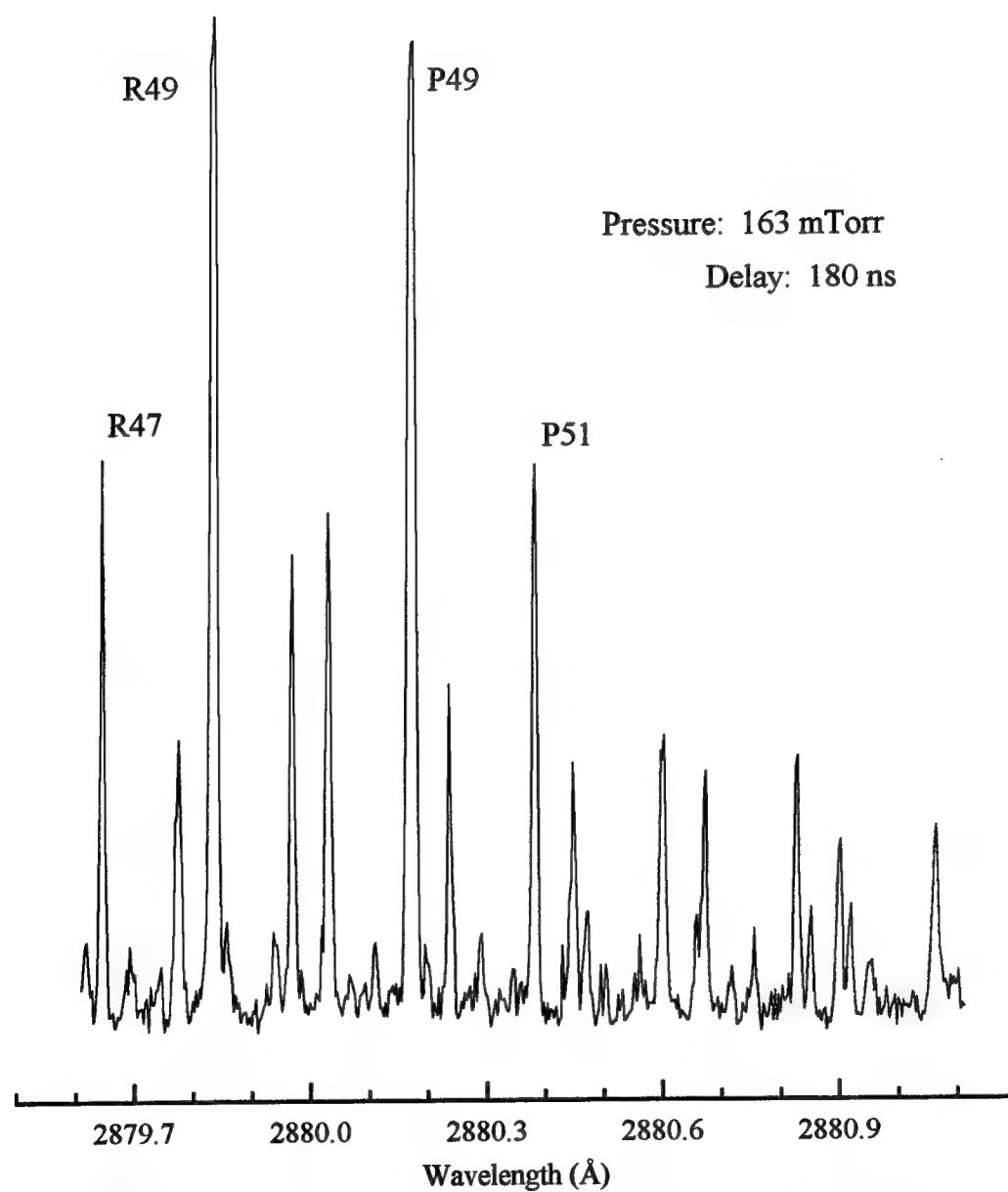
Figure 6.7: SEP-LIF Spectrum of I_2 $(D,v'=10 \leftarrow X,v''=38)$ with N_2
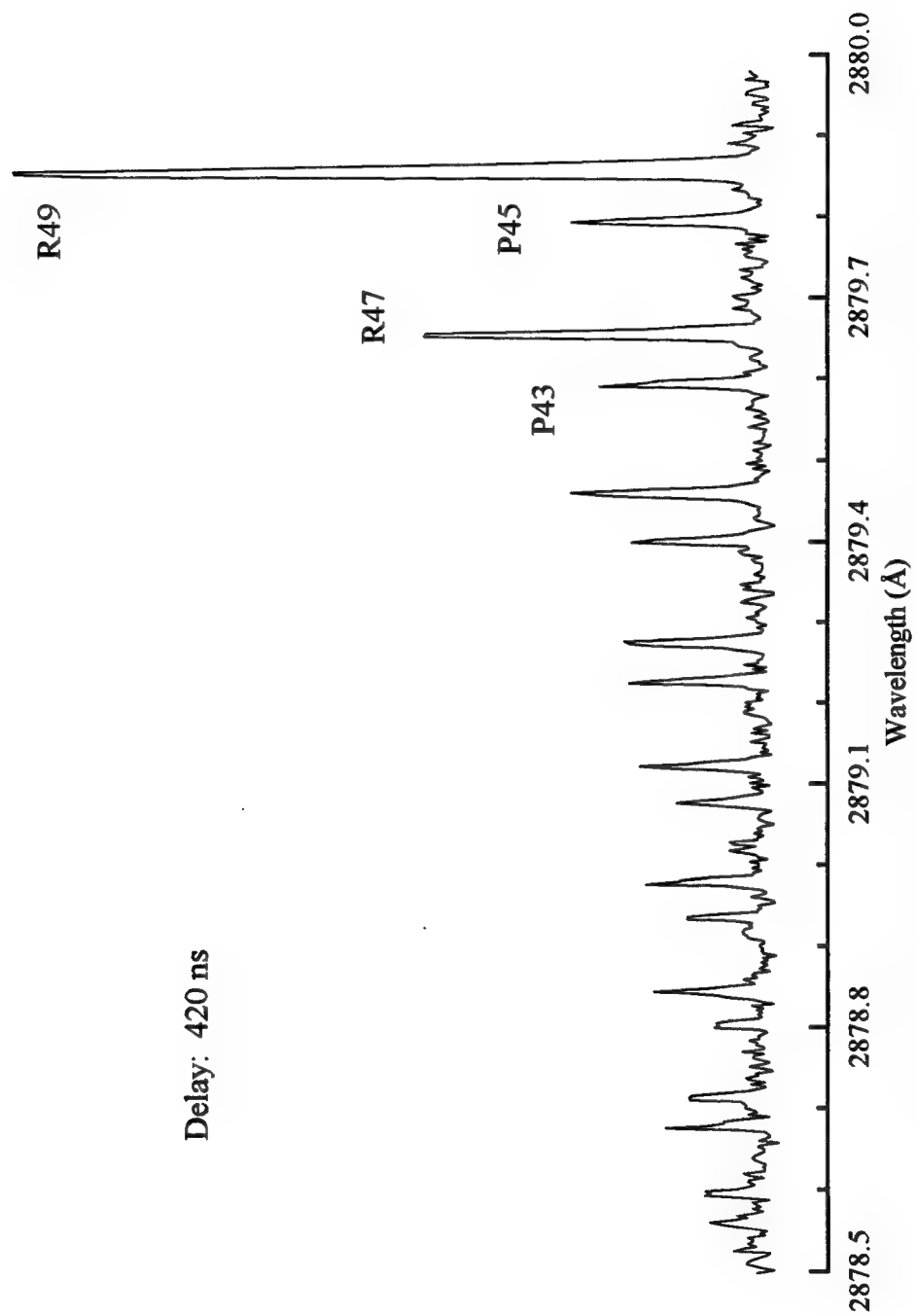
Figure 6.8: SEP-LIF Spectrum of I_2 ($D, v'=10 \leftarrow X, v''=38$) with O_2
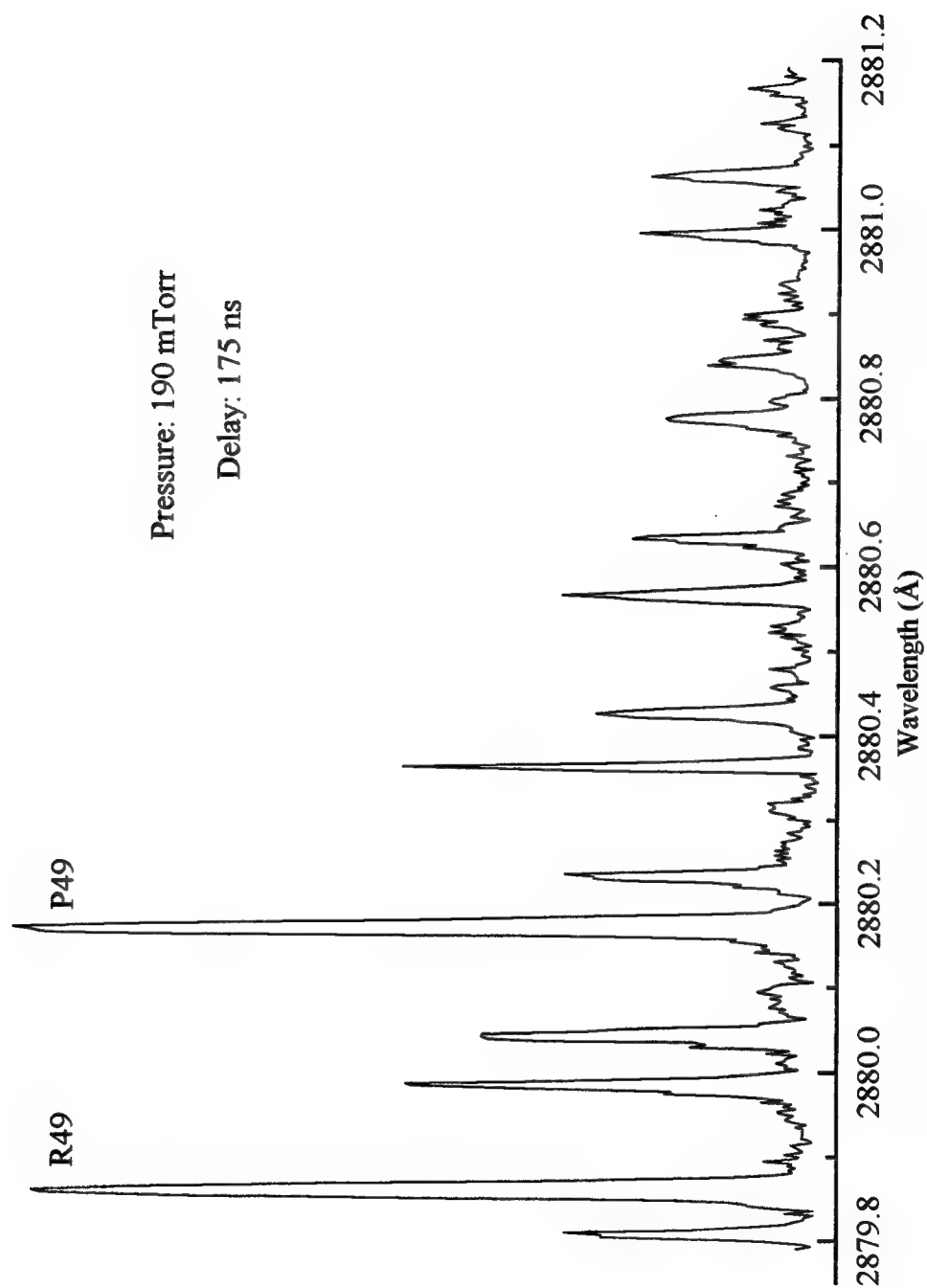
Figure 6.9: SEP-LIF Spectrum of I_2 ($D, v'=10 \leftarrow X, v''=38$) with Cl_2
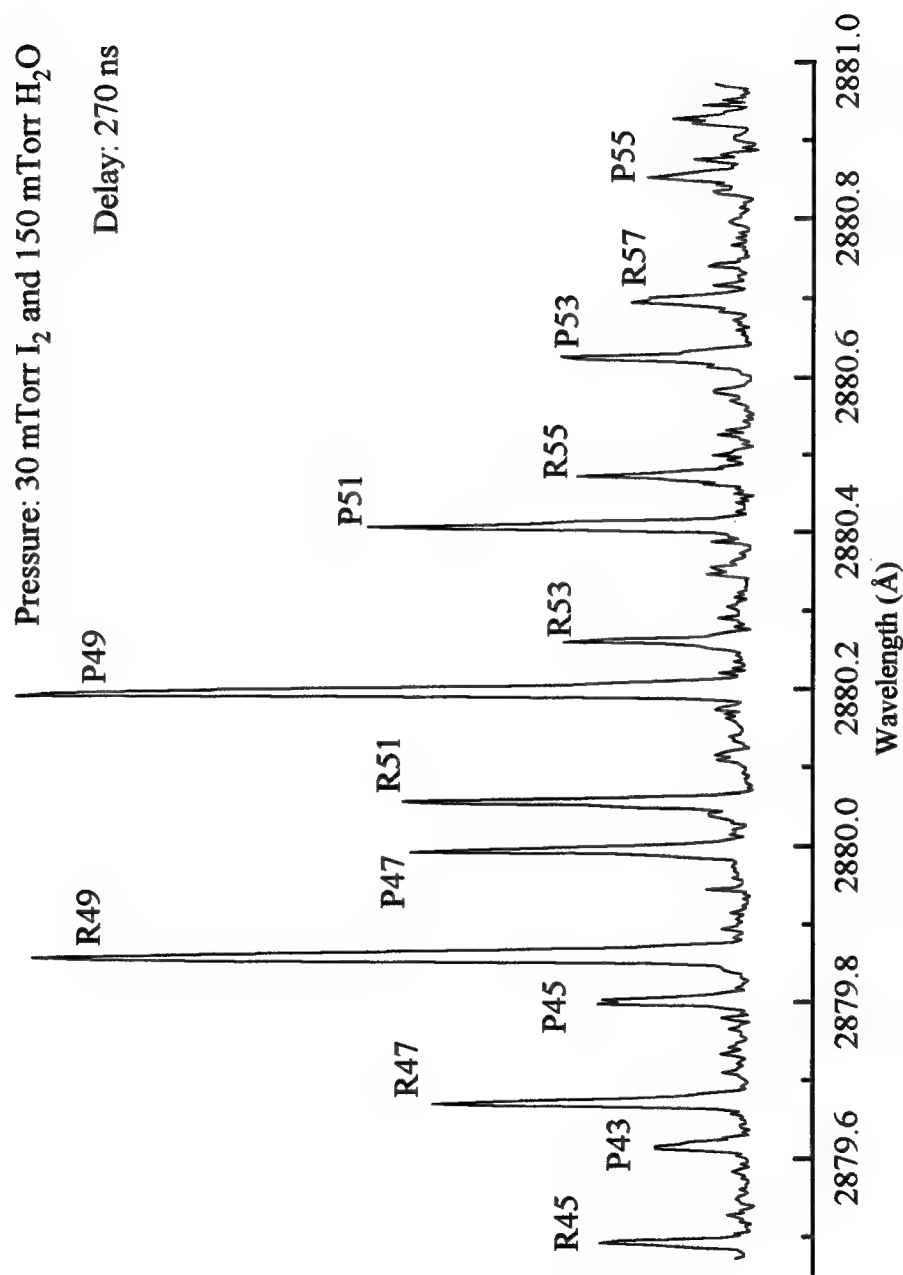
Figure 6.10: SEP-LIF Spectrum of I_2 ($D, v' = 10 \leftarrow X, v'' = 38$) with H_2O
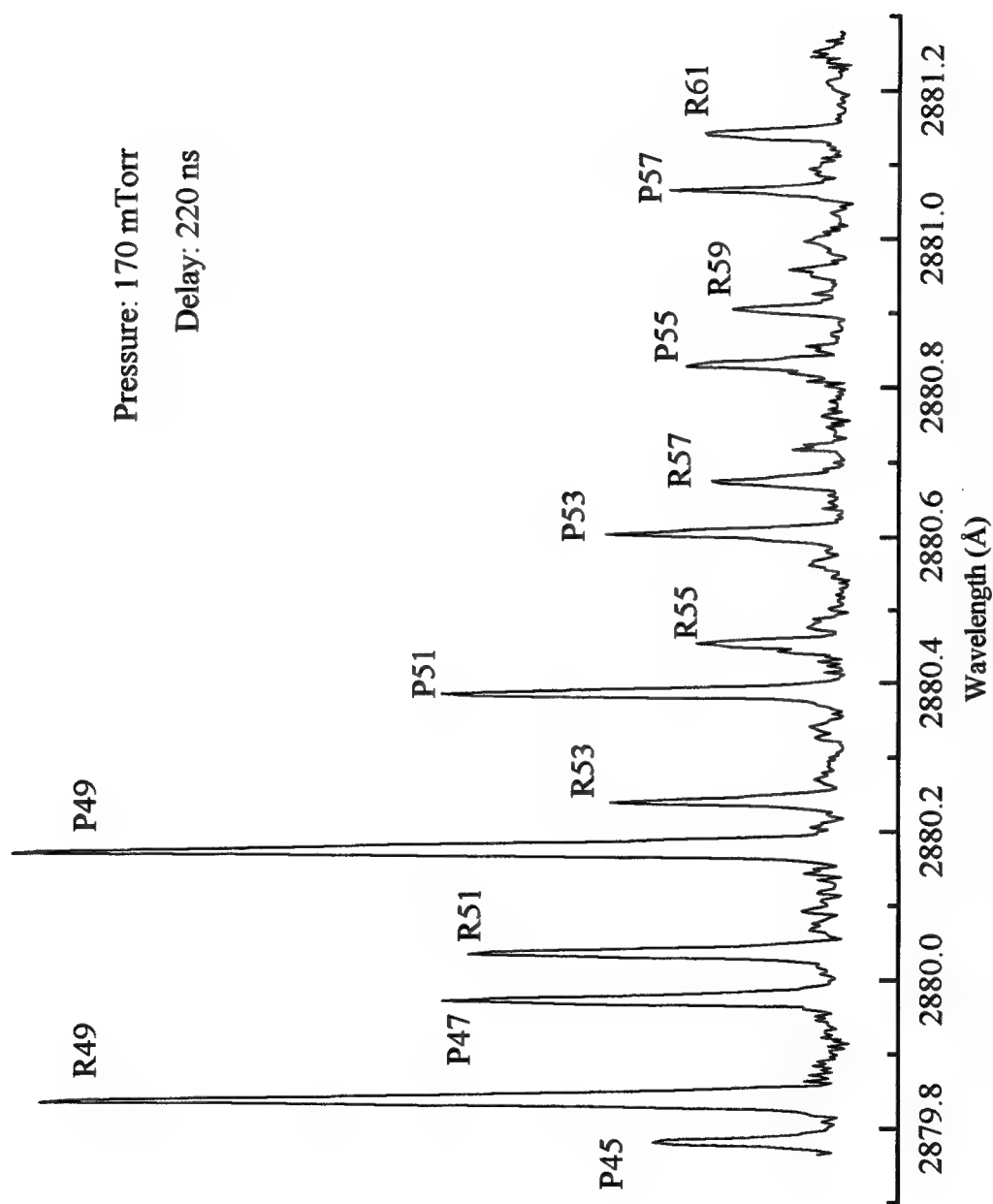
Figure 6.11: SEP-LIF Spectrum of I_2 (D,v'=10←X,v''=38) with D_2O

relaxation was governed by a strong $\Delta v=-1$ propensity. Some rotational memory is evident as J=49 is the strongest feature. Figure 6.12 shows a high resolution LIF spectrum with Ar diluent. Collision-induced transfer by Ar is evident for both v"=38 and v"=37 (the noise level in v"=42, as discussed in Chapter 5, precluded detection of vibrational transfer by Ar or I_2). Energy transfer with Cl_2 and D_2O are shown in Figures 6.13 and 6.14, respectively. The intensity pattern is remarkably similar for both of these species except near the end of the scan (< 2873.2 nm) where the intensity of the Cl_2 for v"=38 is slightly decreasing due to the pressure effects previously discussed.

§6.2 ANALYSIS

Ideally, one would always work at pressures sufficiently low and delays sufficiently short that the probability of multiple collisions are negligible. Unfortunately, these restrictive experimental conditions are not necessarily the most favorable for obtaining adequate signal intensity for data gathering. At sufficiently high bath gas pressures and/or long delay times, secondary collisions from the initially populated or collisionally populated levels must be considered . These secondary collisions may repopulate the initially prepared state or the satellite band under investigation. This kinetic process is known as back transfer and it has the delirious consequence of giving rate coefficients which do not accurately reflect the relaxation events under investigation.[3] Thus, corrections are necessary to properly account for these kinetic events if experimental conditions do not warrant single collision. Single-collision conditions in a cell-experiment are given by
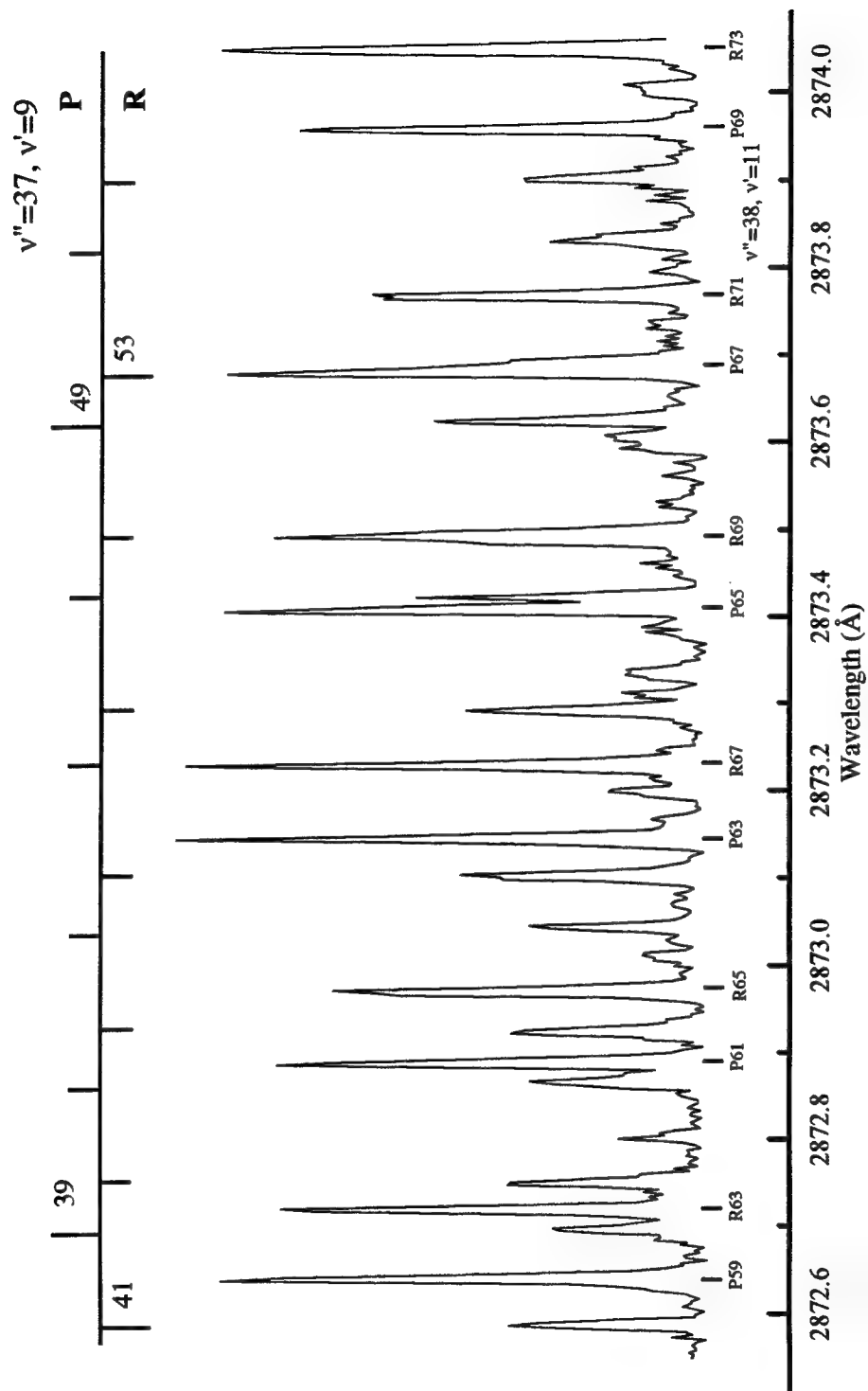
Figure 6.12: High Resolution SEP-LIF Spectrum of I_2 (X) v''=38 and Ar
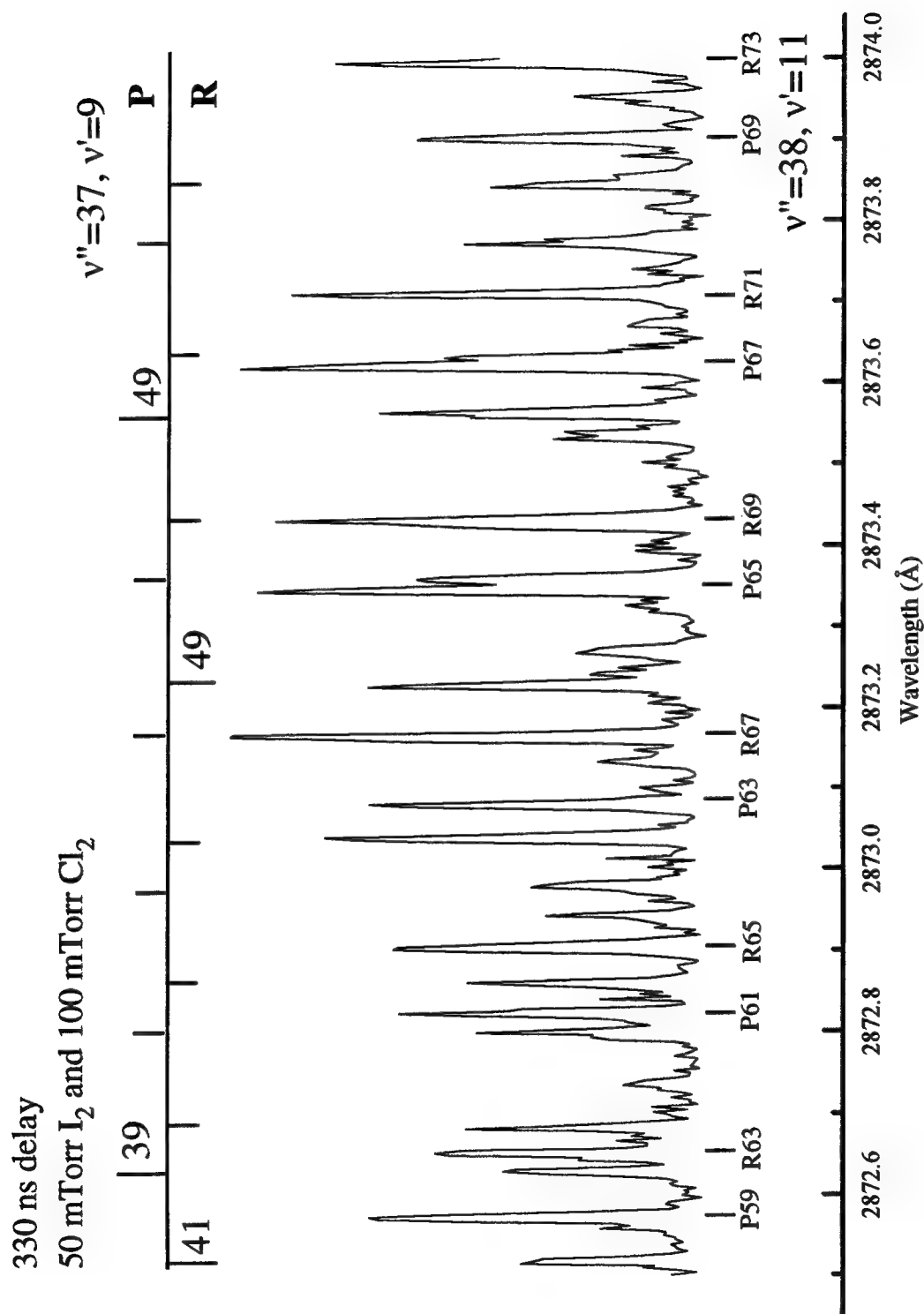
Figure 6.13: High Resolution SEP-LIF Spectrum of I_2 (X; v''=38) with Cl_2
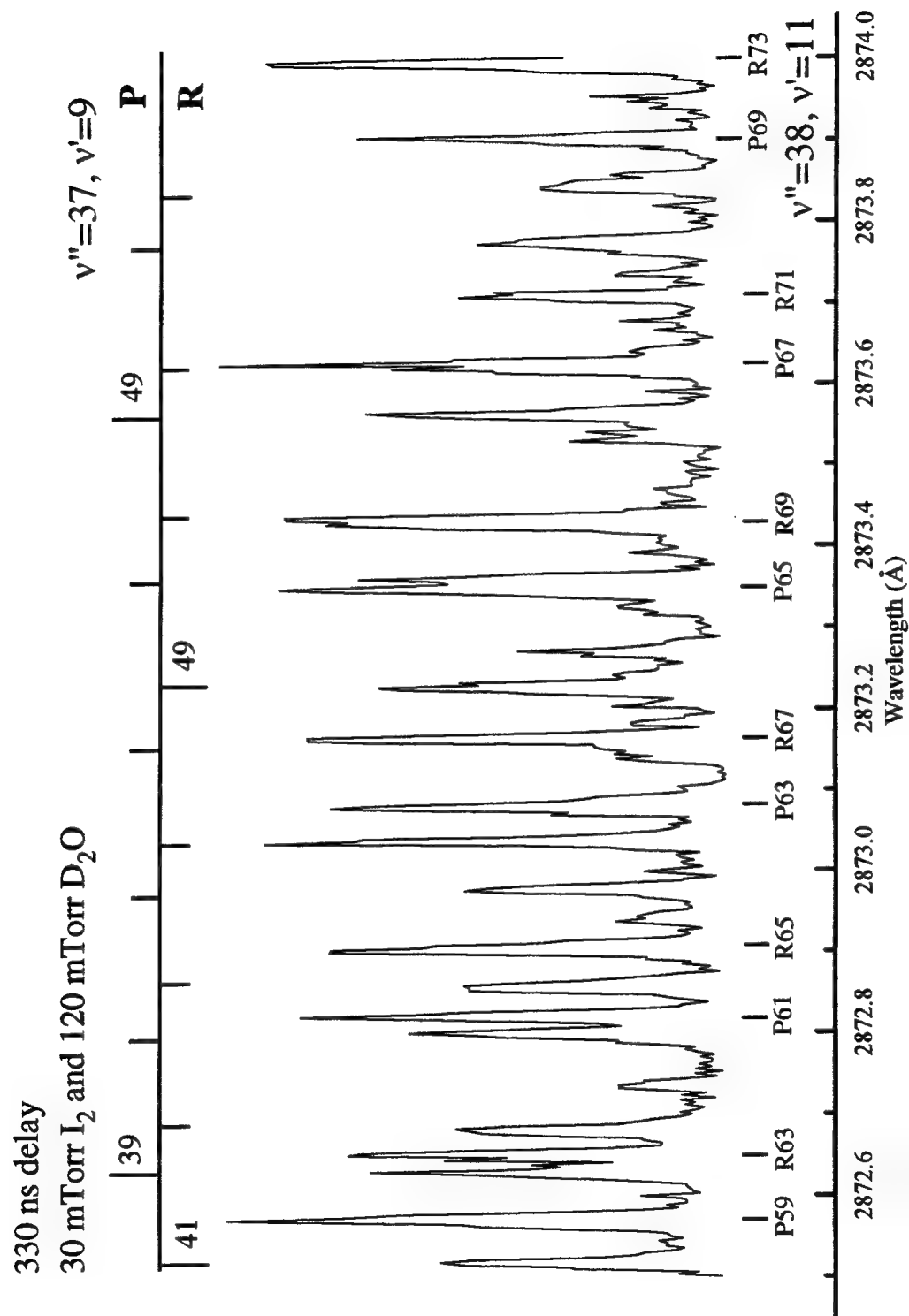
Figure 6.14: High Resolution SEP-LIF Spectrum of I_2 (X; v''=38) with D_2O

$$\lambda > \upsilon\Delta t_0 = l,$$

where υ is the mean speed of the molecule $(8kT/\pi m)^{1/2}$, Δt_0 is the time scale for the

observation, and λ is the mean free path.[4] The mean free path λ, should be larger than

the flight length, l, which occurs within the time scale of the observation time, Δt_0.

However, K. Yamaski and S. R. Leone[4] stated that this inequality is not a sufficient

criterion for single-collision conditions. They observed signals from a large number of

molecules which had undergone multiple collisions under their experimental conditions.

They proposed a stricter criterion for single-collision conditions. With the probability

distribution for the number of collisions being represented by a Poisson distribution, the

probability of one collision in a distance l, should not exceed one-fifth the mean free path

$$0.2\lambda > \upsilon\Delta t_1 = l,$$

where Δt_1 is the predetermined time scale of the observation. The inequality is derived

from the requirement that the number of molecules colliding under single collision

conditions are sufficiently larger than molecules undergoing multiple collisions by a

factor of ten. The number of molecules which do not collide at all is the largest under

this condition.

In follow-on SEP-LIF experiments to those reported in this dissertation, a

program was developed to ascertain the onset of multiple collisions. T. Van Marter and

W. Basinger implemented the integral of J. Derouard and N. Sadeghi[5] in solving the rate

matrix for the ECS scaling law

$$k_{(j_i \to j_f)} = (2j_f + 1)\exp\left[\frac{(E_{ji} - E_{j>})}{kT}\right]\int_0^{\pi} \frac{(2l+1)k(l \to 0)}{4\pi^2 \sin\theta(l+\frac{1}{2})} \times |A_l^{j>}|^2 2\pi \sin\theta d\theta$$

and calculated the populations resulting from multiple collisions. Applying their results to the experimental conditions under which my spectra were sampled (pressure less than 200 mTorr), the single collision approximation is valid through 300 ns at 200 mTorr.

The total loss rate was determined for each diluent by placing the probe laser on the initial populated level and monitoring the decay of the fluorescence intensity as a function of the delay between the *dump* and *probe* lasers. Data was collected in 25-50 ns increments from 100-600 ns. Single exponential decays were observed for all samples and defined by $I(t)=Ae^{-kt}$, where A is a constant and $k=k'_{I_2}[I_2]+k'_M[M]$. k'_{I_2} and k'_M are the total transfer rate constants for I_2 and M, respectively. The total loss rate constants given in Table 6.1 have been corrected for iodine self-transfer.

The rotational energy transfer rate constants were determined from the intensity of the collisionally populated satellite peaks. In determining the intensity, baselining of the spectrum was necessary. The baseline was established by subtracting *pump-probe* from *pump-dump-probe* spectra or by visual inspection. The number densities were determined from the peak heights after resolving if the peak area and peak height was proportional. The respective P and R branches were measured and averaged where the intensity I is the peak height and $I_J = (I_P+I_R)/2$. Applying a simplified form of the statistical power gap law

$$k_{i \to f} = AN|\Delta E|^{-\alpha}$$

Table 6.1: Rate Constants for Total Population Loss of Rotational and Vibrational Energy Transfer from Individual Rovibronic Levels for I_2 (X) $v''=38$, $J_i=49$

Collision Partner	$I_2(X)$ $k_T^{a,b}$	$I_2(X)$ $k_R^{a,b}$	$k_V^{a,c}$	$I_2(B)^d$ k_T^a
I_2	6.6	6.0	0.6	6.5±0.6
Ar	5.5	5.1	0.4	6.8±0.7
He	5.4	4.4	1.0	7.2±0.5
H_2	7.2	-	-	14.0±0.7
N_2	8.0	6.7	1.3	-
O_2	7.0	6.3	0.7	-
Cl_2	4.0	3.1	0.9	-
H_2O	8.8	6.2	2.6	-
D_2O	2.9	2.2	0.7	-

[a] Units of 10^{-10} cm^3 s^{-1}
[b] Error Limits ±0.5 X 10^{-10} cm^3 s^{-1}
[c] Error Limits ±0.7 X 10^{-11} cm^3 s^{-1}
[d] J. Derouard and N. Sadeghi, *Chem. Phys. Lett.* **102**, 324 (1983).

rearranging,

$$\ln \frac{k_{i \to f}}{N} = -\alpha [\ln \Delta E] + \ln A$$

Assuming single collision conditions, the intensity given by the peak height is representative of $k_{1 \to f}$, N is the spin degeneracy factor, α and A are parametric constants, and $\Delta E = B[J_f(J_f+1) - J_i(J_i+1)]$. A plot of $\ln[I_J]/[N]$ vs $\ln(\Delta E/B)$ yielded a slope of α as seen in Figure 6.15. Table 6.2 lists the SPG coefficients and the corresponding spin degeneracy factor. Three spin degeneracy factors were investigated for N: m-randomizing where $N_\Delta = 2j_f + 1$; m-conserving $N_0 = (2j_< + 1)/(2j + 1)$ where $j_<$ is the lesser of j_f or j_i; and m-statistical N_λ. Generally, m-randomizing provided the best correlation except for the light rare-earth gases where the m-conserving model provided a marginally better fit. The exponential and hybrid fitting laws were also modeled, but in all cases the SPG fitting law provided a better representation of the spectra..

After obtaining α for the SPG model, the spectrum would be simulated with the *Display* program (Appendix D) and α optimized. Results of the RET simulation for I_2 and Ar are shown in Figure 6.16. A stimulation of the rotational manifold for J=1 to 101 for RT energy transfer of I_2 + He is shown in Figure 6.17. The rate constants for rotational energy transfer are provided in Table 6.1.

The analysis for energy transfer between vibration-translation was not as straight-forward. The most significant unknown was in determining the rotational distribution of the vibrationally populated level. With the rotational energy transfer of
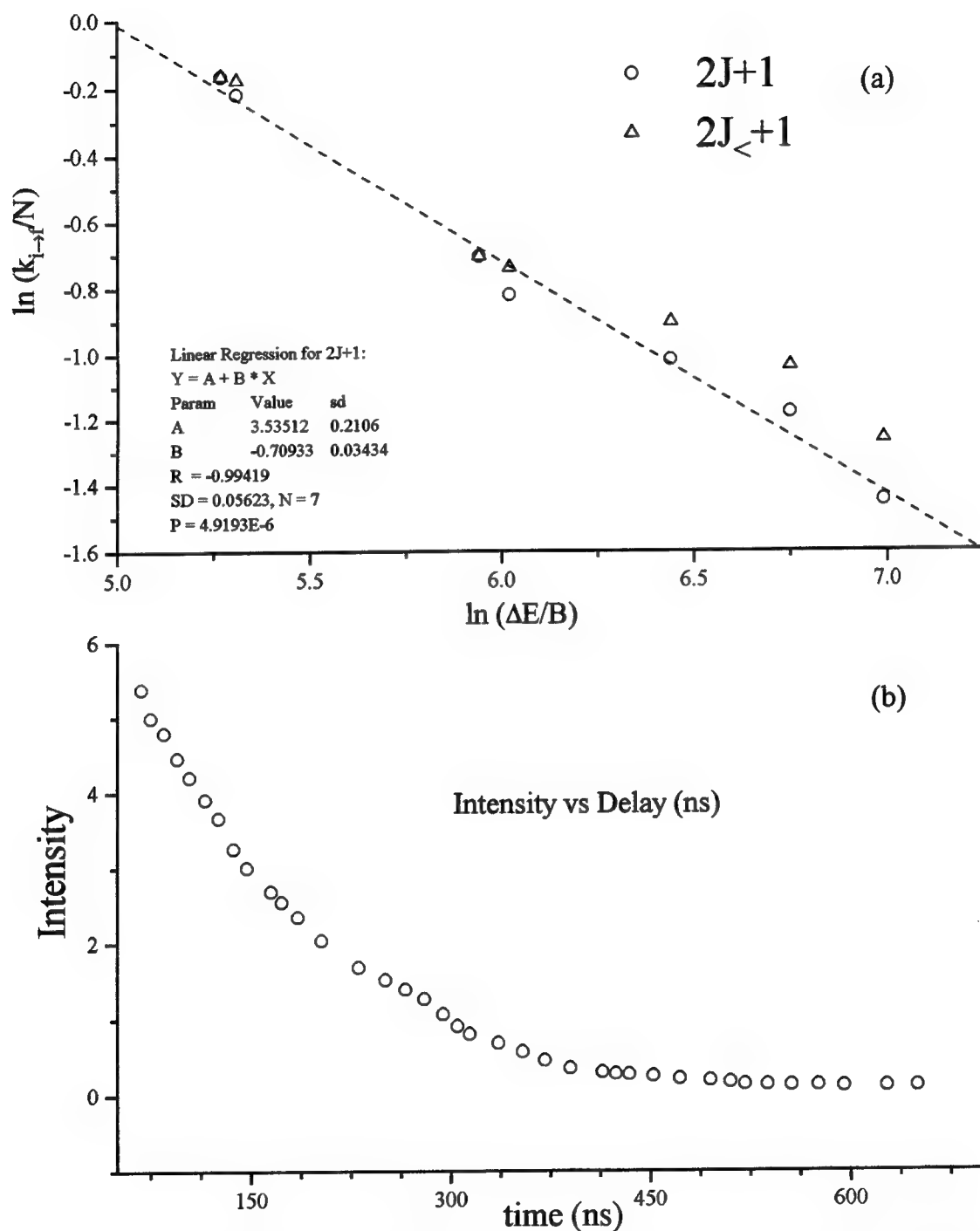
Figure 6.15: (a) ln-ln Plot of $k_{i \to f}/N$ vs $\Delta E/B$ and (b) Decay of Initially Populated $I_2(X)v''=38$, $J_i=49 + Ar$

Table 6.2: Statistical Power Gap Law Coefficients and
Spin Degeneracy (N) for I_2 (X) v''=38, J_i=49

Collision partner	α	N
I_2	0.71	$2J+1$
He	0.54	$2J_<+1$
Ar	0.65	$2J_<+1$
N_2	0.74	$2J+1$
O_2	0.66	$2J+1$
Cl_2	0.76	$2J+1$
H_2O	0.94	$2J+1$
D_2O	0.63	$2J+1$
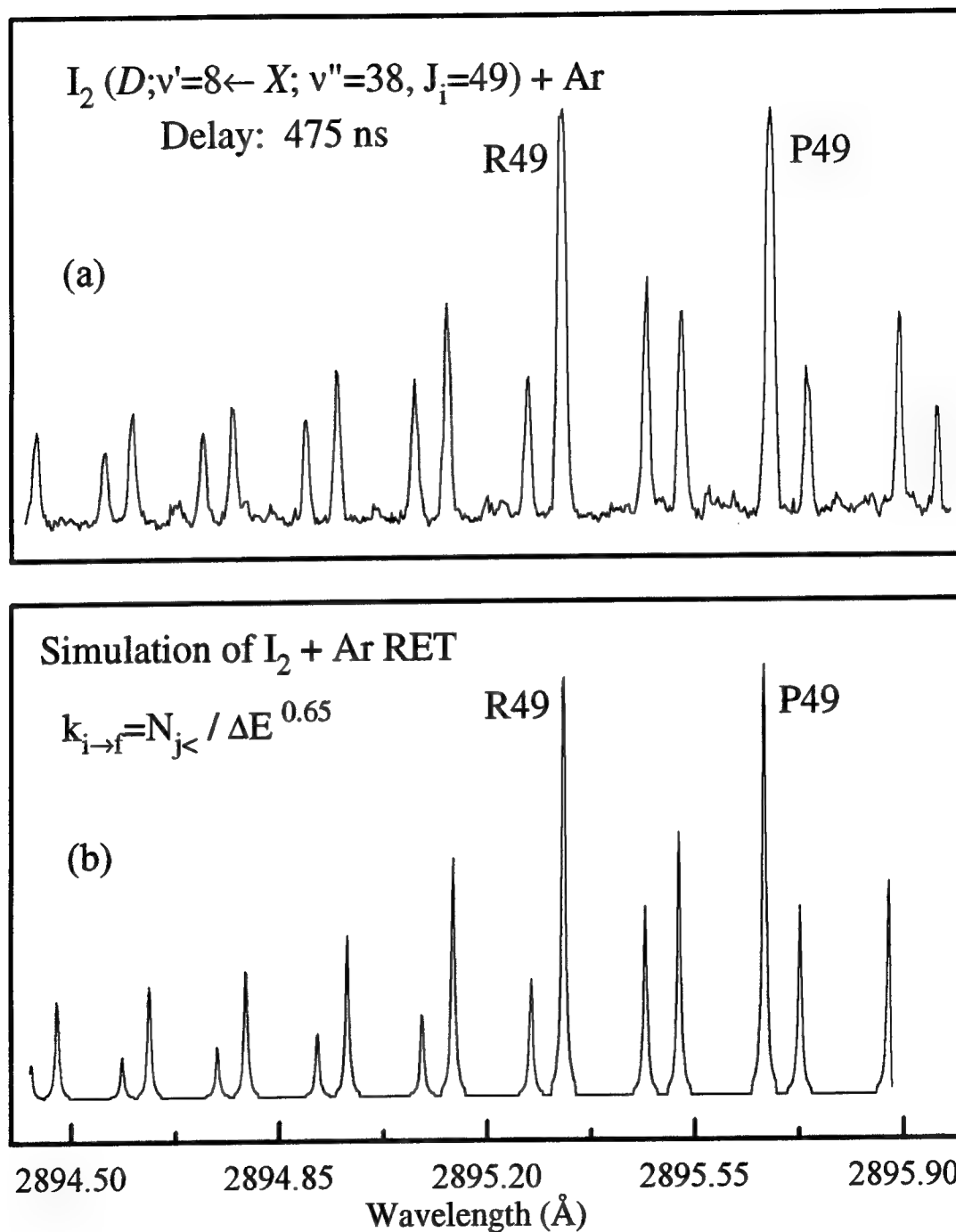
Figure 6.16: (a) SEP-LIF Spectrum of I_2 + Ar and (b) Simulation of I_2 (X) v"=38 + Ar
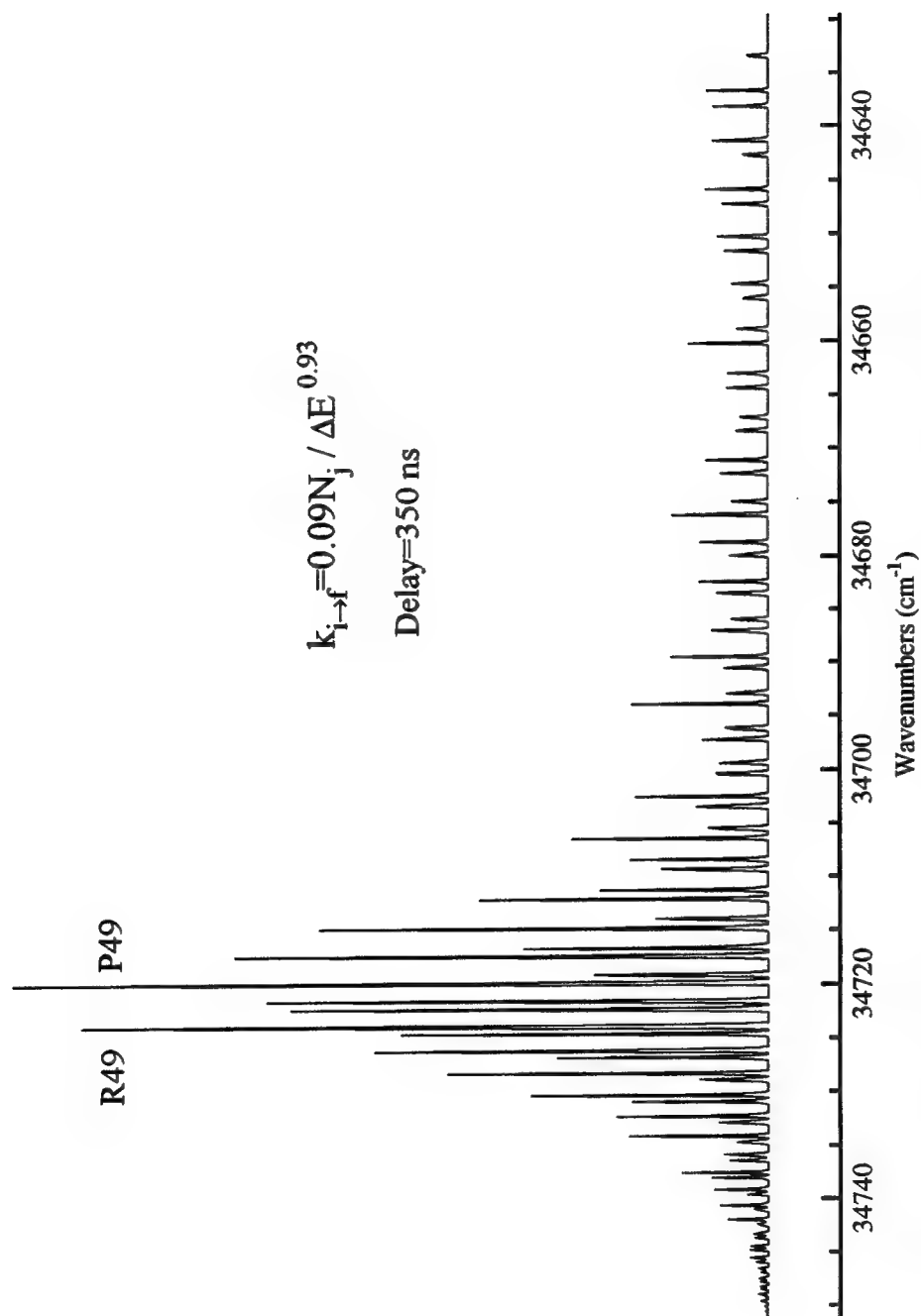
Figure 6.17: Simulation of the rovibrational manifold for J=1→101 with I_2 ($D, v'=10 \leftarrow X, v''=38$) + He

the initially populated level determined, the peak heights of representative rotationally and vibrationally populated levels were compared and scaled by a correction factor to account for the difference in the transition probability (Franck-Condon Factor). When experimental data was available, the observable peaks were individually measured and assigned a rate commensurate with the RET rate. Since the rotational contours of the vibrational energy transfer were consistent with a tendency to conserve angular momentum, the unobserved peaks in the vibrationally populated level were scaled with the α (Table 6.2) of the SPG where

$$k_M(v_i=38 \; J_i=49 \rightarrow v_f=37 \; J_f) = C_{38\text{-}37} N_\Delta |\Delta E_{rot}/B|^{-\alpha}$$

The total vibrational rate constant would then be determined by summing the rates from the observed and SPG distributions. Combining the observed and SPG distributions avoided the singularity at $\Delta E_{rot}=0$. The rate constants for vibrational transfer are listed in Table 6.1.

§6.3 REFERENCES

1. J. P. Bromberg, *Physical Chemistry*, 2nd ed., Allyn and Bacon, Boston (1984).

2. N. N. Greenwood and A. Earnshaw, *Chemistry of the Elements*, Pergamon Press, New York (1982).

3. P. J. Wolf and S. J. Davis, *J. Chem. Phys.* **87**, 3492 (1987).

4. K. Yamasaki and S. R. Leone, *J. Chem. Phys.* **90**, 967 (1989).

5. J. Derouard and N. Sadeghi, *Chem. Phys.* **88**, 171 (1984).

CHAPTER 7

STIMULATED EMISSION PUMPING v"= 23

§7.1 RESULTS

The spectra of v"=23 were the cleanest by far, both experimentally in terms of the

signal to noise, and spectroscopically in terms of no OODR interference or spectral

overlap. Figure 7.1 shows typical low resolution spectra of I_2 self transfer and I_2 with

argon. Unlike the previous two SEP-LIF experiments, v"=42 and v"=38, the *probe* laser

did not excite the $f(0^+_g) \leftarrow B(0^+_u)$ two-photon transition. Fortuitously, unfavorable

Franck-Condon factors for the $f(0^+_g) \leftarrow B(0^+_u)$ transition precluded OODR interference

via the *pump-probe* sequence. The initially populated P and R lines for J_i=57 are clearly

visible in the iodine self-transfer spectrum. Collisionally populated satellite peaks

surrounding the larger parent peaks are observed with the argon diluent.

The fluorescence peaks in Figure 7.2 correspond to the probe transitions from the

initially prepared state (J_i=57) and the rotational energy transfer induced by collisions as

evidenced by the progression of the satellite peaks. The progressions are asymmetric

with the collisions favoring a slight propensity for high J. This is surprising in light of an

increasing energy gap and the fact that the initial level populates J_{max}. The prior

distribution of surprisal theory predicts the final J distribution to be similar to the thermal

distribution. The relative intensity of the peaks reflect the temporal population evolution
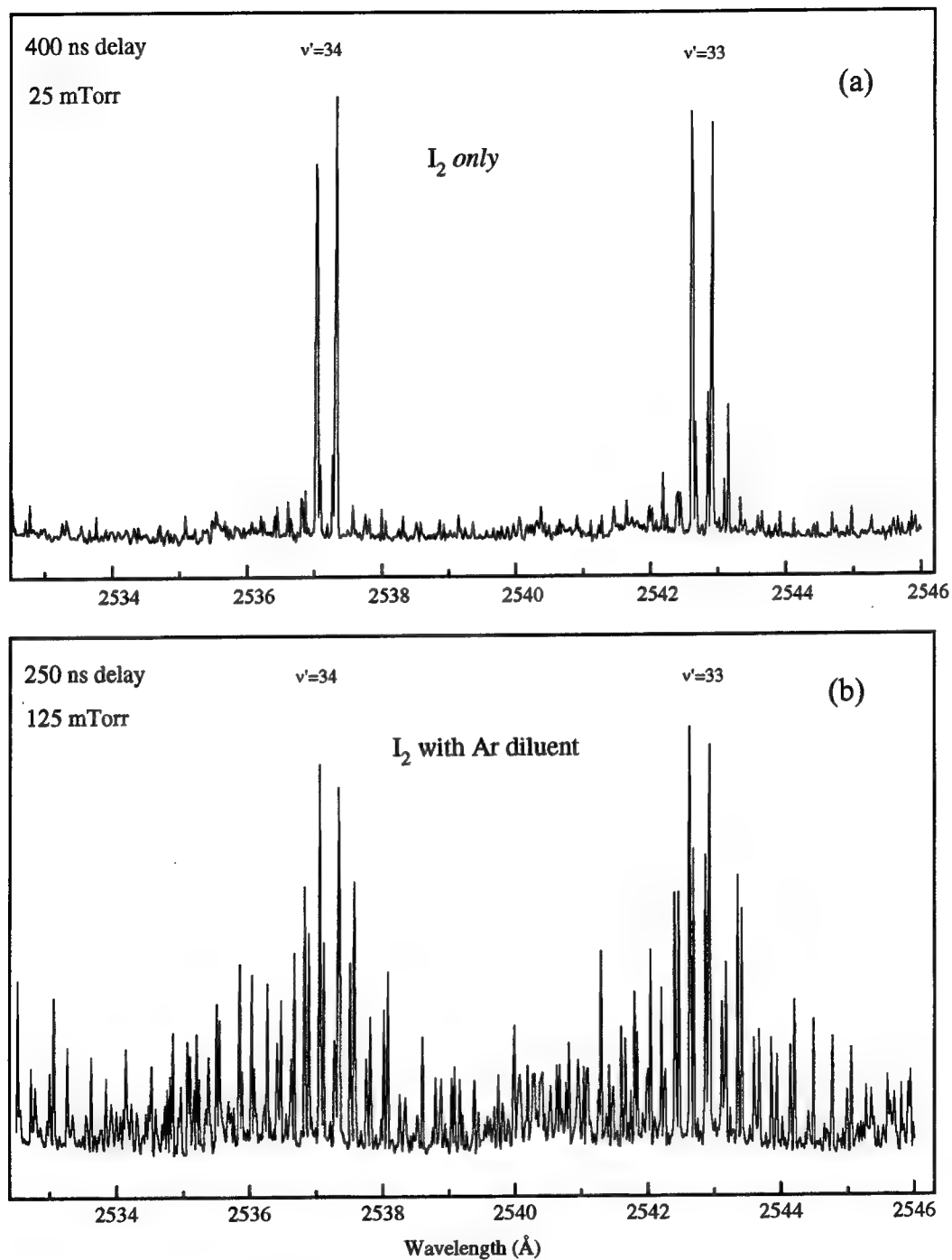
Figure 7.1: Low Resolution Spectra Showing Rotational Energy
Transfer: (a) I_2 (X;v''=23) and (b) I_2 + Ar

100 mTorr Argon
Delay: 400ns

I_2 (D; v'=34 ← X; v''=23)

R57

P57

Wavelength (Å)

2535　2536　2537　2538　2539
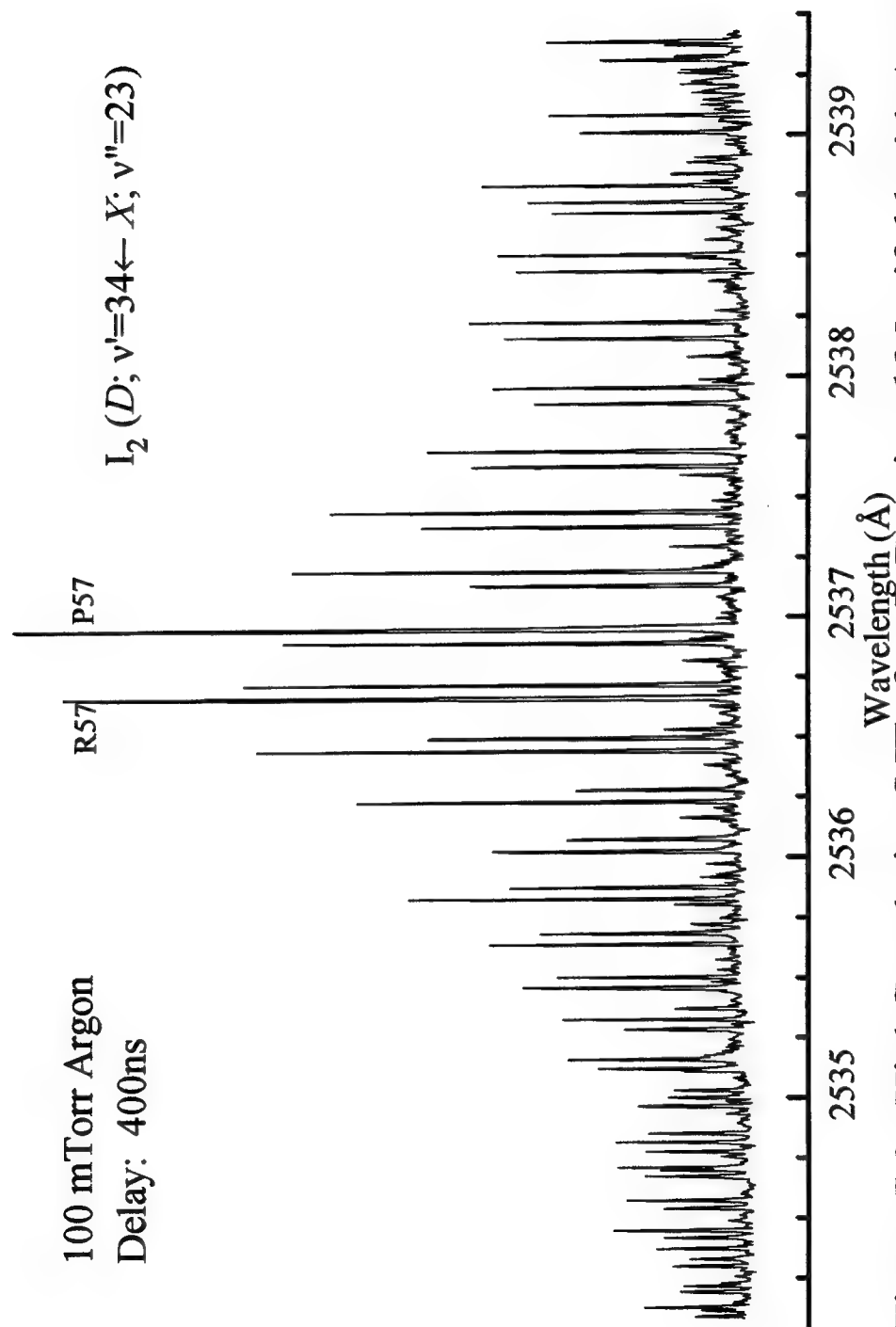
Figure 7.2: High Resolution LIF of an I_2 Rotational Manifold with Argon

of the initially prepared and collisionally populated states. Significant relaxation of the rotational manifold is observed at a 400 ns delay under relatively mild diluent pressures.

The rotational energy transfer in Figures 7.2 and 7.3 shows the same general trends. While the longer delay of the helium spectrum (500 ns) approaches multiple collisions, the spectrum is indicative of the rotational energy transfer. In fact, the energy transfer in Figure 7.2 has populated $J_<$ sufficiently that the bandhead is visible near 2539.1Å for D, v'=33 ←X,v"=23. In Figure 7.4, the propensity for rotational energy distribution over a wide J range for v'=33 and v'=34 can be seen. Once again, rotational transfer for the ground state was spread over significantly more rotational levels than the corresponding transfer in I_2 (B).

While the collision-induced RT bands were prominent, the vibrational transfer peaks were not. Vibration-translation energy transfer is present in both Figure 7.4 with argon and Figure 7.5 with helium. Features due to vibrational energy transfer were observed for all collision partners. For v"=23→22 transfer induced by collision with Ar, we obtained a rate constant of 3×10^{-11} cm^3 s^{-1}. This value is in agreement with the work of Hall et al.[1] Figure 7.6 shows the extensive RT and VT energy transfer with He.

Surprisingly, H_2O was not particularly effective in removing vibrational energy from I_2. To illustrate this point, Figure 7.7 shows a section of the I_2 D-X spectrum of I_2 with H_2O. The delay between the dump and probe pulse was 200 ns. Lines originating from levels populated by rotational energy transfer are prominent in this trace. A few weak features produced by v"=23→22 relaxation can be seen. Lines originating from
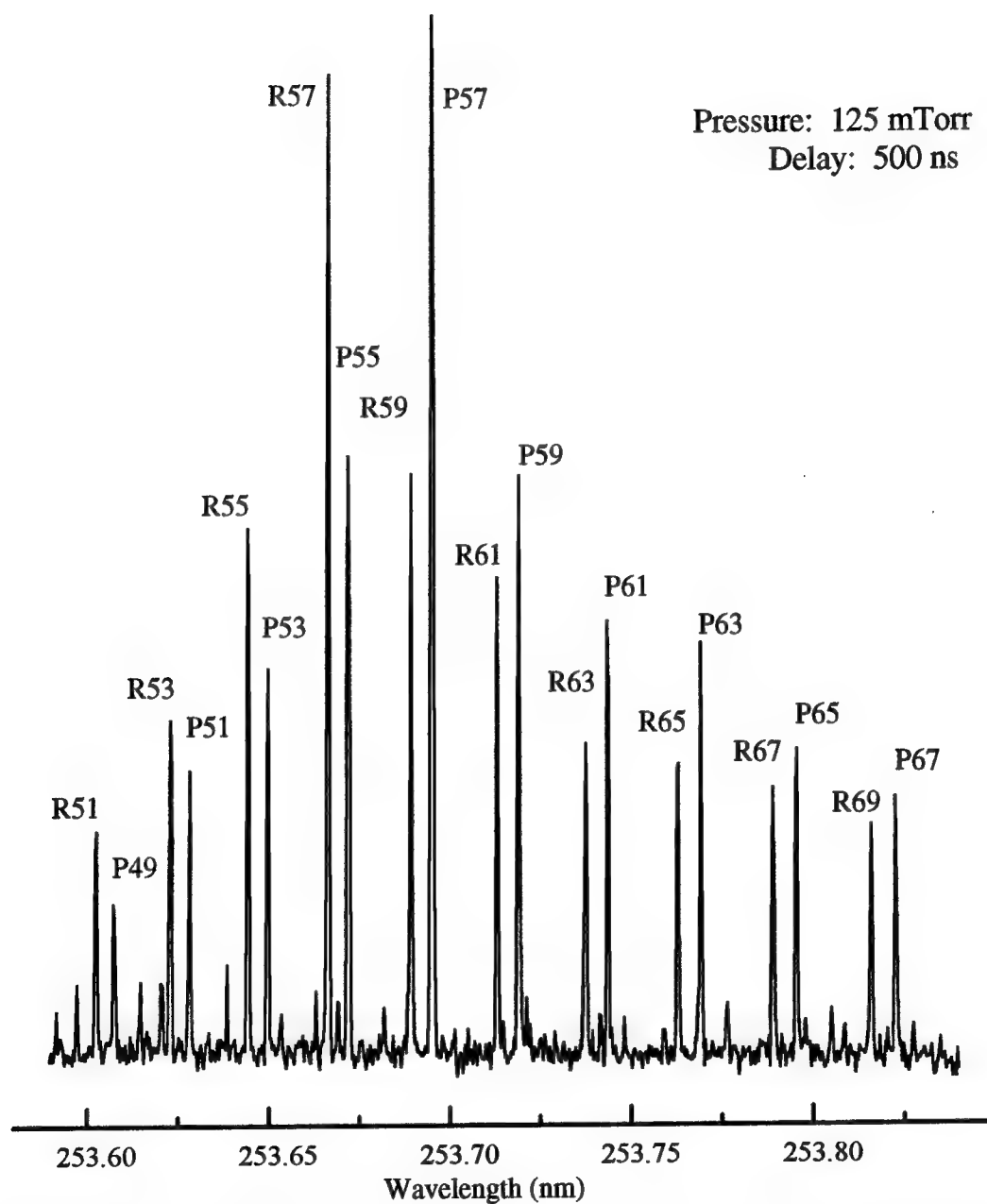
Figure 7.3: High Resolution LIF of I_2 (D; v'=34←X;v"=23, J_i=57) Showing Rotational Energy Transfer with Helium
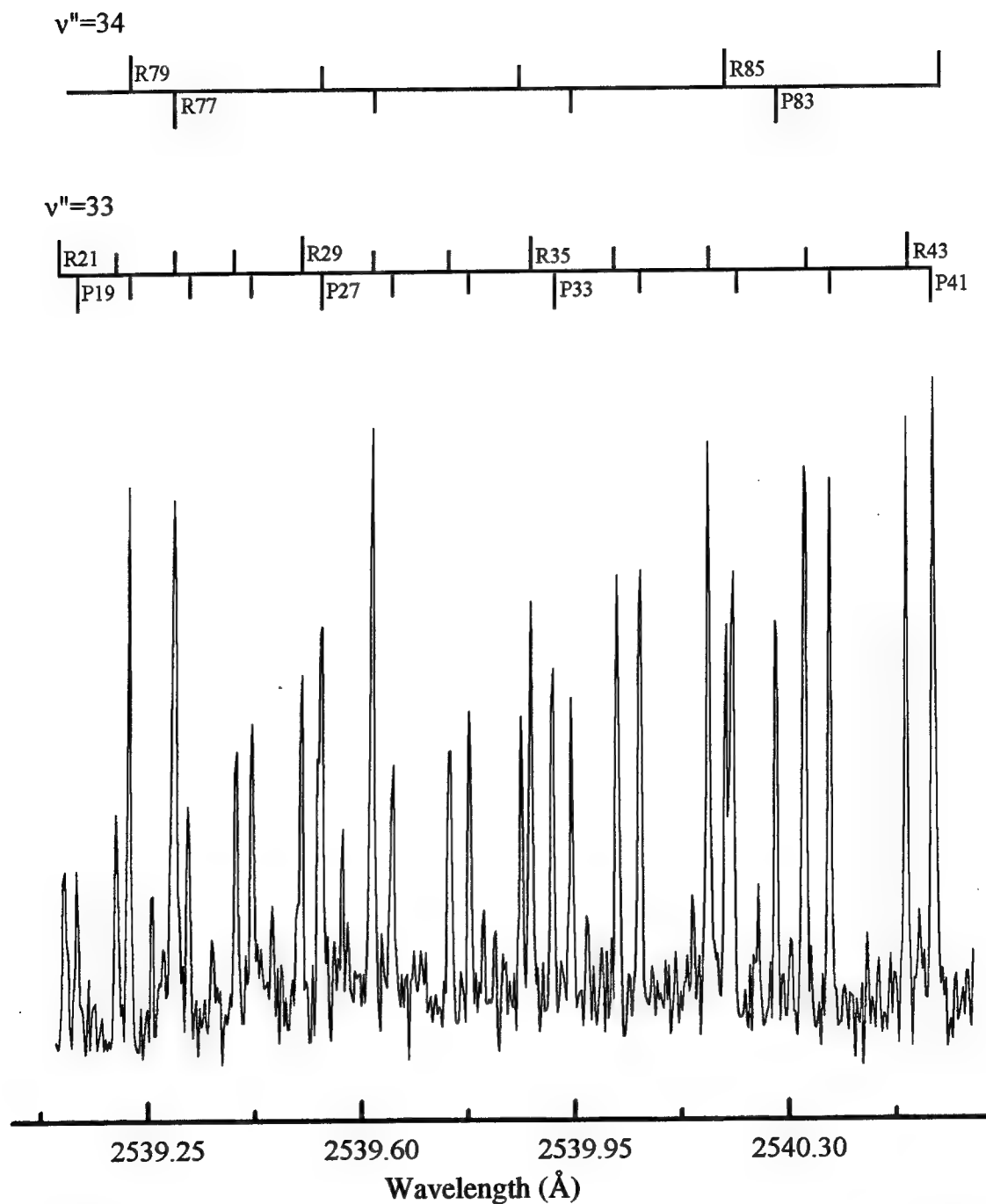
Figure 7.4: High Resolution LIF of I_2 (D,v'=33,34$\leftarrow X,v''$=23) with Ar (400 ns delay, 150 mTorr)
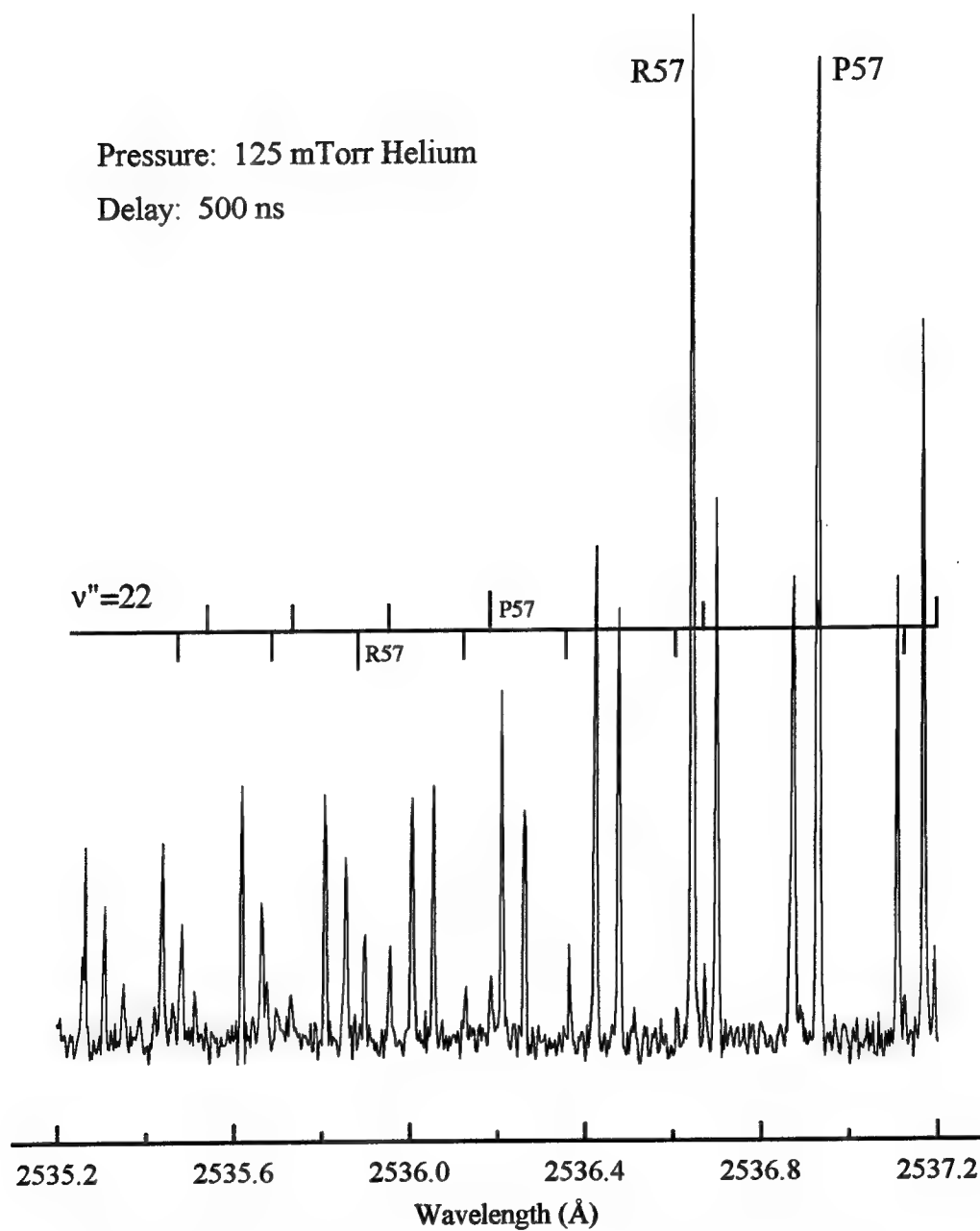
Figure 7.5: SEP-LIF of I_2 (D,v'=34←X,v"=23) with He
Showing Both Rotational and Vibrational
Energy Transfer
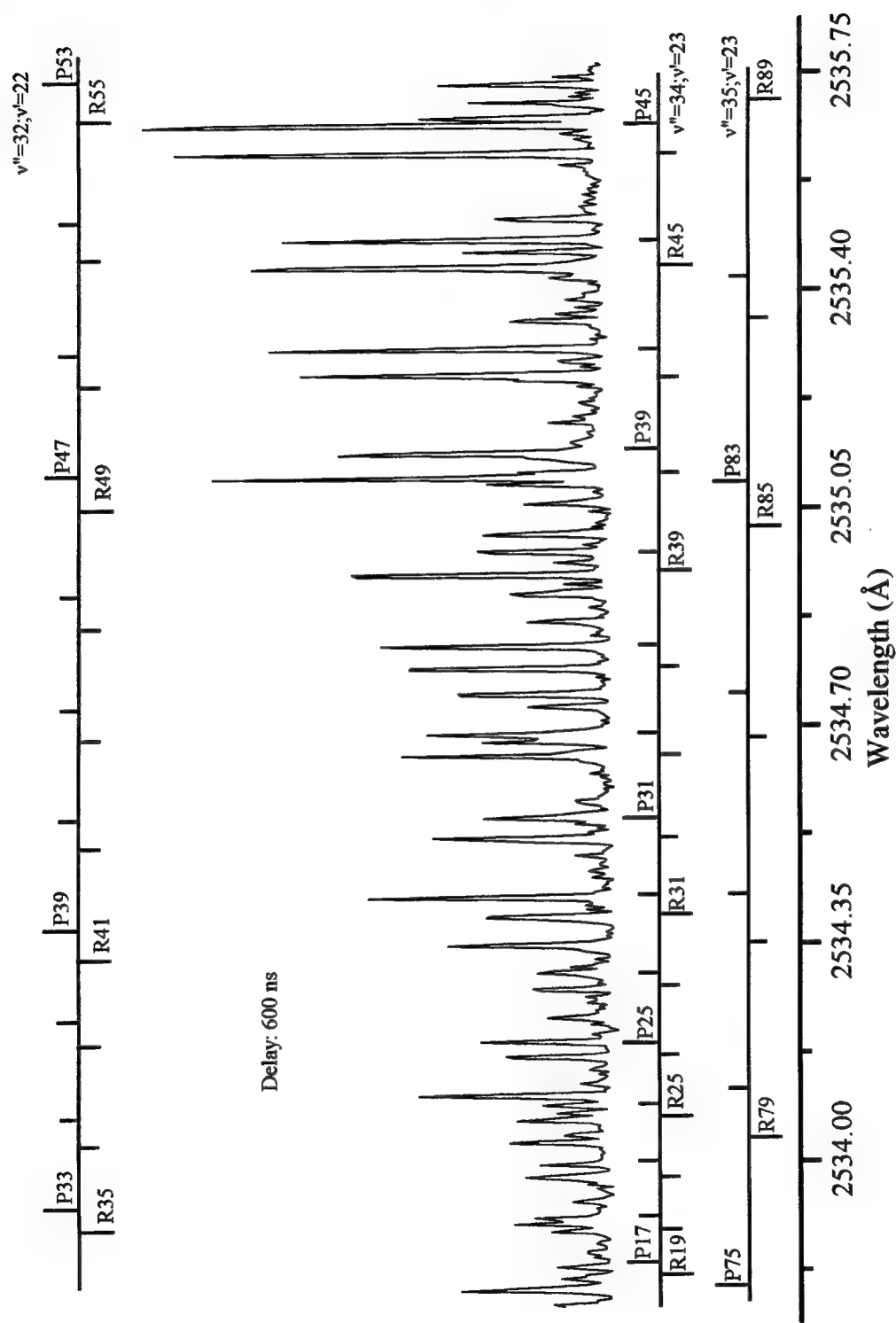
Figure 7.6: High Resolution SEP-LIF Spectrum of I$_2$ (v''=23) with He Diluent
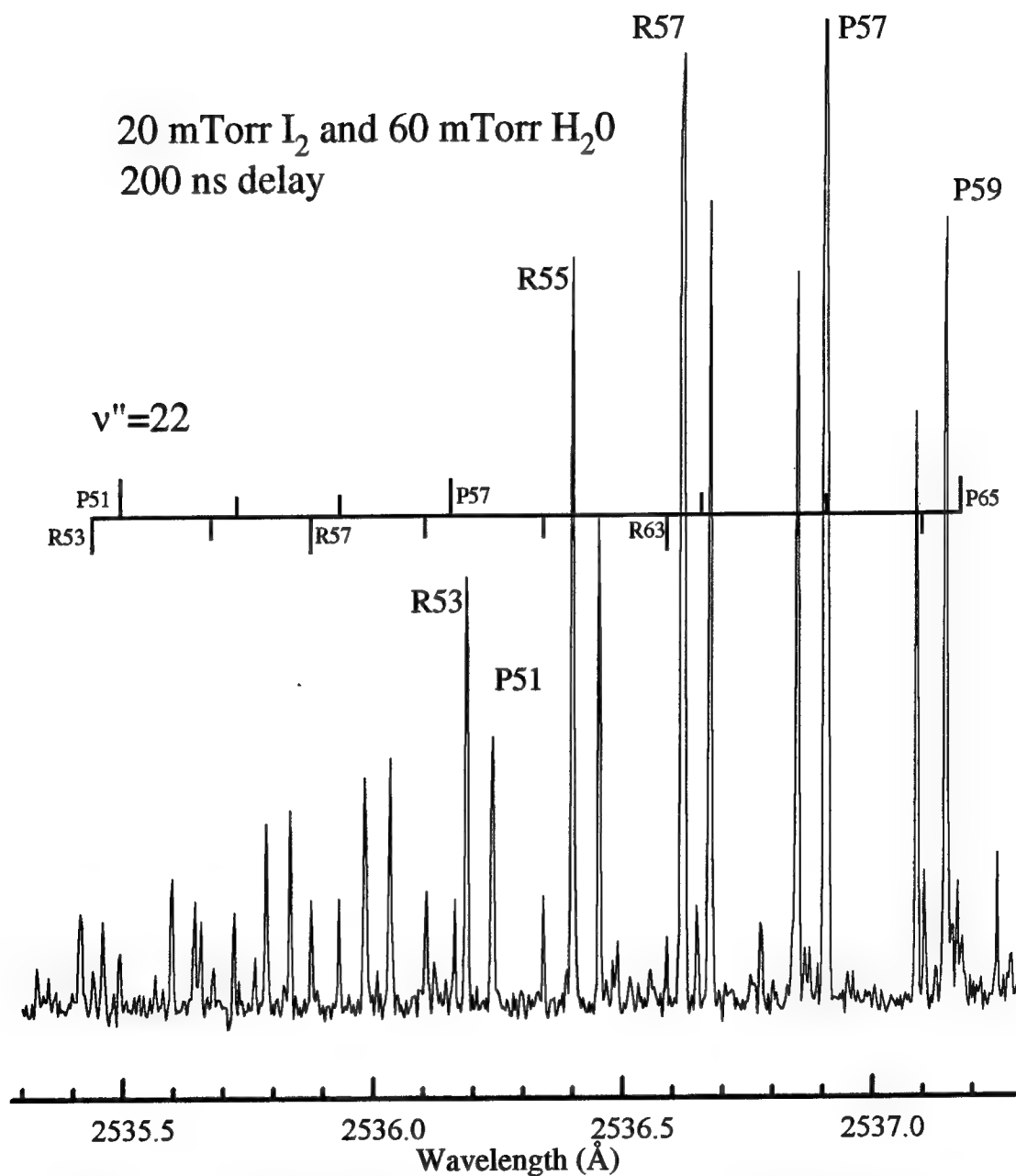
Figure 7.7: High Resolution LIF of I_2 (X; $v''=23$) with H_2O Showing Both Rotational and Vibrational Energy Transfer

collisionally populated v"=22 levels are evident near 2535.8 Å. From spectra recorded at a number of different delays, it could be seen that the population lost from v_i"=23, J_i"=57 was within the experimental error limits accounted for by population transferred to other v"=23 rotational levels. Figure 7.8 allows a qualitative comparison between several diluents under similar experimental conditions. The most notable difference is the relative lack of rotational energy transfer for I_2 self-transfer when compared with other collision partners. The other notable feature is the presence of satellite peaks surrounding R49 in the I_2+He and I_2+H_2O spectra. The presence of these peaks indicate vibrational transfer to v"=22 while this feature is lacking in both the I_2+Ar and I_2 self-transfer spectra.

§7.2 ANALYSIS

The total rate loss constant was determined for each diluent by parking the probe laser onto a parent peak and recording the intensity as a function of the delay between the *dump* and *probe* lasers. The decay of the initially populated level for I_2 (X) v_i=23, J_i=57 + N_2 is shown in Figure 7.9. The rate was obtained by determining the slope and

$$k_T(\tfrac{cm^3}{s}) = \frac{\frac{slope}{3.24 \times 10^{13}}}{pressure(mTorr)} \times 10^9$$

Efforts were made to minimize the iodine concentration in relation to the diluent sample concentration so that iodine self-transfer corrections would be minimal. Unfortunately, these conditions were not always compatible with an adequate signal strength so
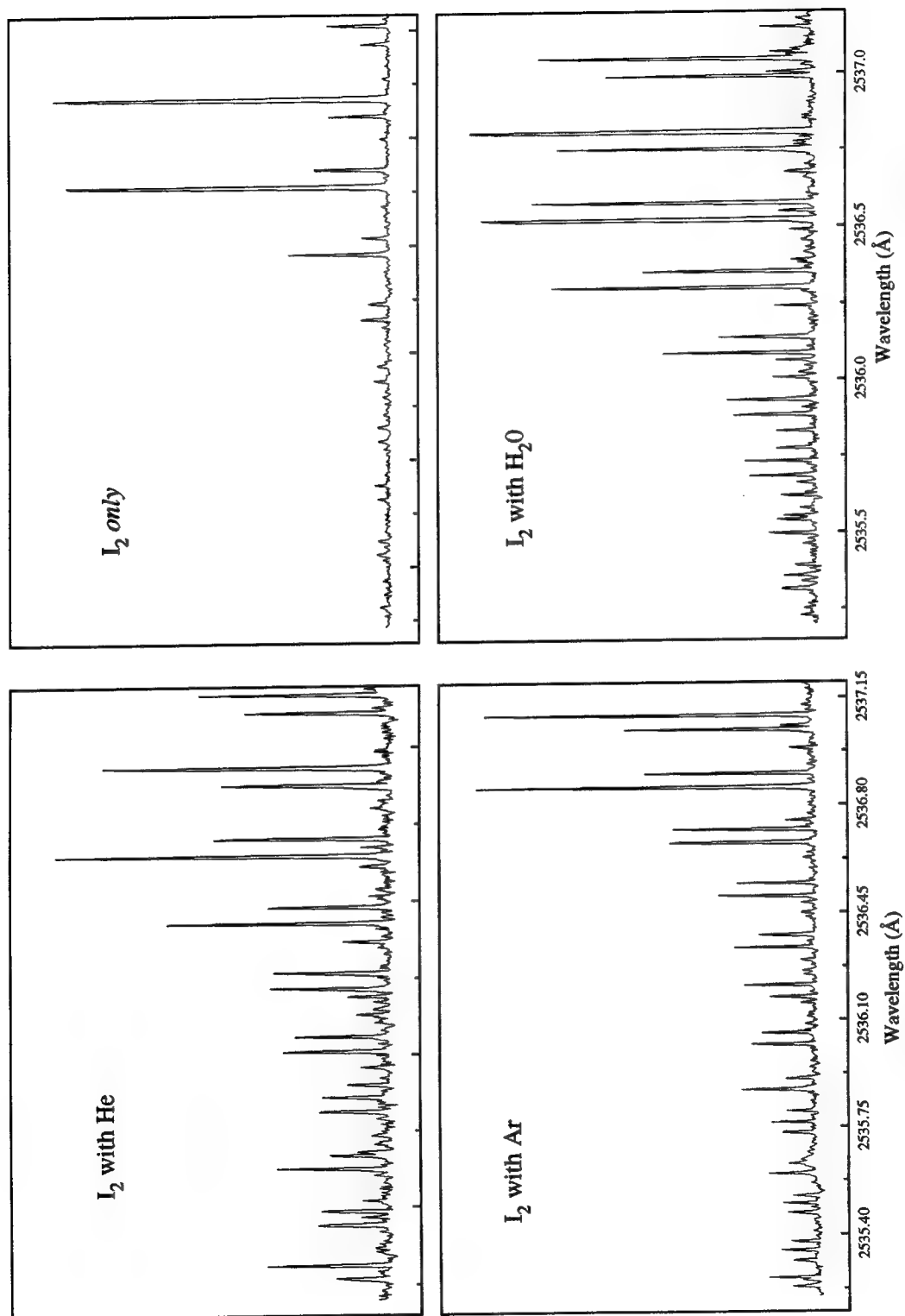
Figure 7.8: Comparison of High Resolution LIF of v''=23 of Iodine with Several Diluents

Fit Y=A*e^{B*X}
A= 0.8159
B= -0.00274
R= 0.99927

32 mTorr I$_2$
90 mTorr N$_2$
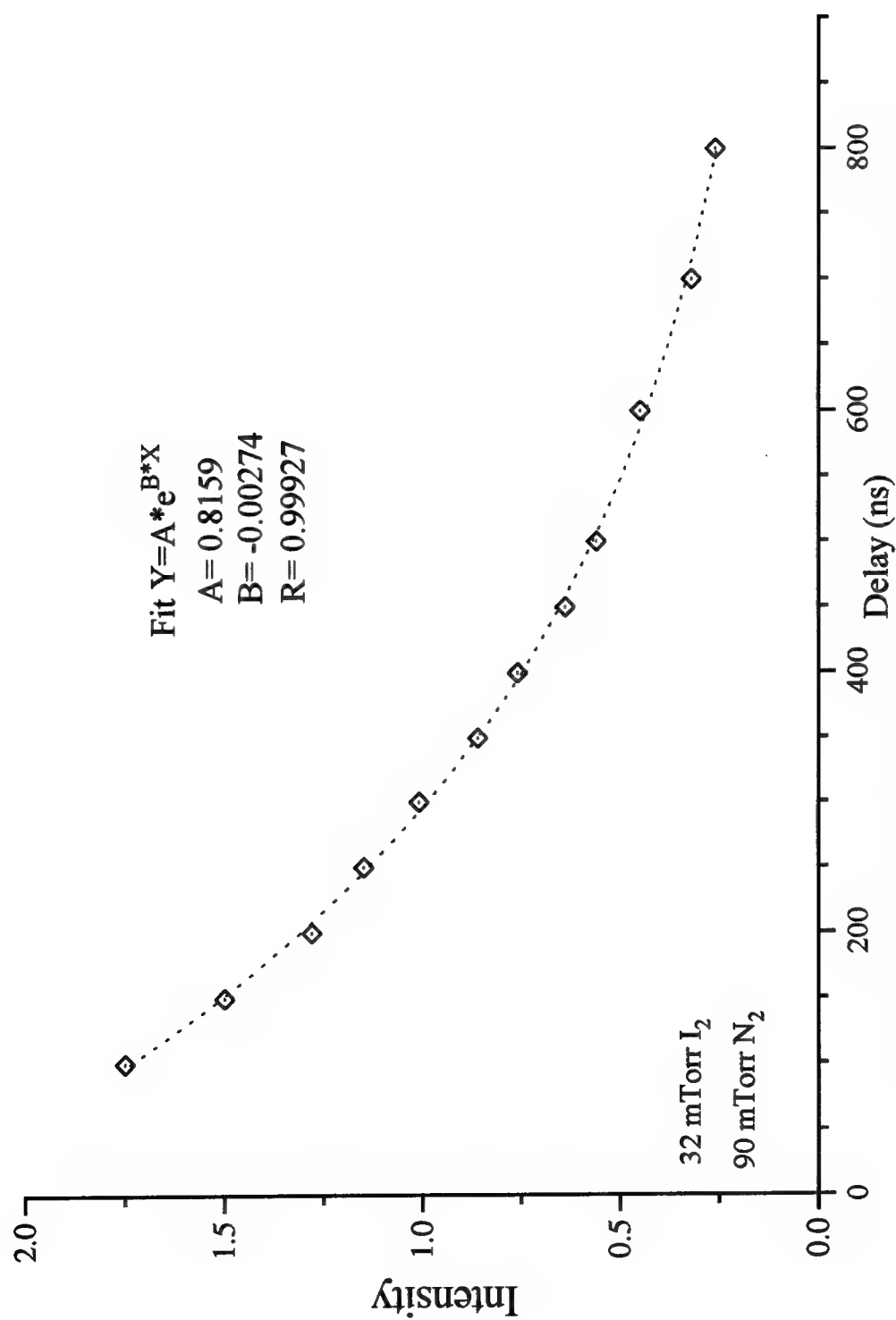
Figure 7.9: Decay of Initially Populated I$_2$ (X) v"=23, J=57 + N$_2$

concentrations were adjusted accordingly. One complication with obtaining ideal mixes was that the McLeod manometer limited total pressures to 200 mTorr. Total loss rate constants in $v''=23$ are given in Table 7.1 with their respective collision partners.

After determining the total loss rate constants, the rotational energy transfer rate constants were determined. Total rotational transfer rate constants are a summation of the state-to-state rotational transfer rate constants. Two methods for determining the RET rate constants were utilized. The first approach involved using an analysis[2] where under single collision conditions, the population of J_f, populated by rotational energy transfer from J_i is

$$\frac{d[N_f]}{dt} = [N_i](t)k_R - [N_f] = 0$$

Rearranging,

$$\frac{[N_f]}{[N_i]} = (t)k_R$$

where $[N_i]$ is the population of the parent peak, $[N_f]$ is the population of the satellite peak, t is delay between *dump* and *probe* laser pulses, and k_R is the energy transfer rate constant. The populations of the parent and satellite peaks were obtained from the experimental data. The number densities were determined from the peak heights after resolving if the peak area and peak height was proportional. For this purpose, a routine by Bevington[3] for calculating peak area was modified and included as the subroutine *Area* in the *Display* program (Appendix D). A cursory analysis indicated proportionality at short delays. In measuring the peak heights, the baseline was first obtained by subtracting a *pump-dump-probe* spectrum from a *pump-probe* spectrum. The respective

Table 7.1: Rate Constants for Total Population
Loss From Individual Rovibronic
Levels for I_2 (X) v''=23

Collision partner	$k_T[I_2(X)]^a$ $(10^{-10} \text{ cm}^3 \text{ s}^{-1})$
I_2	8.7
Ar	5.7
He	6.4
N_2	6.7
O_2	7.1
H_2O	9.3

a. Error Limits $\pm 0.5 \times 10^{-10} \text{ cm}^3 \text{ s}^{-1}$

P and R branches are measured and averaged: where I is the intensity and $I_J = (I_P + I_R)/2$.

Plotting $[I_f]/[I_i]$ vs t yielded a slope of k_R as seen in Figure 7.10.

During collection of the energy transfer data, a concerted effort was made to ensure the initially prepared and collisionally populated lines were on-scale for the purpose of obtaining the ratio of peak heights $[I_{Jf}]/[I_{Ji}]$. However, the limited dynamic range of the transient digitizer resulted in a small signal intensity for $[I_{Jf}]$ as a result of the effort to keep $[I_{Ji}]$ on scale. The shot-to-shot noise in the baseline for large ΔJ was a major limitation for this approach. State-to-state rate constants obtained from fitting the $I_{satellite}/I_{parent}$ ratios for iodine self-transfer were generally consistent with those obtained by computer modeling.

Computer modeling with the statistical power gap law was the second and preferred method of determining state-to-state rate constants. Once again, peak heights were obtained in the same manner as the first method. But the peak height was plotted as a function of the degeneracy where

$$\ln \frac{k_{i \to f}}{N} = -\alpha[\ln \Delta E] + \ln A \qquad (7.1)$$

and

$$k_{i \to f} = AN|\Delta E|^{-\alpha}$$

Under single collision conditions, the peak height is representative of $k_{i \to f}$, N is the spin degeneracy factor, α and A are parametric constants, and $\Delta E = B[J_f(J_f+1) - J_i(J_i+1)]$. Plotting $\ln[I/N]$ vs $\ln[\Delta E/B]$ would yield the fitting parameter, α, as shown in Figure 7.11. Numerous spin degeneracy factors from m-randomizing N_Δ to m-conserving N_0
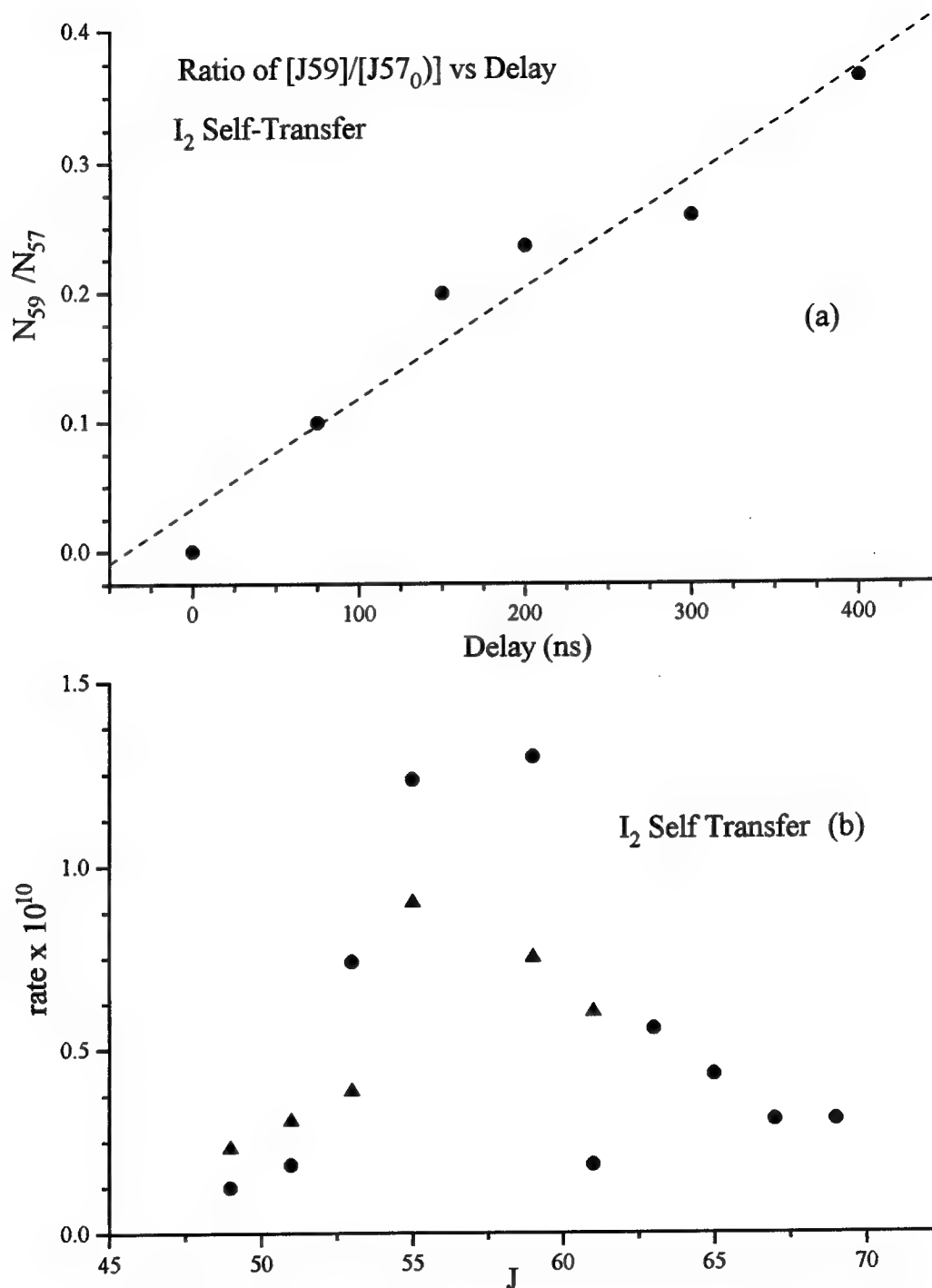
Figure 7.10: (a) Ratio of Experimental Intensities for J59 vs Delay and (b)Observed RET Rates Constants for I_2 Self Transfer
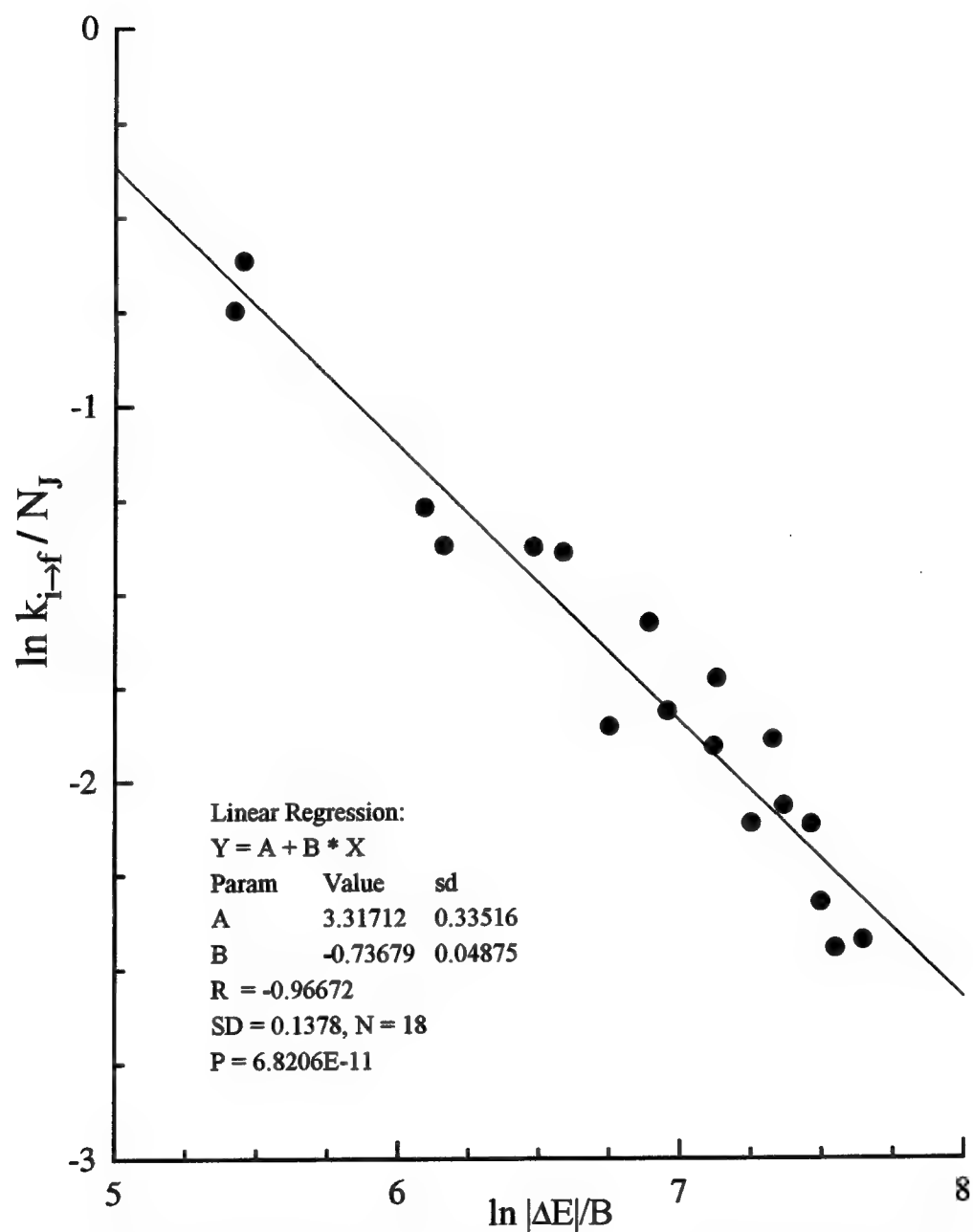
Figure 7.11: Log-log plot of $k_{i \to f}/N_J$ vs. $|\Delta E|/B$ for I_2 (X) $v''=23$, $J_i=57$ + Ar

were modeled (more on this in Chapter 8). Once the fitting parameter was obtained, the

experimental spectrum would be simulated using the computer program *Display*

(Appendix D). The parameters were adjusted to obtain agreement with the experimental

spectrum. The SPG coefficients for $v''=23$ are listed in Table 7.2. Examples of

simulations for iodine self-transfer, I_2+Ar, I_2+He and I_2+H_2O are shown in Figure 7.12 -

7.15, respectively. Individual rotational rate constants are calculated over the range

$1<J<101$ using equation 7.1 and the parameters determined from the simulation.

Rotational transfer rate constants are listed in Table 7.1. A representation of the

individual rotational transfer rate constants for I_2+He is shown in Figure 7.16.

The rotational relaxation rate constants for iodine self-transfer were fit to the

energy corrected sudden scaling law in a program graciously provided by K. Holtzclaw

of Physical Sciences Inc. The program was implemented to calculate the k matrix as

discussed in Chapter 2. The 3j coefficients were calculated by a formula given by Menzel

and Shore[4] as

$$\begin{pmatrix} a & b & J \\ 0 & 0 & 0 \end{pmatrix} = (-1)^g \frac{g! \sqrt{\Delta(abJ)}}{(g-a)!(g-b)!(g-J)!}$$

where

$$\Delta(abJ) \equiv \frac{(a+b-J)!(a-b-J)!(-a+b+J)!}{(a+b+J+1)!}$$

$$2g=a+b+J$$

For the energy corrected sudden scaling fit, values of $a=4.25 \times 10^{-11}$, $a=0.7052$ and

$l_c=0.804$ Å were obtained. Fixing $l_c = 0$ ($[A^{j>}]=1$), allowed for fitting to the infinite order

Table 7.2: Rotational and Vibrational Energy Transfer
Rate Constants with Statistical Power Gap
Law Coefficients

Collision partner	I_2 (X) v"=23			
	γ	N	k_{rot}[b,c]	k_{vib}[b,d]
He	0.83	2J+1	5.2	1.2
Ar	0.67	$2J_<$+1	5.4	0.3
H_2O	0.96	λ=45	7.6	1.7
I_2	0.43[e]	2J+1[e]	8.70	<0.1

a. Coefficients calculated by considering $1 \leq J_f \leq 101$.
b. Units of 10^{-10} cm^3 s^{-1}
c. Error limits $\pm 0.5 \times 10^{-10}$ cm^3 s^{-1}.
d. Error limits $\pm 3 \times 10^{-11}$ cm^3 s^{-1}.
e. γ=1.06 with $N=2J_<$+1
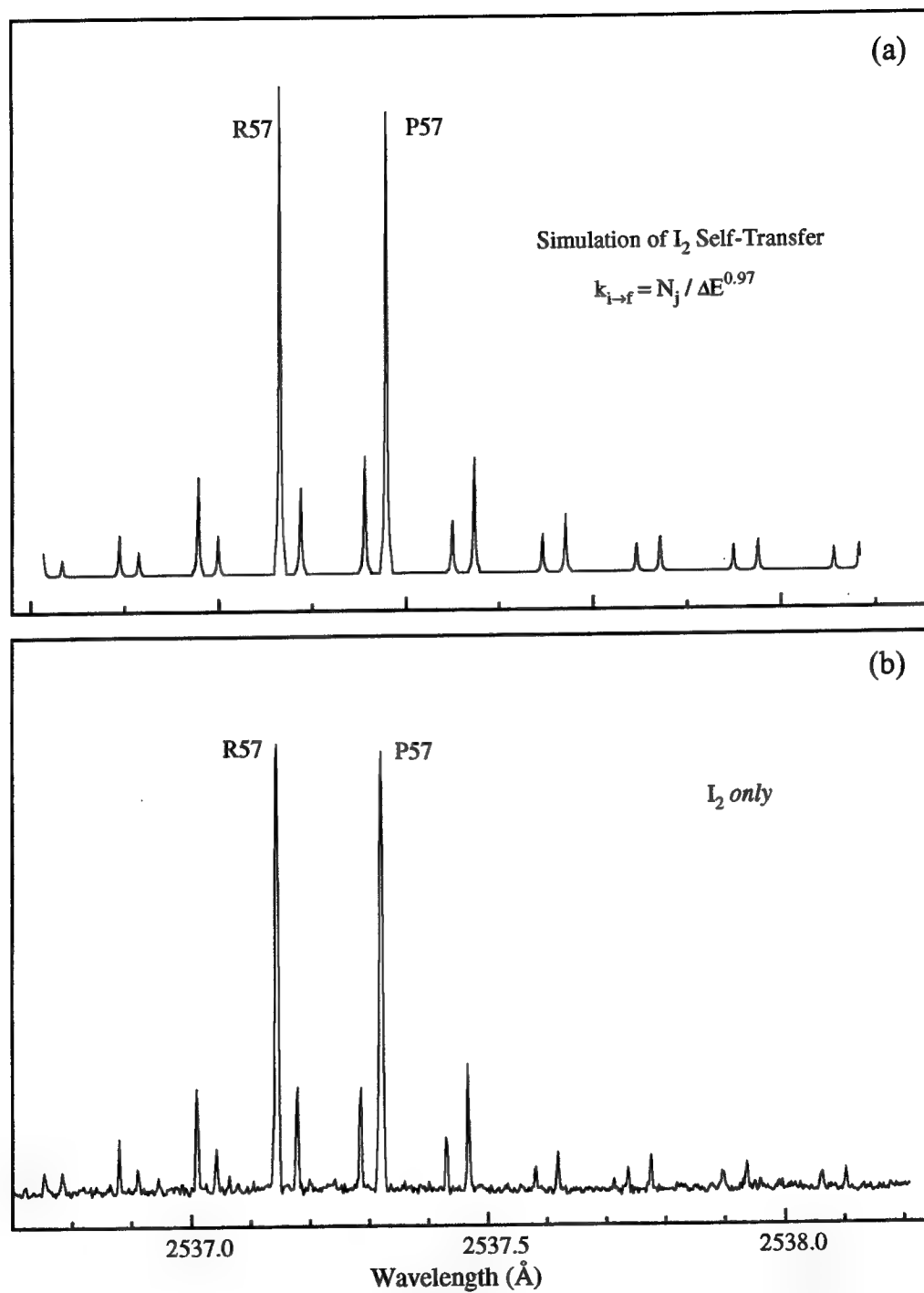
Figure 7.12: (a) Simulation of Iodine Self-Transfer in v"=23 and (b) High
Resolution LIF Showing Self-Transfer of I_2 (D, v'=34← X, v'=23)
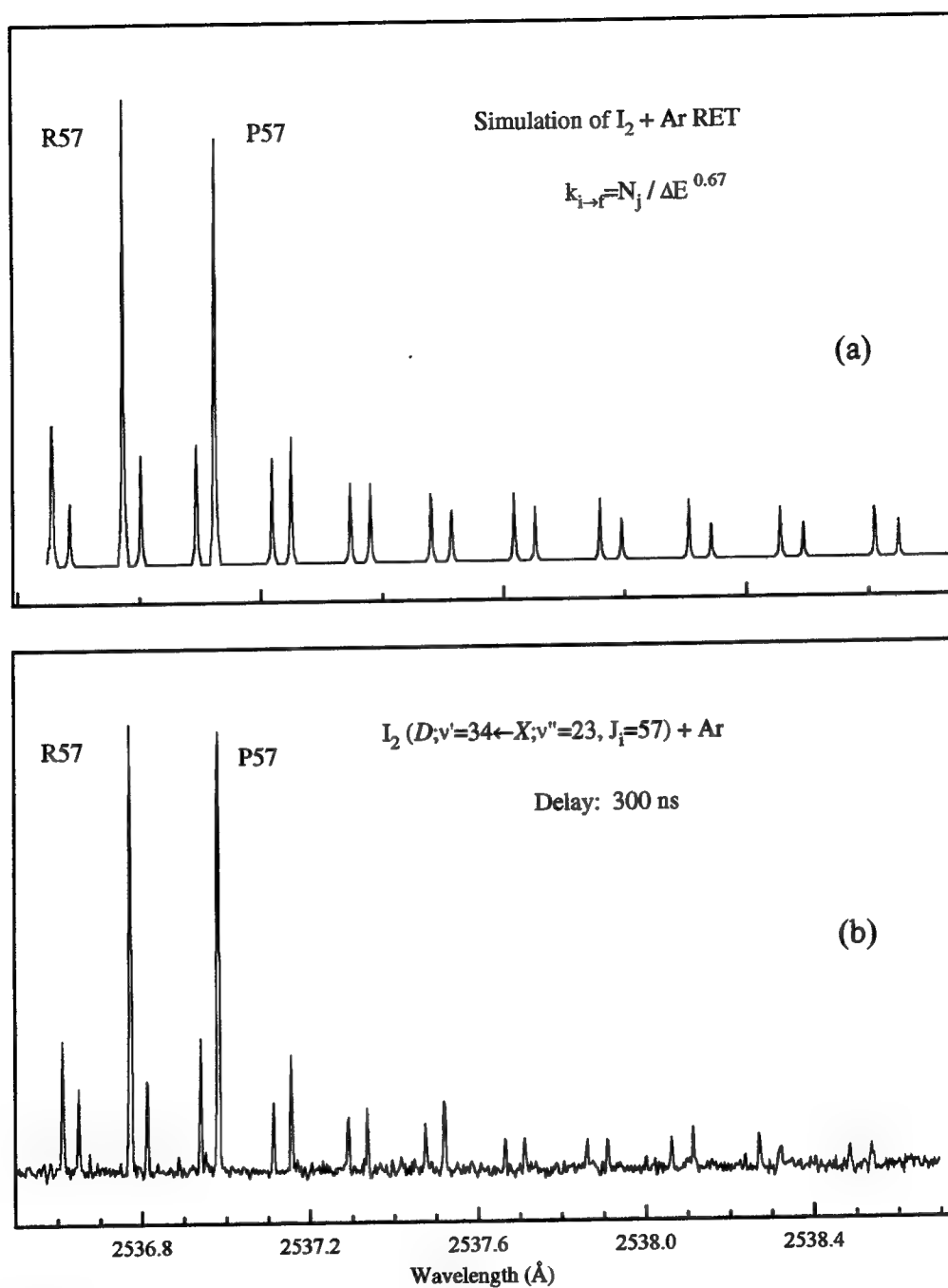
Figure 7.13: (a) Simulation of I_2 (X) v"=23 + Ar and (b) SEP-LIF of I_2 + Ar
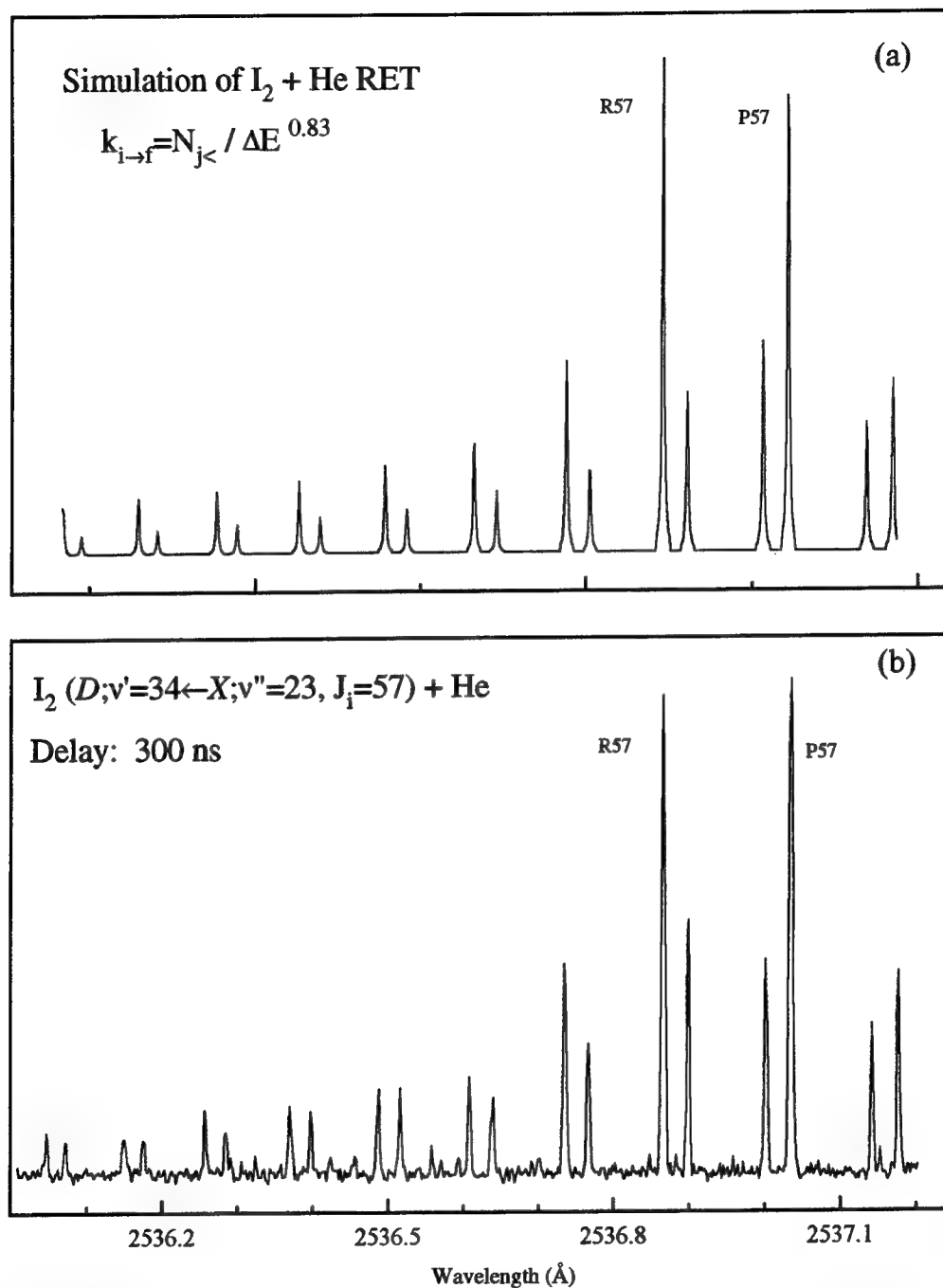
Figure 7.14: (a) Simulation of I_2 (X) v"=23 + He and (b) SEP-LIF of I_2 + He
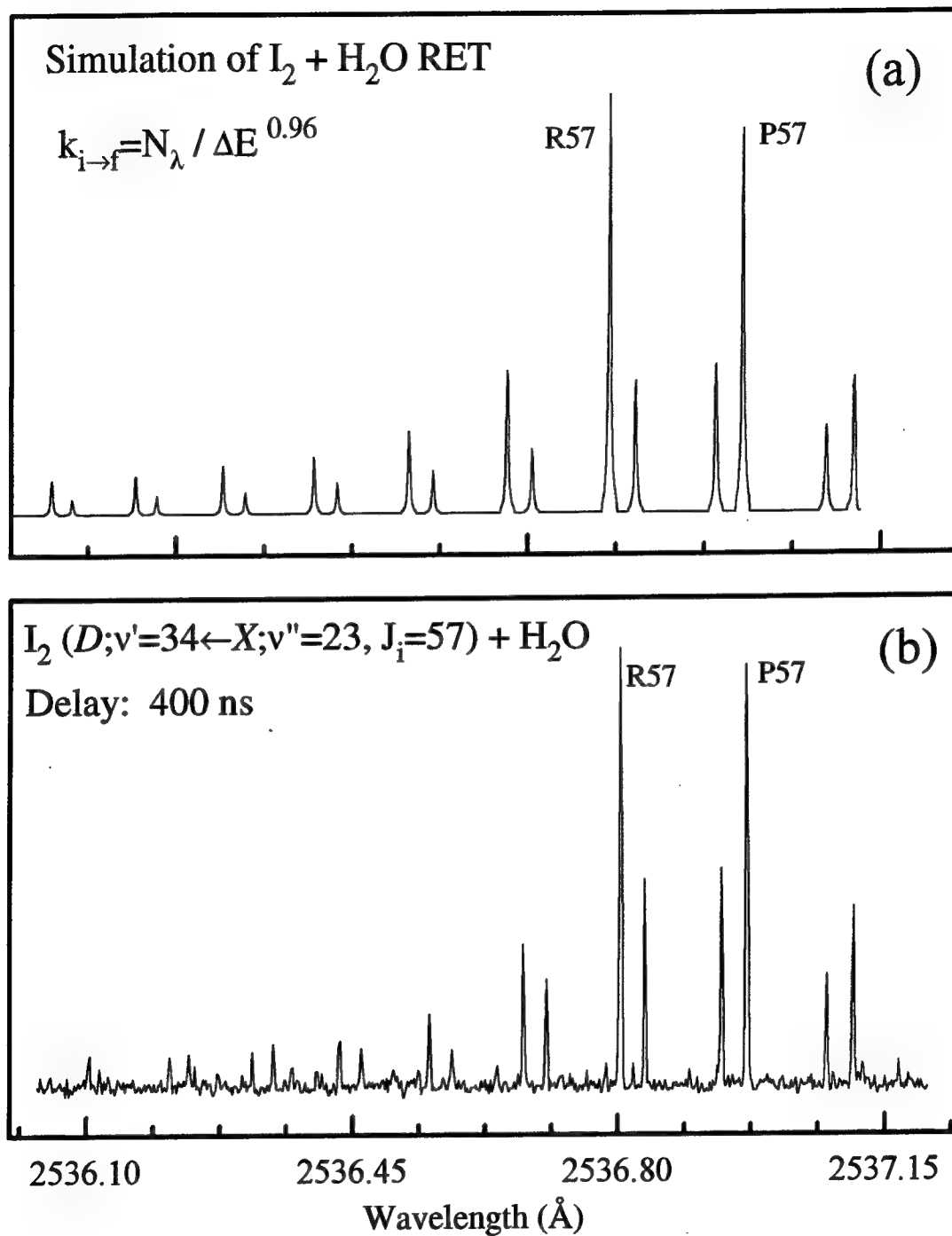
Figure 7.15: (a) Simulation of I_2 (X) v"=23 + H_2O and (b) SEP-LIF of I_2 + H_2O
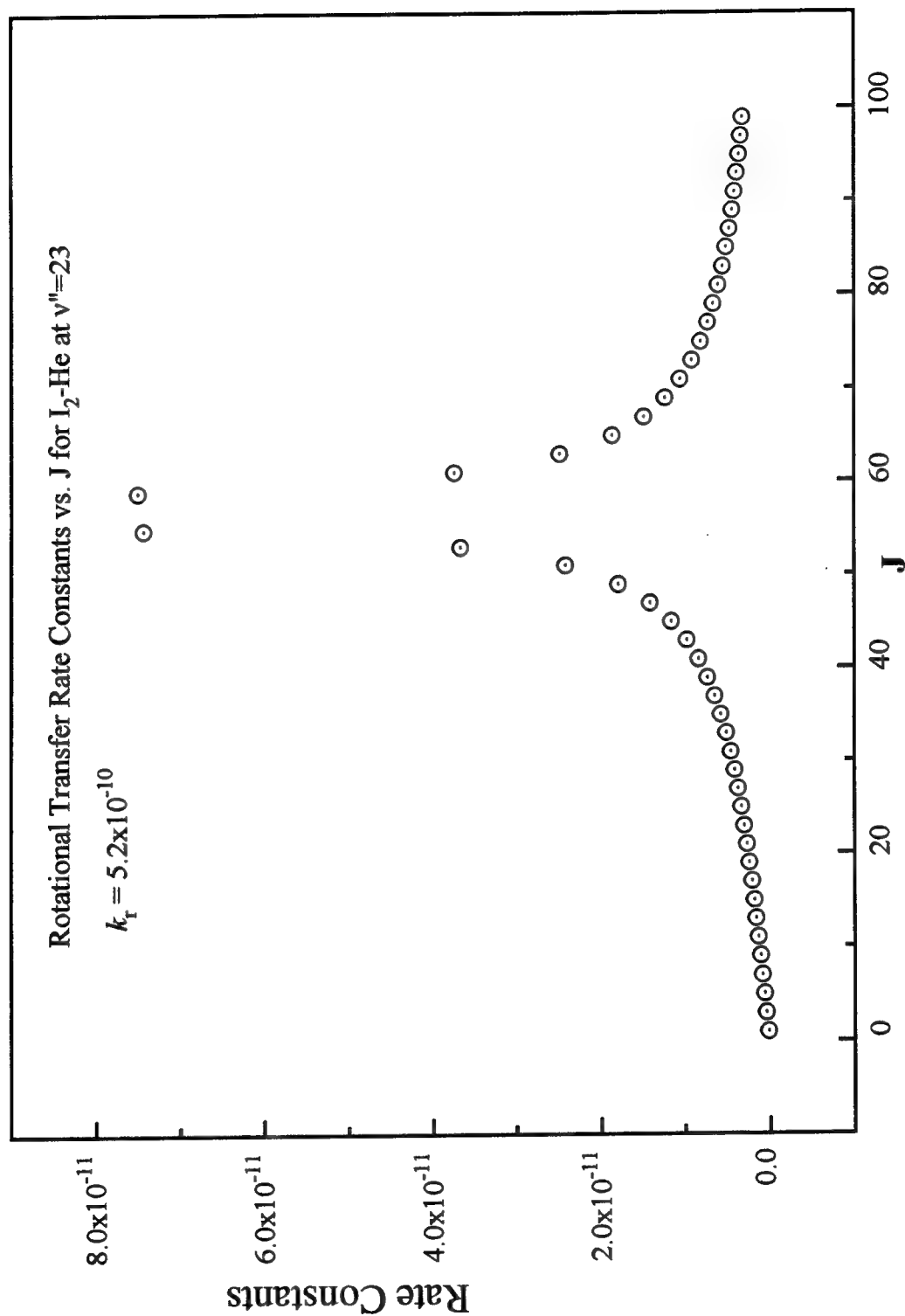
Figure 7.16: Rotational Transfer Rate Constants for Iodine-Helium; I_2 (X) v"=23.

sudden approximation and values of a=4.49x10^{-11} and α=0.7062 were obtained for I$_2$ self transfer.

The vibrational transfer distribution was modeled in the same manner as v"=38 in Chapter 6. First, the rotational transfer rate was determined and transfer peaks of both VT and RT origin were compared. Satellite peaks originating from VT were assigned the same rate constant value as compared to RT peaks with similar heights. When the rotational distribution for the v-1 collisionally populated level was not available, the distribution was modeled with the SPGL. Since the rotational contours of the vibrational energy transfer were consistent with a tendency to conserve angular momentum, the unobserved peaks in the vibrationally populated level were scaled with the α of the SPGL where

$$k_M(v_i=23\ J_i=57\rightarrow v_f=22\ J_f) = C_{23\text{-}22}N_\Delta|\Delta E_{rot}/B|^{-\alpha}$$

The total vibrational rate constant would then be determined by summing the rates from the observed and SPGL distributions. Combining the observed and SPGL distributions avoided the singularity at ΔE_{rot}=0. The vibrational transfer rate constants are listed in Table 7.1

In addition to modeling the v-1 rotational distribution with the SPGL, rotational contours were modeled with Gaussian distributions as shown in Figure 7.17. The rotational and vibrational rate constants were then normalized to the total loss rate. Modeling of the rotational distribution with a Gaussian distribution generally produced a smaller k$_v$ when compared with SPGL modeling.
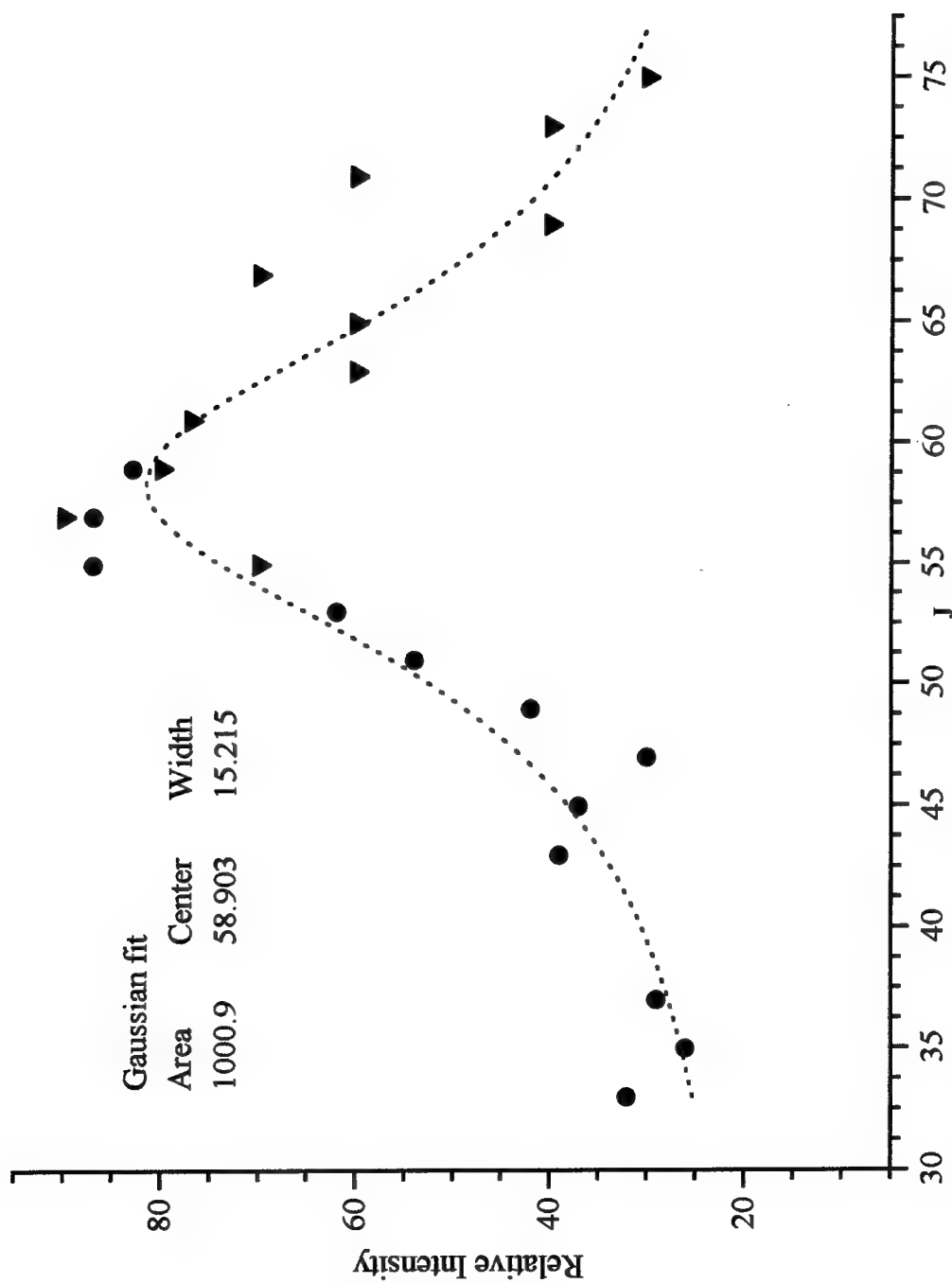
Figure 7.17: Rotational Distribution for VT Transfer of $I_2(X, v''=23, J_i=57 \rightarrow v''=22, J_f)$ + He

A few general trends are suggested by this energy transfer data. For the collisional partners examined, vibrational relaxation was about an order of magnitude slower than rotational redistribution, and governed by a strong $\Delta v=-1$ propensity. Non-reactive molecular collision partners were no more effective than rare gas atoms in causing vibrational transfer. The primary factor controlling the vibrational transfer probabilities appeared to be the mass of the collision partner; light colliders being most effective in transferring energy. These trends are consistent with vibrational-to-translational energy transfer, and can be explained by classical models. Although vibration-to-vibration transfer could occur with O_2 and H_2O, it seems that the mis-matches between the donor and acceptor frequencies are too great for this to be effective.[5] Even for $I_2(X,v''<20) + I_2(X)$ collisions, where the mis-match in vibrational intervals is less severe, V-V transfer does not appear to be of importance.

§7.4 References

1. G. E. Hall, W. J. Marienelli, and P. L. Houston, *J. Phys. Chem.* **87**, 2153 (1983).

2. S. J. Davis and K. W. Holtzclaw, *J. Chem. Phys.* **92**, 1661 (1990).

3. Philip R. Bevington, *Data Reduction and Errror Analysis for the Physical Sciences*, McGraw-Hill, New York (1969).

4. B. W. Shore And D. H. Menzel, *Principles Of Atomic Spectra*, John Wiley&Sons, New York (1968).

5. M. L. Nowlin and M. C. Heaven, *Journal De Physique IV* **4**, CA-729 (1994).

CHAPTER 8

COMPARISON OF COLLISIONAL DYNAMICS AND STUDIES OF E-E TRANSFER

§8.1 COMPARISON OF COLLISIONAL DYNAMICS

Compared to the situation for $I_2(B)$, there have been very few state-resolved studies of the collision dynamics of $I_2(X)$.[1] Gentry and co-workers[2,3] measured relative cross sections for vibrational transfer out of $I_2(X, v''=0)$ and $I_2(X, v''=5)$ induced by collisions with He in crossed molecular beams. This intriguing series of experiments was undertaken, in part, to examine the role of resonances in vibrational energy transfer.[4] Koffend et al.[5] devised an ingenious scheme for extracting energy transfer rate constants from an optically pumped laser system. They obtained upper limits for the rates at which rotational levels of the $v''=42$ and $v''=62$ manifolds were depopulated by collisions with $I_2(X)$. Additional information concerning the rate constants for vibrational relaxation of highly excited levels ($v''>20$) has been obtained incidentally from studies of the electronic to vibrational (E→V) energy transfer processes[6,7]

$$I_2(X) + I(^2P_{1/2}) \rightarrow I_2(X, v'' \approx 26\text{-}42) + I(^2P_{3/2}) \qquad (8.1)$$

and

$$I_2(X) + O_2(^1\Delta) \rightarrow I_2(X, v'' \approx 33\text{-}44) + O_2(^3\Sigma^-) \qquad (8.2)$$
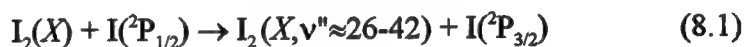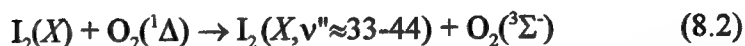
Hall et al.[6] used a pulsed laser to initiate reaction (8.1) in the presence of a large excess of an inert buffer gas (He or Ar). By following the time evolution of the I_2 vibrational

population distribution they determined rate constants for the deactivation of $I_2(X,$ v"=40) by He, Ar, and I_2. All three were found to be efficient vibrational energy transfer agents. From a flow-tube study of reaction (8.2) with He as the carrier gas, van Benthem and Davis[7] obtained supporting evidence that He was effective in relaxing $I_2(X,$ v">20). Both of these studies were inspired by the work of Heidner et al.,[8] who characterized the kinetics occurring in flowing $I_2/O_2(^1\Delta)/Ar$ mixtures. Although vibrationally excited $I_2(X)$ was not observed directly, its participation in the processes leading to electronic excitation and dissociation of I_2 was inferred from kinetic models. Heidner et al. reported a very low rate constant for deactivation of excited $I_2(X)$ by Ar. In this context, deactivation referred to relaxation of the nascent distribution produced by reactions 8.1 and 8.2 to levels with v"<20. As this would required the dissipation of a considerable amount of vibrational energy, the large v→v-1 rate constant obtained by Hall et al. was not considered to be in disagreement with the low deactivation rate. Indeed, David et al.[9] have shown that the flow-tube kinetics can be modeled using the rate constants of Hall et al. Necessary constraints required by the model were that relaxation proceeds via sequential v→v-1 steps, and that the rates for these steps scale linearly with v.

To my knowledge, there have been no other quantitative studies of rotational energy transfer within highly excited vibrational levels of $I_2(X)$, but it is of interest to compare the present results with corresponding data for $I_2(B)$. Selected values for B state rotational transfer rate constants are reproduced in Table 5.2. Here it can be seen

that the rate constants for transfer induced by He and Ar are quite similar. Larger

differences are evident when the rate constants for I_2 and O_2 are compared. It is tempting

to correlate these differences with the fact that both I_2 and O_2 efficiently quench the B

state via collision induced predissociation. Qualitative differences between the X and B

state rotational transfer characteristics are revealed when relative state-to-state rate

constants are compared. Data suitable for this purpose are available for $I_2(B)$+He and

$I_2(B)$+$I_2(X)$. With these collision partners, the probabilities for transferring large amounts

of angular momentum ($|\Delta J|$>15) declined more slowly with increasing $|\Delta J|$ for X, v=42

than for the B state levels. An example of this trend can be seen in Figures 5.4 and 6.7,

where the D-X spectrum shows broader rotational contours than the f-B spectrum

recorded under identical conditions. Figure 8.1 shows a comparison in rotational energy

transfer rate constants between I_2+He for $I_2(X,$ v"=23, J_i=57) and $I_2(B,$v"=15, J_i=59).

Factors which favor the transfer of angular momentum are seen to be favored in the X

state over the B state. Note that the differences between the spectra shown in Figure 5.4

cannot be explained by "energy gap" considerations, as the rotational constant for X,

v"=42 (0.03155 cm^{-1}) is larger than that of B, v'=43 (0.01875 cm^{-1}). Energy gap

considerations are frequently used to explain the relatively rapid rates of vibrational

relaxation from highly excited levels of anharmonic oscillators.[3] The quantum-number

scaling relation is given by

$$\sigma_{m,m-1}(E_m) = m\sigma_{1,0}(E_1)$$
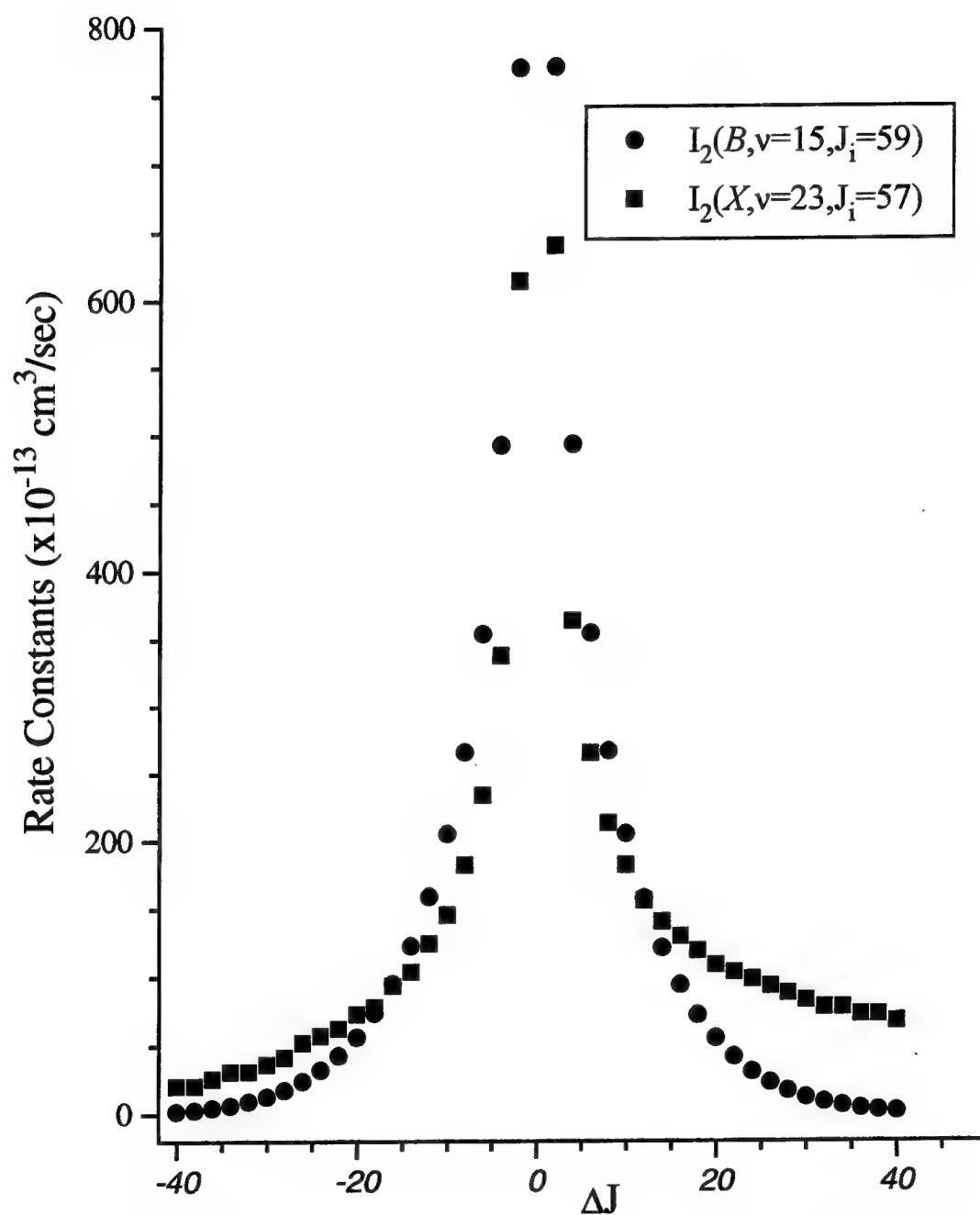
Figure 8.1: Comparison of RET for I_2 + He between I_2 (X,v=23, J_i=57) and I_2 (B, v=15, J_i=59)

where E_i is the kinetic energy of collision in initial state i. This relation shows that highly excited states relax more rapidly than the less excited ones, even in the absence of anharmonic effects.

Pritchard and co-workers[10] reported for $Na_2^* + Xe$ that a different γ was obtained for upward and downward RT transitions until they assumed $\Delta m_J = 0$. Polanyi et al.[11] stated the asymmetry between upward and downward RT transitions was not removed by the assumption of $\Delta m_J = 0$. They explained the difference between their results and Pritchard's was as a consequence of the experimental conditions of the bulb vs. supersonic expansion of a molecular beam apparatus. A bulb experiment assumes an initial equilibrium distribution over m_J states in which all the m_J states are equally populated, whereas the molecular beam experiment cannot. The degeneracy averaged cross-sections for upward and downward transitions are related by

$$\sigma_{i \to f} = (T_f/T_i)(g_f/g_i)\sigma_{f \to i},$$

where T is the translational energies and g is the angular momentum degeneracies for the initial and final states. The cross section is related to the SPGL by

$$\sigma_{J \to J'} \propto N(T_f/T_i)^{1/2}|\Delta E|^{-\gamma} \tag{8.3}$$

Microscopic reversibility can only be satisfied with a single value of γ since $|\Delta E_{J,J'}|^{-\gamma}$ must cancel. Likewise, H. Chun et at.[12] reported different γ for the upward and downward transitions in their RET studies of $I_2 (B^3\Pi)$ with $I_2(X^1\Sigma)$, Ar, and He. In my fits of I_2 self- transfer for $v''=23$, γ was usually 0.03-0.05 smaller for $J_<$ than $J_>$. One possible

explanation for the SEP-LIF fits having two γs is that the m_J distribution with respect to the collision axis may have been non-random[12]. Since the *pump-dump* lasers for SEP preparation would have plane polarization, the molecules could be aligned.

A system which is aligned is defined having equal populations of $+m$ and $-m$ levels, but different $|m|$ levels have different populations. This system would have a net polarization but no net magnetization. An oriented system has unequal populations of $+m$ and $-m$ and has a net magnetization. No polarization experiments were attempted in this dissertation but would be necessary to quantify this alignment. The dye lasers used in these experiments were mostly vertically polarized. However, this explanation appears questionable since the polarization effects were analyzed by Fei et al.[13] in their SEP studies of CN ($X^2\Sigma$) and they found their population to be unaligned. A second explanation may be found in the translational energy factor of equation (8.3). Energy transfer to smaller J_f would result in an increase of higher final translational energy resulting in diffusion of the sample out of the probe beam.

There has been considerable discussion for a $\Delta m=0$ selection rule for rotational relaxation based on experimental evidence from several molecules.[14] The experimental results of my RET simulations for spin-conservation are inconclusive. Generally, spin conservation of the low molecular weight species of He and Ar would be expected. While the fits for Ar had a higher correlation for $2J_<+1$ degeneracy, He was split between $2J_<+1$ for $v"=38$ and $2J+1$ for $v"=23$. For the remainder of the collision partners, a randomized N produced better correlations.

A comparison of the rate constants between common collision partners for the SEP-LIF experiments of v"=42, 38 and 23 are provided in Table 8.1. No trend is readily ascertained from the inspection of these results. In fact, the lack of a trend indicates that for high vibrational levels, the rotational energy transfer is not significantly different than for low lying states. It appears reasonable to conclude that the part of the potential reasonable for RET is at a much larger length than the part giving rise to VT transfer. The long range rotational energy transfer is unaffected by short range vibrational oscillations.[14]

But two other generalizations are worthy of note. The first is factors favorable for the transfer of angular momentum are more prevalent in the X state than the B state as seen in Figure 8.1. Secondly, the B state rotational constants are significantly different from the X state, and that the practice of modeling the ground state energy transfer using excited state constants is questionable. The difference is most pronounced for H_2, O_2 and I_2 RET constants. Generally, energy transfer is comparable for v"=42, 38, and 23. The most striking comparison is for the total loss rate constant for $I_2 + H_2$ between $I_2(X,$ v"=38, J_i=49) and $I_2(B,$ v'=15)[15] with the rate constants of 7.1×10^{-10} and 14.0×10^{-10}, respectively.

Information regarding vibration to translation (V-T) energy transfer derived from this study appears to be in qualitative agreement with the predictions of simple theoretical models. Typically, the models indicate that the v"→v"-1 rate constants will increase with v", and decrease as the collision reduced mass increases. Some years ago,

Table 8.1: Comparison of Rate Constants for Common Collision Partners for the SEP-LIF Experiments of Individual Rovibronic Levels for I_2 (X) v"=42, 38, and 23.

Collision Partner	$k_T[I_2(X)](10^{-10}$ cm^3 s^{-1})		
	v"=42	v"=38	v"=23
I_2	8.6	6.6	8.7
He	6.6	5.4	6.4
Ar	5.0	5.5	5.7
O_2	7.8	7.0	7.1
H_2O	-	8.8	9.3
	$k_R[I_2(X)](10^{-10}$ cm^3 s^{-1})		
I_2	8.6	6.0	8.7
He	6.0	4.4	5.2
Ar	5.0	5.1	5.4
O_2	7.2	6.3	-
H_2O	-	6.2	7.6
	$k_V[I_2(X)](10^{-11}$ cm^3 s^{-1})		
I_2	<1	6.0	1.0
He	5.5	10.0	12.0
Ar	<1	4.0	3.0
O_2	4.5	7.0	-
H_2O	-	26.0	17.0

Nesbitt and Hynes[16,17] examined a classical model of I_2 + M (M=He,Ar,Xe) vibrational energy transfer. Their calculations indicated that, for v"=40, He was a more efficient transfer agent than Ar by a factor greater than two. Gentry and co-workers have argued that $I_2(X)$ + He V-T transfer can for low vibrational levels, be adequately described by a forced harmonic oscillator model. In the low energy region, they proposed that the cross sections for v"→v"-1 transfer ($\sigma_{v",v"-1}$) scale linearly with v", which is the first observation of the simple prediction of the SSH theory of vibrational energy transfer.

When the V-T rate constants were known only for the lowest-lying vibrational states, it was possible to predict the values for the vibrationally excited levels using SSH theory. SSH theory predicts the probability of transition from state v to v-1 as[18]

$$P_{v,v-1} = P(T)(v/(1-\chi_e v)) F(Y_{v,v-1})$$

where

P(T) is a function related to the 1-0 transition

χ_e is the anharmonicity of the molecule

$Y_{v,v-1} = (0.5)^{3/2}(\theta/T)^{1/2}(1-2\chi_e v)$

$F(Y) = 0.5(3-e^{-2Y/3})(e^{-2Y/3})$

and θ is the characteristic temperature for VT energy transfer and is defined

$$\theta = (0.8153 M h^2 v^2 l^2) /k^2$$

where

M is the molecular weight of the gas

v is the frequency of vibration of the lowest vibrational state

h is Planck's constant

l is the characteristic interaction distance (≈ 0.2Å)

In a crossed molecular beam experiment, Ma et al. measured the $\sigma_{5,4}$ cross section relative to the hard sphere scattering cross section, σ_a. At a collision energy of 0.38 meV

(equivalent to 290°K) they obtained a ratio of $\sigma_{5,4}/\sigma_a=0.0045$. Assuming linear v"scaling, this result extrapolates to $\sigma_{42,41}/\sigma_a=0.04$. Furthermore, if we equate σ_a with the total removal rate constant for He (Table 5.1), this extrapolation predicts a V-T rate constant of 2.6×10^{-11} cm^3 s^{-1}. Considering the crudeness of this model, the agreement with the SEP result is reasonable. In addition, there are two plausible reasons why this extrapolation would result in an underestimation. First, the total inelastic scattering cross-section includes contributions from velocity-changing collisions. Hence the ratio of $\sigma_{5,4}$ to the cross section for rotational and vibrational energy transfer will be greater than $\sigma_{5,4}/\sigma_a$. Second, anharmonicity has been ignored, and we are dealing with a level that is three quarters of the way towards dissociation. An important effect of the anharmonicity is reduction of the v"→v"-1 energy spacing with increasing v". Figure 5.4 may provide an indication of the influence the anharmonicity has on the V-T transfer probabilities. Within the ground state, only $\Delta v=-1$ transfer was observed. The v"=42, $\Delta v\pm1$ energy spacings are 151 and -153 cm^{-1}. In the B state, where $\Delta v=\pm1$ and ±2 transfer was easily seen, the n'=43 $\Delta v=\pm1$ energy spacings are 42 and -44 cm^{-1}. Note that the $\Delta v\pm2$ processes were present because v'=43 and the surrounding levels are close to the dissociation limit, and therefore highly anharmonic.

Computer modeling of the kinetics yielded a rate constant for v"=23→22 transfer induced by H$_2$0 at $\approx9\times10^{-11}$cm^3 s^{-1}. This value is a factor of three smaller than the rate constant for H$_2$0 deactivation estimated by Heidner et al. and used in COIL system

computer models. The actual discrepancy is greater than an order of magnitude, because the deactivation process represents transfer from levels around v"=40 to levels below v"=20. As it may take many transfer to achieve deactivation, these results imply that the effective rate constant will be of the order of 10^{-12} cm^3 s^{-1}.

Vibration-translation transfer probabilities are crucial for modeling the deactivation of vibrationally excited iodine and its role in dissociation in the COIL. A model for vibrational deactivation of I$_2$† by He in the COIL device has been analyzed by M. C. Heaven utilizing the rate constants determined from these SEP-LIF experiments. His model was based on the following assumptions: V-T is controlled by $\Delta v = \pm 1$ selection rule; rate constants for downward transfer ($k_{v-1 \leftarrow v}$) scale linearly with the vibrational quantum number (SSH) where $k_{v-1 \leftarrow v} = vk_{0 \leftarrow 1}$; upward energy transfer rate constants are calculated from detailed balance where $k_{v \leftarrow v-1} = k_{v-1 \leftarrow v} \exp(-E_v - E_{v-1})/k_b T$); and where the rotational distributions are thermalized. A coupled rate equation describe the V-T process is given by

$$d[I_2, v]/dt = (k_{v \leftarrow v-1}[I_2, v-1] + k_{v \leftarrow v+1}[I_2, v+1] - (k_{v+1 \leftarrow v} + k_{v-1 \leftarrow v})[I_2, v])[He]$$

The calculation was performed using $k_{0 \leftarrow 1} = 1.4 \times 10^{-12}$ cm^3 s^{-1}, a pressure of 10 Torr He, and a temperature of T=298°K. The initial population of I$_2$† at time t=0 is assumed as a Gaussian distribution defined as

$$N_v = N_0 \exp - [\tfrac{\upsilon - \upsilon_0}{\Delta \upsilon}]^2$$

where v_0 is the distribution center (≈ 40), Δv is the width (≈ 10), and N_0 is a constant normalized to give a total number density of 3×10^{10} cm^{-3}. Some results of the model were:

(i)   The effective rate constant is independent of He pressure

(ii) The model indicates that a single pressure independent rate constant for $I_2^\dagger$ + He is adequate

(iii) The effective rate constant is not strongly dependent on the temperature or the initial state distribution

§8.2 Studies of E-E Transfer: I_2 + CF$_3$I and I_2 + O$_3$

This section serves as historical documentation of experiments which were hypothesized as populating highly vibrational excited levels in I_2 (X), but populated the A' state instead. Translationally hot $I(^2P_{1/2})$ was generated by 248 nm photolysis of CF$_3$I.

$$CF_3I + hv\ (248\ nm) \rightarrow CF_3 + I(^2P_{1/2})$$

$$I(^2P_{1/2}) + I_2 \rightarrow I(^2P_{3/2}) + I_2\ (A')$$
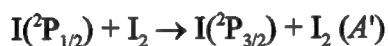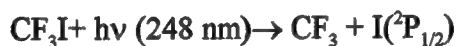
Surprisingly, collisions of I_2 (X) with hot $I(^2P_{1/2})$ resulted in direct excitation of $I_2(A')$, indicating that both electronic and kinetic energy was transferred.

The experimental apparatus is similar to Figure 3.1 with the exception that the photolysis laser was a Lumonics KrF laser instead of a Nd:YAG laser. Trifluoromethyl iodide was chosen as an $I(^2P_{1/2})$ precursor because it is an inefficient quencher of $I(^2P_{1/2})$. Hall et al. were able to detect vibrationally excited I_2 (X) produced by collisional energy

transfer between I_2 and $I(^2P_{1/2})$, where $I(^2P_{1/2})$ was prepared by photolysis of CF_3I at 266 nm. For our experiments, the delay times between the photolysis (KrF: 248 nm) and probe laser were varied from 4 to 9 μs. Pressures were nominally 100 mTorr CF_3I, 200 mTorr I_2, and 500 mTorr Ar. Delays and pressures were varied as well as using a flowing system with CF_3I in order to produce vibrationally excited I_2 (X). Results of the $CF_3I + I_2$ generating D'-A' are shown in Figure 8.2 along with a comparison of the corresponding D-X system of $I_2(X)$ with cold $I(^2P_{1/2})$.

The second experiment which populated I_2 (A') was the energy transfer between photolyzed ozone and iodine.

$$O_3 + h\nu\ (248\ nm) \rightarrow O_2(^3\Sigma, v) + O(^3P)$$
$$\rightarrow O_2(^1\Delta) + O(^1D)$$
$$O(^1D) + I_2\ (X) \rightarrow I_2\ (A') + O(^3P)$$
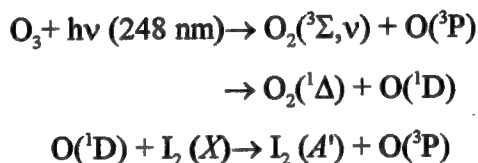
An ozone generator producing a corona discharge generated ozone from oxygen with 98% efficiency. The ozone was photodissociated at 248 nm producing $O_2(^1\Delta)$, $O_2(^3\Sigma, v)$, $O(^3P)$, and $O(^1D)$. The experimental apparatus was the same as in the $CF_3I + I_2$ studies. Indirect confirmation of the presence of $O_2(^1\Delta)$ was required because of its long radiative lifetime. A germanium detector observed $I(^2P_{1/2})$ emission at 1.315 μm resultingfrom the near resonant collisional energy transfer between $O_2(^1\Delta) + I(^2P_{3/2}) \rightarrow O_2(^3\Sigma) + I(^2P_{1/2})$. In addition, a PMT monitored $O_2(^1\Sigma) \rightarrow O_2(^3\Sigma) + h\nu$ emission at 762 nm where $2O_2(^1\Delta) \rightarrow O_2(^1\Sigma) + O_2(^3\Sigma)$. Pressures in the chamber were nominally 600 mTorr O_3 and 100 mTorr I_2. As with the $CF_3I + I_2$ experiment, direct population of the A' state was
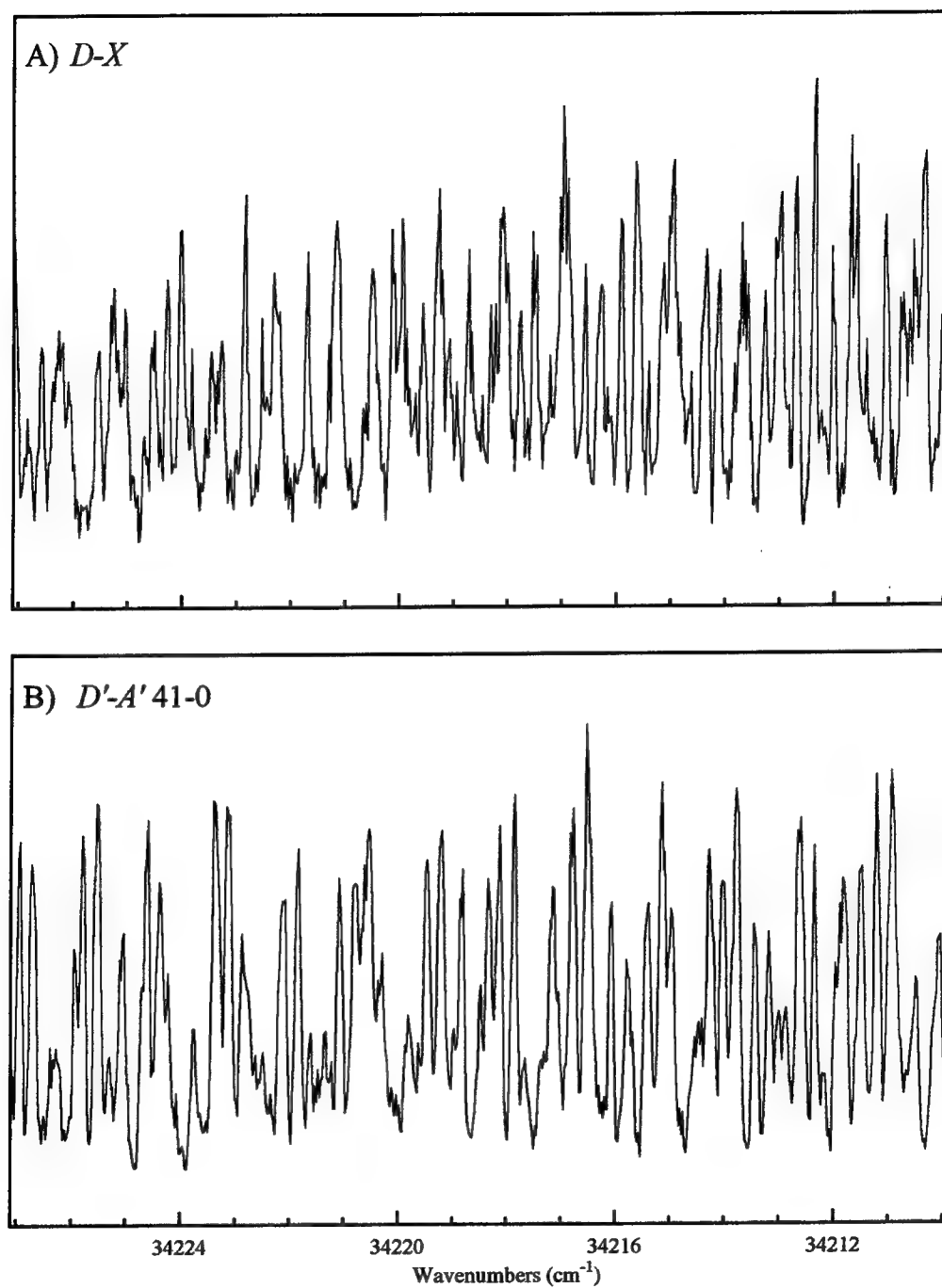
Figure 8.2: (a) Comparison of cold $I(^2P_{1/2}) + I_2$ producing D-X Fluorescence and (b) hot $I(^2P_{1/2}) + I_2$ populating D'-A' System

observed for the collisional energy transfer between O^1D and I_2. Results of the D'-A' spectrum for $O_3 + I_2$ are shown in Figure 8.3.

In addition to photolyzing O_3 at 248 nm, I attempted to produce $O_2(^1\Delta)$ by pumping $O_2 (X^3\Sigma)$ at 1.064μm with the fundamental of a Nd:YAG laser. No signal was observed from the PMT while monitoring 321 nm (D-X), 340 nm (D'-A'), 762 nm $(O_2(^1\Sigma) \rightarrow O_2(^3\Sigma) + h\nu)$, or with the Ge detector at 1.315 μm $[I(^2P_{1/2}) \rightarrow I(^2P_{3/2}) + h\nu]$.

§8.3 REFERENCES

1. J. I. Steinfeld, *J. Phys. Chem. Ref. Data* **13**, 445 (1984); **16**, 903 (1987).

2. G. Hall, K. Liu, M. J. McAuliffe, C. F. Giese, and W. R. Gentry, *J. Chem. Phys.* **81**, 5577 (1984).

3. Z. Ma, D. D. Jons, C. F. Giese, and W. R. Gentry, *J. Chem. Phys.* **94**, 8608 (1991).

4. W. R. Gentry, *J. Chem. Phys.* **81**, 5737 (1984).

5. J. B. Koffend, F. J. Wodarczyk, R. Bacis, and R. W. Field, *J. Chem. Phys.* **72**, 478 (1980).

6. G. E. Hall, W. J. Marienelli, and P. L. Houston, *J. Phys. Chem.* **87**, 2153 (1983).

7. M. H. van Benthem and S. J. Davis, *J. Phys. Chem.* **90**, 902 (1986).

8. R. F. Heidner, C. E. Gardner, G. I. Segal, and T. M. El-Sayed, *J. Phys. Chem.* **87**, 2348 (1983).

9. D. David, V. Joly, and A. Fausse, *Proceedings of the 7th International Symposium on Gas Flow and Chemical Lasers*, Springer Proceedings in Physics Springer, Berlin (1987), p. 156.

10. T. A. Brunner, R. D. Driver, N. Smith, and D. E. Pritchard, *J. Chem. Phys.* **70**, 4155 (1979).
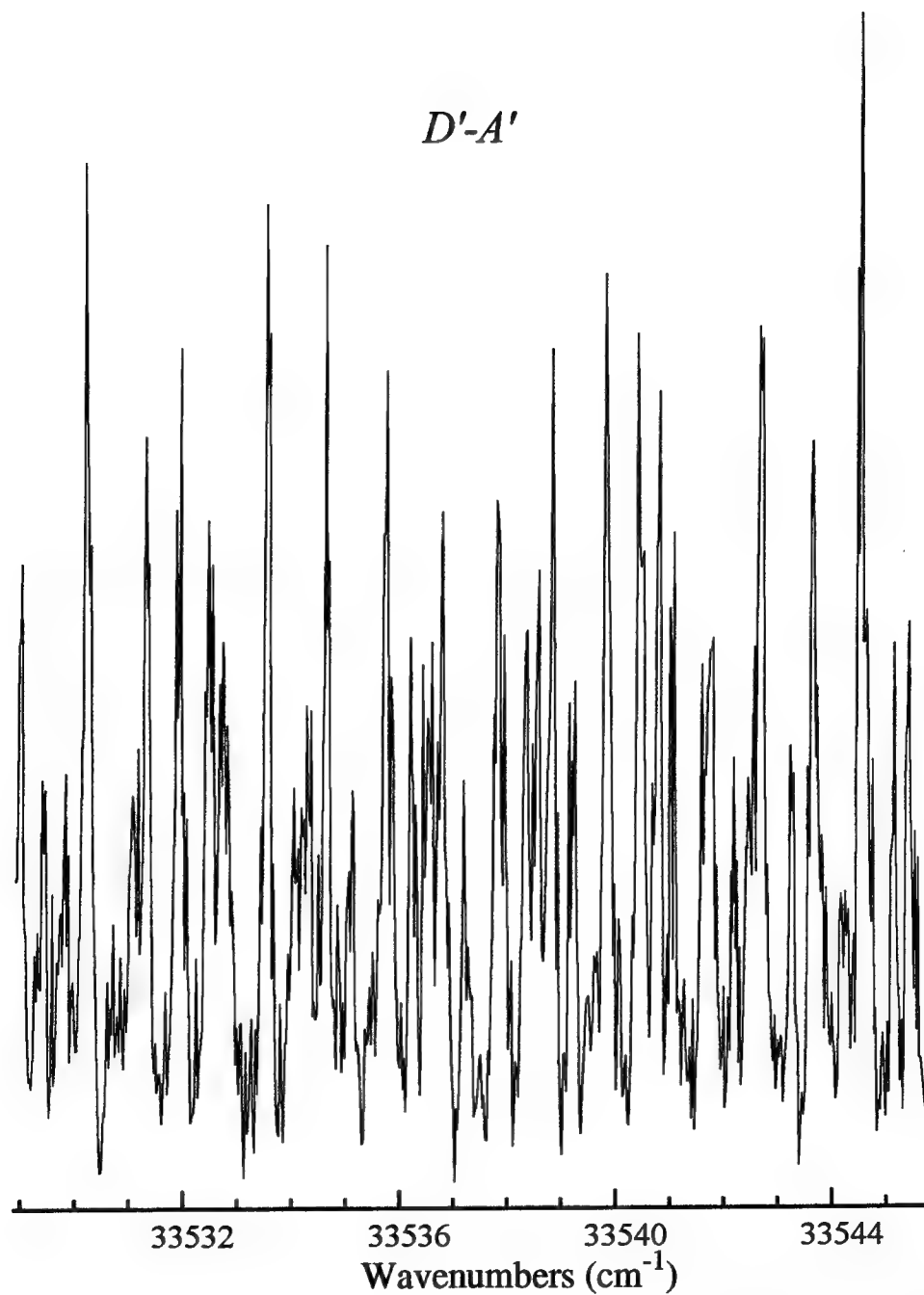
Figure 8.3: Energy Transfer of $I_2 + O_3$ After Photolysis of O_3 at 248 nm Producing $O_2(^1\Delta) + O^1D$

11. J. A. Barnes, M. Keil, R. E. Kutina, and J. C. Polanyi, *J. Chem. Phys.* **76**, 913 (1982).

12. H. Chun, H. Ruiping, and Z. Cunhao, *Appl. Phys. B* **41**, 251 (1986).

13. R. Fei, H. M. Lambert, T. Carrington, S.V. Filseth, C. M. Sadowski, and C. H. Dugan, *J. Chem. Phys.* **100**, 1190 (1994).

14. A. J. McCaffery, M. J. Proctor, and B. J. Whitaker, *Ann. Rev. Phys. Chem.* **37**, 223 (1986).

15. J. Derouard and N. Sadeghi, *Chem. Phys. Lett.* **102**, 324 (1983).

16. D. J. Nesbitt and J. T. Hynes, *Chem. Phys. Lett.* **82**, 252 (1981).

17. D. J. Nesbitt and J. T. Hynes, *J. Chem. Phys.* **76**, 6002 (1982).

18. C. D. King, *Kinetic Studies of Dissociation in Oxygen-Iodine Lasers*, Thesis, Wright-Patterson AFB, Ohio, Air Force Institute of Technology (1989).

BIBLIOGRAPHY

Millard H. Alexander, *Chem. Phys. Lett.* **40**, 267 (1976).

M.Allegrini, G. Alzetta, and M. Civilini, *Chem. Phys. Lett.* **70**,454 (1980).

S. J. Arnold, N. Finlayson, and E. A. Ogryzlo, *J. Chem. Phys.* **44**, 2529 (1966).

R. G. Aviles, D. F. Muller, and P. L. Houston, *Appl. Phys. Lett.* **37**, 358 (1980).

J. A. Barnes, M.Keil, R. E. Kutina, and J. C. Polanyi, *J. Chem. Phys.* **76**, 913 (1982).

J. Bachar and S. Rosenwaks, *J. Appl. Phys.* **62**, 31 (1987).

M. Bartels, R. J. Donovan, A. J. Holmes, P. R. R. Langridge-Smith, M. A. MacDonald, and T. Ridley, *J. Chem. Phys.* **91**, 7355 (1989).

J. Alberto Beswick, R. Monot, J.-M. Philippoz, and H. van den Bergh *J. Chem. Phys.* **86**, 3965 (1987).

Philip R. Bevington, *Data Reduction and Errror Analysis for the Physical Sciences*, McGraw-Hill, New York (1969).

W. Bohn, *Proc. SPIE- Int. Soc. Opt. Eng.* **1810**, 468 (1992).

A. J. Bouvier, R. Bacis, A Bouvier, D. Cerny, S. Churassy, P. Crozet, and M. Nota, *J. Quant. Spectrosc. Radiat. Transfer*, **49**, 311 (1992).

J. C. D. Brand and Rowland J. Hayward, *Chem. Phys. Lett.* **68**, 369 (1979).

J. C. D. Brand and A. R. Hoy, *J. Mol. Spectrosc.* **97**, 379 (1983).

H. P. Broida and Tucker Carrington, *J. Chem. Phys.* **38**, 136 (1963).

Robert L. Brown and W. Klemperer, *J. Chem. Phys.* **41**, 3072 (1964).

M. Broyer, J. Vigue, and J. C. Lehmann, *J. Chem. Phys.* **63**, 5428 (1975).

T. A. Brunner and D. E. Pritchard, *Adv. Chem. Phys.* **50**, 589 (1982).

T. A.Brunner, R. D. Driver, N. Smith, and D. Pritchard, *Phys. Rev. Lett.* **41**, 856(1978).

T. A.Brunner, R. D. Driver, N. Smith, and D. Pritchard, *J. Chem. Phys.* **70**, 4155(1979).

T. A. Brunner, N. Smith, and D. E. Pritchard, *Chem. Phys. Lett.* **71**, 358 (1980).

T. A.Brunner, N. Smith, A. W. Karp, and D. Pritchard, *J. Chem. Phys.* **74**, 3324 (1981).

Michael D. Burrows, *J. Chem. Phys.* **81**, 3546 (1984).

Kirk W. Butz, Hong Du, Douglas J. Krajnovich, and Charles J. Parmenter, *J. Chem. Phys.* **89**, 4680 (1988).

D. Cerny, R.Bacis, A. J. Bouvier, S. Polat, A. Topouzkhanian, and J. Verges, *J. Quant. Spectrosc. Radiat. Transfer* **47**, 9 (1992).

S. Churassy, R. Bacis, A.J. Bouvier, C. Pierre dit Mery, B. Erba, J. Bachar, and S. Rosenwaks, *J. Appl. Phys.* **62**, 31 (1987).

R. Clark and A. J. McCaffery, *Mol. Phys.* **35**, 609 (1978).

J. A. Coxon in *Molecular Spectroscopy* eds. R. F. Barrow, D. A. Long, and D. J. Millen, Specialist Periodic Reports, The Chemical Society, London (1973) Vol. 1, pp 177-227.

D. David, V. Joly, and A.Fausse, *Proceedings of the 7th International Symposium on Gas Flow and Chemical Lasers*, p 156, Springer Proceedings in Physics, Berlin (1987).

H. L. Dai, C. L. Korpa, J. L. Kinsey and R. W.Field, *J. Chem. Phys.* **82**, 1688 (1985).

S. J. Davis and K. W. Holtzclaw, *J. Chem. Phys.* **92**, 1661 (1990).

A. E. DePristo and H. Rabitz, *Chem. Phys.* **24**, 201 (1977).

A. E. DePristo and H. Rabitz, *J. Chem. Phys.* **72**, 4685 (1980).

A. E. DePristo, S. D. Augustin, R. Ramaswamy and H. Rabitz, *J. Chem. Phys.* **71**, 850 (1979).

J. Derouard, *Chem. Phys.* **84**, 181 (1984).

J. Derouard and N. Sadeghi, *Chem. Phys. Lett.* **102**, 324 (1983).

J. Derouard and N. Sadeghi, *J. Chem. Phys.* **81**, 3002 (1984).

J. Derouard and N. Sadeghi, *Chem. Phys.* **88**, 171 (1984).

R. G. Derwent and B. A. Thrush, *Chem. Phys. Lett.* **9**, 591 (1971).

R. G. Derwent and B. A. Thrush, *Disc. Faraday Soc.* **53**, 162 (1972).

R. G. Derwent and B. A. Thrush, *J. Chem. Soc. Faraday Trans. II*, **68**, 720 (1972).

R. G. Derwent and B. A. Thrush, *Trans. Faraday Soc.* **67**, 2036 (1971).

R. G. Derwent , D. R. Kearns B. A. Thrush, *Chem. Phys. Lett.* **6**, 115 (1970).

S. L. Dexheimer, M. Durand, T. A. Brunner and D. E. Pritchard, *J. Chem. Phys.* **76**, 4996 (1982).

R. E. Drullinger and R. N. Zare, *J. Chem. Phys.* **51**, 5532 (1969).

R. E. Drullinger and R. N. Zare, *J. Chem. Phys.* **59**, 4225 (1973).

Suli Fei, Xiaonan Zheng, M. C. Heaven and Joel Tellinghuisen, *J. Chem. Phys.* **97**, 6057 (1992).

R. Fei, H. M. Lambert, Tucker Carrington, S. V. Filseth, C. M. Sadowski and C. H. Dugan, *J. Chem. Phys.* **100**, 1190 (1994).

G. A. Fisk and G.N. Hays, *J. Chem. Phys.* **77**, 4965 (1982).

G. A. Fisk and G.N. Hays, *Appl. Phys. Lett.* **42**, 3 (1983).

A. Gelb, R. Kapral and G. Burns, *J. Chem. Phys.* **59**, 2908 (1973).

W. Ronald Gentry, *J. Chem. Phys.* **81** 5737 (1984).

S. Gerstenkorn and P. Luc, *Atlas du Spectre d'Absorption del la Molecule d'Iode*, Laboratoire Aime Cotton, CNRS II, Orsay, France, 1977.

John W. Glessner, *Amplified Spontaneous Emission of the Iodine* $B^3\Pi(0^+_u).-X^1\Sigma(0^+_g)$. *System*, Dissertation, Wright-Patterson AFB, Ohio, Air Force Institute of Technology (1986).

R. Goldflam, S. Green and D. J. Kouri, *J. Chem. Phys.* **67**, 4149 (1977).

G. E. Hall, Sivaram Arepalli, P. L. Houston, and J. R. Wiesenfeld, *J. Chem. Phys.* **82**, 2590 (1985).

Gregory Hall, Kopin Liu, Michael J. McAuliffe, Clayton F. Giese and W. Ronald Gentry, *J. Chem. Phys.* **81**, 5577 (1984).

G. E. Hall, W. J. Marinelli, and P.L. Houston, *J. Phys. Chem.* **87**, 2153, (1983).

Charles E. Hamilton, James L. Kinsey, and Robert W. Field, *Ann. Rev. Phys. Chem.* **37**, 493 (1986).

Michael C. Heaven, *Chem. Soc. Rev.* **15**, 405 (1986).

R. F. Heidner III, C. E. Gardner, G. I. Segal, and T. M. El-Sayed, *J. Phys. Chem.* **87**, 2348, (1983).

G. Herzberg, *Molecular Spectra and Moleculat Structure I. Spectra of Diatomic Molecules* (Van Nostrand Rheinhold, 1950).

A. J. Hoy and R. H. Lipson, *Chem. Phys.* **140**, 187 (1990).

J. M. Hutson, S. Gerstenkorn, P. Luc. and J. Sinzelle, *J. Mol. Spec.* **96**, 266 (1982).

Takashi Ishiwata and Ikuzo Tanaka, *Laser Chem.*, 7, 79, (1987).

S. R. Jeyes, A. J. McCaffery, M. D. Rowe, and H. Kato, *Chem. Phys. Lett.*, **48**, 91 (1977).

S. R. Jeyes, A. J. McCaffery, M. D. Rowe, P. A. Madden, and H. Kato, *Chem. Phys. Lett.*, **47**, 550 (1977).

Andreas Joig, Ulrich Meier, and Katarina Kohse-Hoinghaus, *J. Chem. Phys.* **93**, 6453 (1990).

V. Khare, D. J. Kouri and D. K. Hoffman, *J. Chem. Phys.* **74**, 2275 (1981).

Carter Kittrell, Evan Abramson, J. L. Kinsey, Stephen A. McDonald, David E.Reisner, Robert W. Field and Daniel H. Katayama, *J. Chem. Phys.* **75**, 2056 (1981).

J. Brooke Koffend and Robert W. Field, *J. Appl. Phys.* **48**, 4468 (1977).

J. Brooke Koffend, R. Bacis and Robert W. Field, *J. Chem. Phys.* **72**, 2366 (1979).

J.B. Koffend, F. J. Wodarczky, R. Bacis and R. W. Field, *J. Chem. Phys.* **72**, 478(1980).

Douglas J. Krajnovich, Kirk W. Butz, Hong Du, and Charles. S. Parmenter, *J. Chem. Phys.* **91**, 7705 (1989).

R. B. Kurzel and J. I. Steinfeld, *J. Chem. Phys.* **53**, 3293 (1970).

Richard B. Kurzel, E. O. Degenkob and J. I. Steinfeld, *J. Chem. Phys.* **56**,1784 (1972).

R. B. Kurzel, J. I. Steinfeld, D. A. Halzenbuhl, and G. E. Leroi, *J. Chem. Phys.* **55**, 4822 (1971).

J. D. Lambert, *Vibrational and Rotational Relaxation in Gases,* Clarendon Press, Oxford (1977).

W. D. Lawrance and A. E. W. Knight, *J. Chem. Phys.* **79**, 6030 (1983).

R. D. Levine, R. B. Bernstein, P. Kahana, I. Procaccia and E. T. Upchurch , *J. Chem. Phys.* **64**, 796 (1976).

J. Li and K. Balasubramanian, *J. Mol. Spectrosc.* **138**, 162 (1989).

H. V. Lilenfeld, P. A. G. Carr, and F. E. Hovis, *J. Chem. Phys.* **81**, 5730 (1984).

Yaomin Lin, *Spectroscopic and Dynamic Studies of Br2 and Open-Shell van der Waals Complexes,* Dissertation, Emory University, Atlanta (1991).

P. Luc, *J. Mol. Spectrosc.* **80**, 41 (1980).

Zhiliu Ma, Steven D. Jons, Clayton F. Geise and W. Ronald Gentry, *J. Chem. Phys.* **94**, 8608 (1991).

F. Marten, R. Bacis, S. Churassy and J. Verges, *J. Mol. Spectrosc.* **116**, 71 (1986).

A. J. McCaffery, *J. Phys. Chem.* **91**, 5451 (1987).

A. J. McCaffery, M. J. Proctor and Whitaker, *Ann Rev Phys Chem* **37**, 223 (1986).

A. J. McCaffery, M. J. Proctor, E. A. Seddon, and A. Ticktin, *Chem. Phys. Lett.* **132**, 181 (1986).

A. J. McCaffery, Z. T. Alwahabi, M. A. Osborne and C. J. Williams, *J. Chem. Phys.* **98**, 4586 (1993).

W. E. McDermott, N. R. Pchelkin, D. J. Benard, and R.R. Bousek, *Appl. Phys. Lett.* **32**, 469 (1978).

Michael J. McQuaid, *Spectroscopic Characterization of Metal-Based Complexes and Metal-Based Complex Oxidation Processes,* Dissertation, Georgia Institute of Technology, Atlanta (1989).

D. F. Muller, R. H. Young, P. L. Houston, and J. R. Wiesenfeld, *Appl. Phys. Lett.* **38**, 404 (1981).

Robert S. Mulliken, *J. Chem. Phys.* **55**, 288 (1971).

David J. Nesbitt and James T. Hynes, *Chem. Phys. Lett.* **82**, 252 (1981).

David J. Nesbitt and James T. Hynes, *J. Chem. Phys.* **76**, 6002 (1982).

M. Nota, A. J. Bouvier, R. Bacis, A.Bouvier, P. Crozet, S. Churassy and J. B.Koffend, *J. Chem. Phys.* **91**, 1938 (1989).

M. L. Nowlin and M. C. Heaven, *J. Chem. Phys.* **99**, 5655 (1993).

M. L. Nowlin and M. C. Heaven, *Journal De Physique IV Colloque C4, supplement au Journal de Physique III*, **4**, 729 (1994).

Mark A. Osborne and Anthony J. McCaffery, *J. Chem. Phys.* **101**, 5604 (1994).

Donald O'Shea, W. Russell Callen and William T. Rhodes, *An Introduction to Lasers and Their Applications,* (Addison-Wesley, Reading Massachusetts, 1978).

G. P. Perram and G. D. Hager, *AFWL-TR-88-50*, Phillips Laboratory, NM (1988).

D. Pritchard, N. Smith, R. Driver and T. A. Brunner, *J. Chem. Phys.* **70**, 2115 (1979).

I. Procaccia and R. D. Levine, *J. Chem. Phys.* **64**, 808 (1976).

Qi, F. Hao, W. Chengdong, S. Guohe, and Z. Cunhao, *Proc. SPIE-Int. Soc. Opt. Eng.* **1810**, 501 (1992).

Katharine L. Reid and Anthony J. McCaffery, *J. Chem. Phys.* **96**, 5789 (1992).

M. Rubinson, B. Garetz and J. I. Steinfeld, *J. Chem. Phys.* **60**, 3082 (1974).

Timothy D. Russell, Benjamin M. DeKoven, Joseph A. Blazy, and Donald H. Levy, *J. Chem. Phys.* **72**, 3001 (1980).

R. N. Schwartz, Z. I. Slovky, and K. F. Herzfeld, *J. Chem. Phys.* **20**, 1591 (1952).

A. N. Schweid and J. I. Steinfeld, *J. Chem. Phys.* **58**, 844 (1973).

R. F. Shea, *Overview of the Singlet Oxygen-Iodine Laser System* **355**, Phillips Laboratory, NM (1984).

K. Shimizu, T. Sawano, T. Tokuda, S. Yoshida, and I. Tanaka, *J. Appl. Phys.* **69**, 79 (1991).

N. Smith and D. E. Pritchard, *J. Chem. Phys.* **74**, 3939 (1981).

J. I. Steinfeld and A. N. Schweid, *J. Chem. Phys.* **53**,3304 (1970).

J. I. Steinfeld, *J. Chem. Phys.* **46**, 4550 (1967).

Jeffrey I. Steinfeld and William Klemperer, *J. Chem. Phys.* **42**,3475 (1965).

J. I. Steinfeld, P. Ruttenberg, G. Millot, G. Fanjoux and B. Lavorel, *J. Phys. Chem.* **95**, 9638(1991).

Tetsuo Suzuki and Eizi Hirota, J. Chem. Phys. **88**, 6778 (1988).

Joel Tellinghuisen, Mark R. McKeever, and Abha Sur, *J. Mol. Spectrosc.* **82**, 225 (1980).

Joel Tellinghuisen, *J. Chem. Phys.* **76**, 4736 (1982).

Joel Tellinghuisen, *Can. J. Phys.* **62**, 1933 (1982).

J. Tellinghuisen, S. Fei, X. Zheng, and M.C. Heaven, *Chem. Phys. Lett.* **176**, 373 (1991).

Friedrich Temps, Scott Halle, Patrick H. Vaccaro, Robert W. Field, and James L. Kinsey, *J. Chem. Soc. Faraday Trans. II*, **84**, 1457 (1988).

J. Toennies, *Ann. Rev. Phys. Chem.* **27**, 225 (1976).

K. A. Truesdall and S. E. Lamberson, *Proc. SPIE-Int. Soc. Opt. Eng.* **1810**, 476 (1992).

W. Ubachs, I. Aben, J. B. Milan, G. J. Somsen, A. G. Stuiver, and W. Hogervorst, *Chem. Phys.* **174**, 285 (1993).

L. J. van de Burgt and M. C. Heaven, *Chem. Phys.* **103**, 407 (1986).

M. H. van Benthem and S. J. Davis, *J. Phys. Chem.*, **90**, 902, (1986).

Joseph T. Verdeyen, *Laser Electronics*, 2nd edition, (Prentice Hall, NJ, 1989).

P. J. Wolf and S. J. Davis, *J. Chem. Phys.* **87**, 3492 (1987).

Paul J.Wolf, Janice H. Glover, Leonard Hanko, Robert F. Shea and Steven J. Davis, *J. Chem. Phys.* **82**, 2321 (1985).

J. Wu, R. Huang, M. Gong, A. Saury, and E. Carrasquillo M., *J. Chem. Phys.* **99**, 6474 (1993).

K. Yamasaki and S. R. Leone, *J. Chem. Phys.* **90**, 964 (1989).

X. Yang and A. M. Wodtke, *J. Chem. Phys.* **92**, 116 (1990).

Xueming Yang and Alec M. Wodtke, *J. Chem. Phys.* **96**, 5123 (1992).

Xueming Yang, Eun H. Kim, and Alec M. Wodtke, *J. Chem. Phys.* **96**, 5111 (1992).

X. Yang, J. M. Price, J. A. Mack, C. G. Morgan, C. A. Rogaski, D. McGuire, E. H. Kim, and A. M. Wodtke, *J. Phys. Chem.* **97**, 3944 (1992).

X. Zheng, S. Fei, M. C. Heaven and J. Tellinghuisen, *J. Mol. Spectrosc.* **149**, 399 (1991).

Xiaonan Zheng, *Laser Spectroscopy of Metastable and Transient Species*, Dissertation, Emory University, Atlanta (1993).

APPENDIX A

SPECTROSCOPIC CONSTANTS

The Hamiltonian for a diatomic molecule with n electrons is

$$H = \sum_{N=1}^{2} \frac{-\hbar^2}{2m_N}\nabla_N^2 + \sum_{i=1}^{2} \frac{-\hbar^2}{2m_e}\nabla_i^2 + \frac{1}{4\pi\varepsilon_0} \sum_{i<j}^{n} \frac{e^2}{|r_i - r_j|} - \frac{1}{4\pi\varepsilon_0} \sum_{i=1}^{n}\sum_{N=1}^{2} \frac{Z_N e^2}{|r_i - R_N|} + \frac{1}{4\pi\varepsilon_0}\frac{Z_A Z_B e^2}{|R_A - R_B|} + H_{so}$$

which include the nuclear kinetic energy, the electronic kinetic energy, the electron-electron repulsions, the electron-nuclear attractions, the nuclear-nuclear repulsion, and the spin orbit coupling, respectively. The Born-Oppenheimer approximation allows us to separate the electronic and nuclear motion. Since the nuclei are much more massive than the electrons, the electrons adjust instantaneously to the motion of the nuclei. In this time reference, the nuclei are considered fixed at nuclear separation **R** while the electronic motion is solved. The electronic Schrodinger is written

$$(H_{el} + V_{NN})\psi_{el} = U\psi_{el}$$

$$H_{el} = \sum_{i=1}^{2} \frac{-\hbar^2}{2m_e}\nabla_i^2 + \frac{1}{4\pi\varepsilon_0} \sum_{i<j}^{n} \frac{e^2}{|r_i - r_j|} - \frac{1}{4\pi\varepsilon_0} \sum_{i=1}^{n}\sum_{N=1}^{2} \frac{Z_N e^2}{|r_i - R_N|}$$

$$V_{NN} \equiv \frac{1}{4\pi\varepsilon_0}\frac{Z_A Z_B e^2}{|R_A - R_B|}$$

After separating out the translational motion, the coordinate system of the kinetic energy operator ∇^2 is transformed from cartesian coordinates into spherical polar coordinates and the angular momentum operator L^2 as shown

$$-\frac{h^2}{2\mu}\left(\frac{2\partial\psi}{r\partial r}+\frac{\partial^2\psi}{\partial r^2}\right)+\frac{L}{2\mu r^2}\psi+V(r)\psi=E\psi$$

The resulting differential equation is separable into radial and angular parts, with the

angular portion assuming a product form of the spherical harmonics Y_{lm} for the

eigenfuction ψ

$$\psi(r,\theta,\phi)=Y_{lm}(\theta,\phi)R(r)$$

Applying the L^2 operator and dividing by $2\mu r^2$

$$\frac{L^2}{2\mu r^2}\psi=\frac{l(l+1)h^2}{2\mu r^2}Y_{lm}$$

Substituting the L^2 product into the Schrodinger Equation and dividing by the spherical

harmonic produces $\qquad -\frac{h^2}{2\mu}(\frac{2\partial R}{r\partial r}+\frac{\partial^2 R}{\partial r^2}-\frac{l(l+1)}{r^2}R)+V(r)R=ER$

This differential equation is only in terms of the electronic separation r.   A displacement

variable s is introduced into the radial Schrodinger equation.

$$S(s)=S(r-r_e)\equiv rR(r)$$

$$\frac{\partial^2 S}{\partial s^2}=r(\frac{2\partial R}{r\partial r}+\frac{\partial^2 R}{\partial r^2})$$

After substituting the displacement variable s and multiplying by r, the radial Schrodinger

equation becomes

$$-\frac{h^2}{2\mu}\left[\frac{\partial^2 S(s)}{\partial s^2}-\frac{l(l+1)}{(s+r_e)^2}S(s)\right]+V(s+r_e)S(s)=ES(s)$$

A power series expansion of the displacement variable s and truncating the expansion

after the first term

$$\frac{1}{(s-r_e)^2} = \frac{1}{r_e^2} - \frac{2s}{r_e^3} + \frac{6s^2}{r_e^4} - \frac{24s^3}{r_e^5} + \ldots.$$

and the radial Schrodinger equation approximated in terms of a vibrating-rotating

diatomic molecule (this approximation neglects the coupling of the vibrational and

rotational motions) is

$$-\frac{\hbar^2}{2\mu}\frac{\partial^2 S(s)}{\partial s^2} + V(s+r_e)S(s) = E'S(s)$$

$$E' \equiv E - \frac{\hbar^2 l(l+1)}{2\mu r_e^2}$$

Substituting the solution for the energy of the harmonic oscillator problem, the possible

eigenstate energies for the diatomic may be approximated

$$E_{nJ} = (n+\tfrac{1}{2})\hbar\omega + \frac{\hbar 2J(J+1)}{2\mu r_e^2}$$

The quantum mechanical analysis of the energy depends on the vibrational

quantum number v and the rotational quantum number J. The J dependence is

expressed as $J(J+1)$, and the v dependence as $(v+\tfrac{1}{2})$. The energy of a vJ level may be

expressed as

$$
\begin{aligned}
E_{vJ} = Y_{00} &+ Y_{10}(v+\tfrac{1}{2}) + Y_{20}(v+\tfrac{1}{2})^2 + Y_{30}(v+\tfrac{1}{2})^3 \\
&+ Y_{01} J(J+1) + Y_{11}(v+\tfrac{1}{2})J(J+1) + Y_{21} J(J+1)(v+\tfrac{1}{2})^2 \\
&+ Y_{02} J^2(J+1)^2 + Y_{12}(v+\tfrac{1}{2})J^2(J+1)^2 \\
&+ Y_{03} J^3(J+1)^3
\end{aligned}
$$

and written in the general form known as the Dunham expansion

$$E_{vJ} = \sum_{k,n} Y_{nk}(\upsilon + \tfrac{1}{2})^n [J(J+1)]^k$$

where

Y_{00} - electronic term energy; T_e

Y_{10} - harmonic (equilibrium) vibrational frequency constant; ω_e

Y_{20} - equilibrium anharmonicity constant; $-\omega_e\chi_e$

Y_{30} - second equilibrium anharmonicity constant; $\omega_e y_e$

Y_{01} - equilibrium rotational constant; B_e

Y_{02} - equilibrium centrifugal distortion constant; $-D_e$

Y_{03} - second equilibrium centrifugal distortion constant; H_e

Y_{11} - vibration-rotational coupling constant ; $-\alpha_e$

Y_{21} - γ_e

Y_{12} - β_e

Y_{nk}'s are called Dunham coefficients. If B_e^2/w_e^2 is small, the Y's can be related to the ordinary band spectrum constants. For most molecules, the ratio B_e^2/w_e^2 is of the order 10^{-6}. For iodine, the ratio of B_e^2/w_e^2 for the D state is $4.755 10^{-8}$. Now substituting the Dunham coefficients with the common spectroscopic constants,

$$E_{vJ} = T_e + \omega_e(v+\tfrac{1}{2}) - \omega_e\chi_e(v+\tfrac{1}{2})^2 + \omega_e y_e(v+\tfrac{1}{2})^3$$

$$+ B_e J(J+1) - \alpha_e J(J+1)(v+\tfrac{1}{2}) + \gamma_e J(J+1)(v+\tfrac{1}{2})^2$$

$$- D_e J^2(J+1)^2 + \beta_e J^2(J+1)^2(v+\tfrac{1}{2})$$

$$+ H_e J^3(J+1)^3$$

The complete description of the energy levels in a vibrating-rotating diatomic molecule require numerous fitting parameters. In order to reduce the number of parameters, molecular constants e.g. G_v, B_v, D_v, H_v ... are often reported in the literature. The vibrational energy of a rotationless molecule is defined as

$$G_v = \omega_e(v+\tfrac{1}{2}) - \omega_e\chi_e (v+\tfrac{1}{2})^2 + \omega_e y_e (v+\tfrac{1}{2})^3$$

Both the rotational and centrifugal distortion constants are dependent upon the vibrational quantum number. The rotational molecular constant, B_v is defined as

$$B_v = B_e - \alpha_e (v+\tfrac{1}{2}) + \gamma_e (v+\tfrac{1}{2})^2$$

During rotation of the molecule, the chemical bonds stretch as centrifugal force pushes the nuclei farther apart. As the vibrational quantum number v increases, both B_v and D_v decrease. The centrifugal distortion constant D_v, is given by

$$D_v = D_e + \beta_e (v+\tfrac{1}{2})$$

Including the second order anharmonicity constant H_v, the rotational energy is

$$F_J = B_v J(J+1) - D_v J^2(J+1)^2 + H_v J^3(J+1)^3$$

The energy levels of the molecules are given in terms of the electronic, vibrational and rotational quantum numbers. With the energy partitioned according to its electronic, vibrational, and rotational energy states, the total energy can be expressed in the consise form

$$E_{vJ} = T_e + G_v + F_J$$

Polynomial representations are extremely useful as they express the molecular constants in a concise form. From a pragmatic view, computational code for calculations of the spectroscopic energy is simplified since only a fraction of the terms are required. For example, for the I_2 B-X system, 62 molecular constants are represented by a 9 term polynomial expansion. The references for the spectroscopic constants of the respective electronic state of iodine are provided below.

REFERENCES

I. N. Levine, *Molecular Spectroscopy*, Wiley, New York (1975).

C. H. Townes and A. L. Schwalow, *Microwave Spectroscopy*, McGraw-Hill, New York (1955).

X State Constants

J. Tellinghuisen, R. McKeever, and A. Sur, *J. Mole. Spectrosc.* **82**, 225 (1980).

R. Bacis, D. Cerny, and F. Martin, *J. Mol. Spectrosc.* **118**, 434 (1986).

B State Constants

P. Luc, J. Mol. Spectrosc. **80**, 41(1980).

J. Hutson, S. Gerstenkorn, P. Luc, and J. Sinzelle, *J. Mol. Spectrosc.* **96**, 226 (1982).

D State Constants

T. Ishiwata and I. Tanaka, *Laser Chem.* 7, 79 (1987).

A. J. Hoy and R. H. Lipson, *Chem. Phys.* **140**, 187 (1990).

M. Bartels, R. J. Donovan, A. J. Holmes, P. R. R. Langridge-Smith, M. A. MacDonald, and T. Ridley, *J. Chem. Phys.* **91**, 7355 (1989).

M. L. Nowlin and M. C. Heaven, *Chem. Phys. Lett. (To Be Submitted)*.

Table A.1: Resonant Transitions of the 1064.55 nm
Nd:YAG Fundamental Used for the
SEP-LIF *Dump* Laser of the I_2 *B-X* system

			cm^{-1}				cm^{-1}
pump	v"=0	J=107	16,343.934	*pump*	v"=0	J=76	16,840.159
pump	v"=1	J=107	16,131.961	*pump*	v"=1	J=76	16,627.528
pump	v"=2	J=107	15,921.224	*pump*	v"=2	J=76	16,416.132
dump	v'=6	J=108	9,393.513	*dump*	v'=10	J=77	9,393.782
probe	v"=37	J=109		*probe*	v"=40	J=78	
pump	v"=0	J=47	16,542.000	*pump*	v"=0	J=81	16,814.970
pump	v"=1	J=47	16,328.955	*pump*	v"=1	J=81	16,602.430
pump	v"=2	J=47	16,117.144	*pump*	v"=2	J=81	16,391.125
dump	v'=7	J=48	9,393.614	*dump*	v'=10	J=82	9,393.011
probe	v"=38	J=49		*probe*	v"=40	J=83	
pump	v"=0	J=48	16,541.142	*pump*	v"=0	J=88	17,134.887
pump	v"=1	J=48	16,328.108	*pump*	v"=1	J=88	16,922.484
pump	v"=2	J=48	16,116.308	*pump*	v"=2	J=88	16,711.316
dump	v'=7	J=49	9,393.116	*dump*	v'=10	J=89	9,393.316
probe	v"=38	J=50		*probe*	v"=42	J=90	

Sample Calculation of Vibrational Energies (G_v) For I_2 $D(0^+_u)$
Using Dunham Expansion Coefficients of M. L. Nowlin and
M. C. Heaven

ORIGIN $\equiv 0$ Y00 $:= 41026.16614$

Y10 $:= 95.11746327$ Y50 $:= -1.408244378 \cdot 10^{-8}$

Y20 $:= -0.111495227$ Y60 $:= 2.6873688 \cdot 10^{-11}$

Y30 $:= -5.792874546 \cdot 10^{-4}$ Y70 $:= -2.3114805 \cdot 10^{-14}$

Y40 $:= 4.205281828 \cdot 10^{-6}$

$$GV1(n) := Y10 \cdot (n+0.5) + Y20 \cdot (n+0.5)^2 + Y30 \cdot (n+0.5)^3 + Y40 \cdot (n+0.5)^4$$
$$GV2(n) := Y50 \cdot (n+0.5)^5 + Y60 \cdot (n+0.5)^6 + Y70 \cdot (n+0.5)^7$$
$$GV(n) := GV1(n) + GV2(n)$$
$$TV(n) := GV(n) + Y00$$

b $:= 0..20$ c $:= 21..41$ d $:= 42..62$

b	GV(b)	TV(b)	c	GV(c)	TV(c)	d	GV(d)	TV(d)
0	47.5308	41073.6969	21	1988.5661	43014.7322	42	3808.5544	44834.7205
1	142.4234	41168.5895	22	2078.1	43104.2661	43	3891.9893	44918.1554
2	237.0879	41263.2541	23	2167.3553	43193.5214	44	3975.1251	45001.2912
3	331.5211	41357.6872	24	2256.3303	43282.4964	45	4057.9613	45084.1274
4	425.7197	41451.8859	25	2345.0236	43371.1898	46	4140.4976	45166.6637
5	519.6807	41545.8469	26	2433.4338	43459.6	47	4222.7336	45248.8997
6	613.4011	41639.5672	27	2521.5595	43547.7257	48	4304.6691	45330.8352
7	706.878	41733.0441	28	2609.3994	43635.5655	49	4386.3038	45412.4699
8	800.1085	41826.2746	29	2696.9522	43723.1183	50	4467.6375	45493.8036
9	893.09	41919.2561	30	2784.2168	43810.3829	51	4548.67	45574.8361
10	985.8198	42011.9859	31	2871.192	43897.3581	52	4629.4012	45655.5674
11	1078.2953	42104.4615	32	2957.8767	43984.0429	53	4709.8311	45735.9972
12	1170.5142	42196.6804	33	3044.27	44070.4362	54	4789.9595	45816.1256
13	1262.474	42288.6401	34	3130.3709	44156.5371	55	4869.7864	45895.9526
14	1354.1724	42380.3386	35	3216.1785	44242.3447	56	4949.3119	45975.478
15	1445.6073	42471.7734	36	3301.692	44327.8581	57	5028.5359	46054.7021
16	1536.7763	42562.9425	37	3386.9105	44413.0766	58	5107.4586	46133.6248
17	1627.6776	42653.8438	38	3471.8333	44497.9994	59	5186.0801	46212.2463
18	1718.3091	42744.4753	39	3556.4597	44582.6258	60	5264.4005	46290.5667
19	1808.6689	42834.8351	40	3640.7891	44666.9552	61	5342.42	46368.5861
20	1898.7552	42924.9213	41	3724.8208	44750.987	62	5420.1388	46446.3049

Sample Calculation for SEP Experiment for $v''=38$

$$\text{Energy} = G_v + B_v*J*(J+1) - D_v*J^2*(J+1)^2 + H_v*J^3*(J+1)^3$$

$$T_{v,j} = \Sigma Y_{nk}(v+1/2)^n \, J^k(J+1)^k$$

Calculate Energy for Pump Transitions from I_2 (X; $v''=2$, $J=47$)

$\text{Pump} := 425.375 + 0.0370811 \cdot 47 \cdot 48 - 4.62 \cdot 10^{-9} \cdot 47^2 \cdot 48^2 - 6.4 \cdot 10^{-16} \cdot 47^3 \cdot 48^3$

$\text{Pump} = 509.006 \quad cm^{-1}$

Calculate Energy for Pump/Dump Transitions for I_2 (B; $v'=7$, $J=48$)

$\text{Dump} := 16560.7847 + 0.027808113 \cdot 48 \cdot 49 - 7.16672 \cdot 10^{-9} \cdot 48^2 \cdot 49^2 - 4.142 \cdot 10^{-15} \cdot 48^3 \cdot 49^3$

$\text{Dump} = 16626.15 \quad cm^{-1}$

Calculate Energy for Dump Transitions to I_2 (X; $v''=38$, $J=49$)

$\text{Probe} := 7153.625 + 0.032225 \cdot 49 \cdot 50 - 6.74 \cdot 10^{-9} \cdot 49^2 \cdot 50^2 - 3.51 \cdot 10^{-15} \cdot 49^3 \cdot 50^3$

$\text{Probe} = 7232.536 \quad cm^{-1}$

$\text{Dumptransition} := \text{Dump} - \text{Probe}$

$\dfrac{1 \cdot 10^7}{\text{Dumptransition}} = 1064.553 \quad nm$

$\text{Dumptransition} = 9393.614 \quad cm^{-1}$

Calculate Energy for Probe Transitions from I_2 (X; $v''=38$, $J=49$) to I_2 (D; $v'=10$, $J=48,50$)

$\text{org} := 42011.891 - 7260.740$ 　　　　$J := 49$ 　　　　$\text{Bpp} := 0.0322252$

$\text{Bp} := 0.020246$

For R: $m := J + 1$

$R := \text{org} + ((\text{Bp} + \text{Bpp}) \cdot m) + (\text{Bp} - \text{Bpp}) \cdot (m)^2$ 　　$R = 34723.827 \quad cm^{-1}$

For P: $m := -J$

$P := \text{org} + ((\text{Bp} + \text{Bpp}) \cdot m) + (\text{Bp} - \text{Bpp}) \cdot (m)^2$ 　　$P = 34719.818 \quad cm^{-1}$

Optical-Optical Double Resonance for I_2 (f; $v'=44$, $J=49$) *Resonant with* I_2 (B; $v''=7$, $J=48$)

$Y00 := 47025.917$ 　　$Y02 := -3.32 \cdot 10^{-9}$ 　　　$Y11 := -5.728 \cdot 10^{-5}$

$Y10 := 104.1804$ 　　$Y01 := 0.0208042$

$Y20 := -0.21324$ 　　$Y30 := 0.000246$ 　　　$Y21 := 5.8 \cdot 10^{-8}$

$\text{OODR1} := Y00 + Y10 \cdot 44.5 + Y20 \cdot 44.5^2 + Y30 \cdot 44.5^3 + Y01 \cdot 49 \cdot 50 + Y02 \cdot 49^2 \cdot 50^2$

$\text{OODR2} := Y11 \cdot 44.5 \cdot 49 \cdot 50 + Y21 \cdot 44.5^2 \cdot 49 \cdot 50$

$\text{OODR} := \text{OODR1} + \text{OODR2}$

$\text{OODR} = 51306.341 \quad cm^{-1}$ 　　　　$\text{OODR} - \text{Dump} = 34680.191 \; cm^{-1}$

Calculation of Molecular Constants for I_2 $D(0^+_u)$ With Error Analysis

This section generates Tanaka's data   [Mathcad 5.0]

$i := 0..5$ $c_0 := 41028.584$

$c_1 := 94.9928$ $c_2 := -0.10919$ $c_3 := -5.805 \cdot 10^{-4}$ $c_4 := 3.686 \cdot 10^{-6}$ $c_5 := -7.61 \cdot 10^{-9}$

$$E(v) := \sum_i c_i \left[(v + 0.5)^i \right]$$

$p := 0..7$

$E(119) = 50396.56640423$

$x_p := p + 4$

This section reads the SEP-LIF data points

$pp := 8..15$

$k := 16..66$ $x_k := k + 58$

$x_{pp} := pp + 22$

$y_k := E(x_k)$

$p2 := 67..232$

$y_0 := 41451.971$ $y_1 := 41545.835$

$x_{p2} := p2 + 58$

$y_2 := 41639.559$ $y_3 := 41733.007$ $y_4 := 41826.277$

$y_5 := 41919.192$ $y_6 := 42011.985$ $y_7 := 42104.469$

$y_8 := 43810.369$ $y_9 := 43897.365$ $y_{10} := 43984.051$ $y_{11} := 44070.471$

$y_{12} := 44156.549$ $y_{13} := 44242.345$ $y_{14} := 44327.845$ $y_{15} := 44413.091$

Bartels, Donovan, Holmes, Langridge-Smith, MacDonald, and Ridley; J Chem Phys 7355 (1989)

y_i where $i = v-58$ e.g. $y_{67} = v(125)$ VDP0   107.115   VDP1   320.419

$y_{67} := 50653.7 + VDP0$ $y_{68} := 50713.4 + VDP0$ $y_{69} := 50773.3 + VDP0$ $y_{70} := 50832.5 + VDP0$

$y_{71} := 50891.8 + VDP0$ $y_{72} := 50950.6 + VDP0$ $y_{73} := 51009.4 + VDP0$ $y_{74} := 51067.6 + VDP0$

$y_{75} := 51125.8 + VDP0$ $y_{76} := 51183.3 + VDP0$ $y_{77} := 51240.6 + VDP0$ $y_{78} := 51297.9 + VDP0$

$y_{79} := 51355.4 + VDP0$ $y_{80} := 51411.9 + VDP0$ $y_{81} := 51468.8 + VDP0$ $y_{82} := 51525.0 + VDP0$

$y_{83} := 51367.8 + VDP1$ $y_{84} := 51423.7 + VDP1$ $y_{85} := 51480.3 + VDP1$ $y_{86} := 51748.2 + VDP0$

$y_{87} := 51590.2 + VDP1$ $y_{88} := 51858.0 + VDP0$ $y_{89} := 51913.1 + VDP0$ $y_{90} := 51967.8 + VDP0$

$y_{91} := 52021.8 + VDP0$ $y_{92} := 52076.1 + VDP0$ $y_{93} := 52129.9 + VDP0$ $y_{94} := 52183.4 + VDP0$

$y_{95} := 52236.5 + VDP0$ $y_{96} := 52289.3 + VDP0$ $y_{97} := 52343.2 + VDP0$ $y_{98} := 52395.7 + VDP0$

$y_{99} := 52448.2 + VDP0$ $y_{100} := 52500.5 + VDP0$ $y_{101} := 52552.5 + VDP0$ $y_{102} := 52603.9 + VDP0$

$y_{103} := 52656.2 + VDP0$ $y_{104} := 52707.9 + VDP0$ $y_{105} := 52758.5 + VDP0$ $y_{106} := 52810.0 + VDP0$

$y_{107} := 52860.8 + VDP0$ $y_{108} := 52910.8 + VDP0$ $y_{109} := 52961.6 + VDP0$ $y_{110} := 53011.9 + VDP0$

$y_{111} := 53061.6 + VDP0$ $y_{112} := 53112.0 + VDP0$ $y_{113} := 53161.5 + VDP0$ $y_{114} := 53210.7 + VDP0$

$y_{115} := 53259.5 + VDP0$ $y_{116} := 53308.8 + VDP0$ $y_{117} := 53144.1 + VDP1$ $y_{118} := 53193.0 + VDP1$

$y_{119} := 53241.6 + VDP1$ $y_{120} := 53289.3 + VDP1$ $y_{121} := 53550.8 + VDP0$ $y_{122} := 53598.7 + VDP0$

$y_{123} := 53646.6 + VDP0$ $y_{124} := 53693.8 + VDP0$ $y_{125} := 53741.2 + VDP0$ $y_{126} := 53788.0 + VDP0$

$y_{127} := 53835.5 + VDP0$ $y_{128} := 53881.7 + VDP0$ $y_{129} := 53928.5 + VDP0$ $y_{130} := 53974.8 + VDP0$

$y_{131} := 54020.8 + VDP0$ $y_{132} := 54067.2 + VDP0$ $y_{133} := 54112.9 + VDP0$ $y_{134} := 54158.3 + VDP0$

$y_{135} := 54203.5 + VDP0$ $y_{136} := 54249.1 + VDP0$ $y_{137} := 54294.1 + VDP0$ $y_{138} := 54339.1 + VDP0$

$y_{139} := 54383.7 + VDP0$ $y_{140} := 54428.7 + VDP0$ $y_{141} := 54473.1 + VDP0$ $y_{142} := 54517.2 + VDP0$

$y_{143} := 54561.2 + VDP0$

Hoy and Lipson, Chemical Physics 140, 187 (1990)

y_{144}	54604.92	y_{145}	54648.57	y_{146}	54691.93	y_{147}	54735.17		
$y_{148} := 54778.25$		$y_{149} := 54821.33$	$y_{150} := 54864.26$		$y_{151} := 54906.92$	$y_{152} := 54949.28$			
$y_{153} := 54991.42$		$y_{154} := 55033.62$	$y_{155} := 55075.79$		$y_{156} := 55117.57$	$y_{157} := 55159.43$			
$y_{158} := 55200.85$		$y_{159} := 55242.10$	$y_{160} := 55283.12$		$y_{161} := 55324.11$	$y_{162} := 55365.06$			
$y_{163} := 55405.85$		$y_{164} := 55446.25$	$y_{165} := 55486.69$		$y_{166} := 55526.98$	$y_{167} := 55567.09$			
$y_{168} := 55607.17$		$y_{169} := 55646.87$	$y_{170} := 55686.43$		$y_{171} := 55725.97$	$y_{172} := 55764.80$			

$y_{173} := 55804.19$ $y_{174} := 55843.21$ $y_{175} := 55882.37$ $y_{176} := 55921.10$ $y_{177} := 55959.98$

$y_{178} := 55997.98$ $y_{179} := 56036.31$ $y_{180} := 56074.53$ $y_{181} := 56112.62$ $y_{182} := 56150.31$

$y_{183} := 56188.08$ $y_{184} := 56225.63$ $y_{185} := 56263.17$ $y_{186} := 56300.36$ $y_{187} := 56337.61$

$y_{188} := 56374.61$ $y_{189} := 56411.59$ $y_{190} := 56448.31$ $y_{191} := 56484.95$ $y_{192} := 56521.36$

$y_{193} := 56557.73$ $y_{194} := 56593.87$ $y_{195} := 56629.89$ $y_{196} := 56665.80$ $y_{197} := 56701.57$

$y_{198} := 56737.21$ $y_{199} := 56772.68$ $y_{200} := 56807.94$ $y_{201} := 56843.23$ $y_{202} := 56878.44$

$y_{203} := 56913.47$ $y_{204} := 56948.28$ $y_{205} := 56983.13$ $y_{206} := 57017.75$ $y_{207} := 57052.14$

$y_{208} := 57086.49$ $y_{209} := 57120.64$ $y_{210} := 57154.84$ $y_{211} := 57188.79$ $y_{212} := 57222.56$

$y_{213} := 57256.16$ $y_{214} := 57289.93$ $y_{215} := 57323.29$ $y_{216} := 57356.69$ $y_{217} := 57389.61$

$y_{218} := 57422.6$ $y_{219} := 57455.48$ $y_{220} := 57488.37$ $y_{221} := 57520.84$ $y_{222} := 57553.38$

$y_{223} := 57585.67$ $y_{224} := 57617.96$ $y_{225} := 57650.02$ $y_{226} := 57682.09$ $y_{227} := 57713.73$

y_{228} 57745.08 y_{229} 57776.96 y_{230} 57808.06 y_{231} 57839.16 y_{232} 57870.01

$r \quad 0 .. 15$

$sd_r := 0.01$

Loading W=s x s weight matrix

$r := 16 .. 66$

$sd_r := 0.03$

where v=4 to 11 and 30 to 37 sd =0.01 SEP-LIF data

$r := 67 .. 143$

$sd_r := 0.5$

v=74 to 124   sd=0.03   Ishiwata and Tanaka

v=124 to 201 sd =0.5   Bartels, Donovan,Holmes,Langridge-Smith,
                        MacDonald, and Ridley

$r := 144 .. 232$

$sd_r := 0.5$

v=202 to 290   sd=0.5   Hoy and Lipson

$hh := 144 .. 232$

$y_{hh} := y_{hh} + 107.115$

$y_{176} = 56028.215$

$$s := 0..232 \quad m := 7 \quad t := 0..m \qquad np := rows(y)$$

$$A_{s,t} := \left(x_s + 0.5\right)^t$$

Molecular constants for $I_2\,D$

$$W_{s,s} := \frac{1}{\left[\left(sd_s\right)^2\right]}$$

$$B := \left(A^T \cdot W \cdot A\right)^{-1} \cdot A^T \cdot W \cdot y$$

$$B = \begin{bmatrix} 4.102616614 \cdot 10^4 \\ 95.11746327 \\ -0.111495227 \\ -5.792874546 \cdot 10^{-4} \\ 4.205281828 \cdot 10^{-6} \\ -1.408244378 \cdot 10^{-8} \\ 2.68736882 \cdot 10^{-11} \\ -2.3114805 \cdot 10^{-14} \end{bmatrix}$$

$$B_3 \cdot 10^4 = -5.7928745$$

$$B_4 \cdot 10^6 = 4.2052818$$

Residuals:

$$r \quad y \quad A \cdot B$$

Variance

$$Var \quad \frac{r^T \cdot r}{np \quad m}$$

$$Var = 0.1307648$$

Standard deviation

$$Sdev := \sqrt{Var_0}$$

$$Sdev = 0.3616142$$

Variance – Covariance

$$VCM := Var_0 \cdot \left(A^T \cdot A\right)^{-1}$$

Residuals   plot

$i := 0 .. np - 1$ $ii := 0 .. 10$

$i := 0 .. 232$
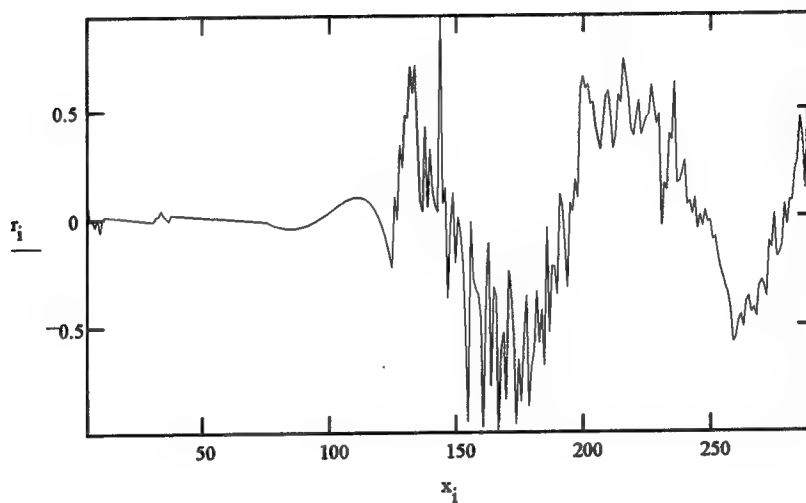
Standard Deviation for fitted parameters:

$I \quad 0 .. m$

$ER_I \quad VCM_{I,I}$

$$ER = \begin{bmatrix} 0.291151156 \\ 0.037671533 \\ 0.001433341 \\ 2.424332385 \cdot 10^{-5} \\ 2.111479032 \cdot 10^{-7} \\ 9.860194139 \cdot 10^{-10} \\ 2.345990745 \cdot 10^{-12} \\ 2.232859147 \cdot 10^{-15} \end{bmatrix}$$

Correlation Matrix

$k := 0 .. m$ $j := 0 .. m$

$$c_{k,j} := \frac{VCM_{k,j}}{\sqrt{VCM_{k,k} \cdot VCM_{j,j}}}$$

Error band calculation

$v := 0 .. 290$ $j := 0 .. m$

$$D_{j,v} := (v + 0.5)^j$$

$p := 0 .. 290$

$a := 0 .. m \qquad b := 0 .. m$

$$EB_p := \sum_a \sum_b D_{(b,p)} \cdot VCM_{(b,a)} \cdot D_{(a,p)}$$

$$Eu_p := \sqrt{EB_p} \qquad El_p := -Eu_p$$

PRNPRECISION := 5
PRNCOLWIDTH := 12

WRITEPRN(DXError) := Eu

APPENDPRN(DXError) := El $\qquad m = 7$
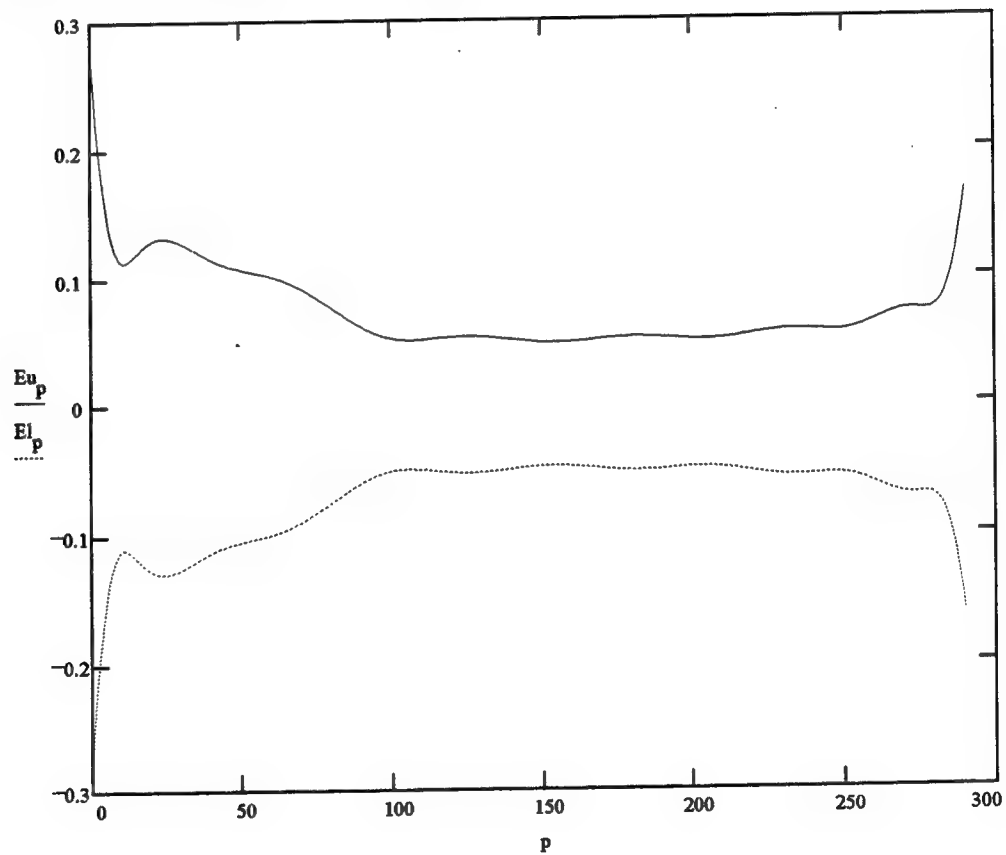
Calculation of Potential Energy Diagram for I₂ X, B and D states using Morse Potential

I_2: X state B state D state

we := 214.5186

bwe := 125.670   dwe := 95.124

De := 12244

bDe := 19881.048   dDe := 63026.128

bTe := 15769.0485   dTe := 41026.128

re := 2.67

bre := 3.016   dre := 3.38

M := 126.904

hbar := $1.0545887 \cdot 10^{-34}$

c := $2.99792458 \cdot 10^{10}$

$redmass := \left(\dfrac{M \cdot M}{M + M} \right) \cdot 1.6605 \cdot 10^{-27}$

$$ax := \frac{we}{\left(\dfrac{hbar \cdot De}{\pi \cdot c \cdot redmass} \right)^{0.5}} \cdot 1 \cdot 10^{-10} \qquad ab := \frac{bwe}{\left(\dfrac{hbar \cdot bDe}{\pi \cdot c \cdot redmass} \right)^{0.5}} \cdot 1 \cdot 10^{-10} \qquad ad := \frac{dwe}{\left(\dfrac{hbar \cdot dDe}{\pi \cdot c \cdot redmass} \right)^{0.5}} \cdot 1 \cdot 10^{-10}$$

ax = 1.881   i := 1 .. 800

$$Ux_i := De \cdot \left[1 - e^{-ax \cdot (r_i - re)} \right]^2$$

ab = 0.865 $r_i := 2.0 + (i \cdot 0.005)$

ad = 0.368

$$Ub_i \quad bDe \cdot \ 1 \quad e^{\ ab \cdot \ r_i \quad bre \quad 2} \quad bTe \quad Ud_i \quad dDe \cdot \ 1 \quad e^{\ ad \cdot \ r_i \quad dre \quad 2} \quad dTe$$

$\dfrac{Ux_i}{}$

Ub_i

Ud_i
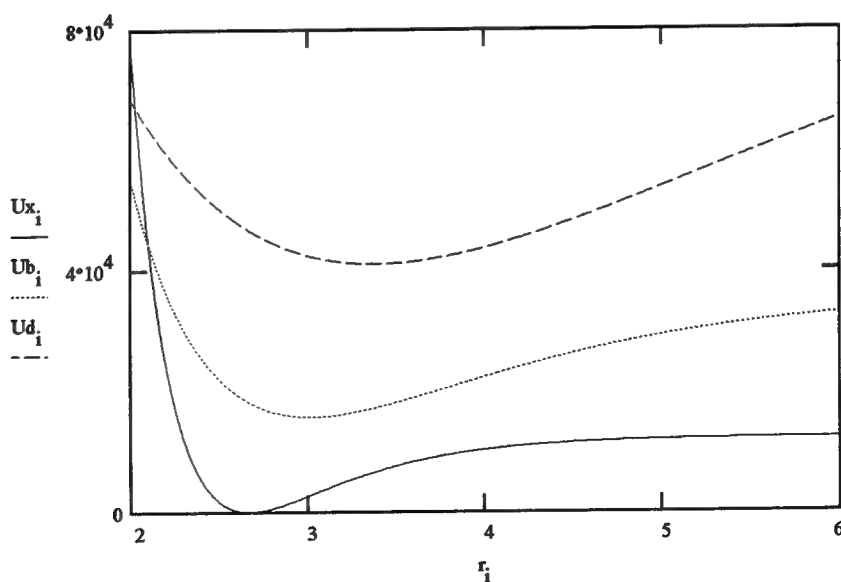
APPENDIX B

LASERS

In commercial laser designs, the source of excitation energy is usually electrical or optical. Both excitation sources pumped the laser radiation sources used in the SEP-LIF studies: excimer (electrical) and Nd:YAG (optical). An overview of both radiation sources, dye lasers, dye structures and optical materials is provided.

The behavior of the rare gas atom can be modified by ionization, or excitation to a higher electronic state, where there is an attractive force with another atom. The two atoms are bound together creating an *excited-state dimer*, or *excimer*. The noble gases upon excitation, forms a bound state with a halide. Since the energy required for the excitation of the noble gas is high, the photons obtained by radiation from the excimer to the ground state are some of the shortest wavelengths (e.g. ArF λ=193 nm) available in commercial lasers. Laser wavelengths become shorter for lighter rare gases which high higher ionization potentials, and heavier halogens, which have lower electron affinities. A potential energy diagram of the XeCl is shown in Figure B.1. The repulsive ground state makes for an ideal two-level laser. The radiative state lifetime (τ=11 ns) of the ionically bound excimer state at 2.9 Å is short by normal electronic transition standards but orders of magnitude longer than the ground state.

In a similar manner, the aurora borealis is a result of rare-gas oxides (ArO*, KrO*, XeO*) in the northern polar sky (southern hemisphere is the aurora australis).
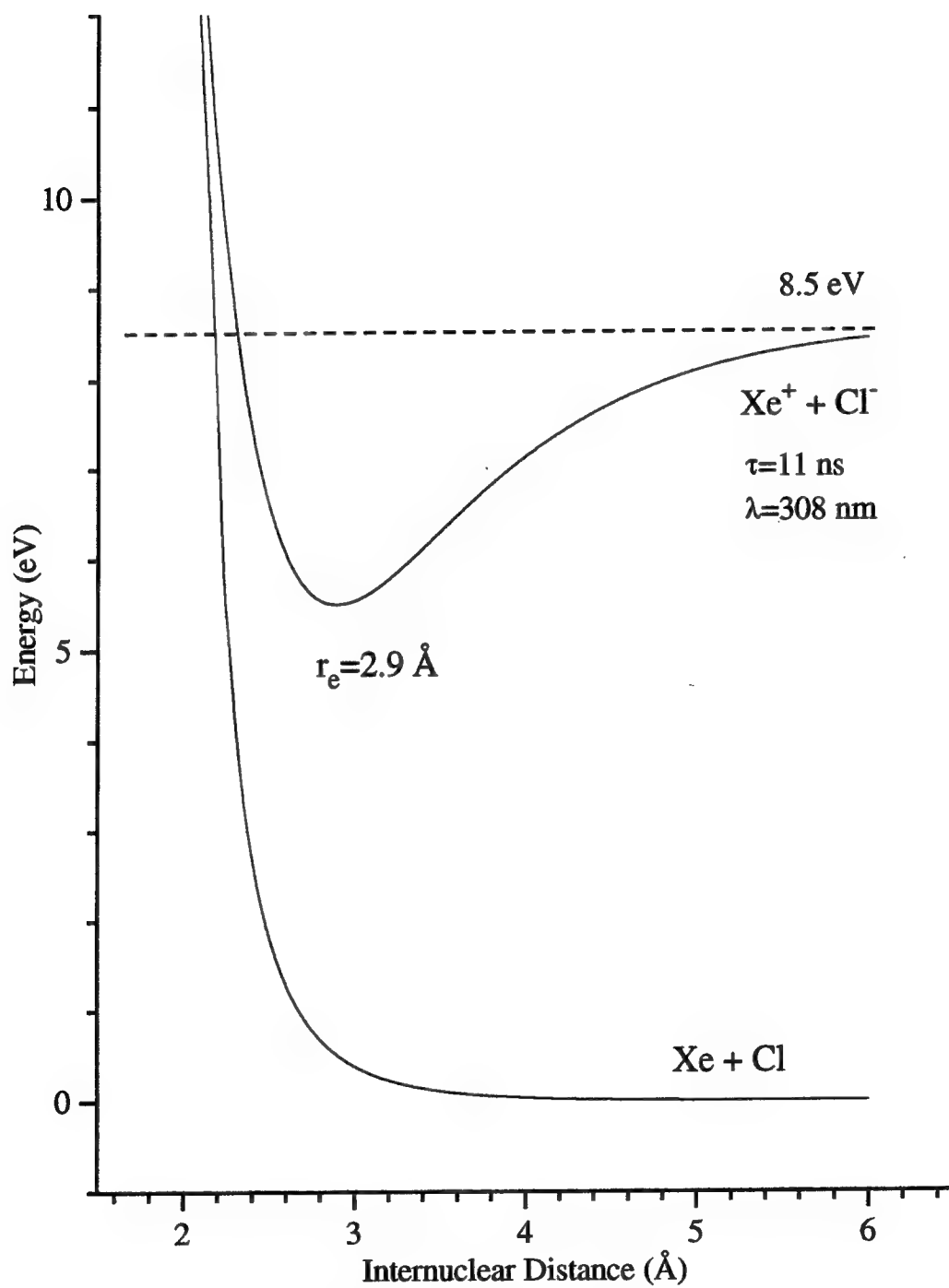
Figure B.1: Potential Energy Diagram for XeCl

The atomic transitions for the neutral oxygen atoms are the $^1S \rightarrow {}^1D$ and $^1D \rightarrow {}^3P$. The rare-gas oxides have lased in the vicinity of 558 nm where the lasing transition for all these systems occur between two excited states of atomic oxygen. Excimer lasers operating off these transitions are known as *aurora* lasers.

Excimer lasers electrically excite gaseous media like the noble gases, whereas optical pumping is successful for a variety of solid state media and organic dyes. The properties of neodymium-doped yttrium aluminum garnet (Nd:YAG) are the most understood of all solid state laser media. Triply ionized neodymium (Nd^{+3}) is optically pumped by krypton flashlamps whose output matches absorption bands in the red and near IR. The energy level diagram for neodymium in yttrium aluminum garnet (Nd:YAG) is shown in Figure B.2. Unlike the excimer laser, the excited level of the Nd^{+3} has a long lifetime (τ=255 μs), and a large population of the excited state can form. In order to prevent laser oscillation during inversion build-up, a Q-switch is employed.

The components of the Q-switch are a polarizer, a quarter-wave polarization rotator, and a Pockels cell. A Q-switch is an electro-optical switch which is opened and closed by application of a voltage. Applying voltage to the Pockels cell changes its polarization retardation characteristics. With no voltage applied, the Pockels cell has no effect on the polarization of radiation. The polarizer vertically polarizes light entering the Q-switch and the quarter-wave polarization rotator converts the radiation to circularly polarized. The cavity mirror reflects the circularly polarized radiation back through the quarter-wave plate converting the radiation to horizontally polarized. Since
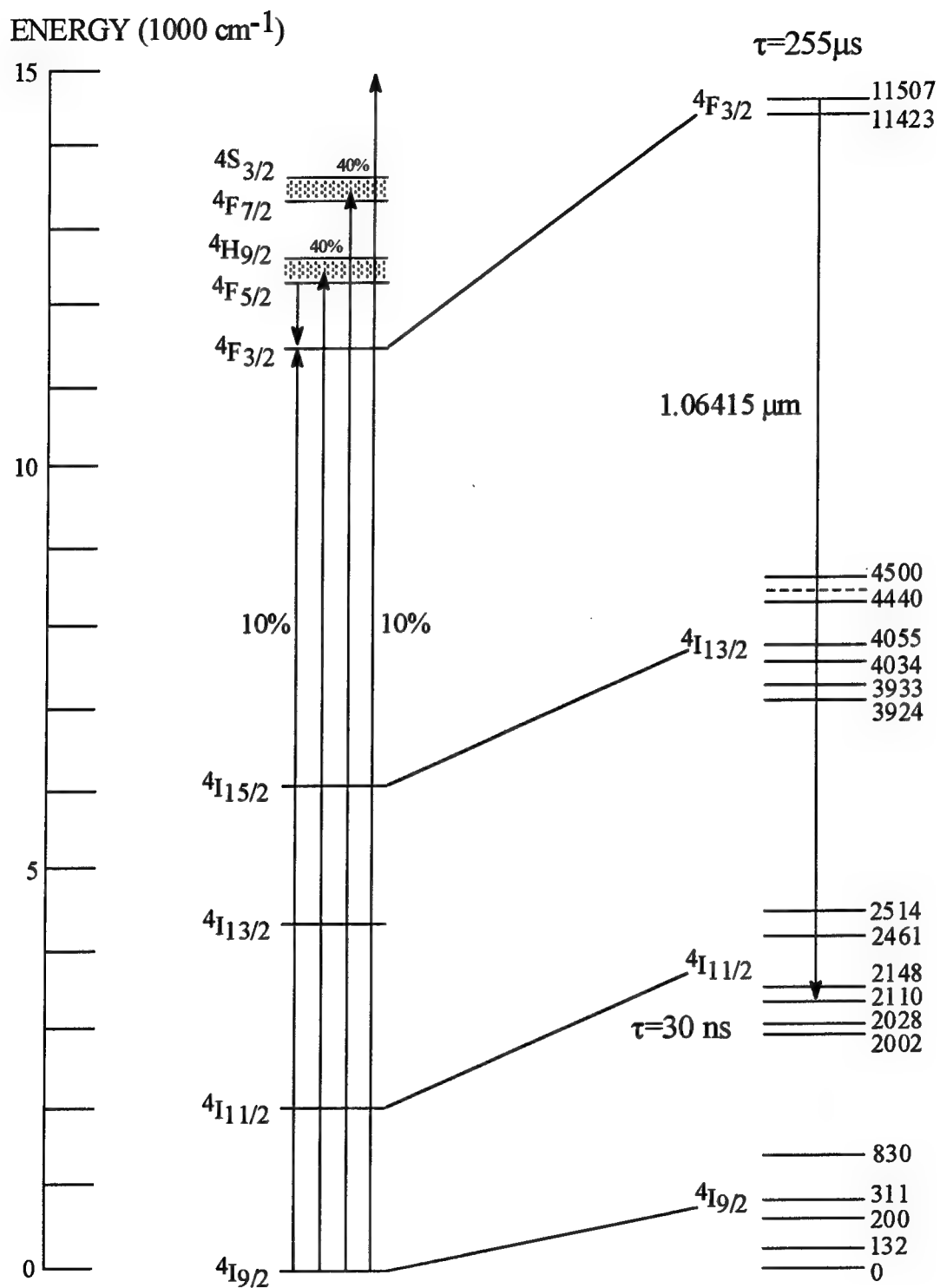
Figure B.2: Energy-Level Diagram for Neodymium in Yttrium Aluminium Garnet

the polarizer only transmit vertically polarized light, oscillation ceases. With voltage applied to the Q-switch, the Pockels cell retards the polarization of the quarter-wave plate. The light reflecting from the cavity mirror remains vertically polarized and the laser oscillates.

The cavity mirror at the output end is called an output coupler. The output coupler allows partial transmittance of the laser light, and the transmitted radiation forms the output of the laser. The unique 'doughnut' beam shape of the Spectra Physics DCR-2 design is due to an unstable resonator design. In resonator design, both cavity length and mirror curvature are important. The stability condition for a resonator is given by $0 \leq g_1 g_2 \leq 1$ where $g_n = 1 - L/R_n$, L is the cavity length and R is the mirror curvature. Unstable resonators have the inherent advantage of having large beam diameters, thereby extracting energy from active media with large cross-sectional areas. The resonator in the Spectra Physics is a diffraction coupled resonator (DCR) and produces a collimated shaped beam.

The collimated shaped beam can be spatially filtered by a process in which the beam intensity is made uniform. Spatial filtering is accomplished by focusing the beam with a positive lens precisely at a pinhole. Since only collimated light is focused at the pinhole. The laser beam diameter at the spatial filter input is determined from $D_{in} = D_L + 2\theta L$ where D_L is the laser beam diameter, θ is the half angle beam divergence in radians (0.0005 radians for PDL-1), and L is the distance from the laser to the filter. The

focused spot size (i.e. the size of pinhole) is given by $S = 1.27 \lambda F_{in}/D_{in}$ where F_{in} is the focal length of the lens.

Both primary radiation excitation sources were used to optically pump liquid dye lasers. When laser dyes are irradiated, higher vibrational levels of the first excited singlet state are populated by optical pumping from thermally populated rovibronic levels in the S_0 ground state. With collisions induced by the solvent molecules (usually methanol or ethanol), the excited dye molecules undergo very fast radiationless transitions into the lowest vibrational level v_0 of S_1 with relaxation times of 10^{-11}-10^{-12} s. The laser transition occurs between the low vibrational levels of S_1 and S_0. With the dense rovibrational manifolds within the S_0 and S_1 states, the broad band emission allows for continuous tuning. The potential energy diagram for a typical dye laser is shown in Figure B.3

As shown in the potential energy diagram, the low-lying vibrational levels of S_1 can be depopulated either by spontaneous emission into different rovibronic levels of S_0 or by radiationless transitions into a lower triplet state T_1 (intersystem crossing). While the intersystem crossing is a forbidden transition due to spin change, sufficient population can build in the T_1 state. Transition from the $T_1 \rightarrow S_0$ (phosphorescence) is also forbidden. Unfortunately, the range of the laser transition frequencies usually coincides with the $T_1 \rightarrow T_2$ transition and this transition can quickly quench laser activity. Flowing dye circulators producing a smooth laminar volume are invariantly used to circumvent this problem by removing the triplet species from the laser gain region.
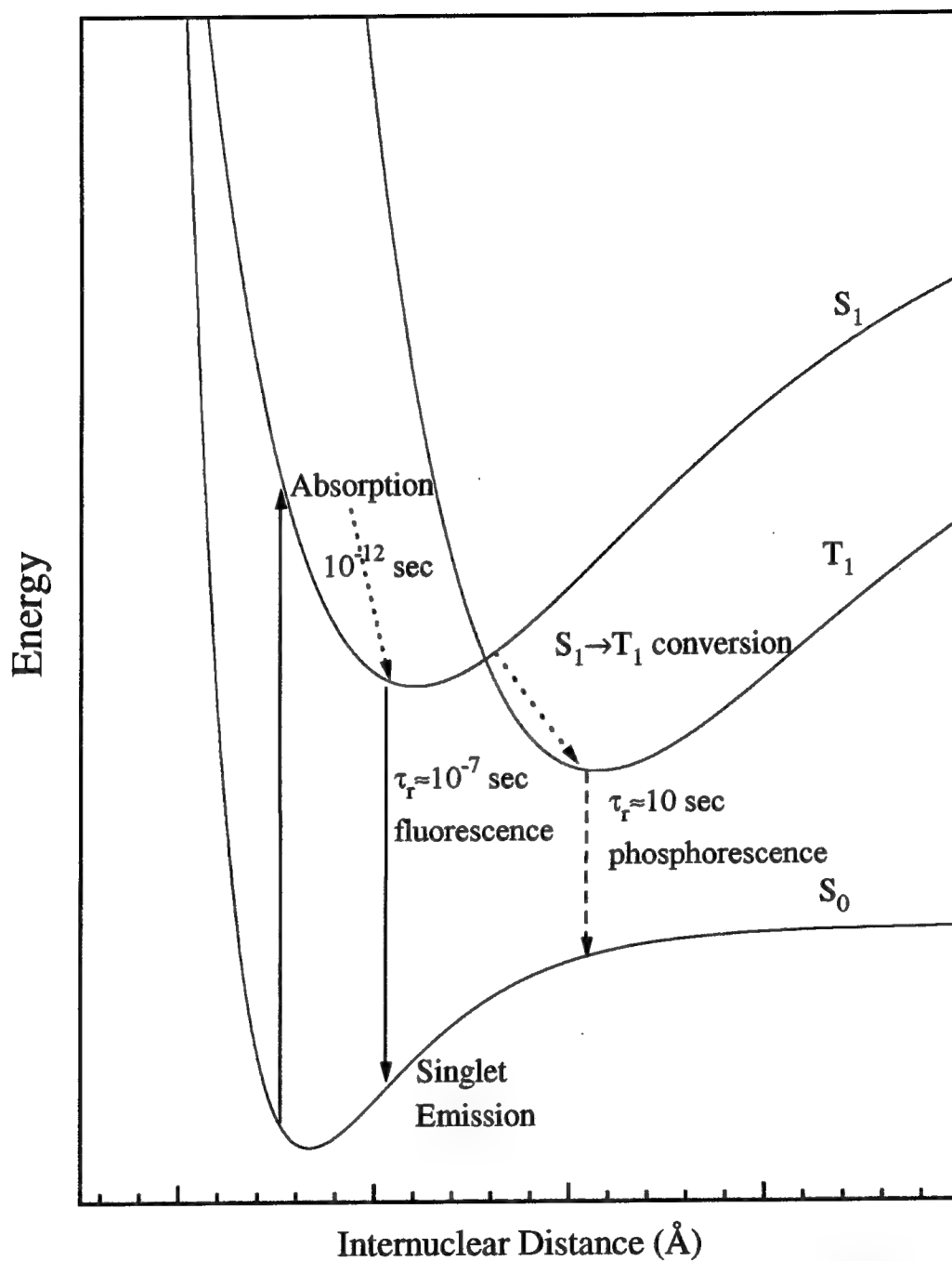
Figure B.3: Potential Energy Diagram for a Dye Laser Showing Intersystem Crossing from Singlet to Triplet

In spite of some of the difficulties associated with the dye laser (e.g. limited lifetime, waste disposal), the broad tuning range made available by different dyes allows continuous tuning over the visible spectrum. The chemical structure of some common laser dyes is shown in Figure B.4 Due to the high gain of many of the dye lasers, a minimum concentration of the dye is used to prevent amplified spontaneous emission (ASE). In most dye lasers, the ASE originates in the oscillator dye cell and is further amplified in the following stages of the dye laser. The advantage of ASE is that it generates intense radiation without an optical cavity. The disadvantage of ASE is that it is a broadband emission which occurs at a lower wavelength and contributes to spectral pollution of the monochromatic source and lower power. The power of the dye laser is also reduced by degradation of the dye. Additives to coumarin dyes can extend the lifetime by over a factor of three. DABCO 1,4-diazabicyclo[2.2.2] octane stabilizes coumarin by quenching singlet oxygen produced by photooxidation of the dye and quenches an excited triplet state.

In addition to dyes, frequency conversion can be produced by nonlinear effects. In 1961, researchers at the University of Michigan focused a ruby laser onto a crystal of quartz and detected two outputs: one, the ruby laser at 694.3 nm and a second at 347.2 nm. A generalized picture of nonlinear optics is if the polarization in not proportional to the electric field, then the system is nonlinear. This is in contrast to a linear system where the polarization is proportional to E. A listing of crystals which lack inversion symmetry and exhibit nonlinear effects are listed in Table B.1

Rhodamine 6G
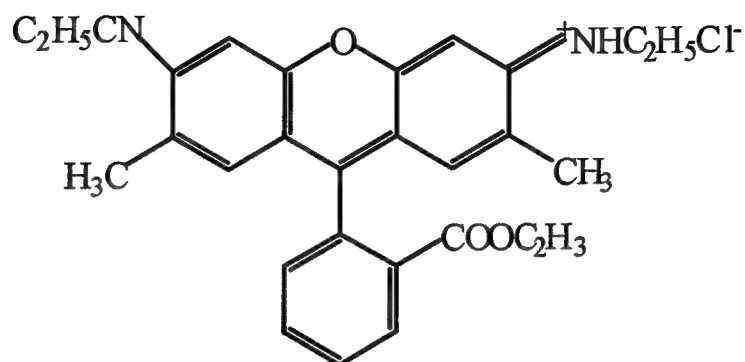
Coumarin
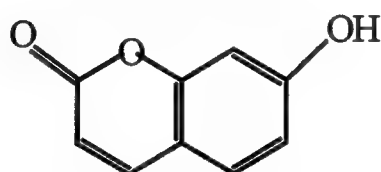
LDS (Stryrl 7)
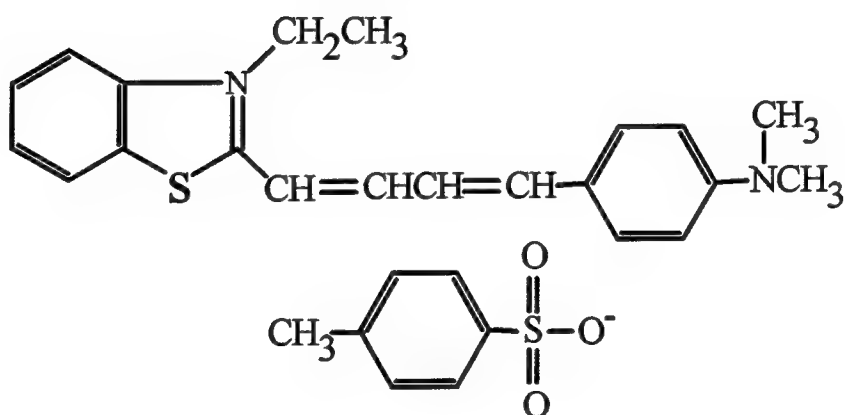
Figure B.4: Molecular Structure of Some Common
         Laser Dyes

While non-linear crystals are used for frequency conversion, another special piece of crystalline glass known as an etalon can be used for frequency narrowing of the laser output. In order to increase the single axial output of from a TEM_{00} laser, an etalon consisting of two surfaces, finely polished to a very fine degree of parallelism, can be inserted into the laser cavity. The etalon acts as a fixed spaced Fabry-Perot cavity whose resonances are broader than the longer laser cavity [If the plate spacing can be varied, the device is called an interferometer]. The resonator frequency spacing is given by $\Delta\omega = \pi c/L$ where L is the cavity length given by $L = \frac{1}{2} q\lambda$ where q is an integer. Secondly, the separations between the etalon resonant frequencies are larger than the laser's. Therefore, losses are introduced into some cavity resonances and the laser operates on a single cavity mode with the smallest loss. Tilting of the etalon with respect to the optical axis of the laser shifts the frequency of the etalon resonances within the laser cavity. The light is dispersed in the oscillator according to the Littrow condition $\lambda_0 = (2\sin\alpha)/(KxN)$, where K is the grating constant (groves/nm) and N is the grating order. Only light matching this condition is reflected back into the oscillator cavity providing the required feedback for lasing. Continuous scanning with an etalon requires a precise synchronization of the etalon tilt with the grating angle for high-Q resonance matching in the oscillator cavity.

REFERENCES

D. C. Oshea, W. R. Callen and W. T. Rhodes, *An Introduction To Lasers And Their Applications*, Addision-Wesley, Reading, Massachusetts (1978).

J. T. Verdeyen, *Laser Electronics*, Prentice Hall, Englewood Cliffs, New Jersey (1989).

Table B.1: Nonlinear Crystals Which Lack Inversion Symmetry

Abbreviation	Crystal Name	Formula
AD*P	Ammonium Dideuterium Phosphate	$(ND_4)D_2PO_4$
KDP	Potassium Dihydrogen Phosphate	KH_2PO_4
CDA	Cesium Dihydrogen Phosphate	CsH_2AsO_4
β-BBO	Barium Metaborate	$BaBO_3$
$LiNbO_3$	Lithium Niobate (V)	LiNbO3
Proustite	Silver Arsenic Sulfide	Ag_3AsS_3
KTP	Potassium Titanyl Phosphate	$KTiOPO_4$
RDA	Rubidium Dihydrogen Arsenate	RbH_2PO_4

APPENDIX C

FRANCK-CONDON PRINCIPLE

The Franck-Condon principle predicts the intensity of transitions between the vibrational levels of different electronic states. The electronic states of a diatomic are represented by a potential energy diagram as a function of the potential energy versus the internuclear distance, r. The Franck-Condon principle states that all electronic transitions occur on a vertical path (r is a constant). The separation between nuclei remains constant in its time reference since bound electrons can readjust their orbits instantaneously compared to the vibrational motion of the more massive nuclei.

Vibrational wavefunctions oscillate much less rapidly near the end points of the potential energy curve than in the region between the turning points. Classically, the turning points correspond to extremes of oscillatory motion where the velocity is zero. The classical turning point is where the vibrational motion changes direction. Since the molecule spends more time near the extremes, the probability of transition is increased. The probability of transitions between two electronic states is dependent upon the overlap of the vertical transition with respect to the vibrational wavefunction. The vertical transition has the highest probability since the relatively massive nuclei have nearly the same positions and velocities before and after an electronic transition.

In the Born-Oppenheimer approximation, the nuclear potential energy is a function of the nuclear coordinates and the nuclear and electronic wavefunctions are

separable. The wavefunction of a vibrating molecule may be written as a product of the electronic and vibrational wavefunction

$$\langle \psi_f | R | \psi_i \rangle = \langle \psi_{ef} \psi_{vf} | R_e + R_v | \psi_{ei} \psi_{vi} \rangle \qquad (C.1)$$

where R_e and R_v are the transition moment operators for transitions between electronic and vibrational states, respectively. Expanding C.1

$$\langle \psi_f | R | \psi_i \rangle = \langle \psi_{vf} | \psi_{vi} \rangle \langle \psi_{ef} | R_e | \psi_{ei} \rangle + \langle \psi_{ef} | \psi_{ei} \rangle \langle \psi_{vf} | R_v | \psi_{vi} \rangle$$

since the electronic wavefunctions are members of the same complete orthogonal set, the second term vanishes and

$$\langle \psi_f | R | \psi_i \rangle = \langle \psi_{vf} | \psi_{vi} \rangle \langle \psi_{ef} | R_e | \psi_{ei} \rangle$$

The integral $\langle \psi_{vf} | \psi_{vi} \rangle$ is known as the Franck-Condon integral and multiplies the electronic transition matrix element. The probability of the electronic transition is

$$| \langle \psi_f | R | \psi_i \rangle |^2 = | \langle \psi_{vf} | \psi_{vi} \rangle |^2 \, | \langle \psi_{ef} | R_e | \psi_{ei} \rangle |^2$$

where $| \langle \psi_{vf} | \psi_{vi} \rangle |^2$ is the Franck-Condon factor for the $v'' \rightarrow v'$ vibrational band of the electronic transition. Summing Franck-Condon factors over all v'

$$\Sigma | \langle \psi_f | R | \psi_i \rangle |^2 = 1$$

Tables C.1 and C.2 contain Franck-Condon factors for I_2 B-X and D-X, respectively. The Franck-Condon factors were calculated by first calculating RKR turning points from the spectroscopic constants. Vibrational wavefunctions were computed for these potentials by the Numerov-Cooley solution from which the Franck-Condon factors and R centroids were obtained by integration of the wave function.

Table C.1: Franck-Condon Factors for I$_2$ B-X

v"\v'	0	1	2	3	4	5	6	7	8	9	10
0	1.66E-09	2.41E-08	1.79E-07	9.12E-07	3.57E-06	1.15E-05	3.18E-05	7.73E-05	1.69E-04	3.36E-04	6.19E-04
1	4.19E-08	5.53E-07	3.73E-06	1.72E-05	6.10E-05	1.77E-04	4.41E-04	9.63E-04	1.89E-03	3.36E-03	5.52E-03
2	5.18E-07	6.17E-06	3.74E-05	1.54E-04	4.91E-04	1.27E-03	2.81E-03	5.43E-03	9.35E-03	1.45E-02	2.08E-02
3	4.18E-06	4.44E-05	2.40E-04	8.81E-04	2.47E-03	5.61E-03	1.08E-02	1.80E-02	2.65E-02	3.49E-02	4.16E-02
4	2.47E-05	2.32E-04	1.10E-03	3.54E-03	8.59E-03	1.68E-02	2.73E-02	3.81E-02	4.59E-02	4.81E-02	4.36E-02
5	1.14E-04	9.38E-04	3.87E-03	1.06E-02	2.18E-02	3.55E-02	4.70E-02	5.15E-02	4.63E-02	3.32E-02	1.74E-02
6	4.29E-04	3.04E-03	1.07E-02	2.46E-02	4.13E-02	5.32E-02	5.31E-02	4.01E-02	2.08E-02	5.15E-03	2.64E-05
7	1.35E-03	8.11E-03	2.37E-02	4.41E-02	5.76E-02	5.38E-02	3.41E-02	1.15E-02	2.75E-04	4.70E-03	1.75E-02
8	3.63E-03	1.81E-02	4.25E-02	6.10E-02	5.66E-02	3.13E-02	6.49E-03	6.47E-04	1.29E-02	2.71E-02	2.90E-02
9	8.45E-03	3.41E-02	6.17E-02	6.28E-02	3.39E-02	4.99E-03	2.58E-03	2.01E-02	3.21E-02	2.49E-02	8.48E-03
10	1.73E-02	5.43E-02	7.13E-02	4.37E-02	6.89E-03	3.29E-03	2.47E-02	3.41E-02	1.97E-02	2.48E-03	2.43E-03

v"\v'	11	12	13	14	15	16	17	18	19	20
0	1.06E-03	1.72E-03	2.63E-03	3.83E-03	5.35E-03	7.17E-03	9.29E-03	1.16E-02	1.42E-02	1.68E-02
1	8.42E-03	1.21E-02	1.63E-02	2.09E-02	2.55E-02	2.97E-02	3.33E-02	3.59E-02	3.74E-02	3.76E-02
2	2.74E-02	3.35E-02	3.83E-02	4.11E-02	4.13E-02	3.89E-02	3.45E-02	2.84E-02	2.16E-02	1.49E-02
3	4.48E-02	4.37E-02	3.84E-02	3.02E-02	2.06E-02	1.16E-02	4.71E-03	8.20E-04	9.89E-05	2.05E-03
4	3.37E-02	2.11E-02	9.73E-03	2.24E-03	1.51E-05	2.59E-03	8.18E-03	1.44E-02	1.93E-02	2.15E-02
5	5.05E-03	5.00E-05	2.76E-03	1.03E-02	1.83E-02	2.33E-02	2.33E-02	1.90E-02	1.24E-02	5.89E-03
6	5.54E-03	1.60E-02	2.42E-02	2.56E-02	2.01E-02	1.13E-02	3.59E-03	9.59E-05	1.43E-03	6.05E-03
7	2.69E-02	2.63E-02	1.71E-02	6.25E-03	3.222E-0	1.71E-03	8.07E-03	1.49E-02	1.82E-02	1.69E-02
8	1.82E-02	5.14E-03	3.90E-06	4.80E-03	1.38E-02	1.97E-02	1.86E-02	1.21E-02	4.63E-03	3.70E-04
9	4.07E-05	5.43E-03	1.65E-02	2.18E-02	1.73E-02	7.83E-03	9.37E-04	8.29E-04	6.18E-03	1.24E-02
10	1.52E-02	2.34E-02	1.83E-02	6.72E-03	1.29E-04	3.20E-03	1.13E-02	1.67E-02	1.54E-02	9.21E-03

Table C.1: Franck-Condon Factors for I$_2$ *B-X* (continued)

v"\v'	0	1	2	3	4	5	6	7	8	9	10
30	3.22E-05	1.02E-03	1.12E-02	5.10E-02	3.57E-06	2.63E-02	1.40E-02	4.06E-02	2.53E-03	3.27E-02	4.59E-03
31	9.23E-06	3.62E-04	5.04E-03	3.08E-02	7.94E-02	6.21E-02	7.35E-05	4.40E-02	8.45E-03	2.86E-02	6.16E-03
32	2.40E-06	1.15E-04	2.02E-03	1.61E-02	5.92E-02	8.44E-02	1.91E-02	1.82E-02	3.78E-02	3.59E-03	3.17E-02
33	5.64E-07	3.31E-05	7.21E-04	7.39E-03	3.70E-02	8.28E-02	5.62E-02	6.20E-05	4.49E-02	7.36E-03	2.87E-02
34	1.20E-07	8.54E-06	2.30E-04	2.98E-03	1.98E-02	6.41E-02	8.29E-02	1.62E-02	1.96E-02	3.72E-02	3.38E-03
35	2.28E-08	1.97E-06	6.52E-05	1.06E-03	9.13E-03	4.08E-02	8.45E-02	5.43E-02	1.10E-04	4.47E-02	8.25E-03
36	3.83E-09	4.04E-07	1.64E-05	3.33E-04	3.65E-03	2.18E-02	6.63E-02	8.31E-02	1.67E-02	1.84E-02	3.89E-02
37	5.68E-10	7.36E-08	3.66E-06	9.20E-05	1.27E-03	9.94E-03	4.20E-02	8.53E-02	5.64E-02	4.40E-07	4.34E-02
38	7.66E-11	1.18E-08	7.18E-07	2.23E-05	3.88E-04	3.89E-03	2.21E-02	6.62E-02	8.52E-02	2.02E-02	1.50E-02
39	9.74E-12	1.64E-09	1.23E-07	4.72E-06	1.02E-04	1.31E-03	9.80E-03	4.10E-02	8.53E-02	6.19E-02	4.35E-04
40	7.36E-13	1.88E-10	1.79E-08	8.61E-07	2.34E-05	3.79E-04	3.67E-03	2.08E-02	6.39E-02	8.85E-02	2.73E-02
41	1.69E-15	1.82E-11	2.29E-09	1.36E-07	4.63E-06	9.44E-05	1.17E-03	8.79E-03	3.79E-02	8.40E-02	7.05E-02
42	7.56E-15	2.05E-12	2.55E-10	1.83E-08	7.79E-07	2.00E-05	3.18E-04	3.11E-04	1.82E-02	5.94E-02	9.18E-02
43	5.37E-14	3.40E-13	2.30E-11	2.05E-09	1.10E-07	3.61E-06	7.31E-05	9.25E-04	7.21E-03	3.30E-02	8.06E-02
44	1.87E-16	6.62E-17	1.07E-12	1.85E-10	1.30E-08	5.44E-07	1.41E-05	2.30E-04	2.36E-03	1.47E-02	5.27E-02
45	4.10E-14	5.90E-14	1.61E-14	1.24E-11	1.23E-09	6.66E-08	2.24E-06	4.74E-04	6.36E-04	5.33E-03	2.68E-02

v"\v'	11	12	13	14	15	16	17	18	19	20
30	2.04E-02	1.48E-02	3.87E-03	2.29E-02	3.42E-03	7.77E-03	1.84E-02	3.15E-03	4.06E-03	1.54E-02
31	2.75E-02	2.09E-04	2.45E-02	6.25E-03	7.59E-03	1.99E-02	1.97E-03	7.43E-03	1.68E-02	4.03E-03
32	4.77E-03	2.03E-02	1.38E-02	4.70E-03	2.24E-02	2.20E-03	9.56E-03	1.73E-02	1.61E-03	6.08E-03
33	6.36E-03	2.68E-02	5.00E-04	2.48E-02	4.55E-03	9.62E-03	1.86E-02	7.27E-04	9.85E-03	1.56E-02
34	3.21E-02	3.71E-03	2.19E-02	1.15E-02	6.75E-03	2.14E-02	7.99E-04	1.23E-02	1.53E-02	3.29E-04
35	2.71E-02	8.16E-03	2.49E-02	1.52E-03	2.51E-02	2.32E-03	1.27E-02	1.62E-02	8.85E-06	1.29E-02
36	2.09E-03	3.35E-02	1.89E-03	2.45E-02	8.05E-03	1.02E-02	1.93E-02	6.17E-06	1.54E-02	1.21E-02
37	1.12E-02	2.38E-02	1.18E-02	2.16E-02	3.97E-03	2.44E-02	4.45E-04	1.66E-02	1.24E-02	7.20E-04
38	4.20E-02	5.34E-04	3.50E-02	2.83E-04	2.73E-02	4.03E-03	1.49E-02	1.54E-02	8.75E-04	1.82E-02
39	4.04E-02	1.66E-02	1.85E-02	1.75E-02	1.64E-02	8.57E-03	2.17E-02	1.86E-04	2.01E-02	7.43E-03
40	9.75E-03	4.56E-02	9.90E-05	3.51E-02	3.67E-04	2.89E-02	7.58E-04	2.02E-02	9.82E-03	4.35E-03
41	2.88E-03	3.47E-02	2.48E-02	1.15E-02	2.49E-02	9.63E-03	1.54E-02	1.63E-02	2.96E-03	2.15E-02
42	3.84E-02	4.03E-03	4.77E-02	2.76E-03	3.20E-02	3.94E-03	2.72E-02	3.07E-04	2.39E-02	3.79E-03
43	8.10E-02	9.39E-03	2.57E-02	3.51E-02	4.27E-03	3.21E-02	3.01E-03	2.31E-02	8.81E-03	9.35E-03
44	9.35E-02	5.37E-02	2.33E-04	4.58E-02	1.05E-02	2.43E-02	1.22E-02	2.09E-02	4.72E-03	2.36E-02
45	7.41E-02	9.13E-02	2.21E-02	1.42E-02	4.48E-02	8.66E-05	3.58E-02	2.79E-06	2.84E-02	1.90E-03

Table C.1: Franck-Condon Factors for I$_2$ B-X (continued)

v"\v'	0	1	2	3	4	5	6	7	8	9	10
20	6.53E-02	7.79E-02	3.44E-03	4.76E-02	9.05E-03	2.15E-02	2.70E-02	2.47E-04	2.51E-02	1.62E-02	3.43E-04
21	4.50E-02	9.42E-02	3.05E-03	5.07E-02	9.66E-04	3.98E-02	3.89E-03	1.91E-03	2.36E-02	1.65E-06	1.88E-02
22	2.84E-02	9.41E-02	2.59E-02	2.90E-02	2.19E-02	2.73E-02	5.37E-03	3.26E-02	2.20E-03	1.61E-02	2.19E-02
23	1.64E-02	8.05E-02	5.84E-02	4.87E-03	4.66E-02	3.55E-03	3.02E-02	1.40E-02	8.44E-03	2.73E-02	1.81E-03
24	8.76E-03	6.03E-02	8.31E-02	2.48E-03	4.57E-02	5.30E-03	3.63E-02	1.51E-04	3.02E-02	7.48E-03	9.48E-03
25	4.28E-03	4.00E-02	8.99E-02	2.60E-02	2.11E-02	3.21E-02	1.35E-02	1.92E-02	2.18E-02	2.94E-03	2.71E-02
26	1.92E-03	2.37E-02	7.96E-02	5.97E-02	1.06E-03	4.86E-02	1.77E-04	3.72E-02	9.05E-04	2.57E-02	1.18E-02
27	7.90E-04	1.26E-02	5.98E-02	8.32E-02	8.46E-03	3.41E-02	1.97E-02	2.17E-02	1.17E-02	2.58E-02	8.51E-04
28	2.97E-04	6.05E-03	3.89E-02	8.65E-02	3.95E-02	7.48E-03	4.51E-02	7.26E-04	3.50E-02	3.09E-03	2.22E-02
29	1.02E-04	2.62E-03	2.22E-02	7.25E-02	7.19E-02	1.68E-03	4.11E-02	1.21E-02	2.66E-02	7.71E-03	2.74E-02
30	3.22E-05	1.02E-03	1.12E-02	5.10E-02	8.65E-02	2.63E-02	1.40E-02	4.06E-02	2.53E-03	3.27E-02	4.59E-03

v"\v'	11	12	13	14	15	16	17	18	19	20
20	1.81E-02	1.79E-02	1.22E-03	6.29E-03	1.79E-02	1.11E-02	4.76E-04	4.41E-03	1.35E-02	1.24E-02
21	1.86E-02	4.08E-04	1.03E-02	1.93E-02	6.31E-03	6.33E-04	1.14E-02	1.53E-02	5.99E-03	2.76E-06
22	4.59E-04	1.27E-02	1.97E-02	3.19E-03	3.74E-03	1.64E-02	1.21E-02	9.05E-04	3.57E-03	1.27E-02
23	1.27E-02	2.09E-02	1.93E-03	7.13E-03	1.88E-02	7.70E-03	2.40E-04	1.01E-02	1.49E-02	5.93E-03
24	2.37E-02	2.14E-03	9.19E-03	1.99E-02	4.52E-03	2.62E-03	1.54E-02	1.21E-02	9.59E-04	3.53E-03
25	4.56E-03	8.96E-03	2.13E-02	3.14E-03	5.58E-03	1.81E-02	7.98E-03	1.89E-04	9.95E-03	1.43E-02
26	5.77E-03	2.38E-02	3.51E-03	7.41E-03	1.95E-02	4.89E-03	2.40E-03	1.50E-02	1.15E-02	6.59E-04
27	2.58E-02	6.43E-03	7.11E-03	2.10E-02	3.52E-03	5.24E-03	1.76E-02	7.35E-03	3.53E-04	1.05E-02
28	1.42E-02	4.13E-03	2.33E-02	3.94E-03	7.02E-03	1.90E-02	4.36E-03	2.87E-03	1.51E-02	1.01E-02
29	2.66E-04	2.48E-02	6.97E-03	6.74E-03	2.06E-02	3.06E-03	5.87E-03	1.73E-02	5.96E-03	8.76E-04
30	2.03E-02	1.48E-02	3.87E-03	2.29E-02	3.42E-03	7.77E-03	1.84E-02	3.15E-03	4.06E-03	1.54E-02

Table C.2: Franck-Condon Factors for I_2 D-X

v"\v'	3	4	5	6	7	8	9	10
33	2.83E-06	1.46E-05	5.98E-05	2.03E-04	5.85E-04	1.46E-03	3.19E-03	6.18E-03
34	9.44E-06	4.53E-05	1.72E-04	5.42E-04	1.44E-03	3.04E-03	6.60E-03	1.16E-02
35	3.04E-05	1.35E-04	4.74E-04	1.37E-03	3.33E-03	6.92E-03	1.25E-02	1.95E-02
36	9.19E-05	3.75E-04	1.21E-03	3.17E-03	6.97E-03	1.30E-02	2.07E-02	2.82E-02
37	2.59E-04	9.66E-04	2.82E-03	6.68E-03	1.31E-02	2.16E-02	2.97E-02	3.42E-02
38	6.81E-04	2.30E-03	6.03E-03	1.27E-02	2.19E-02	3.10E-02	3.59E-02	3.29E-02
39	1.66E-03	5.02E-03	1.17E-02	2.15E-02	3.18E-02	3.75E-02	3.42E-02	2.24E-02
40	3.73E-03	9.99E-03	2.03E-02	3.20E-02	3.92E-02	3.62E-02	2.32E-02	7.72E-03
41	7.72E-03	1.80E-02	3.12E-02	4.07E-02	3.89E-02	2.51E-02	7.99E-03	2.02E-05
42	1.46E-02	2.89E-02	4.14E-02	4.23E-02	2.84E-02	9.19E-03	1.98E-05	6.61E-03
43	2.48E-02	4.08E-02	4.61E-02	3.34E-02	1.17E-02	1.04E-04	6.89E-03	2.02E-02
44	3.75E-02	4.91E-02	4.01E-02	1.63E-02	5.37E-04	6.36E-03	2.12E-02	2.32E-02
45	4.97E-02	4.82E-02	2.39E-02	2.02E-03	4.89E-03	2.15E-02	2.46E-02	1.02E-02

v"\v'	30	31	32	33	34	35	36	37
20	2.45E-03	3.50E-03	4.83E-03	6.45E-03	8.33E-03	1.04E-02	1.26E-02	1.46E-02
21	5.46E-03	7.31E-03	9.43E-03	1.17E-02	1.40E-02	1.62E-02	1.78E-02	1.89E-02
22	1.04E-02	1.29E-02	1.53E-02	1.75E-02	1.90E-02	1.97E-02	1.94E-02	1.79E-02
23	1.64E-02	1.86E-02	2.00E-02	2.04E-02	1.95E-02	1.74E-02	1.43E-02	1.05E-02
24	2.09E-02	2.09E-02	1.96E-02	1.70E-02	1.33E-02	9.11E-03	5.10E-03	1.97E-03
25	1.99E-02	1.67E-02	1.25E-02	8.02E-03	3.94E-03	1.10E-03	5.58E-06	7.68E-04
26	1.22E-02	7.33E-03	3.17E-03	5.92E-04	6.97E-05	1.56E-03	4.48E-03	7.85E-03
27	2.77E-03	3.39E-04	2.61E-04	2.34E-03	5.76E-03	9.29E-03	1.17E-02	1.22E-02
28	4.29E-04	2.96E-03	6.78E-03	1.04E-02	1.25E-02	1.23E-02	9.83E-03	6.12E-03
29	7.46E-03	1.12E-02	1.31E-02	1.23E-02	9.18E-03	5.05E-03	1.55E-03	1.77E-05
30	1.36E-02	1.24E-02	8.79E-03	4.33E-03	9.53E-04	4.41E-05	1.79E-03	5.15E-03
31	8.79E-03	3.99E-03	6.51E-04	2.04E-04	2.60E-03	6.39E-03	9.50E-03	1.03E-02

Table C.2 Franck-Condon Factors for I_2 D-X (continued)

v" \ v'	38	39	40	41
20	1.64E-02	1.78E-02	1.84E-02	1.83E-02
21	1.91E-02	1.83E-02	1.65E-02	1.39E-02
22	1.54E-02	1.22E-02	8.61E-03	5.14E-03
23	6.68E-03	3.31E-03	9.68E-04	1.47E-05
24	2.45E-04	1.74E-04	1.64E-03	4.18E-03
25	3.04E-03	6.11E-03	9.04E-03	1.10E-02
26	1.06E-02	1.18E-02	1.12E-02	8.89E-03
27	1.06E-02	7.46E-03	3.91E-03	1.13E-03
28	2.51E-03	3.17E-04	2.38E-04	2.14E-03
29	9.23E-04	3.68E-03	6.94E-03	9.22E-03
30	8.41E-03	9.99E-03	9.15E-03	6.37E-03
31	8.48E-03	4.98E-03	1.62E-03	2.86E-05

v" \ v'	10	11	12	13	14	15	16	17
20	3.35E-10	1.26E-09	4.41E-09	1.42E-08	4.31E-08	1.22E-07	3.25E-07	8.21E-07
21	1.95E-09	7.08E-09	2.36E-08	7.34E-08	2.12E-07	5.77E-07	1.47E-06	3.56E-06
22	1.05E-08	3.65E-08	1.17E-07	3.48E-07	9.64E-07	2.50E-06	6.11E-06	1.41E-05
23	5.25E-08	1.74E-07	5.35E-07	1.51E-06	4.01E-06	9.95E-06	2.31E-05	5.08E-05
24	2.43E-07	7.72E-07	2.25E-06	6.10E-06	1.53E-05	3.61E-05	7.98E-05	1.66E-04
25	1.04E-06	3.15E-06	8.75E-06	2.24E-05	5.37E-05	1.19E-04	2.50E-04	4.92E-04
26	4.14E-06	1.18E-05	3.12E-05	7.60E-05	1.71E-04	3.61E-04	7.10E-04	1.31E-03
27	1.52E-05	4.12E-05	1.02E-04	2.34E-04	4.98E-04	9.84E-04	1.81E-03	3.12E-03
28	5.14E-05	1.31E-04	3.07E-04	6.60E-04	1.31E-03	2.41E-03	4.14E-03	6.61E-03
29	1.60E-04	3.84E-04	8.39E-04	1.68E-03	3.10E-03	5.30E-03	8.36E-03	1.22E-02
30	4.58E-04	1.02E-03	2.08E-03	3.86E-03	6.56E-03	1.02E-02	1.47E-02	1.94E-02
31	1.19E-03	2.47E-03	4.63E-03	7.89E-03	1.22E-02	1.72E-02	2.22E-02	2.58E-02

Table C.2 Franck-Condon Factors for I₂ D-X (continued)

v" \ v'	18	19	20	21
20	1.96E-06	4.47E-06	9.71E-06	2.01E-05
21	8.15E-06	1.77E-05	3.68E-05	7.29E-05
22	3.08E-05	6.38E-05	1.26E-04	2.37E-04
23	1.05E-04	2.07E-04	3.89E-04	6.93E-04
24	3.27E-04	6.08E-04	1.07E-03	1.80E-03
25	9.12E-04	1.59E-03	2.64E-03	4.16E-03
26	2.27E-03	3.73E-03	5.75E-03	8.38E-03
27	5.05E-03	7.66E-03	1.09E-02	1.45E-02
28	9.84E-03	1.36E-02	1.76E-02	2.12E-02
29	1.65E-02	2.07E-02	2.38E-02	2.50E-02
30	2.34E-02	2.57E-02	2.54E-02	2.22E-02
31	2.69E-02	2.48E-02	1.96E-02	1.25E-02

v" \ v'	11	12	13	14	15
33	1.06E-02	1.63E-02	2.24E-02	2.73E-02	2.91E-02
34	1.79E-02	2.44E-02	2.91E-02	3.01E-02	2.61E-02
35	2.64E-02	3.09E-02	3.08E-02	2.52E-02	1.53E-02
36	3.26E-02	3.13E-02	2.40E-02	1.32E-02	3.44E-03
37	3.20E-02	2.30E-02	1.10E-02	1.97E-03	5.11E-04
38	2.24E-02	9.31E-03	8.95E-04	1.48E-03	9.47E-03
39	8.21E-03	3.24E-04	2.90E-03	1.21E-02	1.90E-02
40	8.56E-05	4.40E-03	1.47E-02	2.02E-02	1.54E-02
41	5.71E-03	1.69E-02	2.11E-02	1.39E-02	3.01E-03
42	1.88E-02	2.16E-02	1.22E-02	1.65E-03	1.73E-03
43	2.23E-02	1.09E-02	6.61E-04	3.28E-03	1.37E-02
44	1.02E-02	1.95E-04	5.28E-03	1.58E-02	1.58E-02
45	3.83E-05	7.16E-03	1.78E-02	1.50E-02	3.23E-03

APPENDIX D

FORTRAN CODE FOR SPECTRA ANALYSIS

The source code for analyzing both $I(^2P_{1/2})+I_2(X)$ energy transfer and $I_2^\dagger + M$ rotational spectra have been included. Numerous fitting laws and spin-degeneracy factors for the parametization of rotational energy transfer data may be modeled . The required files including subroutines, include, and data files for compling, linking and executing this program are:

DISPLAY.FOR	DISPLAY.DAT
RETSIM.FOR	DISPLAY.REF
DXSIM.FOR	FCF.DAT
LAMBDA.FOR	COLORS.H
PEAKLOC.FOR	KEYCODE.H
C_CALLS.FOR	ROW_COL.H

The code was written and complied with Microsoft FORTRAN 5.0 and Microsoft C 5.1. The input list for linking the object files, include files, FORTRAN, C, and graphics libraries is:

```
/NOE /E+
        display+
        lambda c_calls retsim peakloc dxsim


        f:\fortran\lib\llibfor7+
        f:\fortran\lib\graphics+
        f:\c5_1\lib\llibce
```

```fortran
$Storage: 2
$INCLUDE: 'FGRAPH.FI'
*_____*
*                                                *
*   A Graphics Program which allows user input for calibrating   *
*   and fitting data generated by the LAMBDA programs in the    *
*   Laboratory of M. C. HEAVEN.  Source Code by M. Nowlin Oct 93 *
*_____*
      INCLUDE 'FGRAPH.FD'
      INCLUDE 'DISPLAY.DAT' !contains common statements
      INCLUDE 'KEYCODE.H'
      INTEGER    opt
      INTEGER*2   dummy2
      REAL*4     xdummy,ydummy
      CHARACTER   MENU1*78,MENU2*78,name*12,fillay*12
      LOGICAL    Done
*_____*
*                                                *
*  call the application program to read in the user x and y data  *
*_____*
51    CONTINUE
      Write(*,*)
      Write(*,*)
      Write(*,*)'        This program may create up to five files
     + with '
      Write(*,*)'       extensions added to your root name (ente
     +red below):'
      Write(*,*)
      Write(*,*) .        *.dat:  X-Y Format of orginal file (no
     + changes)'
      Write(*,*)'        *.off: File which contains offset of
     +data file.'
      Write(*,*)'                Generated with the input of on
     +ly one'
      Write(*,*)'                calibration point.'
      Write(*,*)'        *.cal: File which contains calibrated
     + data in X-Y format'
      Write(*,*)'                Generated with the input of tw
     +o or more'
      Write(*,*)'                calibration points.'
      Write(*,*)'        *.mel: File which contains peak locat
     +ions and areas'
      Write(*,*)'        cal.ref: File contains input calibratio
     +n points.'
      Write(*,*)'                File is for cross-checking and
     + is over-written'
      Write(*,*)'                each time a data file is calib
     +rated.'
      Write(*,*)
      Write(*,*)'SELECT FILE TYPE (ENTER a or b only; NO RETURN KEY)'
      Write(*,*)
      Write(*,*)'A.  Lambda Data File (Format from MCH Laboratory)'
      Write(*,*)
      Write(*,*)'B.  XY File Format'
      Write(*,*)
      newfile=.false.
      calib=.false.
      done=.false.
      Do While( .not. Done )
       Call checkk( opt )
       SELECT CASE ( opt )
        CASE($CAP_A,$a )    ! call lambda
         call lambda(filnam,yescal,name,oldname)
         OPEN(22,File=name,Err=100,Status='UNKNOWN')
          READ(22,*,err=200,end=300)nume
          Do I=1,nume
           READ(22,*) Xdat(I),Ydat(I),Zdat(I)
          End Do
         CLOSE(22)
         done=.true.
        CASE($CAP_B,$b )    ! read data file
         write(*,*)'Input file name'
         read(*,33)FILLAY
         write(*,*)'Input new file name (Enter root name only)'
         read(*,33)filnam
33       Format(A12)
         oldname=fillay
         OPEN(63,File=FILLAY,ERR=200,STATUS='OLD')
          read(63,*)
          Do jj=1,1000
           read(63,*,END=163)xdat(jj),ydat(jj)
           IF(xdat(jj).gt.9000)then
             temp=xdat(jj)
             xdat(jj)=1e7/temp
           ENDIF
           zdat(jj)=0.0
```

```fortran
          END DO
163       continue
          nume=jj-1
          done=.true.
        CASE( $ESC,$CAP_Q,$q )        ! quit program
         Done = .true.
        CASE DEFAULT
       END SELECT
      END DO
*_____*
*                                                *
*     get the min/max values in the 1d-arrays     *
*_____*
      call minmax(xdat,nume,xdummy,ydummy)
       xmin=dble(xdummy)
        xmax=dble(ydummy)
      call minmax(ydat,nume,xdummy,ydummy)
       ymin=dble(xdummy)
        baselin=ymin
         ymax=dble(ydummy)
      call minmax(zdat,nume,xdummy,ydummy)
       zmin=dble(xdummy)
        zmax=dble(ydummy)
*_____*
*                                                *
*     call the graphics routine and display the data     *
*_____*
      call display
      IF(newfile)goto 51
      call clearscreen ($GCLEARSCREEN)  ! clear screen
      Menu1 ='          PRESS RETURN TO READ ANOTHER DATA'//
     +   ' FILE AND CONTINUE  '
      Menu2 ='     PRESS q OR ESC TO QUIT    '//
     +   ' REMEMBER THE NAMES OF YOUR FILES'
      Call messg(Menu1, 1)
      Call messg(Menu2, 2)
      Done=.false.
      Do While( .not. Done )
       Call checkk( opt )
       SELECT CASE ( opt )
        CASE( $RETURN )          ! load another file
         call clearscreen ($GCLEARSCREEN)  ! clear screen
         dummy2=setvideomode($DEFAULTMODE)
          goto 51
        CASE( $ESC,$CAP_Q,$q )        ! quit program
         Done = .true.
        CASE DEFAULT
       END SELECT
      END DO
      dummy2=setvideomode($DEFAULTMODE)
      stop'end of program'
100   stop'ERROR IN MAIN, cannot open input file, why ?'
200   stop'ERROR IN MAIN, cannot read from input file, why?'
300   stop'ERROR IN MAIN, reached end of input file, why?'
      end

      SUBROUTINE DISPLAY
*_____*
*                                                *
*     graphics routine                            *
*_____*
      INCLUDE 'FGRAPH.FD'
      INCLUDE 'DISPLAY.DAT'
      INCLUDE 'KEYCODE.H'
      INTEGER    opt,iunit,itbnd,ichg
      INTEGER*2   dummy2,id,ix,dstte(5),xstte(5)
      INTEGER*2   ixzum,idzum
      INTEGER*4   itnum,nume2
      REAL*4     alw,press,xxdum(30),yydum(30)
      REAL*4     ymaxsim,ymaxtmp,xdummy,ydummy,fpop
      REAL*8     short,rlong,temp,rmshort,rmlong
      REAL*8     bec,dec,xec,yec,fdum,wgt,based,rate
      CHARACTER   Menu1*78,Menu2*78,dumchar*30,str*7,fillay*12
      CHARACTER   str3*6,str5*20,str2*2,str8*8,str9*9,str10*10
      CHARACTER   dumchr*33
      LOGICAL    done,done3,nex,again,first,fit_all
      LOGICAL    plus,sub,spectro,firstmd,thirtyate
      RECORD/rccoord/ s
      COMMON/SPECT/ spectro,idzum,ixzum,bec,dec,xec,yec,firstmd
      cal_done=.false.
      drawnocal=.false.
      pkhgh=.true.
      spectro=.false.
*_____*
*                                                *
*   read in graphics information from the reference file   *
*   If file is not found....use default values at label 51  *
*_____*
```

```fortran
OPEN(12,ERR=51,FILE='DISPLAY.REF',STATUS='OLD')
READ(12,*,ERR=200,END=300)
READ(12,*,ERR=200,END=300) X1VIEW,Y1VIEW
READ(12,*,ERR=200,END=300)
READ(12,*,ERR=200,END=300) ZSCALE
READ(12,*,ERR=200,END=300)
READ(12,*,ERR=200,END=300) NLC1, NLC2, NLC3, NLC4, NTC
READ(12,*,ERR=200,END=300)
READ(12,*,ERR=200,END=300) COL1, COL2, COL3, COL4, COL5
READ(12,*,ERR=200,END=300)
READ(12,*,ERR=200,END=300) xrange, yvar        !xrange=cur size
READ(12,*,ERR=200,END=300)
READ(12,*,ERR=200,END=300) x_row,x1_col,x2_col
READ(12,*,ERR=200,END=300)
READ(12,*,ERR=200,END=300) put_cur
READ(12,*,ERR=200,END=300)
READ(12,*,ERR=200,END=300) glw
READ(12,*,ERR=200,END=300)
READ(12,*,ERR=200,END=300) iunit,alw
READ(12,*,ERR=200,END=300)
READ(12,*,ERR=200,END=300) rottmp,rotc,rotal,rotap,rotalw,rott
READ(12,*,ERR=200,END=300)
READ(12,*,ERR=200,END=300) inverse,SDeg
READ(12,*,ERR=200,END=300)
READ(12,*,ERR=200,END=300)pop(20),pop(21),pop(22),pop(23) !population for vib
READ(12,*,ERR=200,END=300)pop(24),pop(25),pop(26),pop(27)  !levels of I2 + I*
READ(12,*,ERR=200,END=300)pop(28),pop(29),pop(30),pop(31)  !energy tranfer
READ(12,*,ERR=200,END=300)pop(32),pop(33),pop(34),pop(35)
READ(12,*,ERR=200,END=300)pop(36),pop(37),pop(38),pop(39)
READ(12,*,ERR=200,END=300)pop(40),pop(41),pop(42),pop(43)
READ(12,*,ERR=200,END=300)pop(44),pop(45),pop(46),pop(47)
READ(12,*,ERR=200,END=300)
READ(12,*,ERR=200,END=300)tmpr(20),tmpr(21),tmpr(22),tmpr(23) !temp for vib
READ(12,*,ERR=200,END=300)tmpr(24),tmpr(25),tmpr(26),tmpr(27)!levels of I2 + I*
READ(12,*,ERR=200,END=300)tmpr(28),tmpr(29),tmpr(30),tmpr(31) !energy tranfer
READ(12,*,ERR=200,END=300)tmpr(32),tmpr(33),tmpr(34),tmpr(35)
READ(12,*,ERR=200,END=300)tmpr(36),tmpr(37),tmpr(38),tmpr(39)
READ(12,*,ERR=200,END=300)tmpr(40),tmpr(41),tmpr(42),tmpr(43)
READ(12,*,ERR=200,END=300)tmpr(44),tmpr(45),tmpr(46),tmpr(47)
READ(12,*,ERR=200,END=300)
READ(12,*,ERR=200,END=300)LORENTZ,gowss,ah
READ(12,*,ERR=200,END=300)
READ(12,*,ERR=200,END=300)totJ(20),totJ(21),totJ(22),totJ(23)
READ(12,*,ERR=200,END=300)totJ(24),totJ(25),totJ(26),totJ(27)
READ(12,*,ERR=200,END=300)totJ(28),totJ(29),totJ(30),totJ(31)
READ(12,*,ERR=200,END=300)totJ(32),totJ(33),totJ(34),totJ(35)
READ(12,*,ERR=200,END=300)totJ(36),totJ(37),totJ(38),totJ(39)
READ(12,*,ERR=200,END=300)totJ(40),totJ(41),totJ(42),totJ(43)
READ(12,*,ERR=200,END=300)totJ(44),totJ(45),totJ(46),totJ(47)
rewind 12
Goto 52
51    X1VIEW=85.
      Y1VIEW=85.
      ZSCALE=30.
      NLC1=12
      NLC2=14
      NLC3=11
      NLC4=15
      NTC=4
      COL1=12
      COL2=15
      COL3=15
      COL4=12
      COL5=10
      xrange=6
      yvar=21.0000
      x_row=29
      x1_col=4
      x2_col=71
      put_cur=2
      glw=0.08
      alw=0.06
      iunit=1
      rottmp=301
      rotc=0.2
      rotal=0.0
      rotap=1.0
      rotalw=0.08
      rott=300
      inverse=.false.
      SDeg=4
      pop(20)=0.4 !Steady State Population of Vibration Excited I2
      pop(21)=0.5
      pop(22)=0.9
      pop(23)=0.6
      pop(24)=1.2
      pop(25)=1.3
      pop(26)=0.8
      pop(27)=1.3
      pop(28)=0.9
      pop(29)=0.9
      pop(30)=1.2
      pop(31)=0.9
      pop(32)=1.1
      pop(33)=2.1
      pop(34)=2.4
      pop(35)=3.0
      pop(36)=4.2
      pop(37)=5.3
      pop(38)=5.9
      pop(39)=5.9
      pop(40)=10.2
      pop(41)=4.9
      pop(42)=6.6
      pop(43)=4.2
      pop(44)=3.3
      pop(45)=2.8
      pop(46)=3.3
      pop(47)=1.3
      Do j=20,32 !Nascent Rotational Temperature of Vibration Excited I2
      tmpr(j)=270
      END DO
      tmpr(33)=360
      tmpr(34)=380
      tmpr(35)=380
      tmpr(36)=380
      tmpr(37)=370
      tmpr(38)=360
      tmpr(39)=345
      tmpr(40)=340
      tmpr(41)=340
      tmpr(42)=320
      tmpr(43)=320
      tmpr(44)=320
      tmpr(45)=300
      tmpr(46)=298
      tmpr(47)=298
      LORENTZ=.true.
      gowss=.true.
      ah=0.0002
      Do j=20,47 !Nascent Rotational Temperature of Vibration Excited I2
      totJ(j)=110  !Gaussian distribution
      END DO
52    Continue
*_____*
*        check data from reference file of correctness   *
*_____*
      if(x1view.lt.10.d0.or.x1view.gt.100.d0) goto 901
      if(y1view.lt.10.d0.or.y1view.gt.100.d0) goto 902
      if(zscale.lt.10.d0.or.zscale.gt.100.d0) goto 903
      if(nlc1.lt.0.or.nlc2.lt.0.or.nlc3.lt.0.or.nlc4.lt.0) goto 904
      if(ntc.lt.0)goto 904
*_____*
*                plot the graph                  *
*_____*
      call vidscrn
      call plot
      call axis
*_____*
*          move cursor / select options          *
*_____*
      IF(put_cur.eq.1)then
            curpos=int(nume/2)
          ELSEIF(put_cur.eq.2)then
            curpos=xrange+1
          ELSE
          curpos=nume-xrange-1
      ENDIF
      call setviewport(x1,y1,x2,y2)
      call cursor(curpos,on)
      Done = .false.
      moveone=.false.        !Step second display left or right
      movetwo=.false.        !Second file is dxsim or external
      moveret=.false.        !Second file is RET file
      out_lft=.false.
      out_rgt=.false.
      Menu1 =' Use '//CHAR(27)//' '//CHAR(26)//' keys to move'//
   +    ' cursor        ESC - Return to previous screen'
```

```
Menu2 = ' C - Enter Calibration Mode     '//
+     '      D - Enter Data Mode'
Call messg(Menu1, 1)
Call messg(Menu2, 2)
plotsim=.false.
distwo=.false.
jpcnt=0
jplus=0
jminus=0
Do While( .not. Done )
 Call checkk( opt )
 SELECT CASE ( opt )
  CASE( $LFTAROW, $COMMA, $LT )  ! move Cursor left
   Call Curs_Lft(CurPos)
  CASE( $RGTAROW, $PERIOD, $GT )  ! move Cursor right
    Call Curs_Rgt(CurPos)
  CASE( $CAP_H, $h )       ! move Cursor right
     bbigstep=.true.
    Call Curs_Lft(curpos)
  CASE( $CAP_K, $k )       ! move Cursor right
    bigstep=.true.
       Call Curs_Rgt(curpos)
  CASE( $CAP_J, $j )        ! move Cursor left
    bigstep=.true.
    Call Curs_Lft(curpos)
  CASE( $CAP_L, $l )        ! move Cursor left
    bbigstep=.true.
    Call Curs_Rgt(curpos)
  CASE( $r )            ! refresh screen
    call refresh
    call messg(menu2,2)
  CASE( $CAP_B,$b )         ! baseline
   baselin=ydat(curpos)
   dumchar='BASELINE-              '
Call settextposition(2,37,s)
   Call outtext(dumchar)
    Write(str,'(f7.2)')baselin
   Call settextposition(2,47,s)
   Call outtext(str)
  CASE( $CAP_D,$d )        ! enter data mode
   calib=.false.
   Call Dat_File(CurPos)
  CASE( $CAP_C,$c )        ! enter calibration mode
  calib=.true.
   call Set_CAL(CurPos)
   call cursor(curpos,off)
   calib=.false.
  call axis
  CASE( $F1 )           ! DISPLAY SECOND FILE
  call clearscreen ($GCLEARSCREEN)  ! clear screen
  dummy2=setvideomode($DEFAULTMODE)
  write(*,*)'Input file name'
  read(*,33)FILLAY
33   Format(A12)
  OPEN(63,File=FILLAY,ERR=164,STATUS='OLD')
   read(63,*)
   Do jj=1,2000
    read(63,*,END=163)xcol(jj),ycol(jj)
    If(xcol(jj).gt.9000.)xcol(jj)=1e7/xcol(jj)
   END DO
163   continue
   itwonum=jj-1
   itnum=itwonum
   call minmax(xcol,itnum,xdummy,ydummy)
   xxmin=dble(xdummy)
   xxmax=dble(ydummy)
   call minmax(ycol,itnum,xdummy,ydummy)
   yymin=dble(xdummy)
   yymax=dble(ydummy)
   temp=ymax/yymax
   ydelt=ymin-yymin
   ratio=ymin/ymax
   IF(baselin.gt.0)ydelt=baselin-yymin
   ratio=ymin/ymax
   IF(baselin.gt.0)ratio=baselin/ymax
    Do ja=1,itwonum
     temp2=ycol(ja)
     ycol(ja)=temp2*temp      ! scale data file
     If(ymin.gt.yymin)ycol(ja)=ycol(ja)+ydelt
     If(ymin.lt.yymin)ycol(ja)=ycol(ja)-ydelt
     ycol(ja)=ycol(ja)*(1-ratio)
     IF(ycol(ja).lt.baselin)ycol(ja)=baselin
    End Do
   distwo=.true.          ! display second file
```

```
164   continue
   call vidscrn
   call refresh
   distwo=.false.
  CASE( $F3 )            ! Override No Calibration Data
   yescal=.true.
  CASE( $F4 )            ! DISPLAY D-X Spectroscopy Simulation
   iodx=.true.
  call clearscreen ($GCLEARSCREEN) ! clear screen
  dummy2=setvideomode($DEFAULTMODE)
  short=xdat(1)
  nmshort=short
  IF(short.gt.2000.)nmshort=1e7/short
   rlong=xdat(nume)
   nmlong=rlong
   IF(rlong.gt.2000.)nmlong=1e7/rlong
   IF(nmlong.lt.nmshort)then
    temp=nmshort
    nmshort=nmlong
    nmlong=temp
   ENDIF
   write(*,*)'Input total number of bands (max: 5)'
    read(*,*)itbnd
    Do i=1,itbnd
    write(*,*)'Input D state, X state'
    read(*,*)idzum,ixzum
    dstte(i)=idzum
    xstte(i)=ixzum
   END DO
  call vidscrn
  call refresh
  movetwo=.false.
  spectro=.true.
  nex=.true.
  frstmd=.true.     !erase existing file contents before call
  open(unit=5,file='DXPOS.dat',status='unknown')
     DO i=1,itbnd
     yec=0.
     xec=0.
     dec=0.
     bec=0.
    IF(nex)then
     idzum=dstte(i)
     ixzum=xstte(i)
    END IF
    Write(str2,'(i2)')idzum
     call settextposition(2,10,s)
     call outtext(str2)
     Write(str2,'(i2)')ixzum
     call settextposition(2,14,s)
    call outtext(str2)
    inumq=i
47   call dxsim(nmshort,nmlong)       !calc line positions
    call dxsimtwo(iunit,alw)  !fits line positions with
     wgt=1.0             !line shape
     first=.true.
     plotsim=.true.
    fit_all=.false.
    nex=.true.
   call dxonetime(nex,wgt,first,id,ix,fdum,fit_all)  !scales line
                       !positions based on shape
     distwo=.true.
     itwonum=1501
     call refresh
     distwo=.false.
     done3=.false.
    jminus=0
    jplus=0
    jpcnt=0
    nex=.true.
   Write(str2,'(i2)')idzum
   call settextposition(2,10,s)
  call outtext(str2)
  Write(str2,'(i2)')ixzum
  call settextposition(2,14,s)
  call outtext(str2)
   Write(str10,'(f10.8)')xec
    call settextposition(1,40,s)
    call outtext(str10)
    Write(str10,'(f10.8)')dec
    call settextposition(1,20,s)
    call outtext(str10)
   Write(str3,'(f6.4)')bec
   call settextposition(1,60,s)
```

```
call outtext(str3)                                      done3 = .true.
  Write(str3,'(f6.4)')yec                                nex=.true.
call settextposition(2,60,s)                           CASE( $RETURN)
call outtext(str3)                                       done3 =.true.
  str3='D con-'                                        CASE DEFAULT
  call settextposition(1,13,s)                        END SELECT
  call outtext(str3)                                 END DO
  str3='X con-'                                        IF(.not.nex)goto 47
  call settextposition(1,33,s)                       END DO
  call outtext(str3)                                 iodx=.false.
  str3='BO - '                                       spectro=.false.
  call settextposition(1,53,s)                *******************************************************
  call outtext(str3)                          *      ! DISPLAY D-X NRG TRANSFER SIMULATION       *
  str3='D Dcon'                               *******************************************************
  call settextposition(2,53,s)                    CASE( $F5 )
  call outtext(str3)                                str5='                '
Do While( .not. Done3 )                             call settextposition(8,33,s)
Call checkk( opt )                                  call outtext(str5)
  SELECT CASE ( opt )                               call settextposition(10,33,s)
   CASE( $EQUAL, $PLUS)    !step DXSIM SPECTY display right   call outtext(str5)
     j=0                                            str5=' I2 + I* Simulation '
     jminus=jminus+1                                call settextposition(9,33,s)
       Do k=1,1501                                  call outtext(str5)
         stpx(k)=0.                                iodx=.true.
         END DO                                    short=xdat(1)
         Do k=jminus,1501                          nmshort=short
         j=j+1                                     IF(short.gt.2000.)nmshort=1e7/short
         stpx(j)=ycol(k)                           rlong=xdat(nume)
         END DO                                    nmlong=rlong
         jplus=j                                   IF(rlong.gt.2000.)nmlong=1e7/rlong
         jpcnt=jminus                              IF(nmlong.lt.nmshort)then
          moveone=.true.                             temp=nmshort
          call refresh                               nmshort=nmlong
         moveone=.false.                             nmlong=temp
CASE( $MINUS, $UNDRLIN) !step DXSIM SPECTY display left  ENDIF
jpcnt=jpcnt+1                                      call dxsim(nmshort,nmlong)
     j=0                                           call dxsimtwo(iunit,alw)
       Do k=1,1501                                   inumq=1
         stpx(k)=0.                                  nex=.true.
         END DO                                      wgt=1.0
           Do k=jpcnt,1501                           chg=0.1
           j=j+1                                     fdum=1.0
           stpx(k)=ycol(j)                           first=.true.
           END DO                             34     continue           !allows fitting of each band
           jminus=jpcnt                              plotsim=.true.
           jplus=1501                                call dxonetime(nex,wgt,first,id,ix,fdum,fit_all)
           moveone=.true.                            nex=.true.
           call refresh                              distwo=.true.
           moveone=.false.                            itwonum=1501
     CASE( $CAP_X, $x )                              call refresh
       IF(sub)xec=xec-0.0000001                      distwo=.false.
       IF(plus)xec=xec+0.0000001                   done3=.false.
       nex=.false.                                 again=.false.
       Write(str10,'(f10.8)')xec                    IF(iband-1.lt.inumq-1)then
       call settextposition(1,40,s)                   str5=' Simulation        '
     call outtext(str10)                              call settextposition(1,30,s)
     CASE( $CAP_D, $d )                               call outtext(str5)
       IF(sub)dec=dec-0.0000001                       ELse
         IF(plus)dec=dec+0.0000001                    str5='band -    total -'
       nex=.false.                                    call settextposition(1,30,s)
       Write(str10,'(f10.8)')dec                      call outtext(str5)
       call settextposition(1,20,s)                   Write(str2,'(i2)')iband-1
     call outtext(str10)                              call settextposition(1,53,s)
     CASE( $CAP_B, $b )                               call outtext(str2)
       IF(sub)bec=bec-0.01                            Write(str2,'(i2)')inumq-1
         IF(plus)bec=bec+0.01                         call settextposition(1,38,s)
         nex=.false.                                  call outtext(str2)
         Write(str3,'(f6.4)')bec                    str3='D -  '
       call settextposition(1,60,s)                   call settextposition(2,43,s)
     call outtext(str3)                               call outtext(str3)
     CASE( $CAP_Y, $y )                               Write(str3,'(I2)')id
       IF(sub)yec=yec-0.01                            call settextposition(2,47,s)
         IF(plus)yec=yec+0.01                         call outtext(str3)
         nex=.false.                                str3='X -  '
         Write(str3,'(f6.4)')yec                      call settextposition(2,54,s)
       call settextposition(2,60,s)                   call outtext(str3)
     call outtext(str3)                               Write(str3,'(I2)')ix
     CASE( $COMMA, $LT )                              call settextposition(2,58,s)
       sub=.true.                                     call outtext(str3)
       plus=.false.                                 str3='wgt- '
     CASE( $PERIOD, $GT )                             call settextposition(2,23,s)
       plus=.true.                                    call outtext(str3)
       sub=.false.                                  str3='chg- '
     CASE( $ESC,$CAP_Q,$q)                            call settextposition(2,9,s)
```

```
          call outtext(str3)
str3='pop- '
  call settextposition(2,65,s)
  call outtext(str3)
    Write(str3,'(f6.3)')pop(ix)
    call settextposition(2,70,s)
  call outtext(str3)
str='FCFx100'
  call settextposition(1,57,s)
  call outtext(str)
Write(str8,'(f8.6)')fdum*100
  call settextposition(1,67,s)
  call outtext(str8)
Write(str8,'(f8.6)')chg
  call settextposition(2,13,s)
  call outtext(str8)
Write(str9,'(f9.6)')wgt
  call settextposition(2,30,s)
  call outtext(str9)
ENDIF
jminus=0
jplus=0
jpcnt=0
Do While( .not. Done3 )
Call checkk( opt )
 SELECT CASE ( opt )
  CASE( $F1 )
   done3 =.true.
   again =.true.
   fit_all=.true.
  CASE( $EQUAL, $PLUS)    !step DXSIM display right
   j=0
     jminus=jminus+1
      Do k=1,1501
      stpx(k)=0.
      END DO
      Do k=jminus,1501
      j=j+1
       stpx(j)=ycol(k)
      END DO
     jplus=j
     jpcnt=jminus
     moveone=.true.
     call refresh
     moveone=.false.
CASE( $MINUS, $UNDRLIN) !step DXSIM display left
jpcnt=jpcnt+1
   j=0
    Do k=1,1501
    stpx(k)=0.
    END DO
     Do k=jpcnt,1501
      j=j+1
      stpx(k)=ycol(j)
     END DO
     jminus=jpcnt
     jplus=1501
     moveone=.true.
     call refresh
     moveone=.false.
CASE( $CAP_X, $x)
 nex=.false.
  again=.true.
  done3=.true.
CASE( $CAP_M, $m)
 nume2=1500
  call minmax(ycol,nume2,xdummy,ydummy)
  ymaxsim=dble(ydummy)
  ymaxtmp=ymaxsim*rotap
  Do jms=1,1501
  IF(ycol(jms).gt.ymaxsim)ycol(jms)=ymaxtmp
  ENDDO
  plotsim=.true.
  distwo=.true.
  itwonum=1501
  call refresh
CASE( $CAP_N, $n)
 nex=.true.
  again=.true.
  done3=.true.
CASE( $ONE )
  chg=1.0
    Write(str8,'(f8.6)')chg
    call settextposition(2,13,s)
```

```
          call outtext(str8)
  CASE( $TWO )
   chg=0.1
    Write(str8,'(f8.6)')chg
    call settextposition(2,13,s)
    call outtext(str8)
  CASE( $THREE )
   chg=0.01
    Write(str8,'(f8.6)')chg
    call settextposition(2,13,s)
   call outtext(str8)
  CASE( $FOUR )
   chg=0.001
  Write(str8,'(f8.6)')chg
    call settextposition(2,13,s)
    call outtext(str8)
  CASE( $FIVE )
   chg=0.0001
  Write(str8,'(f8.6)')chg
    call settextposition(2,13,s)
    call outtext(str8)
  CASE( $SIX )
   chg=0.00001
  Write(str8,'(f8.6)')chg
    call settextposition(2,13,s)
    call outtext(str8)
  CASE( $SEVEN)
   chg=0.000001
  Write(str8,'(f8.6)')chg
    call settextposition(2,13,s)
    call outtext(str8)
  CASE( $COMMA, $LT )
    wgt=wgt-chg
    IF(wgt.lt.0.000001)wgt=0.000001
     Write(str9,'(f9.6)')wgt
     call settextposition(2,30,s)
    call outtext(str9)
  CASE( $PERIOD, $GT )
    wgt=wgt+chg
     Write(str9,'(f9.6)')wgt
     call settextposition(2,30,s)
    call outtext(str9)
  CASE( $ESC,$CAP_Q,$q)
    done3 = .true.
    again=.false.
  CASE( $RETURN)
    done3 =.true.
    again =.true.
  CASE DEFAULT
  END SELECT
END DO
IF(inumq.gt.iband)again=.false.
IF(again)goto 34
iodx=.false.
plotsim=.false.
**********************************************************
  CASE( $CAP_P, $p)
   call clearscreen ($GCLEARSCREEN) ! clear screen
   dummy2=setvideomode($DEFAULTMODE)
   Write(*,*)'Relative weights for I2+I* Simulation'
Write(*,*)
Write(*,*)' v=20 ',pop(20)
Write(*,*)' v=21 ',pop(21),'  v=22 ',pop(22),'  v=23 ',pop(23)
Write(*,*)' v=24 ',pop(24),'  v=25 ',pop(25),'  v=26 ',pop(26)
Write(*,*)' v=27 ',pop(27),'  v=28 ',pop(28),'  v=29 ',pop(29)
Write(*,*)' v=30 ',pop(30),'  v=31 ',pop(31),'  v=32 ',pop(32)
Write(*,*)' v=33 ',pop(33),'  v=34 ',pop(34),'  v=35 ',pop(35)
Write(*,*)' v=36 ',pop(36),'  v=37 ',pop(37),'  v=38 ',pop(38)
Write(*,*)' v=39 ',pop(39),'  v=40 ',pop(40),'  v=41 ',pop(41)
Write(*,*)' v=42 ',pop(42),'  v=43 ',pop(43),'  v=44 ',pop(44)
Write(*,*)' v=45 ',pop(45),'  v=46 ',pop(46),'  v=47 ',pop(47)
Write(*,*)
   Write(*,*)'Enter vibrational level to change (21-47)'
   read(*,*)ichg
   Write(*,*)'Enter new weight'
   read(*,*)fpop
   pop(ichg)=fpop
   call vidscrn
   call refresh
  CASE( $CAP_T, $t)
   call clearscreen ($GCLEARSCREEN) ! clear screen
   dummy2=setvideomode($DEFAULTMODE)
   Write(*,*)'Relative rotational temps for I2+I* Simulation'
Write(*,*)
```

```fortran
      Write(*,*)' v=20 ',totJ(20)
      Write(*,*)' v=21 ',totJ(21),'  v=22 ',totJ(22),'  v=23 ',totJ(23)
      Write(*,*)' v=24 ',totJ(24),'  v=25 ',totJ(25),'  v=26 ',totJ(26)
      Write(*,*)' v=27 ',totJ(27),'  v=28 ',totJ(28),'  v=29 ',totJ(29)
      Write(*,*)' v=30 ',totJ(30),'  v=31 ',totJ(31),'  v=32 ',totJ(32)
      Write(*,*)' v=33 ',totJ(33),'  v=34 ',totJ(34),'  v=35 ',totJ(35)
      Write(*,*)' v=36 ',totJ(36),'  v=37 ',totJ(37),'  v=38 ',totJ(38)
      Write(*,*)' v=39 ',totJ(39),'  v=40 ',totJ(40),'  v=41 ',totJ(41)
      Write(*,*)' v=42 ',totJ(42),'  v=43 ',totJ(43),'  v=44 ',totJ(44)
      Write(*,*)' v=45 ',totJ(45),'  v=46 ',totJ(46),'  v=47 ',totJ(47)
      Write(*,*)
      Write(*,*)'Enter vibrational level to change temperature(33-47)'
       read(*,*)ichg
         Write(*,*)'Enter new temperature'
         read(*,*)fpop
         totJ(ichg)=fpop
         call vidscrn
         call refresh
      CASE($CAP_A,$a)             !call subroutine area
      dumchr='AREA-                    '
      Call settextposition(2,31,s)
         Call outtext(dumchr)
         icheck1=Curpos
         done3=.false.
         Do While( .not. Done3 )
         Call checkk( opt )
          SELECT CASE ( opt )
      CASE($LFTAROW,$COMMA,$LT,$CAP_J,$j,$CAP_H,$h) ! move Cursor left
      Call Curs_Lft(CurPos)
      CASE($RGTAROW,$PERIOD,$GT,$CAP_L,$l,$CAP_K,$k) ! move Cursor right
      Call Curs_Rgt(CurPos)
          CASE( $RETURN)
            icheck2=curpos
            done3 = .true.
          CASE DEFAULT
          END SELECT
         END DO
         IF(icheck2.lt.icheck1)then
          itemp=icheck1
          icheck1=icheck2
          icheck2=itemp
         Endif
       npts=icheck2-icheck1+1
       nterms=npts-1
        Do j=1,npts
         jb=icheck2-j+1
         xxdum(j)=xdat(jb)
         yydum(j)=ydat(jb)-baselin
        ENDDO
       retarea=1.
       call area(xxdum,yydum,npts,nterms,retarea)
       jb=npts/2
        OPEN(76,File='AREA.DAT',Status='UNKNOWN')
        Write(76,*)'peak',xxdum(jb),'   area',retarea
        Write(str,'(f7.2)')Retarea
       Call settextposition(2,39,s)
       Call outtext(str)
*****************************************************************************
      CASE( $F10 )             ! enter RET Simulation mode
      moveret=.true.
      movetwo=.false.
      call clearscreen ($GCLEARSCREEN) ! clear screen
      dummy2=setvideomode($DEFAULTMODE)
      based=baselin
      write(*,*)'Input D state, X state, J level (e.g. 7,38,49)'
        read(*,*)dstate,xstate,jlevel
      write(*,*)
      write(*,*)'Input total pressure of sample (mTorr)'
        read(*,*)press
        write(*,*)
      Thirtyate=.false.
      If(xstate.eq.38)then
      Thirtyate=.true.
       Write(*,*)'Select rate constant*10**-10(Enter a,b,c etc.)'
       Write(*,*)' a. O2  7.54'
       Write(*,*)' b. I2  6.59'
       Write(*,*)' c. Ar  5.74'
       Write(*,*)' d. Cl2  3.87'
       Write(*,*)' e. H20  9.1'
       Write(*,*)' f. He  4.62'
       Write(*,*)' g. Enter your own rate'
       Write(*,*)
      Else
       Write(*,*)'Select rate constant*10**-10(Enter a,b,c etc.)'
```

```fortran
       Write(*,*)' a. O2  7.4'
        Write(*,*)' b. N2  6.9'
        Write(*,*)' c. He  6.5'
        Write(*,*)' d. Ar  6.1'
       Write(*,*)' e. I2  8.7'
       Write(*,*)' f. H2O 9.3'
       Write(*,*)' g. Enter your own rate'
       Write(*,*)
      ENDIF
      done3=.false.
       Do While( .not. Done3 )
       Call checkk( opt )
        SELECT CASE ( opt )
       CASE($CAP_A,$a )
         rate=7.4e-10
         IF(Thirtyate)rate= 7.54e-10
         done3=.true.
       CASE($CAP_B,$b )
         rate=6.9e-10
         IF(Thirtyate)rate= 6.59e-10
         done3=.true.
       CASE($CAP_C,$c )
         rate=6.5e-10
         IF(Thirtyate)rate= 5.74e-10
         done3=.true.
       CASE($CAP_D,$d )
         rate=6.1e-10
         IF(Thirtyate)rate= 3.87e-10
         done3=.true.
       CASE($CAP_E,$e )
         rate=8.7e-10
         IF(Thirtyate)rate= 9.1e-10
         done3=.true.
       CASE($CAP_F,$f )
         rate=9.3e-10
         IF(Thirtyate)rate= 4.62e-10
         done3=.true.
       CASE($CAP_G,$g )
         write(*,*)'Enter your rate (e.g. 5.79)'
         read(*,*)rte
         rate=rte*1e-10
         done3=.true.
       CASE DEFAULT
      END SELECT
      END DO
          call vidscrn
          call retdraw(dstate,xstate,jlevel,based,rate,press)
          moveret=.false.
          call refresh
*****************************************************************************
      CASE( $CAP_N,$n )          ! load another file
       call clearscreen ($GCLEARSCREEN) ! clear screen
       dummy2=setvideomode($DEFAULTMODE)
C       rewind 12
       newfile=.true.
       return
      CASE( $ESC,$CAP_Q,$q )        ! return to previous screen
       Done = .true.
      CASE DEFAULT
      END SELECT
      END DO
      RETURN
*------------------------------------------------*
*         get the error messages                 *
*------------------------------------------------*
100  stop'ERROR IN DISPLAY, cannot open file display.ref, why ?'
200  stop'ERROR IN DISPLAY, cannot read from file display.ref, why?'
300  stop'ERROR IN DISPLAY, reached end of file display.ref, why?'
901  stop'ERROR IN DISPLAY, x1view value should be between 10->100!'
902  stop'ERROR IN DISPLAY, y1view value should be between 10->100!'
903  stop'ERROR IN DISPLAY, zscale value should be between 10->100!'
904  stop'ERROR IN DISPLAY, color values have to be larger then 0!'
      END


      SUBROUTINE CURSOR(ix,switch)
*------------------------------------------------*
*  This routine draws or erases a cursor during spectra  *
*  calibration. This cursor is turned on and off by the  *
*  switch: 0 - off, 1 - on                       *
*------------------------------------------------*
      Include 'FGRAPH.FD'
      Include 'ROW_COL.H'
      Include 'COLORS.H'
```

```
Include 'DISPLAY.DAT'
Integer   switch,ix
Integer*2  color,dummy3,dummy2,dummy
Real*4   xwn
Real*8   xs,xd,ys,yd,scale,xsub
Character  Menu1*78,str*10
Record / wxycoord / wxy
Record /rccoord /  rc,s
IF(.not.pkhgh)then           !draws marker for peak height
  call setviewport(x1,y1,x2,y2)
 dummy = setwindow(.true.,xmin,ymax,xmax,ymin)
 IF( switch .eq. 1 ) then
  dummy2 = setcolor(text_clr )
  Call moveto_w(xr(ix),baselin,wxy)
   dummy2 = lineto_w(xr(ix+5),baselin)
    Call moveto_w(xr(ix),ydelt,wxy )
     dummy2 = lineto_w(xr(ix+5),ydelt)
      ELSEIF(switch .eq. 0)then
     dummy2 = setcolor(TWIL_ZONE )
    Call moveto_w(xr(ix),olddel,wxy)
    dummy2 = lineto_w(xr(ix+5),olddel)
   dummy2 = setcolor(text_clr )
  Call moveto_w(xr(ix),ydelt,wxy )
  dummy2 = lineto_w(xr(ix+5),ydelt)
   ELSEIF(switch .eq. 3)then
    dummy2 = setcolor(TWIL_ZONE )
     Call moveto_w(xr(ix),baselin,wxy)
     dummy2 = lineto_w(xr(ix+5),baselin)
    Call moveto_w(xr(ix),ydelt,wxy )
    dummy2 = lineto_w(xr(ix+5),ydelt)
 ENDIF
 Return
 ENDIF
IF( switch .eq. 1 ) then
 IF(calib)then
  dummy2 = setcolor(graph_border)
   Else
    dummy2 = setcolor(PLOT_CURSOR) !set color for cursor
     ENDIF
Elseif( switch .eq. 0 ) then
 IF(calib)then
  dummy2 = setcolor(TWIL_ZONE)
   ELSE
    dummy2=setcolor(TWIL_ZONE)
     ENDIF
Endif
IF(.not.calib)then            ! Data Mode
 call setviewport(x1,y1,x2,y2)
  dummy = setwindow(.true.,xmin,ymax,xmax,ymin)
  yd=yr(ix)-yvar
   ys=yr(ix)+yvar
    ya(ix)=yr(ix)
ELSE
   call setviewport(x1,y1,x2,y3)  ! Calibration Mode
    dummy = setwindow(.true.,xmin,zmax,xmax,zmin)
    yd=zr(ix)-yvar
    ys=zr(ix)+yvar
   ya(ix)=zr(ix)
  If(.not.yescal)then
   dummy = setwindow(.true.,xmin,ymax,xmax,ymin)
    scale=ymax-ymax*0.13
    yd=scale-yvar
    ys=scale+yvar
   ya(ix)=scale
  ENDIF
 ENDIF
Menu1 = '  Wavelength (nm)    '//
+   '   Wavenumber(cm-1)      Signal'
Call messg(Menu1, 1)
xsub=xr(curpos)
If(cal_done)xsub=1e7/calx(curpos)
xwn=1e7/xr(curpos)
If(cal_done)xwn=calx(curpos)
dummy3=settextcolor(15)
Write(str,'(f10.4)')xsub
Call settextposition(1,19,rc)
Call outtext(str)
Write(str,'(f10.4)')xwn
Call settextposition(1,48,s)
Call outtext(str)
Write(str,'(f10.4)')ya(curpos)
Call settextposition(1,66,s)
Call outtext(str)
xdif=xr(ix)-xr(ix-xrange)
```

```
xd=xr(ix)+xdif
xs=xr(ix)-xdif
 dummy2 = ellipse_w($GBORDER,xd,ys,xs,yd)
  Call moveto_w(xr(curpos),yd,wxy)
  dummy2 = lineto_w(xr(curpos),ys)
  Call moveto_w(xs,ya(curpos),wxy )
  dummy2 = lineto_w(xd,ya(curpos))
  dummy2 = setcolor( TWIL_ZONE) ! set color for data point
  dummy2 = setpixel_w( xr(curpos), ya(curpos))
dummy2 = setcolor(color)   ! reset to original color
Return
END


SUBROUTINE CURS_RGT(cp)
*─────────────────────────────────────────────*
*   This routine moves the cursor one data point to the right  *
*─────────────────────────────────────────────*
INCLUDE 'DISPLAY.DAT'
INTEGER  cp,max
IF(out_rgt)goto 51
right=.true.
max=xrange+1
IF(bigstep)max=xrange+15
IF(bbigstep)max=xrange+30
If( cp .gt. max) then
IF(bigstep)then
    Call Cursor(curpos,0 )
     CurPos = CP - 15
      Call Trace (CurPos)
       Call Cursor(curpos,1 )
        out_lft=.false.
         bigstep=.false.
ENDIF
IF(bbigstep)then
    Call Cursor(curpos,0 )
     CurPos = CP - 30
      Call Trace (CurPos)
       Call Cursor(curpos,1 )
        out_lft=.false.
         bbigstep=.false.
ENDIF
    Call Cursor(curpos,0 )
     CurPos = CP - 1
      Call Trace (CurPos)
       Call Cursor(curpos,1 )
        out_lft=.false.
Else
  out_rgt=.true.
ENDIF
51   Continue
Return
End


SUBROUTINE CURS_LFT(cp)
*─────────────────────────────────────────────*
*   This routine moves the cursor one data point to the left  *
*─────────────────────────────────────────────*
INCLUDE 'DISPLAY.DAT'
INTEGER  cp,min
IF(out_lft)goto 51
min = nume-Xrange-1  !array index to data on left side of cursor
IF(bigstep)min=nume-xrange-15
IF(bbigstep)min=nume-xrange-30
If(cp .lt. min) then
If(bigstep) then
    Call Cursor(CP,0)
     CurPos = CP + 15
      Call Trace(CurPos)
       Call Cursor( CurPos,1)
        out_rgt=.false.
         bigstep=.false.
ENDIF
If(bbigstep) then
    Call Cursor(CP,0)
     CurPos = CP + 30
      Call Trace(CurPos)
       Call Cursor( CurPos,1)
        out_rgt=.false.
         bbigstep=.false.
ENDIF
    Call Cursor(CP,0)
     CurPos = CP + 1
      Call Trace(CurPos)
       Call Cursor( CurPos,1)
```

```
          out_rgt=.false.
     Else
        out_lft=.false.
     ENDIF
51   Continue
     Return
     End

     SUBROUTINE MESSG (str,num)
*_____*
*                                                     *
*   This routine will place a message in a dialog window  *
*   on the screen.                                    *
*_____*

     Include 'FGRAPH.FD'
     Include 'COLORS.H'
     Include 'ROW_COL.H'
     Integer Num
     Integer*2 oldcolor,dummy2,l
     Character*(*) str
     Record / rccoord / rc
     oldcolor = gettextcolor()
     dummy2 = settextcolor( MESSG_CLR )
     If( num .eq. 1 ) then
        Call ClearLine(MESSG_ROW1,MESSG_ROW1)
        Call settextposition(MESSG_ROW1,MESSG_COL,rc)
        Elseif( num .eq. 2 ) then
        Call ClearLine(MESSG_ROW2,MESSG_ROW2)
        Call settextposition(MESSG_ROW2,MESSG_COL,rc)
     Endif
     Call gettextposition(rc)
     Call outtext(str)
     l = INDEX(str,':')
     l=l+2
     Call settextposition(rc.row,l,rc)
     dummy2 = settextcolor( oldcolor )
     Return
     END

     SUBROUTINE TRACE (cp)
*_____*
*                                                     *
*   This routine will trace the graph in the region of  *
*   the data indexed by Pos. This data is contained in  *
*   the array data, declared in DISPLAY.DAT           *
*_____*

     Include 'FGRAPH.FD'
     Include 'COLORS.H'
     Include 'DISPLAY.DAT'
     Integer  i,min,max,cp,icor
     Integer*2 dummy2,color
     Record / wxycoord / wxy
     If((.not.yescal).and.(calib))return
     color = getcolor() ! get current color
     icor=0
     IF(bigstep)icor=15
     IF(bbigstep)icor=30
     min = cp - (Xrange*2) -icor
     max = cp + (Xrange*2) -icor
     IF(right)min=min-40
     if( min .lt. 1 ) min = 1+xrange+icor
     IF(right)max=max+80
     right=.false.
     if( max .gt. nume) max = nume-xrange-icor
        dummy2 = setcolor(GRAPH_LINE) !set color to data line (yellow)
     Call moveto_w( xr(min), yr(min),wxy )
     DO i = min,max
        ! retrace region around cursor
        dummy2 = lineto_w(xr(i),yr(i))
     END DO
     dummy2 = setcolor(color)   ! reset to original color
     color = getcolor()         ! get current color
     dummy=setcolor(nlc3)       !set color to calibration line
     Call setviewport(x1,y1,x2,y3)
        dummy = setwindow(.true.,xmin,zmax,xmax,zmin)
     Call moveto_w( xr(min), zr(min),wxy )
     Do i = min,max          ! retrace region around cursor
        dummy2 = lineto_w(xr(i),zr(i))
     End DO
     dummy = setcolor(color)   ! reset to original color
     call setviewport(x1,y1,x2,y2)
     Return
     END
```

```
     SUBROUTINE CLEARLINE( start,end )
*_____*
*                                                     *
*   This routine clears a given block of rows given by  *
*   START and END.                                    *
*_____*

     Include 'FGRAPH.FD'
     Include 'ROW_COL.H'
     Integer start,end
     Character*78 line
     Record / rccoord / rc,s
     Data line(1:78) /' '/
     Call gettextposition(rc)
     Do 10 i = Start,End
        Call settextposition(int2(i),MESSG_COL,s)
        Call outtext(line)
10   Continue
     Call settextposition(rc.row,rc.col,rc)
     Return
     END

     SUBROUTINE Set_Cal(ix)
*_____*
*                                                     *
*   This subroutine normalizes data from calibration  *
*   scan. User should enter five data points          *
*_____*

     Include 'FGRAPH.FD'
     Include 'COLORS.H'
     Include 'ROW_COL.H'
     Include 'DISPLAY.DAT'
     Include 'KEYCODE.H'
     Integer  opt,ix,icnt
     Integer*2 dummy,dummy2,y4
     Character  Menu1*78,Menu2*78,str*25,str2*31
     Character  str3*35,str4*23,str5*10
     Logical   done,word
     Record /wxycoord/ wxy
     Record /rccoord/  rc,s
     curpos=ix
     done =.false.
     word=.false.
     Menu1 =' Use '//CHAR(27)//' '//CHAR(26)//' keys to move'//
     +      '  cursor        ESC - Return to previous screen'
     If(yescal)then
     Menu2 =' S-Set Calibration Pt  F1 - Calibration '//
     +      ' Backspace - Delete Last Entry'
     Else
     Menu2 ='               NO CALIBRATION DATA   '//
     +      ' IN THIS FILE              '
     ENDIF
     Call messg(Menu1, 1)
     Call messg(Menu2, 2)
     icnt=0
     Do While( .not. Done )
      Call checkk( opt )
      SELECT CASE ( opt )
        CASE( $LFTAROW, $COMMA, $LT ) ! move Cursor left
          Call Curs_Lft(CurPos)
        CASE( $RGTAROW, $PERIOD, $GT ) ! move Cursor right
          Call Curs_Rgt(CurPos)
        CASE( $CAP_H, $h )        ! move Cursor right
          bbigstep=.true.
          Call Curs_Lft(curpos)
        CASE( $CAP_J, $j )        ! move Cursor right
          bigstep=.true.
          Call Curs_Lft(curpos)
        CASE( $CAP_L, $l )        ! move Cursor left
          bbigstep=.true.
          Call Curs_Rgt(curpos)
        CASE( $r )
          call refresh
          call messg(menu2,2)
        CASE( $CAP_K, $k )        ! move Cursor left
          bigstep=.true.
          Call Curs_Rgt(curpos)
        CASE( $CAP_S,$s )         ! add data point to file
          icnt=icnt+1
          Call clearline(29,29)
          If(word)then
          Call clearline(30,30)
          dummy2 = settextcolor(messg_clr)
          Call settextposition(30,20,rc)
          str4='Last Calibration Point:'
          Call outtext(str4)
          dummy2 = settextcolor(graph_line)
```

```
        IF(icnt.gt.0)Write(str5,'(f10.3)')xcal(icnt-1)
          Call settextposition(30,44,s)
            Call outtext(str5)
              ENDIF
          Call settextposition(29,20,rc)
         dummy2 = settextcolor(text_clr)
        str='Enter Calibration (cm-1):'
      Call outtext(str)
       Read(*,*)xcal(icnt)
        curtemp(icnt)=curpos
         dummy = setcolor(graph_line)
          Call setviewport(x1,y1,x2,y3)
           Call moveto_w(xn(curpos),y1,wxy)
             y4=(1.15)*zmax
            IF(zmax.le.5)y4=ymin-60
            dummy2 = lineto_w(xn(curpos),y4)
         call setviewport(x1,y1,x2,y2)
       If(.not.word)then
       Call clearline(30,30)
       Call settextposition(30,20,rc)
       dummy2 = settextcolor(messg_clr)
         str4='Last Calibration Point:'
        Call outtext(str4)
         dummy2 = settextcolor(messg_clr)
         Write(str5,'(f10.3)')xcal(icnt)
          Call settextposition(30,44,s)
           Call outtext(str5)
             word=.true.
              ENDIF
        CASE( $DELETE )          ! delete last data point from file
         If(icnt.eq.0)goto 70
           xcal(icnt)=zip
             curtemp(icnt)=zip
             icnt=icnt-1
           Call clearline(29,29)
            Call settextposition(29,25,rc)
              dummy2 = settextcolor(text_err_clr)
               str2='LAST CALIBRATION POINT DELETED!'
           Call outtext(str2)
70        Continue
        CASE( $F1 )            ! calibrates raw data file
          call sort(icnt)
           OPEN(54,FILE='CAL.REF',STATUS='UNKNOWN')
           Do i=1,icnt
             Write(54,*)xcal(i),curtemp(i),zr(curtemp(i))
           END DO
             CLOSE(54)
               IF(icnt.ge.1)then
                 call abscal(icnt)
                  ENDIF
              Call clearline(29,29)
               Call settextposition(29,25,rc)
                 dummy2 = settextcolor(text_err_clr)
                  str3='CALIBRATION OF DATA COMPLETED.....!'
             Call outtext(str3)
               Call messg(Menu1, 1)
                 cal_done = .true.
          CASE( $ESC,$CAP_Q,$q )      ! return to previous screen
            Done = .true.
           CASE DEFAULT
          END SELECT
        END DO
      Menu1 = ' Use '//CHAR(27)//' '//CHAR(26)//' keys to move'//
     +      ' cursor       ESC - Return to previous screen'
      Menu2 = ' F10 - Enter RET Simulation Mode          '//
     +      '      D - Enter Data Mode'
      Call messg(Menu1, 1)
      Call messg(Menu2, 2)
      call clearline(30,30)
      return
      end


      SUBROUTINE SORT(icnt)
*_____*
*  This subroutine sorts the calibration wavenumbers into      *
*  ascending order                                             *
*_____*
      Include 'DISPLAY.DAT'
      Integer   icnt,tmppos
      Real*8    tmpwl
      IF(icnt.eq.1)goto 74
      Do i=2,icnt
       tmpwl = xcal(i)
        tmppos = curtemp(i)
```

```
        Do j=i,2,-1
         IF(xcal(j-1).gt.tmpwl)then
           xcal(j)=xcal(j-1)
            curtemp(j)=curtemp(j-1)
            Else
             xcal(j)=tmpwl
              curtemp(j)=tmppos
           EXIT
          Endif
         End do
        End do
74    continue
      return
      end


      SUBROUTINE AbsCal(icnt)
*_____*
*  This subroutine uses the calibration wavelengths and        *
*  extrapolates a fit to calibrate data file                   *
*_____*
      Include 'FGRAPH.FD'
      Include 'COLORS.H'
      Include 'ROW_COL.H'
      Include 'DISPLAY.DAT'
      Integer   icnt,ihw(30)
      Real*8    datwn,offset,OSdiff
      Real*8    SF(30),Rfirst,Llast,WNMid,Sdum
      IF(icnt.eq.1)then            ! wavelength offset
      call addext(filnam,'off')
       OPEN(53,FILE=fulnam,STATUS='UNKNOWN')
       offset=1e7/xcal(1)
        calcp=curtemp(1)
         datwn=xdat(calcp)
          OSdiff=offset-datwn
          aufset=.true.
        Do i=1,nume
          xoff(i)=1e7/(xdat(i)+osdiff)
           calx(i)=xoff(i)
            Write(53,*)xoff(i),ydat(i)
        END DO
        Close(53)
      ELSE
         Do i=2,icnt
         ihw(i)=int(curtemp(i-1)+curtemp(i))/2
         END DO
        datwn=1e7/xdat(curtemp(1))
        Rfirst=xcal(2)-xcal(1)   !scaling factor start>first cal pt
      IF(curtemp(1).eq.curtemp(2))goto 70
        SF(1)=Rfirst/(curtemp(2)-curtemp(1))
        Do i=1,ihw(2)
         calx(i)=xcal(1)+SF(1)*(i-curtemp(1))
         END DO
70    Continue
      Do i=2,icnt
        IF(i.eq.icnt)goto 71
          WNMid=xcal(i+1)-xcal(i)  !scaling factor for middle
           SF(i)=WNMid/(curtemp(i+1)-curtemp(i))
            k=i
           Do j=ihw(k),ihw(k+1)
            IF(j.LT.curtemp(k))then
              Sdum=SF(k-1)
               ELSE
               Sdum=SF(k)
              ENDIF
            calx(j)=xcal(k)+Sdum*(j-curtemp(k))
          END DO
        END DO
71    Continue
      Llast=xcal(icnt)-xcal(icnt-1) !scaling factor last cal pt>finish
      IF(nume.eq.ihw(icnt))goto 72
        SF(icnt)=Llast/(curtemp(icnt)-curtemp(icnt-1))
         DO i=ihw(icnt),nume
          calx(i)=xcal(icnt)+SF(icnt)*(i-curtemp(icnt))
          END DO
72    Continue
      call addext(filnam,'cal')
       OPEN(52,FILE=fulnam,STATUS='UNKNOWN')
        DO i=1,nume
         write(52,*)calx(i),ydat(i)
        END DO
        CLOSE(52)
      ENDIF
      RETURN
      END
```

```
SUBROUTINE REFRESH
call plot
call axis
Return
END

SUBROUTINE VIDSCRN
*_____*
*                                         *
*      select the video mode              *
*                                         *
*_____*
INCLUDE 'fgraph.fd'
INCLUDE 'display.dat'
INTEGER*2   dummy
RECORD /videoconfig/ myscreen
Call getvideoconfig (myscreen)
SELECT CASE (myscreen.adapter)
CASE($EGA,$OEGA)
  IF(myscreen.monitor .EQ. $MONO)then
    dummy=setvideomode ($ERESNOCOLOR)
  else
    dummy=setvideomode ($ERESCOLOR)
  endif
CASE($HGC)
    dummy=setvideomode ($HERCMONO)
CASE($VGA)
    dummy=setvideomode ($VRES16COLOR)
CASE($OVGA,$MCGA)
    dummy=setvideomode ($VRES2COLOR)
CASE DEFAULT
    dummy=0
END SELECT
Call getvideoconfig (myscreen)
    maxx= myscreen.numxpixels-1
    maxy= myscreen.numypixels-1
  x1=(maxx-int2(maxx*x1view/100.d0))/2
  y1=(maxy-int2(maxy*y1view/100.d0))/2
  x2=maxx-x1
  y2=maxy-y1
  RETURN
  END


SUBROUTINE AXIS
*_____*
*                                         *
*         label the axis                  *
*                                         *
*_____*
INCLUDE 'fgraph.fd'
INCLUDE 'display.dat'
INCLUDE 'keycode.h'
INTEGER   xs
INTEGER*2   dummy,dummy3
REAL*4    xdum
CHARACTER   str*7,dumchar*9
RECORD /rccoord/ rc
    call clearline(29,29)
    dummy3=settextcolor(15)
    xs=int((x1_col+x2_col)/2)
xdum=xr(nume)
If(cal_done)xdum=1e7/calx(nume)  !cal_done - label with cal axis
Write(str,'(f7.3)')xdum
  Call settextposition(x_row,x1_col,rc)
  Call outtext(str)
    dummy3=int(xs*1.36)
  cp1=int(nume*0.333)
  xdum=xr(cp1)
  IF(cal_done)xdum=1e7/calx(cp1)
  Write(str,'(f7.3)')xdum
  Call settextposition(x_row,dummy3,rc)
  Call outtext(str)
    dummy=int(xs*0.7)
  cp2=int(nume*0.67)
  xdum=xr(cp2)
  IF(cal_done)xdum=1e7/calx(cp2)
Write(str,'(f7.3)')xdum
  Call settextposition(x_row,dummy,rc)
  Call outtext(str)
  xdum=xr(1)
  IF(cal_done)xdum=1e7/calx(1)
Write(str,'(f7.3)')xdum
Call settextposition(x_row,x2_col,rc)
  Call outtext(str)
  Call clearline(30,30)
    dummy2 = settextcolor(13)
    dumchar='OLD FILE:'
```

```
  Call settextposition(30,x1_col,rc)
    Call outtext(dumchar)
  Call settextposition(30,x1_col+10,rc)
    Call outtext(oldname)
  dumchar='NEW FILE:'
    Call settextposition(30,dummy3,rc)
  Call outtext(dumchar)
    Call settextposition(30,dummy3+10,rc)
  Call outtext(filnam)
return
end


SUBROUTINE  PLOT
*_____*
*                                         *
*        plot the graph                   *
*                                         *
*_____*
INCLUDE 'fgraph.fd'
INCLUDE 'display.dat'
INCLUDE 'keycode.h'
INTEGER*2   dummy,dummy2,dummy3
Real*8    xx2,yy2
RECORD /wxycoord/  wxy
RECORD /xycoord/   xy
call clearscreen ($GCLEARSCREEN)  ! clear screen
dummy2=setcolor(nlc1)          ! set color for border
dummy2=settextcolor(ntc)       ! set color for text
call setvieworg(0,0,xy)
    dummy = rectangle($GBORDER,x1,y1,x2,y2)
      call setviewport(x1,y1,x2,y2)
    dummy = setwindow(.true.,xmin,ymax,xmax,ymin)
DO i=1,NUME
  xr(i)=dble(xdat(i))
    yr(i)=dble(ydat(i))
      dummy=setpixel_w(xr(i),yr(i))
  dummy2=setcolor(nlc2)      ! set color for line 1
  IF(i.EQ.1)then
    call moveto_w(xr(i),yr(i),wxy)
  ELSE
    dummy = lineto_w(xr(i),yr(i))
  ENDIF
END DO
IF(plotsim)then            ! Plot RET Simulation-call from retsim
icnta=1001
if(iodx)icnta=itwonum
DO i=1,icnta
  dummy3=setcolor(9)       ! set color RET SIMULATION
  xrr=dble(xft(i))
    yr(i)=dble(yft(i))
      dummy=setpixel_w(xrr,yr(i))
  IF(i.EQ.1)then
    call moveto_w(xrr,yr(i),wxy)
  ELSE
    dummy = lineto_w(xrr,yr(i))
  ENDIF
  END DO
If(.not.iodx)then
Do i=1,100            !plot marker lines
  xrr=dble(xps(i))
    yrr=dble(yps(i))
      call moveto_w(xrr,ymin,wxy)
    dummy = lineto_w(xrr,yrr)
END DO
ENDIF
ENDIF
IF(distwo)then            ! Display second file
DO i=1,itwonum
  xx2=dble(xcol(i))
    yy2=dble(ycol(i))
      dummy=setpixel_w(xx2,yy2)
  dummy2=setcolor(nlc4)      ! set color for third line
  IF(i.EQ.1)then
    call moveto_w(xx2,yy2,wxy)
  ELSE
    dummy = lineto_w(xx2,yy2)
  ENDIF
END DO
ENDIF
IF((moveone).or.(moveret))then          !Redraw Simulation Right/Left
DO i=1,jplus
  IF(moveone)xx2=dble(xcol(i))
  IF(moveret)xx2=dble(xft(i))
    yy2=dble(stpx(i))
      dummy=setpixel_w(xx2,yy2)
  dummy2=setcolor(nlc4)          ! set color for third line
```

```
      IF(i.EQ.1)then
        call moveto_w(xx2,yy2,wxy)
      ELSE
        dummy = lineto_w(xx2,yy2)
      ENDIF
      END DO
      ENDIF
*------------------------------------------*
*           draw the calibration line      *
*------------------------------------------*
      IF(.not.drawnocal)then
      y3=y1+int2((maxy*y1view/100.d0)*zscale/100.d0)
       call setviewport(x1,y1,x2,y3)
        dummy = setwindow(.true.,xmin,zmax,xmax,zmin)
       dummy2=setcolor(nlc3)   ! set color for line 2
      DO i=1,NUME
         zr(i)=dble(zdat(i))
          dummy=setpixel_w(xr(i),zr(i))
       IF(i.EQ.1)then
         call moveto_w(xr(i),zr(i),wxy)
       ELSE
         dummy=lineto_w(xr(i),zr(i))
       ENDIF
      ENDIF
      END DO
      call setviewport(x1,y1,x2,y2)
         dummy = setwindow(.true.,xmin,ymax,xmax,ymin)
      ENDIF
      plotsim=.false.
      Return
      End

      SUBROUTINE Dat_File(ix)
*------------------------------------------*
* This subroutine stores peaks and areas by simulating *
* lorentzian or gaussian fit                           *
*------------------------------------------*
      Include 'FGRAPH.FD'
      Include 'COLORS.H'
      Include 'ROW_COL.H'
      Include 'DISPLAY.DAT'
      Include 'KEYCODE.H'
      Integer    opt,opt2,ix,ka,xcur(100)
      Integer*2  dummy,dummy2,y4
      Real*4     ytemp(100),ydiff,yscale,ydum,temp
      Character  Menu1*78,Menu2*78,dumchar*13
      Character  str*7,str2*23,str4*24
      Logical    done,abort,wrtmsg
      Record /wxycoord/ wxy
      Record /rccoord/  rc,s
      curpos=ix
      ka=off
      baselin=0.0
      pkhgh=.true.
      peakmin=ymin
      abort=.false.
      done =.false.
      wrtmsg=.false.         !.true. when message on line 29
      Menu1 = 'F10 - Reset counter   F1 - Set Min peak   ESC -'//
     +     'Return to previous screen'
      Menu2 = 'S-Mark Peak    F-Auto Peak Finder   B- Baseline'//
     +     '     W-Write Data File'
      Call messg(Menu1, 1)
      Call messg(Menu2, 2)
      Do While( .not. Done )
       Call checkk( opt )
       SELECT CASE ( opt )
        CASE( $LFTAROW,$COMMA,$LT )    ! move Cursor left
         Call Curs_Lft(curpos)
        CASE( $RGTAROW,$PERIOD,$GT )   ! move Cursor right
         Call Curs_Rgt(curpos)
        CASE( $CAP_O, $o )     ! Call offscale
         Call Offscale
        CASE( $CAP_H, $h )     ! move Cursor right
         bbigstep=.true.
         Call Curs_Lft(curpos)
        CASE( $CAP_J, $j )     ! move Cursor left
         bigstep=.true.
         Call Curs_Lft(curpos)
        CASE( $CAP_L, $l )     ! move Cursor left
         bbigstep=.true.
         Call Curs_Rgt(curpos)
        CASE( $CAP_K, $k )     ! move Cursor left
         bigstep=.true.
         Call Curs_Rgt(curpos)
```

```
        CASE( $CAP_W,$w )      ! write file
         call addext(filnam,'mel')
         OPEN(51,FILE=fulnam,STATUS='UNKNOWN')
         Do i=1,ka
          IF(cal_done)then
            Write(51,*)calx(xcur(i)),ydat(xcur(i)),ytemp(i)
          ELSE
           temp=xdat(xcur(i))
           IF(xdat(xcur(i)).lt.1000.)temp=1e7/xdat(xcur(i))
           Write(51,*)temp,ydat(xcur(i)),ytemp(i)
          ENDIF
         END DO
      Menu1 = '       Writing peak locations and areas to file'
      Call messg(Menu1, 1)
       Call settextposition(1,60,s)
        Call outtext(FULNAM)
        close(51)
        CASE( $CAP_S,$s )      ! mark peak for fit and location
         ka=ka+1
          If(wrtmsg)then
            call axis
             wrtmsg=.false.
            ENDIF
            Call gauss(curpos)
            ytemp(ka)=yarea
            xcur(ka)=curpos
            dummy = setcolor(nlc1)    ! draw marker
           Call moveto_w(xr(curpos),ymin,wxy)
           y4=ymin+50
          dummy2 = lineto_w(xr(curpos),y4)
        CASE( $CAP_F,$f )      ! auto peak finder
       call cursor(curpos,0)
      Menu1 = ' Use '//CHAR(24)//' '//CHAR(25)//' to adjust for'//
     +     ' min peak height   ESC - Return to previous screen'
      Menu2 = ' Use '//CHAR(45)//' '//CHAR(43)//' to adjust'//
     +     ' scaling factor       Return - Find Peaks'
      Call messg(Menu1, 1)
      Call messg(Menu2, 2)
       pkhgh=.false.
       baselin=ydat(curpos)
       ydiff=ymax-ymin
       ydum=ydiff/4
       yscale=ydiff*0.05          ! step size for peak height
       ydelt=baselin+ydum
       call cursor(curpos,1)
       Do While( .not. pkhgh )      ! set peak height
        Call checkk( opt2 )
         SELECT CASE ( opt2 )
          CASE( $F1 )  !Set minpeak height for peak finder
           peakmin=ydat(curpos)
           dumchar='MIN PEAK -  '
            Call settextposition(2,61,s)
            Call outtext(dumchar)
            Write(str,'(f7.2)')peakmin
            Call settextposition(2,70,s)
           Call outtext(str)
          CASE( $UPAROW, $CAP_I, $i )
           olddel=ydelt
           ydelt=ydelt+yscale
           call cursor(curpos,0)
          CASE( $r )
           call refresh
           call messg(menu2,2)
          CASE( $DWNAROW, $CAP_M, $m )
           olddel=ydelt
           ydelt=ydelt-yscale
           IF(ydelt.lt.baselin)ydelt=baselin+yscale
           call cursor(curpos,0)
          CASE( $EQUAL, $PLUS)
           yscale=abs(yscale+10)
          CASE( $MINUS, $UNDRLIN)
           yscale=abs(yscale-10)
          CASE( $ESC,$CAP_Q,$q)
           call cursor(curpos,3)
           abort = .true.
           pkhgh = .true.
          CASE( $RETURN)
           call cursor(curpos,3)
           pkhgh = .true.
          CASE DEFAULT
         END SELECT
       END DO
       pkhgh = .true.
      IF(.not.abort)then
```

```
        ydelt=ydelt-baselin
        call peakloc
      ENDIF
     call cursor(curpos,1)
    abort=.false.
    Menu1 = 'F10 - Reset counter   F1 - Set Min peak   ESC -'//
   +      'Return to previous screen'
    Menu2 = 'S-Mark Peak     F-Auto Peak Finder   B- Baseline'//
   +      '     W-Write Data File'
    Call messg(Menu1, 1)
    Call messg(Menu2, 2)
     CASE( $r )
      call refresh
      call messg(menu2,2)
       CASE( $F10,$F9 )          ! delete data..reset counter
        ka=0
        Call clearline(30,30)
         dummy2 = settextcolor(messg_clr)
         Call settextposition(30,30,s)
         str4='All Data Points Deleted!'
         Call outtext(str4)
          str=' RESET '
          Call settextposition(2,47,s)
          Call outtext(str)
          wrtmsg=.true.
       CASE( $CAP_B,$b )         ! mark Baseline
         baselin=ydat(curpos)
         dumchar='BASELINE-  '
       Call settextposition(2,37,s)
         Call outtext(dumchar)
          Write(str,'(f7.2)')baselin
         Call settextposition(2,47,s)
          Call outtext(str)
       CASE( $F1 )              ! Set minpeak height for peak finder
        peakmin=ydat(curpos)
         dumchar='MIN PEAK -  '
       Call settextposition(2,61,s)
         Call outtext(dumchar)
          Write(str,'(f7.2)')peakmin
         Call settextposition(2,70,s)
          Call outtext(str)
       CASE( $DELETE )          ! delete last data point from file
        Do i=1,curpos
        If(ka.eq.0)goto 70
         ka=ka-1
         Call clearline(30,30)
          Call settextposition(30,25,rc)
           dummy2 = settextcolor(text_err_clr)
           wrtmsg=.true.
          str2='LAST DATA PEAK DELETED!'
          Call outtext(str2)
        End do
70      Continue
       CASE( $ESC,$CAP_Q,$q )     ! return to previous screen
        Done = .true.
       CASE DEFAULT
      END SELECT
     END DO
     CLOSE(51)
       If(wrtmsg)call axis
    Menu1 =' Use '//CHAR(27)//'  '//CHAR(26)//' keys to move'//
   +     ' cursor        ESC - Return to previous screen'
    Menu2 =' F10 - Enter RET Simulation Mode         '//
   +     '   C - Enter Calibration Mode'
     Call messg(Menu1, 1)
       Call messg(Menu2, 2)
     If(wrtmsg)call axis
    return
    end


    SUBROUTINE GAUSS(cp)

*-----------------------------------------------------*
*    Fit a lineshape to the data and calc area:  in this    *
*    case a lorentzian homogeneous broadened line          *
*-----------------------------------------------------*

    INCLUDE 'fgraph.fd'
    INCLUDE 'display.dat'
    INCLUDE 'keycode.h'
    INTEGER    cp,k,icnt,istp,imax
    INTEGER*2   dummy
    REAL*8    xdum,difflw,test,ddum,xpos,xplus,y
    REAL*8    a1,a2,yrep
    Logical    first
    RECORD /wxycoord/ wxy
```

```
    yarea = 0.0
    icnt = off
    first =.true.
    istp=10
    imax=nume-cp
     IF(imax.lt.10)istp=imax
     IF(imax.lt.2)return
     IF(cp.lt.10)istp=cp
    IF(cp.lt.2)return
    Do k=1,istp
    xpos=1e7/xdat(cp)
    IF(cal_done)xpos=calx(cp)
     xplus=1e7/xdat(cp+k)
    IF(cal_done)xplus=calx(cp+k)
     difflw=abs(xpos-xplus)      !Find the number of cursor positions
       ddum=glw/2          !which are closest to the line width
      icnt=k
       IF(ddum.lt.difflw)then
        a1=abs(ddum-test)
        a2=abs(difflw-ddum)
         IF(a1.lt.a2)then
          icnt=icnt-1
          goto 70
         Else
         goto 70
        ENDIF
       ENDIF
      test=difflw
    End Do
70   Continue
    xpos=1e7/xdat(cp)
    IF(cal_done)xpos=calx(cp)
     dummy = setcolor(15)
      IF(icnt.eq.0)icnt=1        !when stepsize>lzr line width
      Do j=cp-icnt,cp+icnt       ! icnt is counter for cursor position
       xdum=1e7/xdat(j)          !linewidth
       IF(cal_done)xdum=calx(j)
       yrep=ydat(j)
       If(baselin.gt.0)then
        IF(first)then
         yrep=baselin
         ELSEIF(j.eq.cp+icnt)then
         yrep=baselin
         ELSE
         yrep=ydat(j)
         ENDIF
        ENDIF
       y=yrep*(glw/2)**2/((xpos-xdum)**2+(glw/2)**2)
       dummy = setcolor(15)
      If(first)then
      If(baselin.gt.0)y=baselin
      Call moveto_w(xdat(j),y,wxy)
      First=.false.
     Else
      dummy2 = lineto_w(xdat(j),y)
     Endif
    Yarea=Yarea+y
    End Do
    Return
    End


    SUBROUTINE OFFSCALE

*----------------------------------------------------*
*                                                    *
*   This subroutine will attempt to fit offscale peaks   *
*   by fitting a lorentizian lineshape and adjusting Y data  *
*                                                    *
*----------------------------------------------------*

    Include 'FGRAPH.FD'
    Include 'COLORS.H'
    Include 'DISPLAY.DAT'
    Include 'KEYCODE.H'
    Integer   opt,check
    Integer*2  dummy
    REAL*8    temp,store
    CHARACTER str*7,dumchar*13
    Logical   done,first
    Record /rccoord/  s
    first=.true.
    done=.false.
    Do While( .not. Done )
     Call checkk( opt )
      SELECT CASE ( opt )
       CASE( $CAP_H, $h )          ! move Cursor right
         bbigstep=.true.
         Call Curs_Lft(curpos)
```

```
CASE( $CAP_J, $j )          ! move Cursor left
   bigstep=.true.
   Call Curs_Lft(curpos)
CASE( $CAP_L, $l )          ! move Cursor left
   bbigstep=.true.
   Call Curs_Rgt(curpos)
CASE( $CAP_K, $k )          ! move Cursor left
   bigstep=.true.
   Call Curs_Rgt(curpos)
CASE( $LFTAROW, $COMMA, $LT )   ! move Cursor left
   Call Curs_Lft(CurPos)
CASE( $RGTAROW, $PERIOD, $GT )  ! move Cursor right
   Call Curs_Rgt(CurPos)
CASE( $UPAROW, $CAP_I, $i)
   If(first)Temp=YDAT(curpos)
   first=.false.
   TEMP=TEMP+1
   dumchar=' Y data-  '
   dummy=settextcolor(ntc)     ! set color for text
   Call settextposition(2,37,s)
   Call outtext(dumchar)
   Write(str,'(f7.2)')temp
   Call settextposition(2,47,s)
   Call outtext(str)
CASE( $r)
   call refresh
CASE( $DWNAROW, $CAP_M, $m)
   If(first)Temp=YDAT(curpos)
   first=.false.
   TEMP=TEMP-1
   dumchar=' Y data-  '
   dummy=settextcolor(ntc)     ! set color for text
   Call settextposition(2,37,s)
   Call outtext(dumchar)
   dummy=settextcolor(ntc)     ! set color for text
   Write(str,'(f7.2)')temp
   Call settextposition(2,47,s)
   Call outtext(str)
CASE( $EQUAL, $PLUS)
   TEMP=TEMP+10
   dumchar=' Y data-  '
   dummy=settextcolor(ntc)     ! set color for text
   Call settextposition(2,37,s)
   Call outtext(dumchar)
   dummy=settextcolor(ntc)     ! set color for text
   Write(str,'(f7.2)')temp
   Call settextposition(2,47,s)
   Call outtext(str)
CASE( $MINUS, $UNDRLIN)
   TEMP=TEMP-10
   dumchar=' Y data-  '
   dummy=settextcolor(ntc)     ! set color for text
   Call settextposition(2,37,s)
   Call outtext(dumchar)
   Write(str,'(f7.2)')temp
   Call settextposition(2,47,s)
   Call outtext(str)
CASE( $y )
   ymax=TEMP
CASE( $CAP_S, $s)
   YDAT(check)=TEMP
CASE( $ESC,$CAP_Q,$q)
   Done=.true.
CASE( $RETURN)
   call refresh
   check=curpos
   store=ydat(curpos)
   ydat(curpos)=temp
   call gauss(curpos)
   ydat(curpos)=store
CASE DEFAULT
END SELECT
END DO
Return
End

$LARGE
$STORAGE: 2
$DEBUG
   SUBROUTINE DXSIM(short,rlong)
   implicit real*8 (b-h,n-z)
   implicit real*4 (a)
   integer*4 dlevel,xlevel,jd,jx,jp,jpp,J
   dimension dbconst(25),xterm(65),xbconst(50),xhconst(50)
   dimension xdconst(50),VO(30,50),Dlevel(35),Xlevel(35)
   logical  store,viblevel,range,more,spectro,frstrnd
   COMMON/SPECT/ spectro,idzum,ixzum,bec,dec,xec,yec,frstrnd
   data (dbconst(i),i=1,20)/0.020649,0.020605,0.020561,
   c0.020516,0.020472,0.020427,0.020382,0.020337,0.020292,0.020246,
   c0.020201,0.020155,0.020110,0.020064,0.020018,0.019972,0.019925,
   c0.019879,0.019833,0.019786/
   data (xterm(i),i=20,47)/4129.774,4316.736,4502.257,4686.322,
   c4868.917,5050.024,5229.627,5407.710,5584.255,5729.243,5932.657,
   c6104.475,6274.679,6443.247,6610.156,6775.385,6938.908,7100.702,
   c7260.740,7418.996,7575.441,7730.048,7882.785,8033.622,8182.528,
   c8329.47,8474.414,8617.324/
   data (xbconst(i),i=20,47)/0.0348628,0.0347295,0.0345948,0.0344590,
   c0.0343218,0.0341832,0.0340433,0.0339018,0.0337589,0.0336143,
   c0.0334680,0.033200,0.0331701,0.0330182,0.0328642,0.0327081,
   c0.0325496,0.0323887,0.0322252,0.0320589,0.0318898,0.0317176,
   c0.0315423,0.0313636,0.0311813,0.0309953,0.0308054,0.0306114/
   data (xdconst(i),i=20,47)/5.22,5.27,5.33,5.39,5.45,5.51,5.58,5.65,
   c5.73,5.81,5.89,5.98,6.07,6.17,6.27,6.38,6.49,6.61,6.74,6.87,7.01,
   c7.16,7.31,7.48,7.65,7.83,8.02,8.22/
   data (xhconst(i),i=20,47)/11.2,11.8,12.5,13.3,14.1,15.0,15.9,16.9,
   c18.0,19.2,20.5,21.9,23.4,25.0,26.7,28.6,30.6,32.8,35.1,37.6,40.3,
   c43.2,46.4,49.7,53.4,57.3,61.5,66.0/
   TE=41026.16614
   Y10=95.111746327
   Y20=-0.111495227
   Y30=-5.792874546e-4
   Y40=4.205281828e-6
   Y50=-1.408244378e-8
   Y60=2.68736882e-11
   Y70=-2.3114805e-14
   YD=4.43e-9
   IF(spectro)YD=3.63e-9-(yec/1e9)
   IF(.not.spectro)then
     xec=0.
     bec=0.
     dec=0.
     yec=0.
   ENDIF
   itst=999
   store=.false.
   range=.true.
   IF(short.gt.1100.)then
     temp=short
     short=temp/1e7
     temp=rlong
     rlong=temp/1e7
   ENDIF
   IF((short.GT.1000).or.(rlong.GT.1000))then
     cmshort=short
     cmrlong=rlong
     IF(short.LT.rlong)then
       temp=cmshort
       cmshort=cmrlong
       cmrlong=temp
     ENDIF
     GOTO 25
   ENDIF
   IF(short.GT.rlong)then
     temp=short
     short=rlong
     rlong=temp
   ENDIF
25 cmshort=1e7/short
   cmrlong=1e7/rlong
   offset=150.
26 continue
   i1=1
   i2=18
   i3=20
   i4=47
   icount=0
   IF(spectro)then
     i1=idzum      !D state low
     i2=idzum      !Dstate high
     i3=ixzum      !Xstate low
```

```
      i4=ixzum    !Xstate high          aRvis=R/2.
    ENDIF                               aPvis=P/2.
    Do 100 jp=i1,i2                     aPnm=1e7/aPvis
    Do 110 jpp=i3,i4                    aRnm=1e7/aRvis
    vp=jp+0.5              ******************************************
    v1=vp                 *                                        *
    v2=vp**2              *    Calculate intensity of the P and R branches   *
    v3=vp**3              *    Honl-London S(P)=J   S(R)=J+1        *
    v4=vp**4              ******************************************
    v5=vp**5                  aRstrgth=(xbconst(jx)*J*(J+1))-(xdconst(jx)/1e9)*(((J+1)*J)**2)
    v6=vp**6                  aPstrgth=(xbconst(jx)*J*(J-1))-(xdconst(jx)/1e9)*(((J-1)*J)**2)
    v7=vp**7                  IF(aRvis.LE.cmshort .and. aRvis.GE.cmrlong)then
    Bandor=Y10*v1+Y20*v2+Y30*v3+Y40*v4+Y50*v5+Y60*v6+Y70*v7    store = .true.
    VO(jp,jpp)=TE+Bandor-xterm(jpp)          ELSE
C    IF(.not.spectro)then                     aRvis=0.
C      IF(jp.eq.5)then                        aRnm=0.
C        VO(jp,jpp)=VO(jp,jpp)+0.10           ENDIF
C      ENDIF                             IF(aPvis.LE.cmshort .and. aPvis.GE.cmrlong)then
C      IF(jp.eq.6)then                        store = .true.
C        VO(jp,jpp)=VO(jp,jpp)+0.04           ELSE
C      ENDIF                                   aPvis=0.
C    ENDIF                                     aPnm=0.
**********************************************   ENDIF
*  wnrlong and wnshort are the calculated band origins within the region of  *   IF(store)then
*  interest....the input region is doubled      *      IF(aPvis.gt.0)write(5,16)J,aPstrgth,aPvis*2.
**********************************************      IF(aRvis.gt.0)write(5,16)J+500,aRstrgth,aRvis*2.
    wnrlong=2*cmrlong                14    FORMAT(4X,I4,4X,I4,4X,I4)
    wnshort=2*(cmshort+offset)       15    FORMAT(4X,F10.4,4X,F10.4)
    IF((VO(jp,jpp).LE.wnshort).and.(VO(jp,jpp).GE.wnrlong))then   16    FORMAT(4X,I4,4X,E12.6,2X,F10.4)
    icount=icount+1                        store = .false.
    Dlevel(icount)=jp                      viblevel = .false.
    Xlevel(icount)=jpp                     range = .false.
    if(icount.gt.30)goto 28                ENDIF
    ENDIF                             1    continue
110  continue                        2    continue
100  continue                             IF(.not.spectro)endfile 5
28   IF(icount.gt.30)then                 return
    offset=offset-10.                     end
    goto 26
    ENDIF                            SUBROUTINE DXSIMTWO(datanm,alw)
    IF((spectro).and.(.not. frstrnd))then
    open(unit=5,file='DXPOS.dat',access='append',status='unknown')   *_____*
    ELSE                             *                                              *
    open(unit=5,file='DXPOS.dat',status='unknown')   *  This program simulates I2 D-X spectra for the high-lying vibrational *
    ENDIF                            *  levels of ground state iodine               *
    more=.false.                     *_____*
    Do 2 i=1,icount
    viblevel=.true.                       INCLUDE 'display.dat'
    jd=Dlevel(i)                          integer  datanm,idummy,icount(35)
    jx=Xlevel(i)                          integer  jcnt(31,100),ins
    IF(.not.spectro)then                  integer*4 idstate(40),ixstate(40),icnt,jj,k,m
      IF(range)write(5,15)cmshort,cmrlong   real*4   alw,s,ss,xj(31,100),FCFDX(400),mean
      IF(range)write(5,14)itst,jd,jx        real*4   xhgh,xlw,xhigh,xlow,xpos(31,100)
      IF(i.gt.1)more=.true.                 real*4   yr2(100),yp(100),yy,yyr,yst(32,1510)
      IF((viblevel).and.(more))then         real*8   FCF(40),xst,xx,sigma,boltz,xboltz,gauss,distro
        write(5,14)itst,jd,jx               logical  range,more,calcnm,even
        write(5,13)jd,jx                    Common /DX_SIM/ yst,FCF,idstate,ixstate
        ENDIF                               range=.true.
      ELSEIF(spectro)then                   calcnm=.true.
      if(frstrnd)write(5,15)cmshort,cmrlong  Do j=1,20
      if(frstrnd)write(5,14)itst,jd,jx       pop(j)=0.1
      if(.not.frstrnd)write(5,14)itst,jd,jx  END DO
      if(.not.frstrnd)write(5,13)jd,jx       Do j=1,32
      frstrnd=.false.                        tmpr(j)=478.
      ENDIF                                 END DO
13   FORMAT(4X,I4,4X,I4)                    IF(datanm.EQ.0)calcnm=.false.
    Do 1 J=1,150                          Open(unit=5,FILE='DXPOS.DAT',ACCESS='SEQUENTIAL')
    Y=J*(J+1)                             Rewind(5)
    xdum=xbconst(jx)                      IF(range)then
    IF(spectro)xdum=xbconst(jx)-xec        Read(5,16)xhgh,xlw
    X=Y*xdum-(xdconst(jx)/1e9)*Y*Y+(xhconst(jx)/1e16)*Y*Y*Y    Read(5,14)idummy,idstate(1),ixstate(1)
    Y=J*(J-1)                        14    FORMAT(4X,I4,4X,I4,4X,I4)
    xdum=dbconst(jd)                       xhigh=xhgh*2.
    xdum2=VO(jd,jx)                        xlow=xlw*2.
    IF(spectro)xdum=dbconst(jd)-dec        range=.false.
    IF(spectro)xdum2=VO(jd,jx)-bec         ENDIF
    IF(.not.spectro)then                  icnt=0
C      IF(jd.eq.4)YD=2.6e-9               more=.true.
C      IF(jd.eq.7)YD=4.43e-9              Do 11 k=1,35
C      IF(jd.eq.10)YD=4.2e-9             icnt=icnt+1
      ENDIF                              m=0
    P=xdum2+Y*xdum-YD*Y*Y-X              Do 10 i=1,100          !assume less than 100 lines per band
    Y=(J+1)*(J+2)                         IF(more)icount(k)=0    !of a typical scan
    R=xdum2+Y*xdum-YD*Y*Y-X              more=.false.
                                         Read(5,15,END=36)jcnt(k,i),xj(k,i),xpos(k,i)
                                         IF(jcnt(k,i).eq.999)then
                                          m=k+1
                                          Read(5,13)idstate(m),ixstate(m)
```

```
13    Format(4X,I4,4X,I4)
        more=.true.
        goto 35
      ENDIF
      If(jcnt(k,j).gt.0)icount(k)=icount(k)+1
15    FORMAT(4X,I4,4X,E12.6,2X,F10.4)
16    FORMAT(4X,F10.4,4X,F10.4)
10    continue
35    continue
11    continue
36    continue
      iband=icnt+1
      xst=(xhigh-xlow+alw)/1498.
      js=0
      Do j2=1,150
      js=js+1
      END DO
      DO 90 k=1,icnt
      xx=xlow
      DO 91 j=1,icount(k)        !icount=number of P and R lines in band
      IF(jcnt(k,j).lt.499)then
        ins=(-1)**jcnt(k,j)
        ELSE
        jct=jcnt(k,j)-500
        ins=(-1)**jct
      ENDIF
      IF(ins.lt.0)then           !nuclear spin statistics
      even=.false.
      s=7./12.       !s=7/12
      Else
      s=5./12.       !s=5/12
      even=.true.
      ENDIF
      IF(ins.lt.0)then
      even=.true.
      ss=5./12.      !ss=5/12
      ELSE
      ss=7./12.      !ss=7/12
      even=.false.
      ENDIF
      yr2(j)=0.0
      yp(j)=0.0
      boltz=0.6952*tmpr(ixstate(k))
      IF(jcnt(k,j).lt.499)then
        jj=jcnt(k,j)
        xboltz=exp(-xj(k,j)/boltz)   !boltzmann distribution
        mean=js/totJ(ixstate(k))     !gaussian
        gauss=(ah/PI)**0.5*exp(-ah*(jj-mean)**2)
        distro=xboltz
        IF(gowss)distro=gauss
        yp(j)=s*jj*(2*jj+1)*distro
C       If(even) yp(j)=s*jj*(2*jj+1)*xboltz
C       IF(.not.even) yp(j)=s*jj*(2*jj+1)*xboltz*1.3
      ENDIF
      IF(jcnt(k,j).ge.500)then
        jj=jcnt(k,j)-500
        xboltz=exp(-xj(k,j)/boltz)
        mean=js/totJ(ixstate(k))     !gaussian
        gauss=(ah/PI)**0.5*exp(-ah*(jj-mean)**2)
        distro=xboltz
        IF(gowss)distro=gauss
        yr2(j)=ss*(jj+1)*(2*jj+1)*distro
C       If(even) yr2(j)=ss*(jj+1)*(2*jj+1)*xboltz
C       IF(.not.even) yr2(j)=ss*(jj+1)*(2*jj+1)*xboltz*1.3
      ENDIF
91    continue
      Do 80 i=1,1501
      xx=xx+xst
      yy=0.0
      yyp=0.0
      yyr=0.0
      Do ja=1,icount(k)          !sum for the R lines
      IF(yr2(ja).gt.0)then
      if(abs(xpos(k,ja)-xx).gt.(3*alw)) goto 81
      IF(LORENTZ)then
      yyr=yy+yr2(ja)*(1./PI)*(alw/2.)/((xx-xpos(k,ja))**2.+(alw/2.)**2)
      ELSE
      sigma=1/((alw/2.)*(2.*PI)**0.5)
      yyr=yy+yr2(ja)*sigma*exp(-0.5*((xx-xpos(k,ja))/(alw/2.))**2)
      ENDIF
      yy=yy+yyr
      ENDIF
81    IF(yp(ja).gt.0)then
      if(abs(xpos(k,ja)-xx).gt.(3.*alw)) goto 82
```

```
      IF(LORENTZ)then
      yyp=yy+yp(ja)*(1./PI)*(alw/2.)/((xx-xpos(k,ja))**2+(alw/2.)**2)
      ELSE
      sigma=1./((alw/2.)*(2.*PI)**0.5)
      yyp=yy+yp(ja)*sigma*exp(-0.5*((xx-xpos(k,ja))/(alw/2.))**2)
      ENDIF
      yy=yy+yyp
      ENDIF
82    continue
      END DO
      m=k+1
      yst(m,i)=yy
      IF(k.eq.1)then
        IF(.not.calcnm)then
        yst(1,i)=xx
        ELSE
        yst(1,i)=1e7/xx*2.
        ENDIF
      ENDIF
80    continue
90    continue
      jk=0
      Open(unit=13,FILE='FCF.DAT',STATUS='old')
      Do 34 jc=1,328
      READ(13,19,END=37)FCFdum
      IF(FCFdum.lt.1)then
        jk=jk+1
        FCFDX(jk)=FCFdum
      ENDIF
34    continue
37    continue
19    Format(F11.5)
      Close(13,status='keep')
      k=0
      DO 44 m=1,icnt
      k=m+1
      IF((ixstate(m).lt.30).and.(idstate(m).ge.10))then
      IF(idstate(m).eq.10)FCF(k)=1.0e-4
      IF(idstate(m).eq.11)FCF(k)=1.0e-4
      IF(idstate(m).eq.12)FCF(k)=1.0e-4
      IF((idstate(m).eq.13).and.(ixstate(m).eq.29))FCF(k)=1.6835e-3
      IF((idstate(m).eq.13).and.(ixstate(m).le.28))FCF(k)=1.0e-4
      IF((idstate(m).eq.14).and.(ixstate(m).eq.28))FCF(k)=1.312e-3
      IF((idstate(m).eq.14).and.(ixstate(m).eq.29))FCF(k)=3.108e-3
      IF((idstate(m).eq.14).and.(ixstate(m).le.27))FCF(k)=1.0e-4
      IF((idstate(m).eq.15).and.(ixstate(m).eq.27))FCF(k)=9.849e-4
      IF((idstate(m).eq.15).and.(ixstate(m).eq.28))FCF(k)=2.418e-3
      IF((idstate(m).eq.15).and.(ixstate(m).eq.29))FCF(k)=5.301e-3
      IF((idstate(m).eq.15).and.(ixstate(m).le.26))FCF(k)=1.0e-4
      IF((idstate(m).eq.16).and.(ixstate(m).eq.27))FCF(k)=1.815e-3
      IF((idstate(m).eq.16).and.(ixstate(m).eq.28))FCF(k)=4.143e-3
      IF((idstate(m).eq.16).and.(ixstate(m).eq.29))FCF(k)=8.368e-3
      IF((idstate(m).eq.16).and.(ixstate(m).le.26))FCF(k)=1.0e-4
      IF((idstate(m).eq.17).and.(ixstate(m).eq.26))FCF(k)=1.312e-3
      IF((idstate(m).eq.17).and.(ixstate(m).eq.27))FCF(k)=3.129e-3
      IF((idstate(m).eq.17).and.(ixstate(m).eq.28))FCF(k)=6.614e-3
      IF((idstate(m).eq.17).and.(ixstate(m).eq.29))FCF(k)=1.223e-2
      IF((idstate(m).eq.17).and.(ixstate(m).le.25))FCF(k)=1.0e-4
      IF(idstate(m).ge.18)FCF(k)=1.0e-4
        goto 41
      ENDIF
      IF(idstate(m).gt.15)then
        FCF(k)=1.0e-4
        goto 41
      ENDIF
      IF((ixstate(m).lt.30).or.(ixstate(m).gt.47))then
        FCF(k)=1.0e-6
        goto 41
        ENDIF
      jf=((idstate(m)*18)+(ixstate(m)-30))+1
      FCF(k)=FCFDX(jf)
41    continue
44    continue
      close (5)
      return
      end

      SUBROUTINE DXONETIME(nex,wgh,first,id,ix,fdum,fit_all)
*-------------------------------------------------------------------*
*    This program simulates I2 D-X spectra for the high-lying vibrational *
*    levels of ground state iodine one level at a time using scale factor *
*-------------------------------------------------------------------*
      INCLUDE 'display.dat'            !nex-do next band
      integer*4 id,ix,idstate(40),ixstate(40),numne2    !first-first time
```

```
      integer*4 j,jb,k,iex
      real*4  xdummy,ydummy,ysim,yst(32,1510)        !id-v of d state
      real*4  ymaxtemp,ymaxsim
      real*8  fdum,wgh,wegh(40),FCF(40)              !ix-v of x state
      logical nex,wrte,first,fit_all                 !fdum- fcf
      Common /DX_SIM/ yst,FCF,idstate,ixstate
      !inumq steps the simulation through each band determined in
      !subroutine DXSIMTWO
      IF(first)then          !finds ymax for all band in simulation
        ymaxsim=0.
        Do k=2,iband
          Do j=1,1501                    !loads y
            ycol(j)=yst(k,j)*FCF(k)*pop(ixstate(k-1))
          END DO
          nume2=1500          !find max and min of simulation
          call minmax(ycol,nume2,xdummy,ydummy)
          ymaxtemp=dble(ydummy)
          IF(ymaxtemp.gt.ymaxsim)ymaxsim=ymaxtemp
        ENDDO
      ENDIF
91    wrte=.false.           !logical.true. when all bands viewed
      IF(fit_all)nex=.true.
      IF(nex)inumq=inumq+1         !logical nex allows new
        fdum=FCF(inumq)
      IF(inumq.gt.iband)goto 37
      id=idstate(inumq-1)
      ix=ixstate(inumq-1)
      wegh(inumq)=wgh                     !weight for band
      Do j=1,1501                         !loads x and y
        ycol(j)=yst(inumq,j)*FCF(inumq)*wegh(inumq)*pop(ix)
        xcol(j)=yst(1,j)
        END DO
        Do jb=1,1501              !scale intensity of simulation
        ycol(jb)=(((ymax-ymin)/ymaxsim)*ycol(jb))+ymin
      END DO
      first=.false.
                              !sum all bands and write file
37    IF((fit_all).and.(inumq.LE.iband))goto 91
      IF(inumq.GT.iband)then
        open(unit=9, file='simdx.dat',status='unknown')
        wrte=.true.
      ENDIF
      Do j=1,1501
        ysim=0.
        Do k=2,inumq-1        !sum all y's for each x
        iex=ixstate(k-1)
        ysim=ysim+yst(k,j)*FCF(k)*wegh(k)*pop(iex)
        END DO
        xft(j)=yst(1,j)
        yft(j)=ysim
        IF(inumq.GT.iband) xcol(j)=yst(1,j)
        IF(inumq.GT.iband) ycol(j)=ysim
      END DO
        Do jb=1,1501          !scale intensity of simulation
        yft(jb)=(((ymax-ymin)/ymaxsim)*yft(jb))+ymin
        END DO
      IF(inumq.GT.iband)then
        call minmax(ycol,nume2,xdummy,ydummy)
        ymaxsim=dble(ydummy)
        Do jb=1,1501          !scale intensity of simulation
        ycol(jb)=(((ymax-ymin)/ymaxsim)*ycol(jb))+ymin
        write(9,16)xcol(jb),ycol(jb)
        END DO
        close (9)
        plotsim=.false.
        fit_all=.false.
      ENDIF
16    FORMAT(4X,F16.4,4X,F16.6)
      IF(wrte)then
        Open(unit=8,FILE='DXPOS.FCF',status='UNKNOWN')
        Do i=1,iband-1
        write(8,*)'D state -',idstate(i),'   X-',ixstate(i),
     C' weight',wegh(i+1)
        write(8,*)' FCF',FCF(i+1),'  Population', pop(ixstate(i))
        write(8,*)
        END DO
        Close(8)
      ENDIF
99    return
      end
```

```
$STORAGE:2
$INCLUDE:'FGRAPH.FI'
$DEBUG
      SUBROUTINE RETDRAW(ids,ixs,jlvl,blin,rate,press)
*_____*
*                                                 *
*   A Graphics Program which fits and simulates rotational energy *
*   transfer data from the SEP experiment and recorded in the     *
*   LAMBDA programs from the Laboratory of M. C. HEAVEN.          *
*   Source Code by  M. Nowlin  Sep 93    modified Mar 94          *
*_____*
      Include 'FGRAPH.FD'
      Include 'DISPLAY.DAT'
      Include 'KEYCODE.H'
      Integer  opt,jlvl,SSDeg
      Integer*2 iddum,ixdum,dummy,kx,kd,sto1,sto2,sto3,sto4,sto5
      REAL*4  chg,rattmp,ratc,ratal,ratap,ratalw,ratt,scale
      REAL*4  xfit,yfit,press,dumchg
      REAL*8  rettmp,retc,retal,retap,retalw,rett,blin,dume
      REAL*8  large,xpos,ypos,ainv,begin,end,rte,rate,al2s
      REAL*8  rotrana,rotranb,rotranc,rotrand,rotrane,rotranf
      Character str*2,str1*5,str2*4,str3*6,str4*3,str6*15,str7*20
      Logical  doagain,done,plus,sub,first,prostp,IPL,twoslope,sa
      Dimension yfit(3005),xfit(3005),ypos(110),xpos(110)
      Common /RET_SIM/ xfit,yfit,iddum,ixdum,xpos,ypos,IPL,SSDeg,scale
      Common /PAR_SIM/ rettmp,retc,retal,retap,retalw,rett,al2s,twoslope
      Common /RET_LAB/ rattmp,ratc,ratal,ratap,ratalw,ratt,kx,kd
      Common /RET_OUT/ rotrana,rotranb,rotranc,rotrand,rotrane,rotranf
      RECORD /rccoord/ s
      sto1=nlc1        !remember colors for printing graphics
      sto2=nlc2        !load 'graphics laserjetII'
      sto3=nlc3
      sto4=nlc4
      sto5=ntc
      al2s=0.
      first=.true.
      twoslope=.false.
      sa=.false.
      dume=1.0
      scale=1.0
      SSDeg=SDeg                 !pass spin degeneracy choice to RETSIM
      ainv=1.0            !inverse power fit alpha=1.0
      IPL=inverse         !pass logical for inverse fit to RETSIM
      iddum=ids
      kd=iddum
      ixdum=ixs
      kx=ixs
      y2max=ymax
      rotrana=rottmp
      rotranb=rotc
      rotranc=rotal
      rotrand=rotap
      rotrane=rotalw
      rotranf=rott
      begin=xdat(nume)
      end=xdat(1)
      IF(cal_done)then
        begin=calx(1)
        If(calx(1).eq.0)begin=xdat(nume)
        end=calx(nume)
        If(calx(nume).eq.0)end=xdat(1)
      ENDIF
      If(end.LT.9000.)end=1e7/xdat(1)
      If(begin.LT.9000.)begin=1e7/xdat(nume)
      If(begin.LT.end)then
        temp=begin
        begin=end
        end=temp
      ENDIF
      rte=press*3.24e4*rate  !3.24e4 = 3.24e13 molecc/mTorr* 1e-9 s/nanos
100   call retsim(ids,ixs,jlvl,baselin,first,ainv,begin,end,rte,sa)
      first=.false.
      large=1e-2
      DO i=1,1501
        xft(i)=xfit(i)
        yft(i)=yfit(i)
        large=DMAX1(large,yfit(i))
      END DO
      scaldiff=large-blin
      scalfact=y2max/scaldiff
      DO i=1,1501
        ytemp=yft(i)-blin
        yft(i)=ytemp*scalfact+blin
      END DO
      Do i=1,100
```

```
        yps(i)=ypos(i)                                          call settextposition(2,31,s)
        xps(i)=xpos(i)                                          call outtext(str3)
       END DO                                                 CASE( $FOUR )
        plotsim=.true.                                          chg=1.0
       call plot                                                prostp=.true.
       call axis                                                str3='chg'
        rattmp= rettmp                                          call settextposition(2,27,s)
        ratc=retc                                               call outtext(str3)
         ratal=retal                                          Write(str3,'(f6.2)')chg
         ratap=retap                                            call settextposition(2,31,s)
         ratalw=retalw                                          call outtext(str3)
        ratt=rett                                             CASE( $FIVE )
       call retlabel                                            chg=10.
       chg=0.1                                                  prostp=.true.
       sub=.false.                                              str3='chg'
       plus=.true.                                              call settextposition(2,27,s)
       dummy=settextcolor(15)                                   call outtext(str3)
       doagain=.false.                                        Write(str3,'(f6.2)')chg
       done=.false.                                             call settextposition(2,31,s)
       prostp=.false.                                           call outtext(str3)
       jplus=0                                                CASE( $SIX )
       jminus=0                                                 chg=25.
       jpcnt=0                                                  prostp=.true.
       Do While( .not. done )                                   str3='chg'
        Call checkk( opt )                                      call settextposition(2,27,s)
         SELECT CASE ( opt )                                    call outtext(str3)
          CASE( $CAP_W, $w )          ! write file           Write(str3,'(f6.2)')chg
           call addext(filnam,'sim')                           call settextposition(2,31,s)
           OPEN(75,FILE=fulnam,STATUS='UNKNOWN')               call outtext(str3)
            write(75,*)ids,ixs,jlvl,baselin                   CASE( $SEVEN )
            write(75,73)rettmp,retc,retal                      retc=retc/10
            write(75,73)retap,retalw,rett                       ratc=retc
73          format(1X,F8.4,2X,F8.4,2X,F8.4)                    Write(str3,'(f6.3)')ratc
            If(cal_done)then                                   call settextposition(1,21,s)
             Do j=1,1501                                       call outtext(str3)
             ja=j                                            CASE( $LFTAROW )  ! change scale
             IF(ja.gt.nume)ja=nume                             IF(plus)scale=scale+chg
              If(calx(ja).gt.1200)calx(ja)=1e7/calx(ja)        IF(sub) scale=scale-chg
             write(75,54)xfit(j),yfit(j),calx(ja),ydat(ja)     IF(scale.lt.0.01) scale=0.01
             END DO                                            call clearline(30,25)
            Elseif(aufset)then                                 str7='Scale
             Do j=1,1501                                       call settextposition(30,50,s)
             ja=j                                              call outtext(str7)
             IF(ja.gt.nume)ja=nume                            Write(str3,'(f6.2)')scale
              If(xoff(ja).gt.1200.)xoff(ja)=1e7/xoff(ja)       call settextposition(30,58,s)
             write(75,54)xfit(j),yfit(j),xoff(ja),ydat(ja)     call outtext(str3)
             END DO                                          CASE( $RGTAROW )  ! move Cursor right
            Else                                             CASE( $COMMA, $LT )
             Do j=1,1501                                       sub=.true.
             write(75,*)xfit(j),yfit(j)                        plus=.false.
             END DO                                          CASE( $PERIOD, $GT )
            ENDIF                                              plus=.true.
54          Format(2(F8.4,2X,F10.4,2X))                        sub =.false.
          CASE( $CAP_J, $j )        ! move Cursor left       CASE( $F1 )
           bigstep=.true.                                      IF(prostp)then
           Call Curs_Lft(curpos)                               IF(plus)rettmp=rettmp+chg
          CASE( $CAP_K, $k )           ! move Cursor right     IF(sub) rettmp=rettmp-chg
           bigstep=.true.                                      ELSE
           Call Curs_Rgt(curpos)                               IF(plus)rettmp=rettmp+1
          CASE( $ONE )                                         IF(sub) rettmp=rettmp-1
           chg=0.001                                           ENDIF
           prostp=.true.                                       rattmp=rettmp
           str3='chg'                                         Write(str1,'(f5.1)')rattmp
           call settextposition(2,27,s)                        call settextposition(1,10,s)
           call outtext(str3)                                  call outtext(str1)
          Write(str3,'(f6.3)')chg                            CASE( $F2 )
           call settextposition(2,31,s)                        IF(prostp)then
           call outtext(str3)                                  IF(plus)retc=retc+chg
          CASE( $TWO )                                         IF(sub) retc=retc-chg
           chg=0.01                                            ELSE
           prostp=.true.                                       IF(plus)retc=retc+0.1
           str3='chg'                                          IF(sub) retc=retc-0.1
           call settextposition(2,27,s)                        ENDIF
           call outtext(str3)                                  ratc=retc
          Write(str3,'(f6.2)')chg                             Write(str3,'(f6.3)')ratc
           call settextposition(2,31,s)                        call settextposition(1,21,s)
           call outtext(str3)                                  call outtext(str3)
          CASE( $THREE )                                     CASE( $F3 )
           chg=0.1                                             dumchg=10.0
           prostp=.true.                                       IF(SSDEG.eq.5)dumchg=1.0
           str3='chg'                                          IF(prostp)then
           call settextposition(2,27,s)                        IF(plus)retal=retal+chg
           call outtext(str3)                                  IF(sub) retal=retal-chg
          Write(str3,'(f6.2)')chg                              ELSE
```

```
            IF(plus)retal=retal+dumchg
            IF(sub) retal=retal-dumchg
           ENDIF
            ratal=retal
            Write(str3,'(f6.2)')ratal
            call settextposition(1,33,s)
            call outtext(str3)
          CASE( $F4 )
           IF(prostp)then
            IF(plus)retap=retap+chg
            IF(sub) retap=retap-chg
           ELSE
            IF(plus)retap=retap+0.01
            IF(sub) retap=retap-0.01
           ENDIF
            ratap=retap
            IF(inverse)ainv=retap
            Write(str2,'(f4.2)')ratap
           call settextposition(1,46,s)
          call outtext(str2)
          CASE( $F5 )
          IF(prostp)then
            IF(plus)retalw=retalw+chg
            IF(sub) retalw=retalw-chg
            ELSE
            IF(plus)retalw=retalw+0.01
            IF(sub) retalw=retalw-0.01
           ENDIF
            ratalw=retalw
            Write(str2,'(f4.2)')ratalw
            call settextposition(1,56,s)
           call outtext(str2)
          CASE( $F6 )
          IF(prostp)then
            IF(plus)rett=rett+chg
            IF(sub) rett=rett-chg
           ELSE
            IF(plus)rett=rett+50
            IF(sub) rett=rett-50
           ENDIF
            rett=rett
            Write(str1,'(f5.1)')rett
            call settextposition(1,70,s)
            call outtext(str1)
          CASE( $CAP_X,$x)
            IF(plus)ixdum=ixdum+1
            IF(sub) ixdum=ixdum-1
            Write(str4,'(i3)')ixdum
            call settextposition(2,22,s)
           call outtext(str4)
          CASE( $CAP_D,$d)
            IF(plus)iddum=iddum+1
            IF(sub) iddum=iddum-1
            Write(str,'(i2)')iddum
            call settextposition(2,10,s)
            call outtext(str)
          CASE( $ALT_R)
          IF(.not.sa)then
            sa=.true.
           ELSE
            sa=.false.
           ENDIF
          CASE( $CAP_A,$a)
            y2max=ydat(curpos)
             doagain =.true.
            done=.true.
          CASE( $CAP_T,$t)
           IF(.not.twoslope)then
            twoslope=.true.
            ELSE
            twoslope=.false.
           ENDIF
          CASE( $CAP_B,$b)
           IF(twoslope)then
           IF(prostp)then
            IF(plus)dume=dume+chg
            IF(sub) dume=dume-chg
           ELSE
            IF(plus)dume=dume+0.01
            IF(sub) dume=dume-0.01
           ENDIF
            al2s=dume
            str2='ap2-'
            call settextposition(2,39,s)
```

```
            call outtext(str2)
            Write(str2,'(f4.2)')al2s
            call settextposition(2,43,s)
            call outtext(str2)
           ENDIF
          CASE( $CAP_I,$i)
           inverse=.true.
          CASE( $CAP_N,$n)
           IF(plus)SSDeg=SSDeg+1
           IF(sub) SSDeg=SSDeg-1
           IF(SSDeg.LT.1)SSDeg=1
           IF(SSDeg.GT.6)SSDeg=6
           str6='Spin Degeneracy'
           call clearline(30,25)
           call settextposition(30,27,s)
           call outtext(str6)
           Write(str,'(i2)')SSDeg
           call settextposition(30,43,s)
           call outtext(str)
          CASE($CAP_S,$s)
           IPL=.false.
           inverse=.false.
          CASE($CAP_C,$c)
           drawnocal=.true.
          CASE($CAP_P,$p)
            nlc1=col1
             nlc2=col2
              nlc3=col3
               nlc4=col4
               nto=col5
               doagain =.true.
              done=.true.
          CASE( $F9 )              ! big step for temp (100)
           prostp=.false.
          CASE( $F10)
            doagain =.true.
            done=.true.
          CASE( $ESC,$CAP_Q,$q)
            done = .true.
          CASE( $F7 )
           If(jminus.gt.0)jminus=jminus-1
          CASE( $F8 )
           If(jpcnt.gt.0)jpcnt=jpcnt-1
          CASE( $EQUAL, $PLUS)         !step RET display right
            j=0
            jminus=jminus+1
            Do k=1,1501
             stpx(k)=0.
            END DO
            Do k=jminus,1501
            j=j+1
             stpx(j)=yfit(k)
            END DO
            jplus=j
            jpcnt=jminus
             moveret=.true.
            call refresh
            moveret=.false.
            call retlabel
          CASE( $MINUS, $UNDRLIN)  !step RET display left
          jpcnt=jpcnt+1
          j=0
            Do k=1,1501
             stpx(k)=0.
            END DO
            Do k=jpcnt,1501
             j=j+1
             stpx(k)=yfit(j)
            END DO
            jminus=jpcnt
            jplus=1501
            moveret=.true.
            call refresh
            moveret=.false.
            call retlabel
           CASE DEFAULT
          END SELECT
         END DO
       IF(Doagain)goto 100
       Drawnocal=.false.
         nlc1=sto1
         nlc2=sto2
          nlc3=sto3
          nlc4=sto4
```

```
        ntc=sto5
      RETURN
      END

      SUBROUTINE RETLABEL
*----------------------------------------*
*  This routine places labels at top of RET plot   *
*----------------------------------------*
      Include 'FGRAPH.FD'
      Include 'DISPLAY.DAT'
      INTEGER*2    kd,kx,dummy
      REAL*4       rattmp,ratc,ratal,ratap,ratalw,ratt
      CHARACTER    Menu3*78,Menu4*78,str*2,str1*5,str2*4,str4*3
      CHARACTER    str3*6,str5*23
      COMMON /RET_LAB/ rattmp,ratc,ratal,ratap,ratalw,ratt,kx,kd
      RECORD /rccoord/ s,rc
      dummy=settextcolor(14)
      Menu3 = 'D-STATE    X-STATE                    '//
     +   ' W-Write File  F10-RUN '
      Menu4 = 'F1-Temp     F2-C      F3-AL     F4-AP '//
     +   ' F5-LW    F6-TIME    '
      IF(inverse)then
        str5 = '   Inverse Power Fit'
       ELSE
        str5 = ' Statistical Power Fit '
       ENDIF
       call settextposition(29,19,rc)
       call outtext (str5)
       call messg(menu4,1)
        call messg(menu3,2)
         Write(str1,'(f5.1)')rattmp
          call settextposition(1,10,s)
          call outtext(str1)
           Write(str3,'(f6.3)')ratc
          call settextposition(1,21,s)
          call outtext(str3)
          Write(str3,'(f6.2)')ratal
          call settextposition(1,33,s)
          call outtext(str3)
           Write(str2,'(f4.2)')ratap
           call settextposition(1,46,s)
           call outtext(str2)
          Write(str2,'(f4.2)')ratalw
          call settextposition(1,56,s)
          call outtext(str2)
           Write(str1,'(f5.1)')ratt
           call settextposition(1,70,s)
           call outtext(str1)
           Write(str,'(i2)')kd
         call settextposition(2,10,s)
         call outtext(str)
        Write(str4,'(i3)')kx
        call settextposition(2,22,s)
       call outtext(str4)
       Return
       End


      SUBROUTINE RETSIM(ids,ixs,jlvl,blin,first,ainv,begin,end,rte,sa)
*----------------------------------------*
*  This routine simulates RET using statistical power gap   *
*----------------------------------------*
      implicit real*8(a-h,o-z)
      integer    i,ji,ii,jj,jr,jp,jlvl,jcount,jl,SSDeg
      integer*2  ids,ixs,iddum,ixdum,istep
      integer*4  i0low,i0hi,i1low,i1hi
      real*4     scale,xfit,yfit,step
      dimension an(3),ak(200),z(200),x(200),yfit(3005),xfit(3005)
      dimension xterm(45),dterm(44),xbconst(45),dbconst(40)
      dimension xpos(110),ypos(110),xtemp(100),ztemp(100)
      logical   first,rgtonce,IPL,twoslope,hybrid,sa
      Common /RET_SIM/ xfit,yfit,iddum,ixdum,xpos,ypos,IPL,SSDeg,scale
      Common /PAR_SIM/ rettmp,retc,retal,retap,retalw,rett,al2s,twoslope
      Common /RET_OUT/ rotrana,rotranb,rotranc,rotrand,rotrane,rotranf
      data (xterm(i),i=20,42)/4129.774,4316.736,4502.257,4686.322,
     c4868.917,5050.024,5229.627,5407.710,5584.255,5729.243,5932.657,
     c6104.475,6274.679,6443.247,6610.156,6775.385,6938.908,7100.702,
     c7260.740,7418.996,7575.441,7730.048,7882.785/
      data (xbconst(i),i=20,42)/0.0348628,0.0347295,0.0345948,0.0344590,
     c0.0343218,0.0341832,0.0340433,0.0339018,0.0337589,0.0336143,
     c0.0334680,0.033200,0.0331701,0.0330182,0.0328642,0.0327081,
     c0.0325496,0.0323887,0.0322252,0.0320589,0.0318898,0.0317176,
     c0.0315423/
      data (dbconst(i),i=4,40)/0.020516,0.020472,0.020427,0.020382,
     c0.020337,0.020292,0.020246,0.020201,0.020155,0.020110,0.020064,
     c0.020018,0.019972,0.019925,0.019879,0.019833,0.019786,0.019739,
     c0.019693,0.019646,0.019599,0.019552,0.019505,0.019458,0.019410,
     c0.019363,0.019316,0.019268,0.019221,0.019173,0.019126,0.019078,
     c0.019030,0.018983,0.018887,0.018840/
      hybrid=.false.
      DO jp=1,ids
      TE=41026.116
      Y10=95.11746327
      Y20=-0.111495227
      Y30=-5.792874546e-4
      Y40=4.205281828e-6
      Y50=-1.408244378e-8
      Y60=2.68736882e-11
      Y70=-2.3114805e-14
      vp=ids+0.5
       v1=vp
       v2=vp**2
       v3=vp**3
       v4=vp**4
       v5=vp**5
       v6=vp**6
       v7=vp**7
      dterm(ids)=TE+Y10*v1+Y20*v2+Y30*v3+Y40*v4+Y50*v5+Y60*v6+Y70*v7
      END DO
       IF(first)then
       tmp=rotrana
        c=rotranb
        al=rotranc
        ap=rotrand
        alw = rotrane
        t=rotranf
       first=.false.
      rgtonce=.true.
       ELSE
       ids=iddum
       ixs=ixdum
        tmp=rettmp
        c=retc
        al=retal
        ap=retap
        alw=retalw
       t=rett
      rgtonce=.false.
       ENDIF
       OPEN(unit=57,file='rate.ret',status='unknown')
        OPEN(unit=51,file='totsim.dat',status='unknown')
       i0low=0
       i0hi=98
       i1low=1
       i1hi=99
       bu=dbconst(ids)
       bl=xbconst(ixs)
       sig=dterm(ids)-xterm(ixs)
       ii=ji-2*int(ji/2)          !ii=0 or 1
       IF(ii.eq.0)then
        write(57,*)i0low,i0hi
       Else
        write(57,*)i1low,i1hi
       ENDIF
       write(57,*)'   J inital: ',jlvl
       write(57,*)'   J        rate'
      ji=jlvl
      do 20 j=1,50
      jj=ii+2*(j-1)               !Even Delta(J) selection rule
      if (jj.eq.ji) then
       IF(twoslope)then
        aptemp=ap
        ap=al2s
        IF(IPL)then
         aintemp=ainv
         ainv=al2s
        ENDIF
       ENDIF
       goto 20
       ENDIF
       an(1)=jj
       an(2)=ji
       an(3)=al
       de=abs(jj*(jj+1)-ji*(ji+1))    !E/B =abs(jj*(jj+1)-ji*(ji+1))
       do 30 i=1,2
       do 30 k=i+1,3
       IF(an(i).lt.an(k)) then
       temp=an(i)
        an(i)=an(k)              !n1>n2>n3
```

```
      an(k)=temp
     endif
30    continue
     alpha=an(2)+an(3)-an(1)
     if (alpha.lt.0.0) alpha=0.0
     anr=((2.*an(2)+1.)*(2.*an(3)+1.)-alpha*(alpha+1.))/(2.*jj+1.)
      aJ=2.*jj+1.              !spin degeneracy
      jl=ji
      if(jj.le.ji)jl=jj
       ano=(2.*jl+1.)/(2.*ji+1.)        !spin degeneracy |m|=0
       aJl=2.*jl+1.
       IF(SSDeg.eq.1)anl=aJ
       IF(SSDeg.eq.2)anl=ano
       IF(SSDeg.eq.3)anl=aJl
       IF(SSDeg.eq.4)anl=anr
       IF(SSDeg.eq.5)then
        hybrid=.true.
        anl=ano
       ENDIF
      IF(SSDeg.eq.6)hybrid=.false.
      ak(j)=(c*anl)/(de**ap)           !statistical power fit
      IF(IPL)ak(j)=anl/(DE**ainv)       !inverse power fit
      IF(hybrid)ak(j)=(anl*c*exp(-al*0.0001*de))/de**ap !hybrid of power and
20    continue                        !exponential gap law
      ak(int(ji/2)+1)=0.0             !rate of Ji=0.
      t1=0.
      Do i=1,50
       t1=t1+ak(i)             !Sum individual rate constants
      END DO
      DO j=1,50
      jj=ii+2*(j-1)            !Even Delta(J) selection rule
       write(57,*)jj,ak(j),ak(j)/t1
      END DO
      zi=exp(-t1*t)
      z1=exp(-rte*t)
      zinit=z1/(1-z1)*t1
      write(57,*)'Intensity of J initial ',zinit
     IF(rgtonce)Open(60,file='simpos.sim',status='unknown')
     Open(61,file='rate.sim',status='unknown')
      DO i=1,50
      jp=ii+2*(i-1)           !Honl-London S(P)=J; S(R)=J+1
       z(i)=(ak(i)/t1)*(1-zi)*jp       !P-branch intensity
       x(i)=jp*(jp-1)*bu-jp*(jp+1)*bl    !P-branch position
       xpos(i)=1e7/(x(i)+sig)*2
       If(rgtonce)write(60,*)'P',jp,xpos(i),1e7/xpos(i)
       ypos(i)=blin*0.95               !ypos-position marker
       if(jp.eq.ji)ypos(i)=blin*0.75
      END DO
      z(int(ji/2)+1)=zinit*scale        !P-branch initial
      DO i=1,50
      ENDDO
      DO i=1,50
      jr=ii+2*(i-1)
       z(50+i)=(ak(i)/t1)*(1-zi)*jr+1    !R-branch intensity
       x(50+i)=(jr+1)*(jr+2)*bu-jr*(jr+1)*bl  !R-branch position
       xpos(50+i)=1e7/(x(50+i)+sig)*2
       If(rgtonce)write(60,*)'R',jr,xpos(50+i),1e7/xpos(50+i)
       ypos(50+i)=blin*0.975           !ypos-position marker
       if(jr.eq.ji)ypos(50+i)=blin*0.775
      END DO
      z(51+int(ji/2))=zinit*scale        !R-branch initial
      amax=-1e8
      amin=1e8
      jcount=0
      write(61,*)'start',begin,' end',end
     IF(IPL)write(61,*)'inverse',ainv,' Spin Degeneracy',SSDeg
     IF(twoslope.and.IPL)write(61,*)'inverse two ',aintemp
     IF(.not.IPL)then
       write(61,*)'Spin Degeneracy ',SSDeg,' alpha',ap
       write(61,*)' total rate ',t1,' C ',C
       write(61,*)' lambda(spin) ',anl
       IF(twoslope)write(61,*)'slope two ',aptemp
      ENDIF
      Do 70 i=1,100
      xcm=(x(i)+sig)/2
       write(61,*)xcm,' rate- ',z(i)
       if ((xcm.ge.end).and.(xcm.le.begin))then
        jcount=jcount+1
        xtemp(jcount)=x(i)
        ztemp(jcount)=z(i)
       Elseif(sa)then
        jcount=jcount+1
        xtemp(jcount)=x(i)
        ztemp(jcount)=z(i)
```

```
70    ENDIF
      DO j=1,jcount
       x(j)=xtemp(j)
       z(j)=ztemp(j)
      END DO
      Do i=1,jcount
       if(x(i).gt.amax) amax=x(i)
       if (x(i).lt.amin) amin=x(i)
      END DO
      step=1501.
      IF(sa)step=3001.
      xst=(amax-amin+alw)/step
      x0=amin-alw/2.
      istep=1500
      IF(sa)istep=3001
      do 80 i=0,istep
      xx=x0+i*xst
      yy=blin
       do 90 j=1,jcount
       if(abs(x(j)-xx).gt.(3*alw)) goto 90
       yy=yy+z(j)*(alw/2)**2/((xx-x(j))**2+(alw/2)**2)
90     continue
       xx=1e7/(sig+xx)
       IF(sa)write(51,*)xx,yy
       yfit(i+1)=yy
       xfit(i+1)=xx*2
80    continue
      rettmp=tmp
      reto=c
      IF(twoslope)ap=aptemp
      IF(twoslope)ainv=aintemp
      retal=al
      retap=ap
      retalw=alw
      rett=t
      close(61)
      close(51)
      close(57)
      RETURN
      END


      SUBROUTINE AREA (X,Y,NPTS,Nterms,Retarea)
*-------------------------------------------------------------*
*  This routine integrates the area beneath a set of data points  *
*  Bevington "Data Reduction and Error Analysis for the Physcial  *
*  Sciences" McGraw-Hill (1969) p. 273.                          *
*-------------------------------------------------------------*
      implicit real*8(a-h,o-z)
      Dimension X(25),Y(25)
      IF (Nterms.gt.4)Nterms=4
11    sum=0.
      If (NPTS - Nterms) 21, 21, 13
13    Neven =2*(Nterms/2)
      Idelta = Nterms/2-1
      IF (Nterms - Neven) 31, 31, 51
21    X1=X(1)
      X2=X(NPTS)
23    Call INTEG (X,Y,NPTS,1,X1,X2,SUM)
      GOTO 71
31    X1=X(1)
      J=Nterms-IDelta
      X2=X(J)
      Call INTEG (X,Y,NTERMS,1,X1,X2,SUM)
      I1=NPTS-NTERMS+1
      J=I1+IDelta
      X1=X(J)
      X2=X(npts)
39    Call Integ(X,Y,NTERMS,I1,X1,X2,SUM)
      IF(I1-2)71,71,41
41    IMAX=I1-1
      Do 46 I=2,IMAX
      J=I+IDELTA
      X1=X(J)
      X(2)=X(J+1)
46    Call Integ(X,Y,NTERMS,I,X1,X2,SUM)
      Goto 71
51    X1=X(1)
      J=Nterms-IDelta
      X2=(X(J)+X(J-1))/2.
      Call Integ (X,Y,Nterms,1,X1,X2,SUM)
      I1=NPTS-NTERMS+1
      J=I1+IDelta
      X1=(X(J)+X(J+1))/2.
      X2=X(NPTS)
```

```
59  Call INTEG(X,Y,NTERMS,I1,X1,X2,SUM)
    IF(I1-2)71,71,61
61  IMAX=I1-1
    Do 66 I=2,IMAX
    J=I+IDelta
    X1=(X(J+1)+X(J))/2.
    X2=(X(J+2)+X(J+1))/2.
66  Call INTEG(X,Y,NTERMS,I,X1,X2,SUM)
71  Retarea=Sum
    Return
    End


    SUBROUTINE INTEG (X,Y,Nterms,I1,X1,X2,SUM)

*--------------------------------------------------*
*  This routine integrates the area beneath two data points  *
*  Bevington "Data Reduction and Error Analysis for the Physcial  *
*  Sciences" McGraw-Hill (1969) p. 274.       *
*--------------------------------------------------*

    implicit real*8(a-h,o-z)
    Dimension  X(25),Y(25),Array(25,25)
11  Do 17 J=1,Nterms
    I=J+I1-1
    Deltax=X(I)-X(I1)
    XJK=1.
    Do 17 K=1, Nterms
    Array(J,K)=XJK
17  XJK=XJK*Deltax
21  Call Matinv (array,Nterms,Det)
    IF(DET)31,23,31
23  IMID=I1+Nterms/2
    Sum=Sum+Y(IMID)*(X2-X1)
    GOTO 40
31  DX1=X1-X(I1)
    DX2=X2-X(I1)
33  Do 39 J=1,NTERMS
    I=J+I1-1
    A=0.
    Do 37 K=1,Nterms
37  A=A+Y(I)*ARRAY(J,K)
    Denom=J
39  Sum=Sum+(A/Denom)*(DX2**J-DX1**J)
40  Return
    END


    SUBROUTINE MATINV (Array,Norder,DET)

*--------------------------------------------------*
*  This routine integrates the area beneath two data points  *
*  Bevington "Data Reduction and Error Analysis for the Physcial  *
*  Sciences" McGraw-Hill (1969) p. 302.       *
*--------------------------------------------------*

    implicit real*8(a-h,o-z)
    Dimension Array(25,25), IK(25), JK(25)
10  DET=1.
11  Do 100 K=1, Norder
    AMAX =0.
21  Do 30 I=K,Norder
    Do 30 J=K,Norder
23  IF(ABS(AMAX)-ABS(ARRAY(I,J)))24,24,30
24  AMAX=ARRAY(I,J)
    IK(K)=I
    JK(K)=J
30  Continue
*  Interchange rows and columns to put amax in array (k,k)
31  If(AMAX) 41,32,41
32  Det=0.
    Goto 140
41  I=IK(K)
    IF (I-K)21,51,43
43  Do 50 J=1, Norder
    Save=Array(K,J)
    Array(K,J)=Array(I,J)
50  Array(I,J)=-Save
51  J=JK(K)
    IF(J-K)21,61,53
53  DO 60 I=1,NORDER
    SAVE=ARRAY(I,K)
    ARRAY(I,K)=ARRAY(I,J)
60  ARRAY(I,J)=-SAVE

61  Do 70 I=1,NORDER
    IF (I-K) 63,70,63
63  ARRAY(I,K)=-ARRAY(I,K)/AMAX
70  CONTINUE
71  DO 80 I=1,NORDER
```

```
    DO 80 J=1,NORDER
    IF(I-K)74,80,74
74  IF(J-K)75,80,75
75  ARRAY(I,J)=ARRAY(I,J)+ARRAY(I,K)*ARRAY(K,J)
80  Continue
81  Do 90 J=1,NORDER
    IF (J-K)83,90,83
83  ARRAY(K,J)=ARRAY(K,J)/AMAX
90  Continue
    Array(K,K)=1./AMAX
100 Det=Det*AMax
101 Do 130 L=1,Norder
    K=Norder-L+1
    J=IK(K)
    IF(J-K)111,111,105
105 Do 110 I=1,Norder
    Save=Array(I,K)
    Array(I,K)=-Array(I,J)
110 Array(I,J)=Save
111 I=JK(K)
    IF(I-K)130,130,113
113 Do 120 J=1,Norder
    Save=Array(K,J)
    Array(K,J)=-Array(I,J)
120 Array(I,J)=Save
130 Continue
140 Return
    END



    SUBROUTINE LAMBDA(new,gdcal,fulnam,filnm)

*--------------------------------------------------*
*  Lambda reads files with the format of the        *
*  experimental data files found in the lab of M.C. Heaven  *
*--------------------------------------------------*

    Implicit Real*4  (a-h,o-z)
    Real*4     XX(1024),YY(1024),YC(1024)
    Character  Filnm*12,tmpname*12,fulnam*12
    Character*3  ext
    Character*7  GD
    Character*(*)  New
    Logical    First,GDCAL
    first=.true.
    gdcal=.true.
    zip=0.0
92  WRITE(*,*)'Enter name of file to be read: '
    READ(*,30)FILNM
30  FORMAT(A12)
    OPEN(22,FILE=FILNM,ERR=90,STATUS='OLD')
    goto 91
90  WRITE(*,*)'UNABLE TO OPEN THIS FILE...TRY AGAIN'
    goto 92
91  continue
50  READ(22,33)NUME,XMAX,XMIN,YMAX,YMIN,IFILE
33  FORMAT(I4,2X,4(F8.2,1X),I1)
    IF(IFILE.EQ.1)GO TO 42
    READ(22,34)(XX(I),YY(I),I=1,NUME)
34  FORMAT(4(F8.2,1X,F8.2,1X))
    GO TO 43
42  CONTINUE
    IF(GDCAL)then
    READ(22,35,ERR=31)(XX(I),YY(I),YC(I),I=1,NUME)
    ELSE
    READ(22,36,ERR=31)(XX(I),YY(I),GD,I=1,NUME)
    ENDIF
    GOTO 43
31  GDCAL=.false.
    Rewind 22
    GOTO 50
35  FORMAT(3(F7.1,1X,F7.1,1X,F7.1,1X))
36  FORMAT(3(F7.1,1X,F7.1,1X,A7,1X))
43  CLOSE(22,STATUS='KEEP')
    STP=(XMAX-XMIN)/(NUME-1)
    Write(*,*)
    Write(*,*)'          This program simulates RET using the sta
   +tistical'
    Write(*,*)'          power gap law.  The progam requires a ca
   +librated'
    Write(*,*)'          data file.  The program will generate a
   +new file'
    Write(*,*)'          called *.sim which contains the simulati
   +on.'
    Write(*,*)'          and *.ret which contains rate constants'
```

```
        Write(*,*)
        Write(*,*)'          IMPORTANT:  Input new file name without
        +an extension.'
        Write(*,*)'                 e.g. input SEP0727A.DAT  as
        + SEP0727A'
        Write(*,*)
        WRITE(*,*)'Enter NEW FILENAME: '
        READ(*,30)NEW
        Tmpname=New
        length = Len_Trim( tmpname )
        pos = INDEX(tmpname,'.',.false.)
        ext='dat'
        fulnam = tmpname(1:length)//'.'//ext
        OPEN(unit=9,file=fulnam,status='UNKNOWN')
        DO 81 I=1,NUME
         XX(I)=XMAX-STP*(I-1)
          IF(first)then
           WRITE(9,*)NUME,XMAX,XMIN,YMAX
           first=.false.
          ENDIF
          IF(GDCAL)then
          WRITE(9,*)XX(I),YY(I),YC(I)
          Else
          WRITE(9,*)XX(I),YY(I),zip
          ENDIF
81      CONTINUE
48      CONTINUE
        CLOSE(UNIT=9)
        CLOSE(UNIT=22)
        RETURN
        END

        SUBROUTINE ADDEXT(name,ext)
*_____*
*                                       *
*  This routine will add an extention onto a file name.  *
*_____*
        INCLUDE 'display.dat'
        Integer length
        Character*3 ext
        Character tmpname*12, name*12
        tmpname = name
        ! get the length of the name
        length = Len_Trim( tmpname )
        ! find occurance of . starting from end of filename
        pos = INDEX(tmpname,'.',.false.)
        If( pos .ne. 0 ) length = pos - 1   ! Period was found
        fulnam = tmpname(1:length)//'.'//ext
        END

$Storage: 2
$Include: 'FGRAPH.FI'
        SUBROUTINE PEAKLOC
*_____*
*                                       *
*  This subroutine locates peaks by stepping three points  *
*  through the data file using the difference defined in   *
*  the Dat_File                         *
*_____*
        Include 'FGRAPH.FD'
        Include 'COLORS.H'
        Include 'ROW_COL.H'
        Include 'DISPLAY.DAT'
        Include 'KEYCODE.H'
        Integer   jcnt,peakcur(1524),peaktemp(1524),icor
        Integer   head,mid,tail,ipos,opt
        Integer   jpos,temp(500),stor(200,9),tmp(9)
        Integer*2  dummy,dummy2,y4
        Real*4    yup,ydown
        Character  Menu2*80
        Logical   first,done
        RECORD /wxycoord/ wxy
        Done=.false.
        jcnt=1            !Locate the peaks by stepping
        Do mid=3,nume-2    !three peaks separated by two
         head=mid+2        !cursor positions
          tail=mid-2
          yup=ydat(head)-ydat(mid)
          ydown=ydat(mid)-ydat(tail)
           IF((abs(yup).gt.ydelt).and.(ydown.gt.ydelt))then
            IF(yup.lt.0)then
             jcnt=jcnt+1
             peakcur(jcnt)=mid
            ENDIF
           ENDIF
           IF(ydown.gt.ydelt)then
```

```
           IF(yup.lt.0)then
             yupdum=ydat(head+1)-ydat(head)
             IF(yupdum.lt.0)then
             ENDIF
            ENDIF
           ENDIF
          END DO
         First=.false.
         ipos=0
         Do j=1,jcnt
        IF(peakcur(j).GT.0)then        !Sort the peaks by
          IF(.not.first)then           !removing copies and zeros
           ipos=ipos+1                 !Sort - 1
           peaktemp(ipos)=peakcur(j)
           first=.true.
          ENDIF
          IF(first)then
           IF(peaktemp(ipos).ne.peakcur(j))then
           ipos=ipos+1
           peaktemp(ipos)=peakcur(j)
           ENDIF
          ENDIF
         ENDIF
         End Do
         Do k=1,ipos
           temp(k)=peaktemp(k)
         End DO
        icor=5
70      Continue
        Do k=1,ipos
         temp(k)=peaktemp(k)
         End DO
        !Use correct factor to find max peaks
        !looking forward
         Do j=1,ipos
           stor(j,1)=temp(j)
           kk=2
           Do k=j+1,j+icor
             IF(temp(k)-temp(j).le.icor)then
              kk=kk+1
              stor(j,kk)=temp(k)
             ENDIF
            END DO
             stor(j,2)=kk
           END DO
        DO j=1,ipos
         inx=stor(j,2)
         inx2=inx-2
        IF(inx2.eq.0)goto 73
        IF(inx2.eq.1)then
          IF(YDAT(stor(j,3)).gt.YDAT(stor(j,1)))then
           stor(j,1)=stor(j,3)
           goto 73
          ENDIF
        ENDIF
        Do k=3,inx
          tmp(k)=stor(j,k)
        END DO
        DO jj=inx,4,-1
          IF(YDAT(tmp(jj)).gt.YDAT(tmp(jj-1)))then
           tmp(jj-1)=tmp(jj)
          ENDIF
        END DO
        IF(YDAT(tmp(3)).gt.YDAT(stor(j,1)))stor(j,1)=tmp(3)
73      Continue
        END DO
        !looking backward
         Do j=ipos,2,-1
           stor(j,2)=0
           IF(stor(j,1)-stor(j-1,1).le.icor)then
             IF(YDAT(stor(j-1,1)).gt.YDAT(stor(j,1)))then
               stor(j,2)=stor(j,1)
               stor(j,1)=stor(j-1,1)
             ENDIF
           ENDIF
         END DO
         do jc=1,ipos
          temp(jc)=stor(jc,1)
         end do
        first=.true.
        jpos=0
        Do j=1,ipos
        IF(first)then
          IF((temp(j).GT.0).and.(YDAT(temp(j)).GT.peakmin))then
```

```
          jpos=jpos+1
          peakcur(jpos)=temp(j)
          first=.false.
        ENDIF
      ELSEIF(.not.first)then
       IF(peakcur(jpos).ne.temp(j))then
        IF(YDAT(temp(j)).GT.peakmin)then
          jpos=jpos+1
          peakcur(jpos)=temp(j)
        ENDIF
       ENDIF
      ENDIF
     END DO
80       Continue
        DO j=1,jpos
        IF((peakcur(j).le.nume-2).and.(peakcur(j).ge.2))then
          Call gauss(peakcur(j))
          ytempb(j)=yarea
          xcurb(j)=peakcur(j)
          dummy = setcolor(nlc1)
          Call moveto_w(xr(peakcur(j)),ymin,wxy)
          y4=ymin+50
          dummy2 = lineto_w(xr(peakcur(j)),y4)
        ENDIF
        END DO
     Menu2 = ' a-add one point   d-delete point   w-write file '//
     +      ' r-refresh screen   ESC-Quit '
        Call messg(Menu2, 2)
        call cursor(curpos,1)
        Do While( .not. done )
          Call checkk( opt )
           SELECT CASE ( opt )
           CASE( $CAP_X, $x )       ! delete one point
             DO j=1,jpos
               IF(curpos.eq.xcurb(j))then
                 ytempb(curpos)=zip
                 xcurb(curpos)=0
                 peakcur(j)=0
               ENDIF
             END DO
           CASE( $CAP_A, $a )       ! add one point
             jpos=jpos+1
             Call gauss(curpos)
             ytempb(jpos)=yarea
             xcurb(jpos)=curpos
             peakcur(jpos)=curpos
           CASE( $CAP_W, $w,$s,$RETURN) ! write file
             call addext(filnam,'mel')
             OPEN(51,FILE=fulnam,STATUS='UNKNOWN')
             i=0
             Do j=1,jpos
             IF(xcurb(j).GT.0)then
             i=i+1
             IF(cal_done)then
           IF(aufset)then
           Write(51,*)xoff(xcurb(i)),ydat(xcurb(i)),ytempb(i)
           Else
           Write(51,*)cabx(xcurb(i)),ydat(xcurb(i)),ytempb(i)
             ENDIF
             Else
           Write(51,*)xdat(xcurb(i)),ydat(xcurb(i)),ytempb(i)
             ENDIF
             ENDIF
             END DO
           CASE($ONE)
             icor=1
             call refresh
             call messg(menu2,2)
             goto 70
           CASE($TWO)
             icor=2
             call refresh
             call messg(menu2,2)
             goto 70
           CASE($THREE)
             icor=3
             call refresh
             call messg(menu2,2)
             goto 70
           CASE($FOUR)
             icor=4
             call refresh
             call messg(menu2,2)
             goto 70
           CASE($FIVE)
             icor=5
             call refresh
             call messg(menu2,2)
             goto 70
           CASE($SIX)
             icor=6
             call refresh
             call messg(menu2,2)
             goto 70
           CASE($SEVEN)
             icor=7
             call refresh
             call messg(menu2,2)
             goto 70
           CASE($EIGHT)
             icor=8
             call refresh
             call messg(menu2,2)
             goto 70
           CASE($NINE)
             icor=9
             call refresh
             call messg(menu2,2)
             goto 70
           CASE( $F10 )            ! delete all
             jpos=0
             goto 80
           CASE( $F9)
           CASE( $LFTAROW,$COMMA,$LT ) ! move Cursor left
             Call Curs_Lft(curpos)
           CASE( $RGTAROW,$PERIOD,$GT ) ! move Cursor right
             Call Curs_Rgt(curpos)
           CASE( $CAP_H, $h )        ! move Cursor right
             bbigstep=.true.
             Call Curs_Lft(curpos)
           CASE( $CAP_J, $j )        ! move Cursor left
             bigstep=.true.
             Call Curs_Lft(curpos)
           CASE( $CAP_L, $l )        ! move Cursor left
             bbigstep=.true.
             Call Curs_Rgt(curpos)
           CASE( $CAP_K, $k )        ! move Cursor right
             bigstep=.true.
             Call Curs_Rgt(curpos)
           CASE( $r)
             call refresh
             call messg(menu2,2)
           CASE( $ESC,$CAP_Q,$q)
             done = .true.
           CASE DEFAULT
           END SELECT
         END DO
       Close(53)
       Return
       End

       SUBROUTINE MINMAX(a,n,amin,amax)
*---------------------------------------------*
*  this routine finds the min and max in a 1d array  *
*  routine written by Herr Udo Schnupf         *
*---------------------------------------------*
       implicit real*4 (a-h,o-z)
       dimension a(n)
       amin= 1.e30
       amax=-1.e30
       do 10 i=1,n
         amax=max(a(i),amax)
         amin=min(a(i),amin)
10     continue
       return
       end
```

```
*_____*
*                                         *
*    FILE: C_Calls.for                    *
*_____*
$Storage: 2
*
*   This file contains interfaces and functions to use the C function
*   calls GETCH and KBHIT.
■
    INTERFACE TO INTEGER*2 FUNCTION getch [C] ()
    end

    INTERFACE TO INTEGER*2 FUNCTION kbhit [C] ()
    end
    Subroutine Checkk(num)
          Integer num
    Integer*2 getch
    num = getch()
    If( num .eq. 0 ) then
      num = getch() + 128
    Endif
    Return
    END

    Subroutine Key_Hit(num)
    Integer num
    Integer*2 kbhit
    num = 0
    If( kbhit() .ne. 0 ) num = 1
    END
```

```
*_____*
*                                         *
*     KEYCODE.H - ASCII values for keyboard  *
*_____*

INTEGER$LFTAROW,$RGTAROW,$UPAROW,$DWNAROW,$INSERT,$DELETE
INTEGER $HOME,$END,$PAGEUP,$PAGEDWN,$F1,$F2,$F3,$F4,$CTRL_R
INTEGER $F5,$F6,$F7,$F8,$F9,$F10,$ESC,$ALT_D,$ALT_Q,$ALT_R,$ALT_X
INTEGER $RETURN,$ZERO,$ONE,$TWO,$THREE
INTEGER $FOUR,$FIVE,$SIX,$SEVEN,$EIGHT,$NINE
INTEGER $PLUS,$EQUAL,$MINUS,$UNDRLIN,$PERIOD,$GT,$LT,$COMMA
INTEGER $CAP_A,$a,$CAP_B,$b,$CAP_C,$c,$CAP_D,$d,$CAP_E,$e
INTEGER $CAP_F,$f,$CAP_G,$g,$CAP_H,$h,$CAP_I,$i
INTEGER $CAP_J,$CAP_K,$CAP_L,$j,$k,$l,$CAP_M,$m,$CAP_N,$n
INTEGER $CAP_O,$o,$CAP_P,$p,$CAP_Q,$q,$CAP_R,$r,$CAP_S,$s
INTEGER $t,$CAP_T,$CAP_W,$w,$CAP_X,$x,$CAP_Y,$y

PARAMETER($LFTAROW  = 203)
PARAMETER($RGTAROW  = 205)
PARAMETER($UPAROW  = 200)
PARAMETER($DWNAROW  = 208)
PARAMETER($INSERT  = 210)
PARAMETER($DELETE  = 211)
PARAMETER($HOME  = 199)
PARAMETER($END  = 207)
PARAMETER($PAGEUP  = 201)
PARAMETER($PAGEDWN  = 209)
PARAMETER($RETURN  = 13)
PARAMETER($PLUS  = 43)
PARAMETER($COMMA  = 44)
PARAMETER($MINUS  = 45)
PARAMETER($PERIOD  = 46)
PARAMETER($ZERO  = 48)
PARAMETER($ONE  = 49)
PARAMETER($TWO  = 50)
PARAMETER($THREE  = 51)
PARAMETER($FOUR  = 52)
PARAMETER($FIVE  = 53)
PARAMETER($SIX  = 54)
PARAMETER($SEVEN  = 55)
PARAMETER($EIGHT  = 56)
PARAMETER($NINE  = 57)
PARAMETER($LT  = 60)
PARAMETER($EQUAL  = 61)
PARAMETER($GT  = 62)

PARAMETER($F1  = 187)
PARAMETER($F2  = 188)
PARAMETER($F3  = 189)
PARAMETER($F4  = 190)
PARAMETER($F5  = 191)
PARAMETER($F6  = 192)
PARAMETER($F7  = 193)
PARAMETER($F8  = 194)
PARAMETER($F9  = 195)
PARAMETER($F10  = 196)
PARAMETER($ESC  = 27)
PARAMETER($ALT_D  = 160)
PARAMETER($ALT_Q  = 128)
PARAMETER($ALT_R  = 147)
PARAMETER($ALT_X  = 173)
PARAMETER($CAP_A  = 65)
PARAMETER($CAP_B  = 66)
PARAMETER($CAP_C  = 67)
PARAMETER($CAP_D  = 68)
PARAMETER($CAP_E  = 69)
PARAMETER($CAP_F  = 70)
PARAMETER($CAP_G  = 71)
PARAMETER($CAP_H  = 72)
PARAMETER($CAP_I  = 73)
PARAMETER($CAP_J  = 74)
PARAMETER($CAP_K  = 75)
PARAMETER($CAP_L  = 76)
PARAMETER($CAP_M  = 77)
PARAMETER($CAP_N  = 78)
PARAMETER($CAP_O  = 79)
PARAMETER($CAP_P  = 80)
PARAMETER($CAP_Q  = 81)
PARAMETER($CAP_R  = 82)
PARAMETER($CAP_S  = 83)
PARAMETER($CAP_T  = 84)
PARAMETER($CAP_W  = 87)
PARAMETER($CAP_X  = 88)
PARAMETER($CAP_Y  = 89)
PARAMETER($UNDRLIN  = 95)
PARAMETER($a  = 97)
PARAMETER($b  = 98)
PARAMETER($c  = 99)
PARAMETER($d  = 100)
PARAMETER($e  = 101)
PARAMETER($f  = 102)
PARAMETER($g  = 103)
PARAMETER($h  = 104)
PARAMETER($i  = 105)
PARAMETER($j  = 106)
PARAMETER($k  = 107)
PARAMETER($l  = 108)
PARAMETER($m  = 109)
PARAMETER($n  = 110)
PARAMETER($o  = 111)
PARAMETER($p  = 112)
PARAMETER($q  = 113)
PARAMETER($r  = 114)
PARAMETER($s  = 115)
PARAMETER($t  = 116)
PARAMETER($w  = 119)
PARAMETER($x  = 120)
PARAMETER($y  = 121)
PARAMETER($CTRL_R  = 18)
```

```
***************************************************************
*                                                             *
*   ROW_COL.H                                                  *
*   This include file contins constants for row and column positions  *
*   during data review.                                       *
***************************************************************
INTEGER LABEL_ROW,LABEL_COL,NUM_COL,NUM_DATA_ROWS
INTEGER DATA_COL,BOR_START_ROW,MESSG_ROW1,MESSG_ROW2
INTEGER MESSG_COL,IC_COL,NUM_IC_ROWS,SEP_IC_ROWS
INTEGER LFT_BOR_COL,ERROR_ROW,STARTDATAROW
PARAMETER  (LABEL_ROW  =2 )
PARAMETER  (LABEL_COL  =2 )
PARAMETER  (NUM_COL  =80 )
PARAMETER  (STARTDATAROW =5 )
PARAMETER  (NUM_DATA_ROWS=17)
PARAMETER  (DATA_COL  =2 )
PARAMETER  (BOR_START_ROW=1 )
PARAMETER  (LFT_BOR_COL =1 )
PARAMETER  (MESSG_ROW1 =1 )
PARAMETER  (MESSG_ROW2 =2 )
```

```
PARAMETER    (MESSG_COL    = 2 )
PARAMETER    (ERROR_ROW    = 25 )
PARAMETER    (IC_COL       = 22 )
PARAMETER    (NUM_IC_ROWS  = 11 )
PARAMETER    (SEP_IC_ROWS  = 14 )
```

```
*********************************************************************
*   COLORS.H                                                        *
*   This file contains constant declarations used to set the colors of  *
*   text and graphics output to the screen.                         *
*********************************************************************
      INTEGER*2 TEXT_CLR,GRAPH_BORDER,GRAPH_FILL,PLOT_CURSOR
      INTEGER*2 GRAPH_LINE,TEXT_ERR_CLR,GRPH_ERR_CLR
      INTEGER*2 BORDER,FILE_NAME,DATA_PT
      INTEGER*4 TEXT_BK_CLR,GRPH_BK_CLR,MESSG_CLR

      PARAMETER    (TWIL_ZONE  = 0  )   ! ANOTHER DIM
      PARAMETER    (TEXT_BK_CLR = 1  )   ! BLUE
      PARAMETER    (GRPH_BK_CLR = $BLUE)   ! BLUE
      PARAMETER    (DATA_PT    = 7  )   ! WHITE
      PARAMETER    (GRAPH_FILL = 8  )   ! DARK GRAY
      PARAMETER    (FILE_NAME  = 9  )   ! LIGHT BLUE
      PARAMETER    (MESSG_CLR  = 10 )   ! LIGHT GREEN
      PARAMETER    (TEXT_CLR   = 11 )   ! LIGHT CYAN
      PARAMETER    (GRPH_ERR_CLR = 12 )   ! LIGHT RED
      PARAMETER    (PLOT_CURSOR = 12 )   ! LIGHT RED
      PARAMETER    (BORDER     = 13 )   ! LIGHT MAGENTA
      PARAMETER    (GRAPH_LINE = 14 )   ! YELLOW
      PARAMETER    (GRAPH_BORDER = 15 )   ! LIGHT WHITE
      PARAMETER    (TEXT_ERR_CLR = 28 )   ! BLINKING LIGHT RED
```

```
*_____*
*                                                 *
*             DISPLAY.DAT                         *
*_____*

      Integer   xrange,on,off,curpos,itwonum,jlevel,SDeg,icnta,totJ(47)
      Integer*2 inumq,iband
      Integer*2 x1,y1,x2,y2,y3,nlc1,nlc2,nlc3,nlc4,ntc,jplus
      Integer*2 col1,col2,col3,col4,col5
      Integer*2 x_row,x1_col,x2_col,put_cur,curtemp(30)
      Integer*2 xcurb(500),maxx,maxy,dstate,xstate,jminus
      Integer*4 nume
      Real      xdif,ydif
      Real*4    xdat(1524),ydat(1524),zdat(1524),pop(47)
      Real*4    xmax,xmin,ymax,ymin,zmax,zmin,glw,ydelt
      Real*4    xxmax,xxmin,yymax,yymin,tmpr(47)
      Real*4    olddel,xcol(1501),ycol(1501),peakmin
      Real*4    stpx(1501)
      Real*4    xft(1501),yft(1501),xps(110),yps(110)
      Real*8    xr(1024),yr(1024),zr(1024),ya(1024),yvar
      Real*8    xcal(30),calx(1024),caly(1024),zip,xoff(1024)
      Real*8    ytempb(500),X1VIEW,Y1VIEW,ZSCALE,baselin,ah
      Real*8    rottmp,rotc,rotal,rotap,rotalw,rott,PI,yarea
      CHARACTER filnam*12,fulnam*12,oldname*12
      Logical   calib,out_rgt,out_lft,cal_done,yescal,aufset,newfile
      Logical   pkhgh,bigstep,bbigstep,right,plotsim,distwo,iodx
      Logical   moveone,moveret,movetwo,drawnocal,inverse
      Logical   LORENTZ,gowss
      Common /dat_array/ xdat,ydat,zdat,xstate,dstate,jlevel
      Common /dat_win/ xr,yr,zr,ya
      Common /dat_spec/ nume,xmax,xmin,ymax,ymin,zmax,zmin
      Common /dat_integ/ baselin,yarea,plotsim,iodx,glw
      Common /cursize/ xdif,ydif
      Common /view_lo/ x1,y1,x2,y2,y3
      Common          curpos,right,calib,bigstep,bbigstep
      Common /curs_scal/ xrange,yvar
      Common /pref_col/ nlc1,nlc2,nlc3,nlc4,ntc
      Common /axis_lab/ x_row,x1_col,x2_col,put_cur
      Common /outrange/ out_lft,out_rgt
      Common /cal_pnts/ xcal,curtemp,drawnocal
      Common /cal_out/ calx,caly,cal_done,aufset,xoff
      Common /file_dir/ filnam,fulnam,yescal,newfile,oldname
      Common /peak_find/ pkhgh,ydelt,olddel,xcurb,ytempb,peakmin
      Common /par_file/ x1view,y1view,zscale,maxx,maxy
      Common /plot_sim/ xft,yft,xps,yps
      Common /file_two/ xcol,ycol,distwo,itwonum,icnta
      Common /file2_max/ xxmax,yymax,yymin,xxmin
      Common /file2_mov/ movetwo,moveone,moveret,stpx,jplus,jminus
      Common /RET_par/ rottmp,rotc,rotal,rotap,rotalw,rott,inverse
      Common /RET_pmt/ col1,col2,col3,col4,col5,SDeg
      Common /DX_time/ iband,inumq,pop,tmpr,LORENTZ
```

```
      Common /DX_guass/ ah,totJ,gowss
      Parameter (on = 1)
      Parameter (off = 0)
      Parameter (zip = 0.0000)
      Parameter (PI = 3.141592654)
```

```
*_____*
*                                                 *
*             DISPLAY.REF                         *
*_____*
```

X1VIEW,Y1VIEW, size of the orignal window in percent values (real values)
85.,85
ZSCALE RESCALING FACTOR FOR THE REFERENCE SPECTRUM IN
PERCENT (real value)
30
LINE COLORS: border,data,cal,sim,text (integer values)
12,15,12,11,14
LINE COLORS (GRAPHICS PRINT): border,data,cal,sim,text (integer values)
12,15,15,12,10
SCALING FACTORS FOR CURSOR: X-SCALE (integer value), Y-SCALE(real value)
6, 21.0000
SCALING FACTORS FOR X-axis Label: row,col_start,col_stop
29,4,71
START CURSOR(Integer value:0=left,1=middle,2=right)
0
Gaussian Laser Line Width(cm-1)
0.09
IUNIT(1-nm, 2-cm),ALW (RET SIMULATION)
1,0.09
ROTATIONAL ENERGY TRANSFER
SIMULATION:TMP,C,LAMBDA,ALPHA,LINEWIDTH,DELAY
301,0.2,0,0.9,0.08,300
INVERSE POWER RET FIT; SPIN DEGENERACY 1=Nj 2=No 3=Njl 4=Nl
5=J(J+1)
.true.,1
RELATIVE STEADY STATE POPULATION OF VIB EXCITED IODINE
1.5,1.2,1.0,1.2   !21-24
1.5,1.2,1.0,1.2   !25-28
0.3,0.9,0.9,1.2   !29-32
2.5,1.2,3.0,4.2   !33-36
5.3,5.9,5.9,10.2   !37-40
3.9,6.6,4.2,3.3   !41-44
2.8,3.3,1.3   !45-47
I* + I2 ROTATIONAL TEMPERATURE TEMPSIM(distribution temperature)
360,370,380,380   !33-36
310,330,310,310   !37-40
310,340,330,320   !41-44
298,270,278   !45-47
FIT SIMULATION WITH LORENTZ,[GAUSSIAN,1/2sigma,mean sample,(DXSIM)]
.false.,.true.,0.0002,80

```
*_____*
*                                                 *
*               FCF.DAT                           *
*_____*
```

Data file FCF.DAT contains numbers only! in a single column listing!
Modified in its appearance to 5 (five) columns to save space

1.8758e-11	1.7034e-03	9.9999e+04	3.2752e-02	5.6672e-04
9.2388e-11	3.8282e-03	2.2172e-05	2.1961e-02	9.9999e+04
4.3203e-10	7.8994e-03	7.1419e-05	7.3296e-03	6.6671e-03
1.9194e-09	1.4853e-02	2.1280e-04	2.7190e-06	1.2401e-02
8.1015e-09	2.5205e-02	5.8471e-04	7.0555e-03	1.9994e-02
3.2480e-08	3.8064e-02	1.4753e-03	2.0616e-02	2.7252e-02
1.2360e-07	5.0136e-02	3.3997e-03	2.2981e-02	3.0120e-02
4.4706e-07	5.5788e-02	7.1038e-03	9.5978e-03	2.4950e-02
1.5330e-06	4.9572e-02	1.3335e-02	4.1339e-07	1.2803e-02
4.9863e-06	9.9999e+04	2.2195e-02	1.0156e-02	1.7773e-03
1.5366e-05	2.9952e-07	3.2146e-02	9.9999e+04	1.6680e-03
4.4814e-05	1.1674e-06	3.9375e-02	1.0456e-03	1.2448e-02
1.2354e-04	4.2645e-06	3.8830e-02	2.5248e-03	2.0323e-02
3.2156e-04	1.4586e-05	2.7918e-02	5.4881e-03	1.3497e-02
7.8881e-04	4.6632e-05	1.1208e-02	1.0637e-02	1.3994e-03
1.8200e-03	1.3905e-04	3.9236e-04	1.8132e-02	3.6654e-03
3.9397e-03	3.8569e-04	5.3624e-03	2.6651e-02	1.6177e-02
7.9777e-03	9.1189e-04	2.1367e-02	3.2745e-02	1.4623e-02
9.9999e+04	2.3548e-03	2.9208e-02	3.1879e-02	1.5303e-03
4.6503e-10	5.1327e-03	9.9999e+04	2.2016e-02	4.8916e-03
2.1638e-09	1.0203e-02	6.8959e-05	7.8190e-03	9.9999e+04
9.5312e-09	1.8324e-02	2.0760e-04	4.3138e-05	1.0399e-02
3.9759e-08	2.9357e-02	5.7490e-04	6.0997e-03	1.7478e-02
1.5700e-07	4.1220e-02	1.4590e-03	1.9172e-02	2.4956e-02
5.8662e-07	4.9325e-02	3.3732e-03	2.2093e-02	2.9181e-02
2.0724e-06	4.7989e-02	7.0531e-03	9.6062e-03	2.6117e-02
6.9169e-06	3.4562e-02	1.3206e-02	5.0775e-06	1.5364e-02
2.1784e-05	1.4336e-02	2.1847e-02	9.2506e-03	3.4416e-03
6.4644e-05	9.9999e+04	3.1301e-02	2.0889e-02	5.1060e-04
1.8049e-04	1.4958e-06	3.7658e-02	9.9999e+04	9.4738e-03
4.7307e-04	5.4810e-06	3.6080e-02	2.1997e-03	1.9064e-02
1.1609e-03	1.8748e-05	2.4651e-02	4.7188e-03	1.5374e-02
2.6600e-03	5.9776e-05	8.7110e-03	9.3619e-03	3.0143e-03
5.6688e-03	1.7723e-04	4.8778e-05	1.6341e-02	1.7326e-03
1.1183e-02	4.8716e-04	6.8592e-03	2.4620e-02	1.3670e-02
2.0304e-02	1.2368e-03	2.2038e-02	3.1089e-02	1.5824e-02
3.3676e-02	2.8869e-03	2.6576e-02	3.1284e-02	3.2324e-03
9.9999e+04	6.1565e-03	1.2950e-02	2.2668e-02	2.5660e-03
5.7810e-09	1.1899e-02	9.9999e+04	8.9436e-03	1.5254e-02
2.5387e-08	2.0628e-02	1.9001e-04	2.3729e-04	
1.0521e-07	3.1587e-02	5.3322e-04	4.7385e-03	
4.1150e-07	4.1780e-02	1.3681e-03	1.7325e-02	
1.5177e-06	4.6091e-02	3.1920e-03	2.1546e-02	
5.2736e-06	3.9750e-02	6.7220e-03	1.0376e-02	
1.7243e-05	2.3201e-02	1.2649e-02	1.0386e-04	
5.2973e-05	5.5480e-03	2.0974e-02	7.7152e-03	
1.5261e-04	5.5122e-04	3.0033e-02	1.9581e-02	
4.1130e-04	9.9999e+04	3.5973e-02	1.2368e-02	
1.0343e-03	6.2239e-06	3.4086e-02	9.9999e+04	
2.4176e-03	2.1404e-05	2.2758e-02	3.9263e-03	
5.2290e-03	6.8412e-05	7.5627e-03	8.0156e-03	
1.0410e-02	2.2080e-04	1.8794e-06	1.4406e-02	
1.8933e-02	5.5579e-04	7.3714e-03	2.2391e-02	
3.1154e-02	1.4024e-03	2.1635e-02	2.9282e-02	
4.5768e-02	3.2413e-03	2.4438e-02	3.0765e-02	
5.8885e-02	6.8168e-03	1.0586e-02	2.3719e-02	
9.9999e+04	1.2930e-02	7.6443e-06	1.0624e-02	
4.8015e-08	2.1853e-02	9.9999e+04	7.5801e-04	
1.9878e-07	3.2360e-02	4.6896e-04	3.1784e-03	
7.7401e-07	4.0906e-02	1.2230e-03	1.5089e-02	
2.8336e-06	4.2272e-02	2.8952e-03	2.1055e-02	
9.7418e-06	3.2912e-02	6.1775e-03	1.1735e-02	
3.1403e-05	1.5720e-02	1.1761e-02	4.9314e-04	
9.4740e-05	1.7343e-03	1.9704e-02	5.7697e-03	
2.6692e-04	2.9617e-03	2.4630e-02	1.8091e-02	
7.0011e-04	1.8827e-02	3.4346e-02	1.3341e-02	

APPENDIX E

TERM SYMBOLS

The energy state of an atom is represented by its term symbol. The term symbol for the atomic transition is labeled by $N^{2S+1}L_J$ where: N is the orbit number; L is the total orbital angular momentum; S is the total spin angular momentum; and **J** is the total angular momentum $J=L+S$. The left superscript $(2S+1)$ is often referred to as the multiplicity of that term, e.g. ^2P is called 'doublet P'. The right subscript (J) is the level of the term, e.g. $^2P_{3/2}$ is called 'doublet P three halves' with values of $J = L+S,...|L-S|$. Likewise, the molecular term symbol for a diatomic is given by $^{2S+1}\Lambda$. The values of L and Λ correspond to

L	0	1	2	3	4
Atomic (L)	S	P	D	F	G
Molecular (Λ)	Σ	Π	Δ	Φ	Γ

Molecular iodine belongs to Hund's coupling case (c). Figure E.1 shows Hund's case (c) in which the orbital (**L**) and spin (**S**) are mutually coupled to form a resultant $\mathbf{J_a}$. In case (c), the spin-orbit coupling is so strong that the spin and orbital momenta couple strongly at every opportunity. The resultant $\mathbf{J_a}$ precesses about the molecular axis with fixed projection $\Omega\hbar$. The projection Ω couples with the rotational angular momentum N to form the total angular momentum **J**. Since **L** and **S** do not precess independently about the molecular axis in case (c) molecules, Λ and Σ are not good quantum numbers.
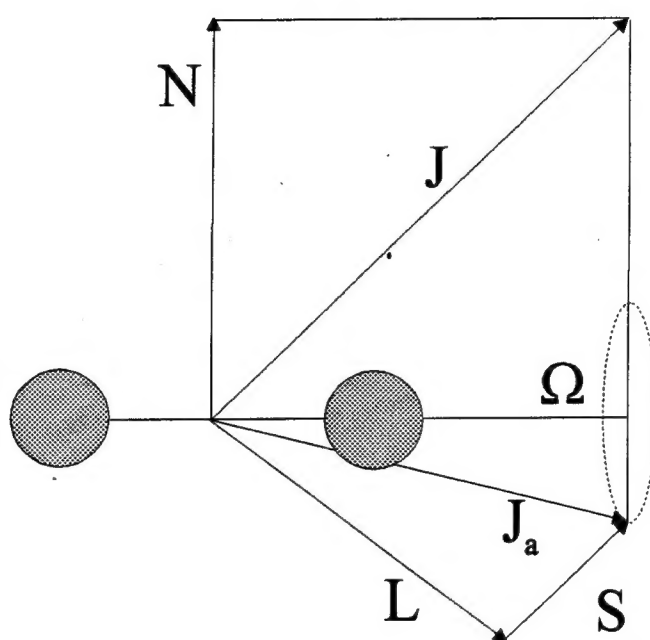
Figure E.1: Hund's Coupling Case (c)

APPENDIX F

LINESHAPES

While the peak height is representative of the intensity, the width of the peak is influenced by the lineshape broadening mechanisms. In a typical absorption measurement, the three most important mechanisms which contribute to broadening the spectral lineshape are: Doppler broadening, collision broadening, and lifetime broadening. If the pressure of the absorbing atoms inside the sample cell is kept low (10-100 mTorr), the line width of the absorption will be governed by the lifetime of the excited state and by Doppler broadening. Doppler broadening is caused by the motion of the atoms due to the Doppler effect, which is an apparent change in radiation when radiating atoms or molecules are moving relative to the observer. Spectral lines are broadened according to the Maxwell-Boltzmann velocity distribution with an observed frequency ω for non-relativistic velocities (v<<c) of $\omega = \omega_0[1+(v_z/c)]$. The atoms in an atomic or molecular gas will have in addition to their internal energies, Brownian kinetic motion through space. The distribution of axial velocities in a gas in thermal equilibrium will be Gaussian and have the form

$$g_G(\upsilon) = \exp[\frac{-Mc^2(\upsilon-\upsilon_0)^2}{2kT(\upsilon_0)^2}]$$

where $g_G(\nu)$ is the Gaussian linewidth, M is the atomic mass, k is the Boltzmann constant, c is the speed of light, and ν_0 is line center. The lineshape of a spectral feature does not occur at one precise frequency, but has a finite linewidth. The width of the resonance transition is often expressed in terms of the *full width at half maximum power*

(FWHM). In the case of a Gaussian lineshape, the linewidth is expressed as 2σ. Also, the Gaussian distribution is applicable to the errors associated with many types of experimental measurements. For this type of distribution, the percentage of measured values that lie within two or three standard deviations is 95.4% or 99.7%, respectively.

With gas pressures greater than 100 mTorr, the absorption line will be further broadened due to collisions with other atoms. This line broadening feature is known as Lorentzian broadening. Broadening of lines can also arise from the finite collisional or natural lifetime of a state. Such broadening gives rise to a Lorentzian lineshape function due to the effective damping of the classically oscillating dipole. The broadening is homogeneous since each particle has the same distribution of transition frequencies. The Lorentzian lineshape function is given by

$$g_L(\upsilon) = \frac{\Delta\upsilon_h}{2\pi\left[(\upsilon_0-\upsilon_x)^2+(\frac{\Delta\upsilon_h}{2})^2\right]}$$

where g_L is the Lorentzian line width (FWHM).

At moderate pressures, the lineshape is influenced by both Doppler and collision broadening. With still increasing pressures (>1 Torr), a convolution between Doppler velocity distribution and first order collisional relaxation is mathematically described by the Voigt function. In reality, Gaussian and Lorentzian lineshapes are a convolution of the collision and Doppler broadening, but the influence of these factors are such that they can be accurately described by a closed mathematical expression. A good approximation of the Voigt profile is assuming that each velocity group in the Gaussian shaped doppler profile is broadened to the same extent by the Lorentzian profile. The

combined profile is intermediate as it appears Lorentzian in the wings and Gaussian near the line center. The Voigt function is defined as

$$W(z) = \frac{i}{\pi} \int_{-\infty}^{\infty} \frac{\exp\{-t^2\}}{z-t} dt$$

with the customary definitions, $z = x - iy$

$$x = \frac{\sqrt{\ln 2}\,(\upsilon - \upsilon_0)}{\gamma_D} \qquad\qquad y = \frac{\sqrt{\ln 2}\,\gamma_L}{\gamma_D}$$

where γ_L and γ_D are the collision and Doppler broadened widths, respectively. A highly accurate Voigt function algorithm using an improved Drayson's method, complete with FORTRAN source code has been published by Z. Shippony and W. G. Read[2].

REFERENCES

1. L. J. Radziemsiki, R. W. Solarz, and J. A. Paisner, Eds., *Laser Spectroscopy and its Applications*, Marcel Dekker, New York (1987).

2. Z. Shippony and W. G. Read, *J. Quant. Spectrosc. Radiat. Transfer* **50**, 635 (1993).